TAL TECH

DOCTORAL THESIS

Biodegradability Assessment of Emerging Green Solvents, Bioactive Heterocycles, and Hybrid Nanomaterials

Nandish Mudegowdru Nagappa

TALLINNA TEHNIKAÜLIKOOL
TALLINN UNIVERSITY OF TECHNOLOGY
TALLINN 2026

TALLINN UNIVERSITY OF TECHNOLOGY
DOCTORAL THESIS
43/2026

Biodegradability assessment of emerging green solvents, bioactive heterocycles, and hybrid nanomaterials

NANDISH MUDEGOWDRU NAGAPPA

TAL TECH PRESS

TALLINN UNIVERSITY OF TECHNOLOGY
School of Science
Department of Chemistry and Biotechnology
This dissertation was accepted for the defence of the degree 29/06/2026

Supervisor: Dr. Yevgen Karpichev
Department of Chemistry and Biotechnology
Tallinn University of Technology
Tallinn, Estonia

Opponents: Assist. Prof. Paresh Kumar Samantaray
Department of Chemical & Materials Engineering
University of Alabama in Huntsville
Huntsville, Alabama, USA

Dr. Monika Mortimer
Laboratory of Environmental Toxicology
National Institute of Chemical Physics and Biophysics
Tallinn, Estonia

Defence of the thesis: 10/08/2026, Tallinn

Declaration:
Hereby I declare that this doctoral thesis, my original investigation and achievement, submitted for the doctoral degree at Tallinn University of Technology has not been submitted for doctoral or equivalent academic degree.

Nandish Mudegowdru Nagappa

---
signature

European Union
European Regional
Development Fund

Investing
in your future

ISSN 2585-6898 (paperback)
ISBN 978-9916-80-523-7 (paperback)
ISSN 2585-6901 (PDF)
ISBN 978-9916-80-524-4 (PDF)
https://doi.org/10.23658/taltech.43/2026

Nagappa, N. M. (2026). *Biodegradability assessment of emerging green solvents, bioactive heterocycles, and hybrid nanomaterials* [TalTech Press]. https://doi.org/10.23658/taltech.43/2026

TALLINNA TEHNIKAÜLIKOOL
DOKTORITÖÖ
43/2026

Tekkivate roheliste lahustite, bioaktiivsete heterotsüklite ja hübriidnanomaterjalide biolagunevuse hindamine

NANDISH MUDEGOWDRU NAGAPPA

TAL TECH
KIRJASTUS

Contents

List of Publications

The list of author's publications, based on which the thesis has been prepared:

I **Nagappa, N. M**.; Mero, A.; Husanu, E.; Usmani, Z.; Oliva, M.; Sanches, M. V.; Fumagalli, G.; Mele, A.; Mezzetta, A.; Gathergood, N.; Guazzelli, L.; Pretti, C.; Karpichev, Y. Biodegradability and Ecotoxicity Profiles of Choline Acetate, Betaine, and L-Proline NADESs: A Hidden Threat for Eutrophication? *Molecules* 2026, *31* (2), 262. https://doi.org/10.3390/molecules31020262.

II Bondar, D.; Smirnova, O.; **Nagappa, N. M**.; Heinmaa, I.; Soukup, O.; Kobrlova, T.; Opravil, J.; Hrabinova, M.; Jun, D.; Starkov, P.; Spuul, P.; Kuča, K.; Mochalin, V. N.; Karpichev, Y. Nanodiamond Mediated Delivery of Pyridinium Oxime Antidotes to Central Nervous System for Potential Treatment of Exposure to Nerve Agents. *Chem.-Biol. Interact.* 2025, *420*, 111711. https://doi.org/10.1016/j.cbi.2025.111711.

III Severin, O. O.; Bondar, D.; Bragina, O.; **Nagappa, N. M**.; Olev, J.; Brovarets, V. S.; Semenyuta, I. V.; Karpichev, Y. In Vitro Anticancer Activity and In Silico Target Profiling of 5-(Piperazin-1-Ylsulfonyl)-1,3-Oxazole-4-Carbonitriles. *Int. J. Mol. Sci.* 2026, *27* (4), 1936. https://doi.org/10.3390/ijms27041936.

Author's contribution to the publications

Contributions to the papers in this thesis are:

I The author performed OECD 301D biodegradability tests for all investigated NADESs with experimental guidance from Zeba Usmani, analysed the biodegradation data, and evaluated the ready biodegradability classifications of both the NADESs and their individual components. The author contributed to the discussion and interpretation of the environmental implications of the study by integrating the biodegradability results generated during the OECD 301D experiments with the ecotoxicity findings reported by collaborators, including discussion of potential eutrophication-related risks. The author made significant contributions to the preparation of the manuscript and the compilation of the Supporting Information.

II The author performed biodegradability assessment of the oxime-functionalized nanodiamonds and participated in their physicochemical characterisation, including DLS sample preparation, measurements, and data interpretation, as well as FT-IR spectroscopy data interpretation, for the samples prepared for the biodegradability test.

III The author contributed to the conceptualisation of the biodegradability study and experimental design, performed biodegradability assessment of the oxazole derivatives, and contributed to interpretation of the high-performance liquid chromatography (HPLC) characterization data. The author contributed to biodegradation data analysis, environmental interpretation of the results, and manuscript preparation.

Introduction

The global production and use of synthetic chemicals and advanced materials have increased drastically over the past few decades, driven by rapid development in the pharmaceuticals, materials science, agriculture, and consumer products. It is estimated that tens of thousands of chemicals are currently registered for commercial use, with hundreds to thousands of new substances entering the market annually[1]. Once released during production, use, or disposal, many of these substances inevitably enter environmental compartments, particularly aquatic systems, where they may persist, transform, or interact with biological systems. Predicting the environmental fate of such a diverse and continuously expanding chemical space represents one of the central endeavours in contemporary environmental chemistry.

Biodegradation plays a key role in determining environmental fate. It refers to the microbial transformation of organic substances into simpler compounds and ultimately inorganic products such as carbon dioxide, water, and mineral salts. Biodegradation data indicate whether a chemical is rapidly removed from the environment or remains available for prolonged exposure, thereby influencing persistence, bioaccumulation, biomagnification, and long-term ecological risk[2,3]. Accordingly, biodegradability assessment is widely recognized as a first-tier screening tool in environmental risk assessment frameworks.

To harmonize and standardize biodegradability testing across regulatory jurisdictions, the Organisation for Economic Co-operation and Development (OECD) established internationally accepted test guidelines in the late 1980s and early 1990s. Among these, the OECD 301 series of "ready biodegradability" tests were developed to identify substances that are rapidly and completely mineralized under aerobic aqueous conditions[4]. These methods, including the closed bottle test (OECD 301D), are intentionally conservative. They operate under favourable conditions to assess the intrinsic biodegradation potential of a substance rather than its full environmental behaviour. While these tests provide essential information for screening persistence, it is increasingly recognized that biodegradability outcomes should be interpreted alongside molecular structure, degradation kinetics, and environmental context to fully understand their environmental relevance[5–7].

In recent years, growing attention has been directed towards emerging greener classes of chemicals and materials that defy conventional biodegradability assumptions. One such class is Natural Deep Eutectic Solvents (NADESs), which are formed by hydrogen-bonded mixtures of naturally occurring components such as choline, amino acids, and organic acids. NADESs have been widely described as "green solvents" due to their low volatility, tunable properties, and renewable origins[8,9]. However, despite being composed of naturally derived constituents, uncertainty remains regarding their biodegradability, ecotoxicity, and potential indirect environmental impacts, such as increased biological oxygen demand or nutrient-driven eutrophication following release into aquatic systems[10].

Another relevant group comprises synthetic heterocyclic compounds**,** including oxazole derivatives, which are commonly used in medicinal chemistry due to their significant pharmaceutical application. The presence of heteroaromatic rings and electron-withdrawing substituents can impart high chemical stability, potentially limiting microbial degradation and increasing environmental persistence[11,12]. Given the

continuous introduction of new bioactive molecules, understanding the biodegradability of such structures is essential for early identification of persistence risks[7].

The increasing application of emerging biocompatible carbon nanomaterials such as carbon dots (CDs)[13] and nanodiamonds (NDs)[14,15] in drug delivery, bioimaging, and sensors, has raised critical questions regarding their environmental fate[16,17], as these materials can enter aquatic and terrestrial ecosystems through manufacturing, consumer use, and disposal. Carbon-based nanomaterials are generally considered non-biodegradable due to their highly stable lattice structures, yet they are often functionalized with organic surface moieties to enhance dispersibility and functionality[18,19]. In such hybrid systems, environmental behaviour is influenced by the degradability of the surface-bound organic corona as well as the long-term persistence of the nanomaterial core, posing hurdles for conventional biodegradation assessment frameworks.

Understanding the environmental fate of chemicals and advanced materials is among the central questions of the contemporary sustainable chemistry[20], particularly in the context of increasing structural complexity and the emergence of novel material classes[21]. Biodegradation screening tests, such as the OECD 301D Closed Bottle Test, are commonly employed to assess the ready biodegradability or persistence of the substances[22]. However, their applicability to diverse and non-conventional materials remains insufficiently explored[23]. Together, these compound classes represent emerging anthropogenic substances whose environmental persistence and biodegradation profile should be evaluated proactively prior to widespread industrial, pharmaceutical, or biomedical application.

The conceptual framework of this thesis is therefore based on the hypothesis that standardized biodegradation screening, when interpreted in the context of molecular structure and physicochemical properties, can provide a transferable basis for early-stage environmental persistence assessment. This approach allows systematic comparison between simple bio-based molecules, hybrid nanomaterials, and structurally complex pharmaceutical compounds. Within this framework, the OECD 301D Closed Bottle Test is employed not merely as a routine laboratory method, but as an analytical platform to examine how structural features influence biodegradation behaviour under controlled conditions.

By integrating results across these distinct systems, this thesis contributes to a broader understanding of potential relationships between molecular structure and environmental persistence, while critically assessing the applicability of standardized biodegradation tests to emerging materials. The results provide a basis for more informed environmental assessment strategies and support the development of sustainable, benign-by-design chemical systems evaluated already at early stages of their lifecycle

Abbreviations

2-PAM	Pralidoxime
AChE	Acetylcholinesterase
API	Active pharmaceutical ingredient
BBB	Blood–brain barrier
BcA	Blank control A
BcB	Blank control B
Bet	Betaine
BPA	Bisphenol A
BOD	Biological oxygen demand
CA	Citric acid
CBT	Closed Bottle Test
ChA	Choline acetate
ChBt	Choline bitartrate
ChOAc	Choline acetate
ChTA	Choline tartrate
CNS	Central nervous system
CYP2M	Cytochrome P450
DES	Deep eutectic solvents
DGA	Diglycolic acid
DLLME	Dispersive liquid–liquid microextraction
DLS	Dynamic light scattering
DOC	Dissolved organic carbon
EG	Ethylene glycol
EP	End point
ESI	Electrospray ionization
FTIR	Fourier Transform Infrared spectroscopy
GA	Glycolic acid
GB	Sarin
Gly	Glycerol
HBA	Hydrogen bond acceptor
HBD	Hydrogen bond donor
HCCA	α-Cyano-4-hydroxycinnamic acid
HI-6	HI-6 oxime
HPLC	High-performance liquid chromatography
HRMS	High-resolution mass spectrometry
Im	Imidazole
L-LacA	L-Lactic acid
LA	Levulinic acid
LPME	Liquid-phase microextraction
L-Pro	L-Proline
MA	Malic acid
MALDI-TOF	Matrix-Assisted Laser Desorption/Ionization Time-of-Flight
MITI	Ministry of International Trade and Industry test
MS/MS	Tandem mass spectrometry
m/z	Mass-to-charge ratio

NADES	Natural deep eutectic solvents
NAMs	New approach methodologies
ND	Nanodiamond
ND-4a	4-pyridinium oxime linked to PEG-diamine
NGS	Next-generation sequencing
NSAIDs	Nonsteroidal anti-inflammatory drugs
OECD	Organisation for Economic Co-operation and Development
OP	Organophosphorus
PEG	Polyethylene glycol
PreSens	Precision Sensing GmbH
PTFE	Polytetrafluoroethylene
QcA	Quality control A
QcB	Quality control B
QSBR	Quantitative Structure–Biodegradation Relationship
RP-LC	Reversed-phase liquid chromatography
SDME	Single drop microextraction
SP	Start point
TestA	Test substance A
TestB	Test substance B
ThOD	Theoretical oxygen demand
ToxA	Toxicity control A
ToxB	Toxicity control B
UHPLC	Ultra-high-performance liquid chromatography
WWTP	Wastewater treatment plant

1 Literature overview

1.1 Biodegradation

Biodegradation is a fundamental ecological process through which organic compounds are transformed and mineralized by microorganisms, in simple terms, microorganisms utilize organic compounds as sources of carbon and energy, thereby transforming complex molecules into simpler compounds or completely mineralizing them, enabling the continuous cycling of carbon and nutrients in the environment. From an evolutionary perspective, microorganisms represent Earth's earliest and most effective degraders of organic matter. Through the development of diverse metabolic pathways and enzymatic systems, microbial communities have enabled the decomposition of a wide range of natural biomolecules, ensuring that organic carbon does not accumulate indefinitely in ecosystems[24].

Billions of years ago, during the early stages of Earth's history, microorganisms emerged as Earth's earliest biodegraders, initiating the natural breakdown and recycling of organic matter. Under present-day oxygen-rich conditions, microbial communities are highly efficient at degrading and mineralizing organic compounds, thereby ensuring the rapid turnover of carbon within the ecosystems[25]. However, during ancient geological periods, this was not always the case, during the Carboniferous and Mesozoic eras, organic matter often escaped complete microbial degradation due to its anoxic environment. This incomplete mineralization led to the burial, and long-term transformation of biomass into fossil fuels which ultimately enabled modern industrial and technological development, a process that contrasts strongly with the rapid biodegradation seen today.

In the modern era, the omnipresence of microbes, their metabolic diversity and oxygen-rich environment together have allowed for the decomposition of most naturally occurring organic matter[26]. This continuous microbial turnover prevents the accumulation of organic matter in natural ecosystems. Earth's earliest microorganisms were nature's first recyclers, initiating the decomposition of organic materials. In today's world, a different challenge has emerged, the increasing use of synthetic and structurally complex compounds, particularly in the pharmaceutical and biotechnology industries, has raised concern about their environmental fate and persistence. Unlike natural biomolecules, many of these anthropogenic compounds may resist microbial degradation, leading to persistence and potential ecological risks. For example, many fish and amphibians have undergone feminization and other estrogenic effects due to exposure to endocrine disruptors like BPA[27] and Ethinylestradiol[28]. These are only two examples among many complex compounds that are having an adverse effect on our environment by their limited biodegradation and increased environmental persistence.

Numerous historical cases demonstrate that chemicals initially considered safe can have severe and unforeseen environmental consequences, as indicated in Table 1. A prominent example is diclofenac. The case of diclofenac exemplifies a critical failure in environmental risk assessment, where a drug deemed safe for humans and livestock led to the catastrophic collapse of vulture populations across South Asia. The substance's environmental persistence, a property not initially assessed, allowed it to remain in livestock carcasses. The scavenging vultures, which were the victims of this case, were exquisitely sensitive to diclofenac's renal toxicity, which was discovered later, due to this they suffered mass mortality[29], causing population declines exceeding 97%. This case

underscores the paramount importance of biodegradation testing. Such assessments directly screen for a chemical's persistence: Environmental persistence contributed to prolonged exposure and ecological impact. By identifying persistent substances early, biodegradation testing acts as a crucial first-tier warning, triggering deeper investigation into potential bioaccumulation and specific toxicological threats long before a chemical is widely released, thereby helping to prevent such unforeseen and devastating consequences.

" A chemical's resistance to biodegradation is a prerequisite for its potential to undergo biomagnification.**"**

Table 1*. Environmental and biological impacts of selected pharmaceutical compounds detected in aquatic environments.*

Pharmaceutical type	**Impact**	**Affected organism/system**	**References**
β-blockers (Bisoprolol)	Immobilization	*Daphnia similis*	[30,31]
β-blockers (Bisoprolol)	Mortality	Green algae	[32]
β-blockers (Bisoprolol)	Mortality	Fish	[32]
β-blockers (Propranolol)	Growth and developmental problems	*Synechococcus leopolensis*, *Cyclotella meneghiniana*	[33]
β-blockers (Propranolol)	Mortality	Crustacean (*Ceriodaphnia dubia*)	[34]
β-blockers (Propranolol)	Embryonic developmental abnormalities	*Danio rerio*	[35]
NSAIDs and Analgesics (Acetaminophen)	Cardiovascular abnormalities, altered hatch and motor behaviour, disruption of oocyte maturation/ovulation	*Danio rerio*	[36–38]
NSAIDs and Analgesics (Diclofenac)	Population decline	*Gyps* vultures	[39]
NSAIDs and Analgesics (Diclofenac)	Damage to gills, liver, and kidneys	*Salmo trutta fario*	[40–42]
NSAIDs and Analgesics (Diclofenac)	Histological and cytological alterations; impaired ionic regulation	*Oncorhynchus mykiss*	[40–42]
NSAIDs and Analgesics (Diclofenac)	Inhibition of CYP2M enzyme	*Cyprinus carpio*	[43–45]

Pharmaceutical type	Impact	Affected organism/system	References
NSAIDs and Analgesics (Diclofenac)	Oxidative stress and biomarker responses	*Mytilus galloprovincialis*	[46]
NSAIDs and Analgesics (Ibuprofen)	Inhibition of CYP2M enzyme	*Cyprinus carpio*	[47]
NSAIDs and Analgesics (Ibuprofen)	Alteration of breeding patterns	*Oryzias latipes*	[48]
NSAIDs and Analgesics (Ibuprofen)	Cardiovascular abnormalities and developmental effects	*Danio rerio*	[43–45]
NSAIDs and Analgesics (Ibuprofen)	Reduced plant growth and physiological functions	*Vigna unguiculata*	[49]

Following the recognition of the importance of biodegradation, a clear definition of this concept and its underlying mechanisms is essential. Biodegradation is defined as the transformation of chemical substances by microorganisms through enzymatic processes, ultimately resulting in structural modification or complete mineralization[3]. These processes are driven by diverse microbial metabolic pathways that utilize organic compounds as sources of carbon and energy. Depending on the extent of transformation, biodegradation can range from partial molecular transformation to complete mineralization into inorganic end products. Consequently, biodegradation is not a singular phenomenon but encompasses multiple stages and outcomes that differ in environmental relevance, kinetics, and regulatory interpretation[50]. Biodegradation is commonly categorized into primary and ultimate biodegradation. Primary biodegradation describes the initial structural alteration of a compound, resulting in the loss of its original chemical identity or biological activity through the formation of transformation products. While such changes may reduce functionality or toxicity, they do not necessarily eliminate environmental persistence. In contrast, ultimate biodegradation refers to the complete mineralization of organic compounds into carbon dioxide, water, and inorganic salts, representing the definitive removal of organic carbon from the environment. This distinction is particularly important for environmental risk assessment, as ultimate biodegradation ensures the long-term elimination of a substance from aquatic ecosystems.

Building on this distinction, biodegradation is usually investigated under different conceptual and experimental frameworks, depending on the purpose of the assessment and the environmental compartment of interest [3,51]. Biodegradation studies are typically organized into hierarchical levels of assessment, including screening tests, simulation tests, and field-based observations [51] , as shown in Figure 1. Screening tests are designed to rapidly assess whether a substance has the intrinsic potential to biodegrade under favourable conditions, providing an initial indication of environmental persistence [52]. Simulation tests, in contrast, aim to reproduce specific environmental compartments such as activated sludge, surface waters, sediments, or soils, allowing for a more realistic evaluation of degradation kinetics and transformation pathways [53]. Field studies offer

the highest level of environmental relevance but are often limited by complexity, variability, and lack of mechanistic control [54]. Each of these approaches serves a distinct role within environmental risk assessment, with screening tests acting as the first and most critical step for identifying substances that may warrant further investigation [51,55].

Among screening approaches, standardized ready biodegradability tests play a central role in regulatory frameworks, as they provide conservative and comparable assessments of a chemical's potential to undergo ultimate biodegradation [51]. These tests are intentionally stringent, employing low microbial densities and non-adapted inoculum to identify substances that biodegrade rapidly and completely under aerobic conditions [56]. A positive outcome in such tests implies a low likelihood of environmental persistence, whereas failure does not necessarily indicate recalcitrance but rather triggers the need for higher-tier studies [57]. Given the widespread use and release of organic compounds into aquatic environments, biodegradation under aerobic aqueous conditions is of relevance. Consequently, this thesis focuses on comparative assessment of the environmental biodegradability and persistence behaviour of diverse emerging compounds and materials under standardized aerobic aqueous conditions using the OECD 301D Closed Bottle Test, a widely accepted screening method for assessing ultimate biodegradation based on oxygen consumption [56]. By applying this standardized approach, the work aims to systematically evaluate mineralization behaviour, persistence potential, and structure-related biodegradation trends across diverse classes of organic substances.

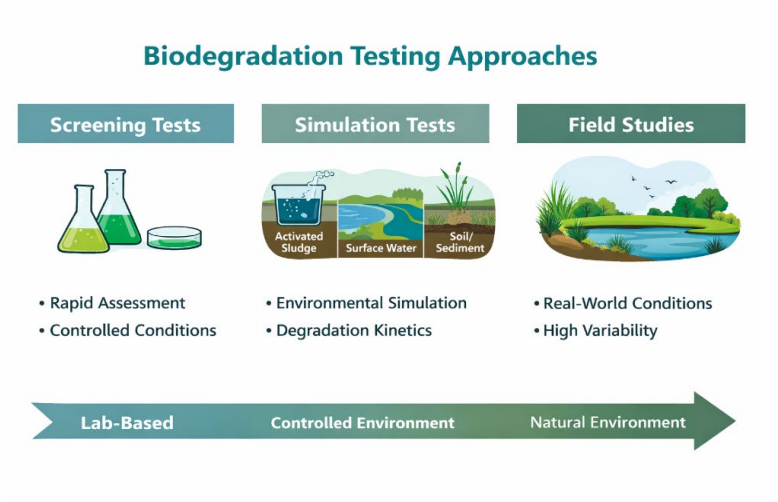

Figure 1. *Conceptual overview of different biodegradation testing approaches, including screening tests, simulation tests, and field studies. The figure was generated with assistance from ChatGPT (OpenAI) and edited by the author.*

Most organic pollutants, regardless of whether they are released directly into surface waters, ultimately reach aquatic environments through processes such as runoff, leaching, and atmospheric deposition. Consequently, understanding their behaviour in aquatic systems is essential for predicting their persistence, transformation, and potential adverse effects on aquatic flora and fauna. Accordingly, assessing the environmental fate and biodegradability of chemical compounds at early stages of

development: ideally during their design and synthesis: rather than after-market release, is consistent with environmentally conscious chemical design principles, as it enables structural modification of substances to reduce environmental persistence and ecological risks before widespread use. According to OECD guidelines, biodegradability tests are classified based on the level of environmental realism and the type of information they provide regarding the degradation behaviour of a substance. These tests are generally organized into three categories: screening tests, inherent biodegradability tests, and simulation tests. Screening tests are stringent methods designed to identify substances that are readily biodegradable under favourable aerobic conditions. Inherent biodegradability tests evaluate whether a substance possesses the potential to biodegrade under optimized conditions, even if degradation is slower or incomplete. Simulation tests provide the highest level of environmental relevance by reproducing specific environmental compartments, such as activated sludge systems, surface waters, sediments, or soils, to estimate degradation kinetics and transformation pathways under realistic conditions.

Among these categories, the OECD 301 series represents the standard screening-level tests for ready biodegradability assessment. These methods differ primarily in their analytical principle and suitability for compounds with different physicochemical properties. The applicability of selected OECD ready biodegradability tests is summarized in Table 2.

Table 2. *Applicability of test methods based on OECD guidelines for ready biodegradability tests.*

Test	**Analytical method**	**Suitability for compounds which are:**		
		poorly soluble	**volatile**	**adsorbing**
DOC Die-Away (301 A)	Dissolved organic carbon	-	-	+/-
CO_2 Evolution (301 B)	Respirometry: CO_2 evolution	+	-	+
MITI (I) (301 C)	Respirometry: oxygen consumption	+	+/-	+
Closed Bottle (301 D)	Respirometry: dissolved oxygen	+/-	+	+
Modified OECD Screening (301 E)	Dissolved organic carbon	-	-	+/-
Manometric Respirometry (301 F)	Oxygen consumption	+	+/-	+

1.2 Biodegradation of metabolites and natural biomolecules

Natural metabolites such as amino acids, organic acids, simple sugars, and related biomolecules are generally expected to be readily utilized by microorganisms as they align with their central metabolic routes. Amino acids such as glycine and alanine can be rapidly deaminated and incorporated into cellular metabolism, while organic acids such as acetate and lactate serve as key intermediates in microbial energy production pathways. Similarly, monosaccharides such as glucose and fructose are efficiently utilized

through glycolysis by a wide range of microorganisms[58]. Experimental work in aquatic systems has demonstrated that dissolved amino acids can be substantially mineralized by microbial communities, with microbial metabolism often dominating their fate under relevant environmental conditions[59]. Due to this easy metabolism, amino acids have been used as indicators of organic matter degradation status in aquatic and sedimentary environments, reflecting their role in biogeochemical cycling and microbial processing[60]. Although these compounds are typically biodegradable, their effective turnover can still be influenced by environmental constraints such as sorption interactions, community composition, and redox conditions[59]. These compounds are generally readily metabolized by microbial communities, although the surrounding environmental conditions can affect how fast this breakdown can happen.

1.3 Biodegradation of bio-based molecules and materials

Bio-based molecules and materials are usually assumed to be environmentally benign due to their natural origin. However, bio-based origin does not automatically imply rapid biodegradation under all conditions. OECD has emphasized that standards and test methods (including biodegradability testing) are important for substantiating environmental claims associated with bio-based products[61]. Reviews of biodegradable bio-based polymers highlight substantial variability in biodegradation performance depending on polymer chemistry, crystallinity, molecular weight, additives, and environmental conditions, emphasizing the need for standardized testing and cautious interpretation of "biodegradable" labels[62]. Complementary assessments comparing standard methods and real-world conditions further underline that biodegradation outcomes can differ across matrices and that standardized tests provide controlled, comparable data rather than direct field rate predictions[63].

Accordingly, research suggests that the incorporation of bio-based and biodegradable fragments into synthetic platforms, such as ionic liquids (ILs) and surface-active ionic liquids (SAILs), has emerged as a promising strategy to enhance biodegradability and support a benign-by-design approach. Early studies on amino acid-derived ionic liquids have demonstrated that the use of naturally occurring building blocks, such as L-phenylalanine and related amino acids, can improve environmental compatibility by reducing microbial toxicity while maintaining or enhancing biodegradation potential[64]. For example, L-phenylalanine-derived SAILs have been shown to combine surface activity with improved biodegradation profiles, demonstrating the potential of amino acid-based building blocks in environmentally compatible materials[65]. Similarly, toxicity profiling of structurally related ionic liquids has revealed that the choice of cation and alkyl chain length significantly influences biological effects, highlighting the importance of molecular design in reducing environmental impact[65]. More recent studies on dipeptide-based ionic liquids further confirm that incorporating biodegradable fragments can enhance both biodegradability and reduce toxicity, reinforcing the concept of sustainable molecular design[66]. In addition, systematic investigations have established design rules indicating that structural features such as ester linkages and shorter alkyl chains play a key role in improving environmental degradability, providing a rational framework for the development of greener ionic liquids[67].

1.4 Biodegradation of simple synthetic molecules

Many structurally simple synthetic molecules, such as low-molecular-weight oxygenated compounds, are generally biodegradable because their chemical structures closely resemble naturally occurring substrates and can be readily assimilated into existing microbial metabolic pathways[3]. Nevertheless, biodegradation rates and extents reported in the literature vary depending on environmental conditions, microbial community composition, and nutrient availability[68]. Methodological literature comparing respirometry tests emphasizes that experimental parameters (including endogenous respiration and inoculum characteristics) can influence oxygen-consumption-based biodegradation curves, reinforcing the role of guideline structure, validity criteria, and appropriate controls in interpretation[68]. In practical terms, simple molecules may pass ready tests readily, but standardized conditions are still necessary to ensure comparability across substances and laboratories.

1.5 Biodegradation of complex synthetic molecules and pharmacophores

As molecular complexity increases—through aromaticity, heteroatoms in rigid ring systems, halogenation, strong electron-withdrawing groups, or multiple functional substitutions—biodegradation can become less favourable due to reduced enzymatic accessibility or lack of suitable catabolic pathways. Aromatic and heteroaromatic compounds have long been recognized as environmentally relevant because they are prevalent pollutants and may exhibit persistence depending on substitution patterns and environmental conditions[69]. This is particularly relevant for pharmaceuticals, where structural motifs designed for biological stability (pharmacophores) can contribute to reduced biodegradability and longer environmental residence times.

Reviews on pharmaceuticals in aquatic environments summarize that many active ingredients are continuously introduced into surface waters and wastewater systems, and their removal is often incomplete; biodegradation is one of the key attenuation mechanisms, but outcomes vary strongly by compound class and system conditions[70,71]. Importantly, pharmaceuticals can undergo primary biotransformation to transformation products that may retain biological activity or persistence, meaning that ultimate biodegradation cannot be assumed from partial loss of the parent compound[4,70]. For heterocyclic and structurally rigid pharmacophores, persistence concerns are frequently emphasized in environmental fate discussions[72]. Experimental work focusing on heterocyclic aromatic contaminants similarly indicates that many such structures do not meet ready biodegradability criteria, reinforcing the link between aromatic heterocycle stability and reduced biodegradation under screening conditions[73].

1.6 Biodegradation and transformation of engineered nanomaterials

Engineered nanomaterials present a distinct challenge for biodegradability assessment due to their hybrid composition, typically consisting of a stable inorganic or carbonaceous core combined with diverse surface functionalizations. The biodegradation and transformation of such materials depend strongly on particle characteristics, including core composition, surface chemistry, functional groups, and interactions with biological systems, such as bio-corona formation[74]. Environmental fate-oriented synthesis further describes how colloidal behaviour, aggregation, and surface

reactions govern transport and bioavailability, which in turn influence observed biodegradation or biotransformation[75]. In contrast, studies on organic nanoparticles have demonstrated that materials composed of biodegradable constituents can undergo significant transformation and mineralization in aqueous environments, although degradation rates remain highly dependent on particle structure, size, and surface properties[76]. For carbon-based nanomaterials in particular, recent reviews summarize evidence that enzymatic and microbially mediated oxidation processes may occur under certain conditions, but rates and extents can be limited, and outcomes depend heavily on material properties and environmental context[77].

1.7 OECD 301D Ready Biodegradability (Closed Bottle Test)

Often referred to as the closed bottle test (CBT), this test uses a respirometric analytical method to assess the biological oxygen demand caused by the test substance. In the assessment of chemical environmental fate, the OECD 301D Closed Bottle Test serves as a stringent screening tool. The test simulates a "worst-case" scenario for biodegradation by modelling a pristine receiving water body. It is therefore considered one of the stringent tests for biodegradation among the other tests available because of the following reasons:

1. *Low inoculum concentration:* this test uses a highly diluted inoculum, typically obtained from wastewater treatment plant effluent, thereby mimicking environmentally dilute conditions such as surface waters distant from pollution sources.
2. *Lack of pre-adaptation*: the microorganisms used in this test are not previously exposed or acclimatized to the test substances, whereas in the real world these microorganisms can adapt over time, so this test requires microorganisms to degrade the test substance with a non-adapted microbial community thereby increasing the stringency of the test.
3. *Low test substance concentration*: the concentration of the test substance used in this test is very low compared to other OECD biodegradability tests, it is also below the threshold value that would allow the metabolic pathways to be metabolically favourable for microorganisms.

For a substance to be classified as readily biodegradable according to OECD 301D Closed Bottle Test it must meet these two criteria, within the standard 28-day test period:

1. *The extent of degradation*: The biodegradation value must reach a minimum of 60%. This is calculated based on the percentage of the theoretical oxygen demand (ThOD) of the substance that is consumed by the microbes. This indicates that the majority of the test substance has been mineralized (broken down to CO_2 water and biomass).
2. *The speed of degradation*: This is the critical criterion for *readiness*. The 60% degradation must occur within a 10-day window that begins when biodegradation first reaches 10%.

1.7.1 Limitations of OECD screening tests and emerging improvements

Although OECD ready biodegradability tests, such as the 301D Closed Bottle Test, are extensively applied as first-tier screening tools, their stringent design introduces several limitations that can affect the interpretation of results. These tests employ low microbial inoculum concentrations, non-adapted communities, and low quantity of test

substances, which may not adequately represent environmentally relevant conditions. As a result, many chemicals fail to meet the criteria for ready biodegradability, not necessarily due to true persistence, but because the test conditions limit microbial activity and diversity. This can lead to conservative and, in some cases, overly pessimistic assessments of biodegradation potential.

To address these limitations, recent approaches aim to improve both realism and efficiency in biodegradability assessment. High-throughput and miniaturized screening methods[78] allow variation of key parameters such as inoculum density and exposure conditions, enabling a more nuanced understanding of biodegradation as a continuum rather than a binary outcome. In addition, the integration of experimental data with computational tools, such as QSBR models and machine learning, is emerging as a promising strategy to enhance persistence predictions[79]. These developments contribute to new approach methodologies, which complement traditional OECD tests within a broader, multi-tiered framework for environmental fate assessment. The present work does not aim to develop a novel OECD biodegradability methodology, but rather employs an optode-based adaptation of the standard OECD 301D protocol for continuous oxygen monitoring and improved experimental reproducibility.

1.8 Natural Deep Eutectic Solvents

Deep eutectic solvents were developed as a greener and cheaper alternative to the traditional solvents such as ionic liquids, whose environmental benignity remains debated in the current available literature. DESs can be obtained by simply mixing two naturally derived components, which are inexpensive, renewable, and biodegradable and are capable of self-association often through hydrogen bonding to form a eutectic mixture. The resulting mixture generally exhibits a lower melting point than that of the individual components[80] . Eutectic is a word derived from the Greek *eutektos* meaning easy melting, which here is considered in the context of phase behaviour. DESs usually consist of two components, a hydrogen bond acceptor (HBA) and hydrogen bond donor (HBD). Natural Deep Eutectic Solvents (NADES) are a subclass of DESs composed of naturally derived metabolites[81]. Most of the available NADESs currently consist of primary or biosynthetically derived metabolites. Based on their chemical nature, these components can be grouped into 5 main categories: quaternary ammonium compounds, organic acids, amino acids, sugars, and fatty acids.

NADESs have rapidly transitioned from a bio-inspired solvent concept to practical tools across analytical chemistry, biocatalysis, pharmaceutics, and biomass valorisation. Their respective applications are presented in Table 3:

Table 3. *Reported applications of NADESs.*

Application area	Description / Key points	References
Plant and food extraction	Extraction of polyphenols, flavonoids, alkaloids, pigments; greener alternative to organic solvents.	[82]
Analytical sample preparation	Used in LPME, DLLME, SDME; improves selectivity and reduces solvent toxicity.	[83]
Enzyme stabilization & biocatalysis	Enhances enzyme stability, activity, and selectivity, compatible with many biocatalysts.	[84]

Application area	Description / Key points	References
Pharmaceutical solubilization	Increases solubility and stability of poorly soluble drugs;	[85]
Drug delivery and biomedical use	Works as carriers/co-solvents; improves permeability and drug release behaviour.	[86]
Biomass processing and valorization	Useful for lignocellulosic biomass fractionation; extraction from agro residues.	[87]
Natural products research	Proposed as natural intracellular solvents helping metabolite storage and stability.	[88]
General green solvent applications	Applied in catalysis, electrochemistry, separations, and other sustainable processes.	[89]

The broad and expanding industrial use of NADESs increases the likelihood of environmental release, reinforcing the need for systematic biodegradability assessment. Although NADESs are composed of naturally occurring constituents, they cannot be assumed to be inherently safe or environmentally benign. Similar assumptions were previously made for DESs, based on the established safety profiles of their individual components as reported in material safety data sheets; however, subsequent studies have demonstrated that such mixtures may exhibit unexpected toxicity[90]. This highlights that the properties of eutectic mixtures cannot be reliably inferred from those of their individual components, even when these are naturally derived metabolites [91]. This highlights the need to evaluate the actual environmental behaviour of these eutectic mixtures.

In this regard, the present study investigates the biodegradability of 15 NADESs, alongside selected individual components. The assessed systems, including their hydrogen bond acceptor (HBA), hydrogen bond donor (HBD), and molar ratios, are summarized in Table 4.

Table 4. *List of the NADESs assessed for their biodegradability with their composition and molar ratio.*

NADES	HBA	HBD	Molar Ratio
1.Bet:EG	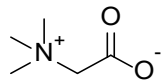 Betaine	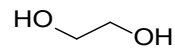 Ethylene Glycol	**1:4**
2.Bet:CA	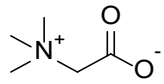 Betaine	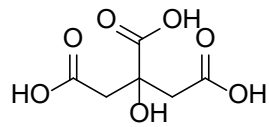 Citric Acid	**2:1:6(water)**
3.Bet:Gly	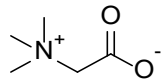 Betaine	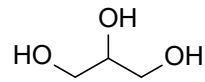 Glycerol	**1:2**

NADES	HBA	HBD	Molar Ratio
4.Bet:LA	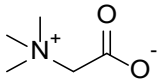 Betaine	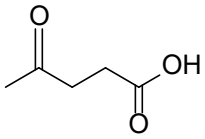 Levulinic Acid	**1:2**
5.Bet:L-LacA	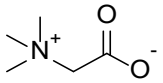 Betaine	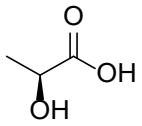 L-Lactic Acid	**1:1**
6.L-Pro:Gly	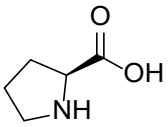 L-Proline	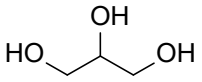 Glycerol	**1:2.5**
7.L-Pro:L-LacA	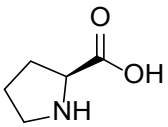 L-Proline	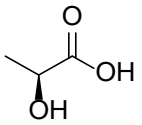 L-Lactic Acid	**1:1**
8.L-Pro:LA	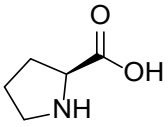 L-Proline	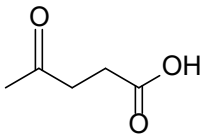 Levulinic Acid	**1:2**
9.L-Pro:MA	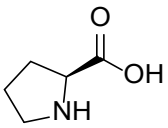 L-Proline	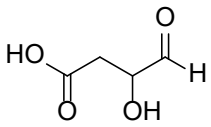 Malic Acid	**1:1**

NADES	HBA	HBD	Molar Ratio
10.ChBt:CA	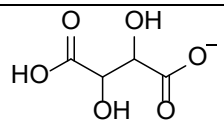 Choline bitartrate	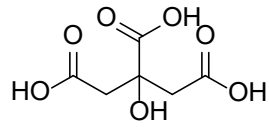 Citric Acid	**1:1**
11.ChA:Im	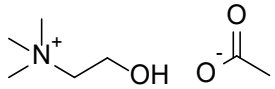 Choline Acetate	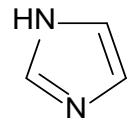 Imidazole	**1:1**
12.ChA:LA	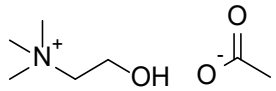 Choline Acetate	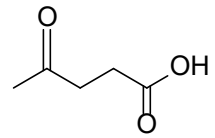 Levulinic Acid	**1:1**
13.ChA:GA	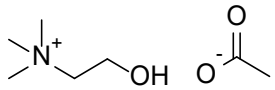 Choline Acetate	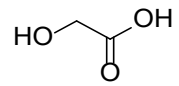 Glycolic Acid	**1:1**
14.ChA:DgA	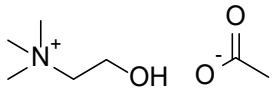 Choline Acetate	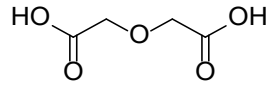 Di-glycolic Acid	**1:1**
15.ChA:CA	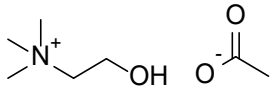 Choline Acetate	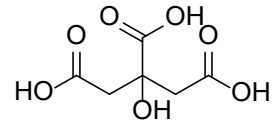 Citric Acid	**1:1**

1.9 Nanodiamond-based drug delivery systems

Nanotechnology-based drug delivery systems have attracted increasing interest due to their ability to improve bioavailability and transport across biological barriers. In the present work, this is particularly relevant for oxime-functionalized nanodiamonds, whose environmental persistence and biodegradability remain poorly understood[92,93]. Nanocarriers offer advantages such as enhanced solubility of poorly water-soluble drugs, controlled release, and the ability to overcome biological barriers, including the blood–brain barrier (BBB)[93,94]. These features make nanotechnology particularly valuable in the treatment of complex diseases, including cancer and central nervous system (CNS)

disorders. Among various nanomaterials, carbon-based nanomaterials have attracted considerable attention due to their unique physicochemical properties, including high surface area, chemical stability, and ease of functionalization[95]. This class includes carbon nanotubes, graphene, fullerenes, and nanodiamonds, each exhibiting distinct structural and biological characteristics[95]. Their versatile surface chemistry allows for conjugation with drugs, biomolecules, and targeting ligands, making them promising candidates for drug delivery applications[96].

Nanodiamonds (NDs) are carbon-based nanoparticles characterized by a diamond-like sp^3 hybridized carbon core and a surface rich in functional groups such as carboxyl, hydroxyl, and carbonyl moieties[97]. These surface functionalities enable facile chemical modification and conjugation with therapeutic agents. NDs exhibit excellent biocompatibility, low cytotoxicity, and high colloidal stability compared to other carbon nanomaterials, making them particularly suitable for biomedical applications[97,98]. In addition, NDs have demonstrated the ability to interact with biological membranes and facilitate cellular uptake, which is critical for effective drug delivery. Their nanoscale size and surface properties allow them to act as carriers for both hydrophilic and hydrophobic drugs[97,99].

Surface functionalization of NDs is a crucial strategy to enhance their performance as drug delivery systems. Functionalization can be achieved through covalent or non-covalent approaches, enabling the attachment of polymers, drugs, and targeting ligands[100]. Among these, polyethylene glycol (PEG) modification is widely employed to improve solubility, reduce aggregation, and increase circulation time in biological systems[101]. Functionalized NDs have been investigated for a variety of biomedical applications, including targeted drug delivery, imaging, and gene therapy[97]. Importantly, surface modification also influences the biological fate and potential biodegradation of NDs. Although NDs are generally considered highly stable, emerging studies suggest that surface-functionalized carbon nanomaterials can undergo gradual transformation under oxidative biological conditions, which may facilitate their clearance and improve their safety profile[102].

Building upon these advancements, NDs have been functionalized with oxime groups to develop novel therapeutic systems for the treatment of organophosphorus (OP) poisoning. Oximes, such as pralidoxime (2-PAM), obidoxime, and HI-6, are nucleophilic agents capable of reactivating acetylcholinesterase (AChE) inhibited by OP compounds[103]. These clinically used oxime antidotes typically contain quaternary nitrogen (pyridinium) groups, which confer a permanent positive charge and enhance their reactivity toward phosphorylated AChE[104,105]. However, this permanent positive charge significantly limits their ability to cross the blood–brain barrier (BBB), thereby reducing their effectiveness in reactivating AChE within the central nervous system[106]. To address this limitation, oxime moieties have been covalently conjugated to ND surfaces through linker systems, often incorporating polyethylene glycol (PEG) spacers (Figure 2). This strategy aims to enhance the delivery of oxime functionalities by improving their transport across biological barriers and increasing their bioavailability. In addition, the incorporation of variable spacer lengths allows modulation of molecular flexibility and spatial orientation of the active oxime group, which may influence interaction with biological targets and overall therapeutic efficiency. Oxime-functionalized NDs therefore represent a promising approach for improving the efficacy of antidotes against nerve agents and pesticide poisoning, particularly in scenarios where rapid CNS penetration and reactivation of AChE are critical.

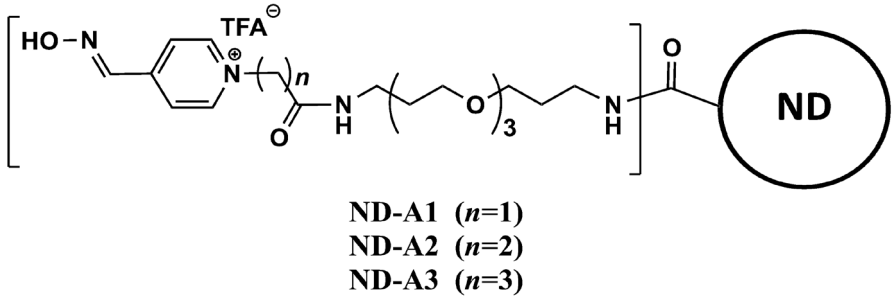

ND-A1 (*n*=1)
ND-A2 (*n*=2)
ND-A3 (*n*=3)

Figure 2. *4-Oximinopyridinium-functionalized nanodiamond conjugates (ND-A1–ND-A3). Source: Reproduced from Publication II, with permission from Elsevier.*

Evaluating the biodegradation of oxime antidotes and their ND conjugates is essential because these therapeutic systems are designed for deployment in scenarios involving chemical warfare agents and organophosphate contamination, where large-scale or repeated use may lead to environmental release[107]. Oxime molecules, especially when modified or delivered through engineered nanoparticles, may persist in aquatic or soil ecosystems if they are not readily biodegradable. Persistence can lead to long-term accumulation, potential toxicity to microorganisms, and disruption of natural biodegradation cycles. ND conjugation introduces an additional concern: although NDs are considered chemically stable, their surface-functionalized forms may interact differently with microbial communities and may alter degradation pathways[108]. Therefore, biodegradation analysis helps determine whether the ND oxime constructs break down into harmless products, how fast this occurs, and whether the nanocarrier or the oxime moiety contributes to environmental persistence. Although the structural properties of quaternary oximes and ND-based carriers strongly indicate that these compounds are unlikely to be readily biodegradable[108], experimental biodegradation testing remains essential to confirm their environmental persistence, understand degradation pathways of surface functional groups, and support ecological risk assessments for potential large-scale or emergency-response applications.

1.10 Biodegradation and environmental fate of oxazole-derived pharmaceuticals

The widespread use of pharmaceuticals in the modern era has led to their continuous release into the environment, particularly into aquatic systems through wastewater effluents, hospital discharges, and agricultural runoff[109]. These compounds, commonly referred to as active pharmaceutical ingredients (APIs), are designed to exert biological effects at low concentrations and are often not completely removed during conventional wastewater treatment processes[7]. As a result, pharmaceuticals are increasingly detected in surface water, groundwater, and even drinking water supplies, raising concerns about their potential impact on both human health and ecosystems. Their continuous input and pseudo-persistent nature make pharmaceutical pollution an emerging global environmental issue[110,111].

A significant proportion of pharmaceuticals contain heterocyclic moieties, which play a crucial role in modulating biological activity, pharmacokinetics, and molecular stability. Heterocycles, defined as cyclic compounds containing at least one heteroatom such as

nitrogen, oxygen, or sulphur, are present in the majority of small-molecule drugs[112]. Their structural diversity and ability to participate in various intermolecular interactions make them highly valuable in drug design. However, these same features, particularly aromaticity and chemical stability can contribute to environmental persistence, making heterocyclic pharmaceuticals an important class to evaluate in environmental studies[113]. Among heterocyclic compounds, azoles represent a prominent class of five-membered aromatic rings containing nitrogen and, in some cases, additional heteroatoms such as oxygen or sulphur. These compounds are broadly utilized in medicinal chemistry due to their stability, versatility, and broad spectrum of biological activities, including antifungal, antibacterial, antiviral, and anticancer properties[114,115].

The aromatic character of azoles can contribute to increased resistance to biodegradation, which may result in prolonged environmental persistence. Consequently, azole-containing pharmaceuticals have attracted attention in environmental research due to their potential to accumulate and exert long-term ecological effects[7,113].

Within the azole family, oxazoles are five-membered aromatic heterocycles containing one oxygen atom and one nitrogen atom in a 1,3 arrangement. The aromaticity of the oxazole ring imparts rigidity, planarity, and significant chemical stability, while the presence of heteroatoms creates an electron-deficient system capable of hydrogen bonding interactions[116,117]. These physicochemical properties make oxazole derivatives valuable scaffolds in medicinal chemistry, where they are frequently employed as bioisosteres of amide groups. Because oxazole derivatives are structurally stable heteroaromatic compounds commonly used in medicinal chemistry, their potential environmental persistence following pharmaceutical release warrants biodegradability assessment, including those with anticancer and antiviral activities [117,118]. However, their structural stability may also contribute to reduced biodegradability, necessitating further investigation into their environmental behaviour[119].

The oxazole derivatives investigated in this study were synthesized (Figure 3), structurally characterized, and evaluated for anticancer activity by collaborators from partnering institutions, together with Dr. Denys Bondar, TalTech. Active pharmaceutical ingredients (APIs) can persist in aquatic environments and negatively affect both human and ecological health, making it essential to evaluate their environmental behaviour during early stages of drug development [7]. Assessing the biodegradability of the synthesized oxazole derivatives is crucial because APIs and their transformation products are increasingly recognized as environmental pollutants. Since these oxazole derivatives showed promising anticancer activity and structural stability, it is necessary to determine whether they are capable of degrading under aerobic environmental conditions.

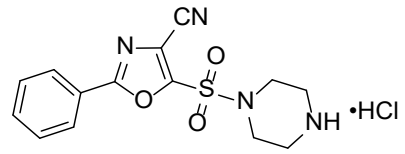

7a

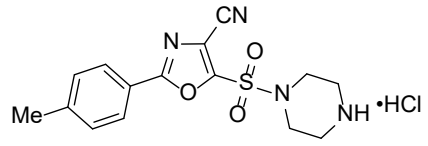

7b

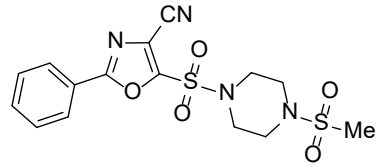

8aa

Figure 3. *Structures of the 5-(piperazin-1-ylsulfonyl)-1,3-oxazole-4-carbonitrile derivatives 7a, 7b, and 8aa, for which biodegradation assessments were performed in the present study. Synthesis of these compounds was carried out by co-authors as reported in the original publication. Source: Reproduced from Publication III, under CC-BY 4.0 licence.*

2 Research objectives

The increasing introduction of structurally diverse chemicals and advanced materials into the environment requires systematic approaches for assessing their persistence and environmental impact. This thesis addresses this challenge within a unified framework focused on emerging materials, including green solvents, pharmaceutical scaffolds, and hybrid nanomaterials.

The objectives of the present work are:

- To perform a comparative evaluation of the aerobic biodegradability of representative compounds from these distinct chemical classes: natural deep eutectic solvents (NADESs), oxime-functionalized nanodiamonds (NDs), and oxazole derivatives using the OECD 301D Closed Bottle Test as a common experimental platform.
- To analyze how molecular structure, chemical complexity, and hybrid material architecture may influence biodegradation behaviour under controlled screening conditions. Particular attention is given to identifying trends in biodegradability across simple bio-based systems, structurally complex pharmaceutical molecules, and surface-functionalized hybrid nanomaterials.
- To interpret the biodegradation results within the broader context of environmental persistence and environmental relevance, including indirect effects such as eutrophication potential, persistence of nanomaterial systems, and environmental behaviour of bioactive molecules.

Overall, this work aims to contribute experimental data and a comparative framework that can support early-stage environmental assessment and inform future development of safer and more sustainable chemical systems within a benign-by-design perspective.

3 Experimental methods

The biodegradation of all three compound classes was evaluated following the OECD guidelines for testing the biodegradability of chemicals. For this purpose, a modified OECD 301D Closed Bottle Test protocol was employed. The materials and procedures used in this modified 301D test are detailed below.

The NADESs used in our research were provided by collaborators from the Ionic Liquids group at the University of Pisa, Italy. The information about their commercial components, purity and suppliers is as follows: Choline acetate (ChA, 98%) was obtained from IOLITEC (Germany). Betaine (Bet, >99%) and L-proline (L-Pro, >99%) were purchased from Tokyo Chemical Industry (Japan). Ethylene glycol (EG, 99%), levulinic acid (LA, 98%), imidazole (Im, 99%), and cholinium bitartrate (ChTA, >98%) were supplied by Thermo Fisher (USA). Glycerol (Gly, 99%), glycolic acid (GA, 99%), malic acid (MA, >99%), diglycolic acid (DGA, 98%), and L-lactic acid (L-LacA, ≥98%) were obtained from Sigma-Aldrich (Merck, Germany). Ultrapure deionized water (Milli-Q system) was used throughout. Potassium dichromate ($K_2Cr_2O_7$, ≥99%, 1 g/L, ACS grade) from Sigma-Aldrich was used as a reference toxicant in the algal growth inhibition assay. The composition and the molar ratio of the NADESs assessed are listed in Table 4. The chemicals and reagents used for the synthesis of oxime-functionalized nanodiamonds, and oxazole derivatives are as reported in our publications.

3.1 Aerobic biodegradation according to modified OECD 301D

Aerobic biodegradation was assessed using a modified closed bottle test (CBT) based on OECD 301D guidelines[57]. In this modified setup, biological oxygen consumption was monitored using an optode oxygen sensor system equipped with PTFE-lined PSt3 oxygen sensor spots (Fibox 3, PreSens, Regensburg, Germany), allowing continuous biological oxygen demand (BOD) measurements without opening the flasks. This approach reduces the number of parallel samples required for each compound, thereby increasing test throughput, and has been reported to improve reproducibility[120] compared to the original OECD 301D protocol. Among standard aerobic biodegradation tests, the CBT is particularly suited for evaluating compounds with diverse physiochemical properties. Moreover, it is considered one of the most stringent ready biodegradability tests, as it uses a very low inoculum concentration. Consequently, compounds that pass the CBT are expected to exhibit good biodegradation not only under artificial wastewater treatment conditions but also in soil and groundwater environments.

The optode-based setup employed in this study enabled continuous dissolved oxygen monitoring through the bottle wall without opening the test bottles (Figure 4) or disturbing the test bottles[120]. This adaptation is increasingly used in biodegradation research for substances that require precise oxygen tracking and stable closed-system conditions. The optode setup preserves the integrity of the closed bottle environment, prevents changes in headspace composition, eliminates the risk of oxygen re-equilibration during manual sampling, and enables high-resolution monitoring of oxygen consumption throughout the 28-day test period. Importantly, this modification does not alter the underlying principles or stringency of the closed bottle test: the inoculum concentration, nutrient medium composition, test substance concentration, and ready-biodegradability pass criteria (≥60% ThOD within a 10-day window) remain unchanged. The use of optode therefore represents an analytical improvement that enhances

measurement accuracy and repeatability while fully maintaining the conservative nature of the original OECD 301D method.

Figure 4. *Modified oxygen measurement system used in the closed bottle test, employing a PreSens fiber-optic sensor integrated with OxyView software.*

3.2 Closed bottle test experimental setup

Each CBT experiment was conducted with four series of flasks as mentioned in Table 5, each run in duplicate, to assess biodegradation, reference activity, toxicity, and background oxygen consumption. The series were as follows:

1. Quality control series:
    - Purpose: To monitor microbial activity and validate the inoculum.
    - Procedure: Readily biodegradable sodium acetate (6.41 mg/L) was added to mineral medium inoculated with effluent from a wastewater treatment plant (WWTP).
    - Rationale: Sodium acetate is rapidly degraded by microbes and serves as a positive control for the activity of the inoculum.
2. Test series:
    - Purpose: To evaluate the biodegradability of the compound of interest.
    - Procedure: The test compound was added as the sole carbon source to the inoculated mineral medium at a concentration corresponding to a theoretical oxygen demand (ThOD) of ~5 mg/L.
    - Notes: ThOD calculations assumed nitrification would occur, as all 25 studied compounds contained nitrogen atoms.
3. Measured toxicity series:

- Purpose: To assess potential inhibitory or toxic effects of the test compound on the inoculum.
- Procedure: Both sodium acetate (as reference) and the test compound were added to the inoculated medium at their respective concentrations.
- Interpretation: If biodegradation of sodium acetate in these flasks was significantly lower than in the reference series, the test compound was considered potentially inhibitory or toxic to the microbial community.

4. Blank series:
    - Purpose: To account for background oxygen consumption by the inoculum itself.
    - Procedure: Flasks containing only mineral medium and inoculum, without any added carbon source, were included in each CBT run.
    - Data Treatment: The oxygen consumption measured in blank flasks was subtracted from all other series to correct for background microbial activity.

    This setup ensured that the CBT provided reliable, reproducible, and interpretable biodegradation data for all test compounds, while simultaneously controlling for microbial activity and potential toxicity.

Table 5. *Composition and purpose of each series in the CBT.*

Series	Purpose	Contents
Blank series	Measures background oxygen consumption of inoculum only	Mineral medium + inoculum (no added carbon source)
Reference series	Verifies microbial activity; ensures test validity	Mineral medium + inoculum + sodium acetate (readily biodegradable reference compound)
Test series	Evaluates biodegradability of the test compound	Mineral medium + inoculum + test compound (at concentration equal to ~5 mg/L ThOD)
Toxicity series	Assesses inhibitory/toxic effects of test compound	Mineral medium + inoculum + sodium acetate + test compound

3.3 Inoculum collection and preparation

In the closed Bottle Test (CBT, OECD 301D), the inoculum serves as the source of microorganisms responsible for degrading the test compounds. In this study, the inoculum was obtained from effluent of the Paljassaare municipal wastewater treatment plant in Tallinn, Estonia (59°27'55.5"N, 24°42'08.8"E). Before use, the effluent was filtered through a Whatman cellulose filter paper to remove large particulates while retaining the microbial community. These microorganisms metabolize the test compounds, consuming oxygen in the process, and this oxygen uptake is measured to evaluate biodegradability. The validity of the inoculum is verified using reference substances such as sodium acetate, confirming sufficient microbial activity. Its low concentration in the CBT makes the test stringent, such that only compounds capable of ready biodegradation under limited microbial conditions will pass, and it can reveal any toxic or inhibitory effects of the test compound on the microbial community.

In accordance with OECD Guideline 301D (CBT), the inoculum used in this study was derived from secondary effluent of a municipal wastewater treatment plant and represents a non-adapted microbial population, as no prior exposure, acclimation, or enrichment with the test substance or structurally related compounds was carried out. Microbial community analysis, sequencing analysis and bioinformatic processing of the inoculum was performed using 16S rRNA gene amplicon sequencing by Microbiome Research Group at TFTAK, Tallinn.

3.4 Physicochemical characterization methods

- Dynamic light scattering (DLS) measurements used for characterization of oxime-functionalized nanodiamonds were performed in collaboration with Dr. Denys Bondar, TalTech. The author participated in sample preparation, experimental measurements, and analysis of the DLS data together with Dr. Denys Bondar and was responsible for interpretation of the results in the context of biodegradability assessment.
- Fourier-transform infrared (FT-IR) spectroscopy measurements were performed by Dr. Denys Bondar, while the author contributed to interpretation of the FT-IR spectra in relation to biodegradability assessment.
- High-performance liquid chromatography (HPLC) characterization data for oxazole derivatives were generated together with Dr. Denys Bondar, the author contributed to analysis of the chromatographic data and was responsible for interpretation of the results in relation to biodegradability assessment and environmental relevance.
- MALDI-TOF mass spectrometry analysis used for preliminary characterization of the microbial inoculum in Publication I, was performed by Dr. Olga Bragina and Daria Maljuk (TalTech). The author contributed to the interpretation of the microbial profiling results in the context of inoculum suitability and environmental relevance.

3.5 Mineral media preparation

Mineral medium is a defined, nutrient-balanced solution that provides microorganisms with all essential inorganic nutrients needed for growth except for an organic carbon source. It contains specific amounts of phosphate buffers, magnesium sulphate, calcium chloride, and ferric chloride, which together supply nitrogen, phosphorus, trace elements, and maintain pH stability. The mineral medium is required because it creates a controlled, standardized environment where the test compound is the only source of organic carbon. This ensures that any oxygen consumption measured during the test can be attributed solely to the biodegradation of the test substance and not to other organic impurities.

Before the test, a mineral media stock solution is usually prepared in four different bottles and named A to D, the composition of each of these bottles is mentioned in Table 6 below.

Table 6. *Mineral media stock solution composition and concentration.*

Stock solution	Substances	Concentration in g/L
A	Potassium Dihydrogen Phosphate	8.50
	Di-Potassium Hydrogen Phosphate	21.75
	Di-Sodium Hydrogen Phosphate dihydrate	33.40
	Ammonium Chloride	0.50
B	Calcium Chloride Dihydrate	36.40
C	Magnesium Sulfate Heptahydrate	22.50
D	Iron (III)chloride Hexahydrate	0.25

3.6 Closed bottle test procedure

On the day prior to the start of the test, deionised water (approximately 33 L) was aerated with compressed air to achieve oxygen saturation of approximately 9 mg/L O_2. At the beginning of the experiment, a 1 L Schott bottle was filled from the canister for temperature monitoring. The remaining volume in the canister was adjusted to 30 L, after which each of the mineral media stock solutions were added sequentially (1 mL/L each) in the order B, C, D, then A (see Table 6), with thorough mixing after each addition. The inoculum was then added (2 drops/L), and the mixture was homogenised.

The prepared test medium was subsequently distributed into 1 L Schott bottles for individual test preparations. The required quantities of sodium acetate, mineral medium, and test substances were calculated and added according to OECD guidelines. Each preparation was mixed thoroughly prior to transfer.

For each test series, two closed bottle test (CBT) narrow-neck bottles were carefully filled from the corresponding Schott bottle. A separate bottle without sensor spots was prepared for temperature measurement. During filling, care was taken to avoid the introduction of air bubbles, and any trapped air was removed by gentle tapping before sealing. The bottles were capped without leaving headspace and stored in the dark to prevent light exposure.

Oxygen measurements were carried out according to the predefined sequence, and analytical samples were collected from the Schott bottles on day 0 and from the corresponding CBT bottles on day 28. All test bottles were incubated in the dark at 20 °C in a temperature-controlled room. Prior to measurement, the bottles were equilibrated to room temperature for several hours to ensure stable and consistent oxygen readings.

3.7 Evaluation of the results

3.7.1 Evaluation of biodegradation

The biodegradation of the test substance was evaluated according to OECD Guideline 301D (CBT). The degree of biodegradation was calculated based on the biological oxygen demand (BOD), corrected for oxygen consumption in the blank, and related to the theoretical oxygen demand (ThOD). The BOD at time t_x was calculated according to Equation (1):

$$BOD(t_x) = \Delta c(O_2)_T(t_x) - \Delta c(O_2)_{BC}(t_x) \quad (1)$$

Where $\mathrm{BOD}(t_x)$ is the biological oxygen demand at time t_x [mg/L], $\Delta c(O_2)_t(t_x)$ is the decrease in dissolved oxygen concentration in the test preparation at time t_x [mg/L], $\Delta c(O_2)^{Bc}(t_x)$ is the mean decrease in dissolved oxygen concentration in the blank controls at time t_x [mg/L], and t_x represents the selected measurement time point during the biodegradation experiment.

For nitrogen-containing test substances, biodegradation was calculated relative to the theoretical oxygen demand assuming ammonia formation, ThOD(NH_3), as shown in Equation (2):

$$Biodegradation(\%) = (BOD(t_x))/(ThOD(NH_3)) \times 100 \quad (2)$$

Where, *Biodegradation*(%) represents the percentage of biodegradation of the test substance, BOD(t_x) is the biological oxygen demand at time t_x [mg/L], ThOD(NH_3) is the theoretical oxygen demand calculated assuming ammonia formation during biodegradation, and t_x represents the selected measurement time point during the biodegradation experiment.

To account for oxygen consumption associated with nitrification, biodegradation was additionally calculated relative to the theoretical oxygen demand assuming nitrate formation, ThOD(NO_3^-), as shown in Equation (3):

$$Biodegradation(\%) = (BOD(t_x))/(ThOD(NO_3^-)) \times 100 \quad (3)$$

Where *Biodegradation*(%) represents the percentage of biodegradation of the test substance, BOD(t_x) is the biological oxygen demand at time t_x [mg/L] , ThOD(NO_3^-) is the theoretical oxygen demand calculated assuming complete nitrification to nitrate during biodegradation, and t_x represents the selected measurement time point during the biodegradation experiment

In the Excel-supported evaluation, oxygen concentration data recorded using the Fibox3 system were imported into the OECD 301D master worksheet. Start points (SP) and end points (EP) were defined within the plateau phase of the degradation curve, each comprising at least ten measured values. Outliers were excluded where necessary, and consistency between the number of SP and EP values was verified. Calibration data of the corresponding sensor spots were applied to correct the oxygen measurements. Degradation curves were visualized using the respective evaluation worksheets.

3.7.2 Calculated toxicity control

In all closed bottle tests, a calculated toxicity control was used to estimate the expected biodegradation of a mixture containing the test substance and a readily biodegradable reference compound under the assumption that no microbial inhibition occurs. This value was derived from the separately measured biodegradation of the test substance and the reference substance. The blank-corrected oxygen consumption of both components was combined and normalized to the total theoretical oxygen demand (ThOD) of the mixture, calculated from their individual concentrations and ThOD values. The calculated toxicity control therefore represents the biodegradation expected in the absence of inhibitory effects. Comparison of this calculated value with the experimentally measured toxicity control enables the assessment of potential inhibition and helps distinguish between true persistence and toxicity-related suppression of biodegradation.

3.7.3 Validity of the CBT results

The test substance is considered readily biodegradable if biodegradation reaches at least 60% of the theoretical oxygen demand (ThOD) within a 10-day window after biodegradation first exceeds 10%, during the standard 28-day test period. The 10-day window begins once biodegradation exceeds 10%. Substances fulfilling these criteria in the CBT are regarded as readily biodegradable under aerobic aqueous conditions.

According to OECD Guideline 301D, the validity of the closed bottle test is confirmed when the following criteria are fulfilled:

- Oxygen depletion in the blank controls should not exceed 1.5 mg/L during the 28-day incubation period.
- Dissolved oxygen concentrations in all test bottles should remain above 0.5 mg/L throughout the experiment.
- The difference in biodegradation between duplicate bottles should not exceed 20%.
- The reference compound sodium acetate should achieve at least 60% biodegradation within 14 days, confirming adequate microbial activity of the inoculum.
- In the toxicity control containing both the reference compound and the test substance, biodegradation should reach at least 25% within 14 days. Lower degradation values may indicate inhibitory or toxic effects of the test substance on the microbial community.

4 Results and discussion

4.1 Characterization of the microbial inoculum

To confirm the suitability and environmental relevance of the inoculum, microbial community analysis was performed by the Microbiome Research Group at TFTAK using 16S rRNA gene amplicon sequencing targeting the V4 region. The candidate contributed to interpretation of the microbial community composition in the context of inoculum suitability for biodegradation studies. The results indicated a highly diverse bacterial community, with 671 bacterial species, 421 genera, and 226 families detected, and a Shannon diversity index of 4.01, reflecting a well-balanced microbial population without dominance of specific taxa, as illustrated in Figure 5. Such microbial diversity is characteristic of wastewater-derived inoculum recommended for OECD ready biodegradability testing and indicates the presence of a diverse heterotrophic microbial community. These findings confirm that the inoculum is consistent with OECD 301D recommendations, for the use of a non-adapted, environmentally relevant microbial population in closed bottle test studies.

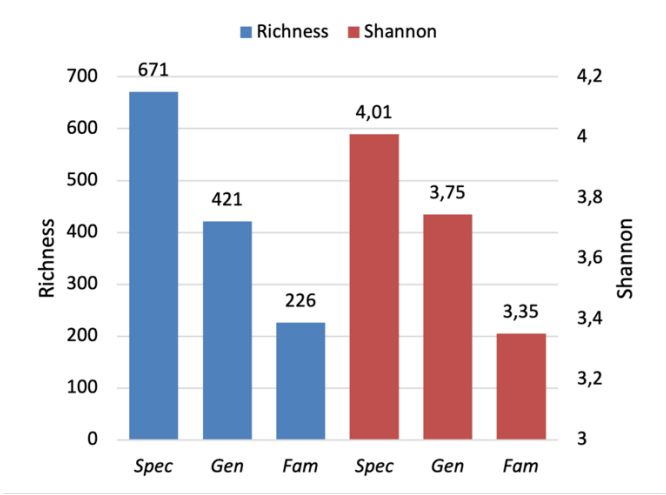

Figure 5. *Taxonomic richness at species (Spec), genus (Gen), and family (Fam) levels, together with corresponding Shannon diversity indices of the microbial community in the inoculum as determined by 16S rRNA sequencing, Figure generated from sequencing data analysis performed by the Microbiome Research Group at TFTAK.*

MALDI-TOF mass spectrometry analysis, performed by Dr. Olga Bragina and Daria Maljuk (TalTech), the author contributed to interpretation of these results in relation to biodegradation testing. The analysis provided insight into the culturable fraction of the microbial community present in the inoculum. High-confidence identifications (score ≥ 2.0) revealed a diverse bacterial assemblage dominated by genera such as *Escherichia*, *Aeromonas*, and *Citrobacter*, which were detected with high frequency across multiple samples. Moderate representation was observed for genera including *Acinetobacter*, *Klebsiella*, and *Pseudomonas*, while *Raoultella* and *Enterococcus* were identified less frequently. The detected taxa belong predominantly to families commonly associated

with wastewater environments, such as *Enterobacteriaceae*, *Aeromonadaceae*, *Moraxellaceae*, and *Pseudomonadaceae*, reflecting the environmental origin of the inoculum. The observed score ranges indicate that most dominant genera were identified with high confidence, while less abundant taxa were supported by moderate-confidence identifications. Overall, the MALDI-TOF results demonstrate the presence of a metabolically diverse and environmentally relevant culturable microbial community, consistent with the requirements for OECD 301D biodegradation testing. A summary of the bacterial taxa identified by MALDI-TOF MS is presented in Table 7. The table highlights the dominant genera detected in the culturable fraction of the inoculum, along with representative isolates, corresponding sample IDs, and score ranges reflecting identification confidence.

The NGS analysis discussed below refers to the same 16S rRNA gene amplicon sequencing dataset described previously. The results obtained from MALDI-TOF MS were further compared with the microbial composition revealed by next-generation sequencing (NGS). While MALDI-TOF analysis identified culturable bacterial taxa represented by 47 species, belonging to 10 families, sequencing revealed a significantly greater microbial diversity, identifying 372 species distributed among 368 genera and 202 families in the inoculum. This corresponds to approximately 7.9 times more species and sequencing revealed substantially broader microbial diversity than MALDI-TOF analysis. The difference can largely be attributed to the methodological scope of MALDI-TOF, which primarily identifies culturable microorganisms and relies on the availability of reference spectra in existing databases. Therefore, MALDI-TOF can be considered a useful rapid screening tool for preliminary microbial identification, while sequencing provides a more comprehensive analysis of microbial diversity. Differences in reported diversity metrics reflect differences in taxonomic filtering and comparative analysis approaches between sequencing-based community profiling and MALDI-TOF identification of culturable microorganisms[121,122].

Table 7*. Summary of microbial taxa identified by MALDI-TOF MS, including representative species, corresponding sample IDs, score ranges, and relative detection frequency within the inoculum.*

Genus	**Representative Species**	**Example Sample ID**	**Score Range**	**Frequency**
Escherichia	*E. coli*	C7, E3, H12	2.16 – 2.42	High
Aeromonas	*A. veronii, A. hydrophila*	B9, F10	2.00 – 2.17	High
Citrobacter	*C. freundii, C. gillenii*	B2, A7	2.13 – 2.19	High
Acinetobacter	*A. johnsonii*	A12, C5	1.77 – 2.09	Moderate
Klebsiella	*K. pneumoniae*	A2, F3	1.71 – 2.15	Moderate
Pseudomonas	*P. koreensis, P. veronii*	A9, D8	1.93 – 2.02	Moderate
Raoultella	*R. planticola, R. terrigena*	D1, E4	1.93 – 2.36	Low–Moderate
Enterococcus	*E. hirae, E. aquimarinus*	D6, H5	1.74 – 1.80	Low

4.2 Biodegradation results and discussion of NADESs

4.2.1 Biodegradation results

All the 15 NADESs compounds and some of their individual components were assessed for their ready biodegradability, using the modified OECD 301D Closed Bottle Test, and the results obtained are deemed to be valid as per the OECD guidelines.

All the tested NADESs, as well as their individual components, were classified as "readily biodegradable", their tested biodegradation values exceeded 60% after 28 days in the closed bottle test (Table 8). The only exception was imidazole (Im), which, when tested as an individual hydrogen bond donor (HBD), showed a markedly lower biodegradation value of 23%. Notably, however, the incorporation of Imidazole into a NADES with choline acetate (ChA) (NADES 11) did not negatively impact the overall biodegradability of the system, which reached 67%. This finding suggests that the eutectic combination may modulate the biodegradation profile of individual components, potentially through altered physicochemical interactions or enhanced microbial accessibility. The biodegradation profiles of the studied NADESs (Figure 6) further support this observation, as all NADESs displayed biodegradation trends consistent with ready biodegradability. Overall, these results indicate that, despite the limited biodegradation of certain individual constituents, their combination into NADESs might yield environmentally benign solvent systems, reinforcing the potential of NADESs as sustainable alternatives to conventional solvents.

Table 8. NADESs and their single components, with the relative structural formula, molar mass, concentration for biodegradation assessment, and biodegradation achieved by CBT 301D (28 days).

NADESs No.	**HBA: HBD** (molar ratio)	**Structural Formula**	**Molar Mass** (g/mol)	**Test Substance** (mg/L)	**Biodegradation** (28 days)
1	Bet: EG (1:4)	$C_{13}H_{35}NO_{10}$	365.42	3.57	76%
2	Bet: CA: water (2:1:6)	$C_{16}H_{42}N_2O_{17}$	371.86	5.06	70%
3	Bet: Gly (1:2)	$C_{11}H_{27}NO_8$	301.34	3.62	67%
4	Bet: LA (1:2)	$C_{15}H_{27}NO_8$	229.66	4.78	68%
5	Bet: L-LacA (1:1)	$C_8H_{17}NO_5$	263.75	3.60	70%
6	L-Pro: Gly (1:2.5)	$C_{13}H_{31}NO_{10}$	387.89	3.76	74%

NADESs No.	**HBA: HBD** (molar ratio)	**Structural Formula**	**Molar Mass** (g/mol)	**Test Substance** (mg/L)	**Biodegradation** (28 days)
7	L-Pro + L-LacA (1:1)	$C_8H_{15}NO_5$	205.21	3.77	65%
8	L-Pro: LA (1:2)	$C_{10}H_{21}NO_4$	347.36	3.29	69%
9	ChTA: CA (1:1)	$C_{12}H_{28}N_2O_6$	445.37	4.97	60%
10	L-Pro: MA (1:1)	$C_9H_{15}NO_7$	249.21	4.58	61%
11	ChA: Im (1:1)	$C_{10}H_{21}N_3O_3$	231.30	3.14	67%
12	ChA: LA (1:1)	$C_{12}H_{25}NO_6$	279.33	3.01	81%
13	ChA: GA (1:1)	$C_9H_{21}NO_6$	239.27	3.56	80%
14	ChA: DGA (1:1)	$C_{11}H_{23}NO_8$	297.30	3.87	77%
15	ChA: CA (1:1)	$C_{13}H_{25}NO_{10}$	373.36	4.32	66%
Single NADES components					
Betaine		$C_5H_{11}NO_2$	117.148	3.05	76%
Ethylene glycol		$C_2H_6O_2$	62.068	3.88	65%
Citric Acid		$C_6H_8O_7$	192.123	6.67	76%
Glycerol		$C_3H_8O_3$	92.094	4.11	75%
Levulinic Acid		$C_5H_8O_3$	116.116	3.30	72%

Single NADES components				
L-Lactic Acid	$C_3H_6O_3$	90.078	4.69	65%
L-Proline	$C_5H_9NO_2$	115.132	3.27	72%
D, L-Malic Acid	$C_4H_6O_5$	134.087	6.98	73%
Choline Acetate	$C_7H_{17}NO_3$	163.21	2.83	75%
Imidazole	$C_3H_4N_2$	68.077	4.25	23%
Glycolic Acid	$C_2H_4O_3$	76.05	7.92	79%
Diglycolic Acid	$C_4H_6O_5$	134.09	6.98	76%
Choline Bitartrate	$C_9H_{19}NO_7$	253.251	4.17	66%

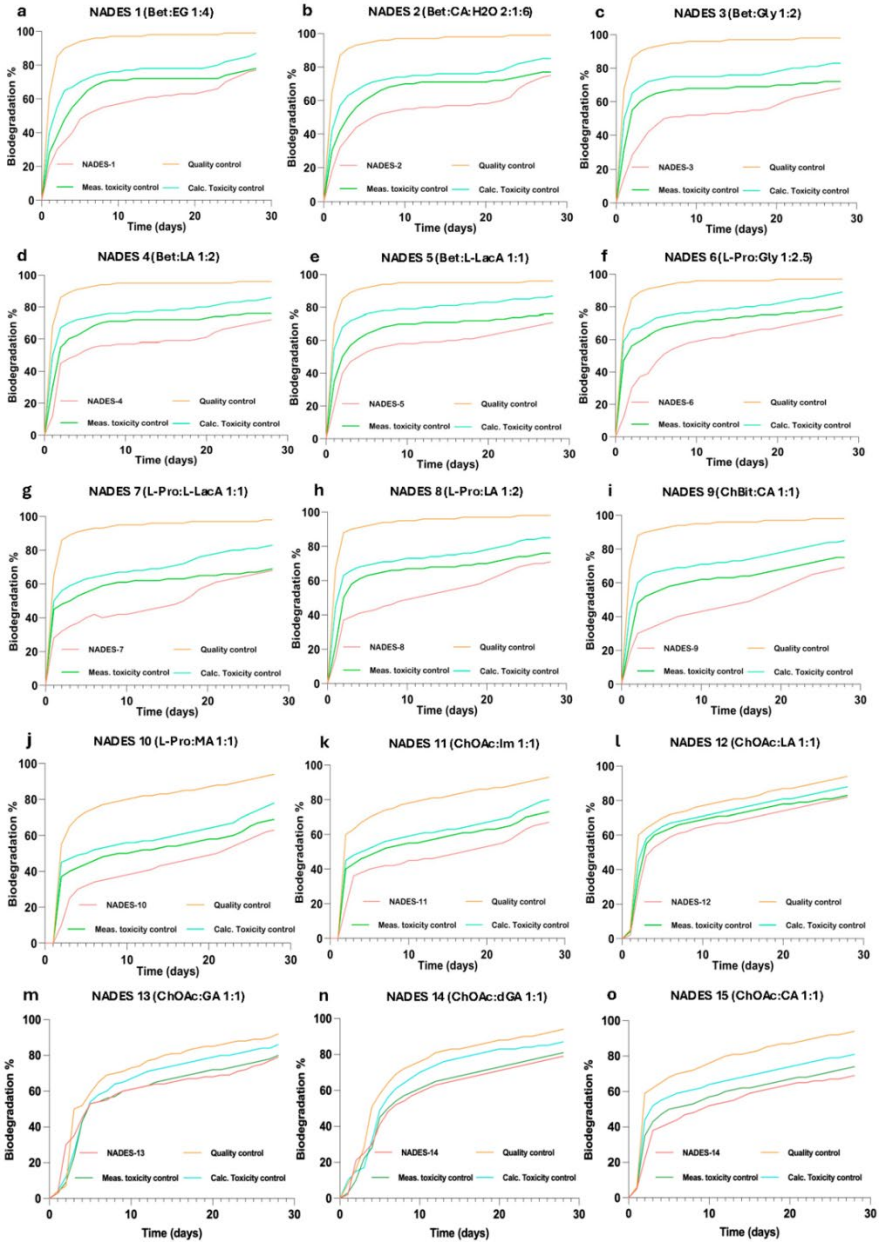

***Figure 6**. Biodegradability profiles obtained from the closed bottle test (OECD 301D, 28 days) for the investigated NADESs: (a) Bet:EG; (b) Bet:CA; (c) Bet:Gly; (d) Bet:LA; (e) Bet:L-LacA; (f) L-Pro:Gly; (g) L-Pro:L-LacA; (h) L-Pro:LA; (i) ChTA:CA; (j) L-Pro:MA; (k) CA:Im; (l) ChA:LA; (m) ChA:GA; (n) ChA:DGA; (o) ChA:CA. Sodium acetate (6.41 mg/L) was used as a reference compound (quality control) to confirm microbial activity and test validity. Toxicity control experiments, containing both sodium acetate and the test compound, were performed to evaluate potential inhibitory effects on microbial activity. Theoretical biodegradation curves were calculated to assess deviations indicating possible toxicity of the tested substances. Source: Reproduced from Publication I under CC-BY 4.0 licence*

4.2.2 Ecotoxicity analysis of NADESs

The ecotoxicological effects of the investigated NADESs were evaluated using the *Raphidocelis subcapitata* growth inhibition bioassay by our collaborators in University of Pisa, and the results are presented in Figure 7 as reported in Publication I. The results are summarised here to provide an integrated environmental profile of the investigated NADESs alongside the biodegradability data obtained in the present work. Overall, the majority of the tested NADESs induced a concentration-dependent algal growth stimulation rather than inhibition when compared to the control. Specifically, thirteen out of fifteen NADESs showed increased algal growth with increasing concentration, indicating a predominantly biostimulatory response. In contrast, NADES 4 (Bet:LA) and NADES 11 (ChA:Im) did not cause statistically significant differences in algal growth relative to the control across the tested concentration range. Differences between NADESs and their individual components were evident, highlighting the role of eutectic formulation in modulating biological responses. Among the individual components, choline acetate exhibited the strongest stimulatory effect on algal growth, consistent across NADESs 11-15, where it acts as the hydrogen bond acceptor. L-proline showed a concentration-dependent dual effect, with slight stimulation at higher concentrations in NADES 7 and 10, followed by growth inhibition at intermediate dilutions, whereas stronger inhibitory effects were observed when equivalent L-proline concentrations were present in NADES 6 and 8. Similar trends were observed for malic acid and L-lactic acid, although growth inhibition was limited to higher concentrations. Betaine and choline tartrate generally promoted algal biomass increase at the highest concentrations tested, while other components showed growth patterns comparable to the control. These results demonstrate that most NADESs formulations exhibit low acute ecotoxicity toward *R. subcapitata*, with biological responses strongly influenced by both component identity and concentration.

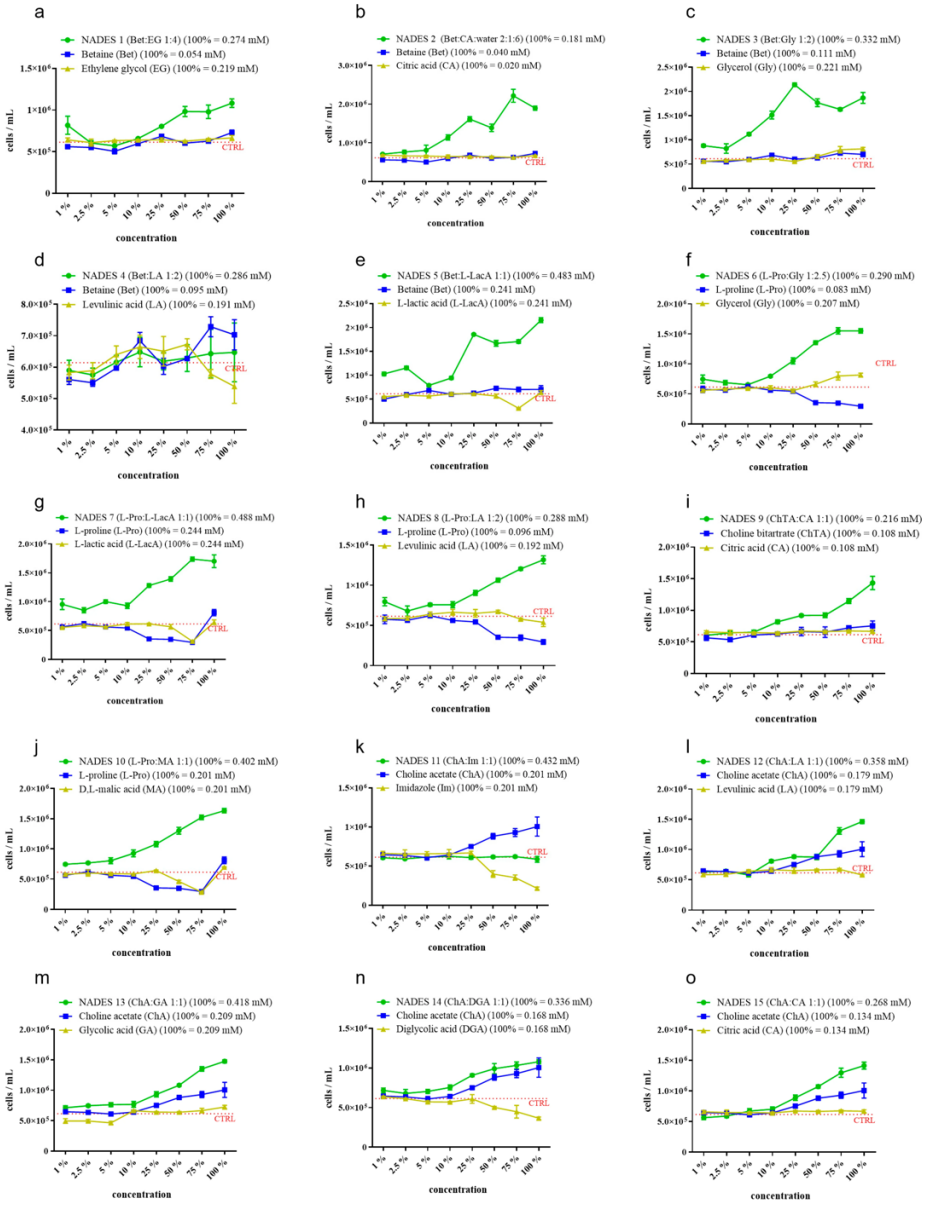

Figure 7. *Concentration–response curves of R. subcapitata exposed to NADESs and their individual components at equivalent relative concentrations. The red dashed line indicates the mean algal density in control samples: (a) Bet:EG; (b) Bet:CA; (c) Bet:Gly; (d) Bet:LA; (e) Bet:L-LacA; (f) L-Pro:Gly; (g) L-Pro:L-LacA; (h) L-Pro:LA; (i) ChTA:CA; (j) L-Pro:MA; (k) CA:Im; (l) ChA:LA; (m) ChA:GA; (n) ChA:DGA; (o) ChA:CA. Results are expressed as mean algal concentration (cells mL^{-1}) ± standard deviation (n = 3). Source: Reproduced from Publication I under CC-BY 4.0 licence*

4.2.3 Discussion and interplay between biodegradability and ecotoxicity of NADESs

The OECD 301D (CBT) biodegradation testing showed that most of the assessed NADESs were readily biodegradable, with degradation values after 28 days ranging between 60% and 81%. Regardless of the abundance of hydroxyl functionalities and the occurrence of oxygen-containing functional groups, including carboxylic acid-related moieties, esters, and amide structures, the biodegradability profiles were considered as "readily biodegradable". While their individual components showed a broader range of biodegradability (23-79%). Imidazole was the only component exhibiting low biodegradability (23%), which may suggest that the microbial inoculum used in the closed bottle test may have lacked effective metabolic pathways for its degradation. Although interestingly, when imidazole was combined with choline acetate in NADESs 11, the biodegradability increased to 67%, which indicates that the interactions between components in NADESs formulations can significantly alter the environmental behaviour of their individual compounds. Overall, the observed biodegradation profiles suggest that molecular composition and hydrogen-bond donor structure may influence biodegradation kinetics and environmental persistence under standardized aerobic conditions. These results indicate that, NADESs doesn't pose an environmental threat as they degrade quickly and not carry the risk of persisting in the aquatic environment compared to conventional solvents, but readily biodegradable materials potentially increase the load of dissolved ions/molecules with nutritional value such as choline which might increase the chances of eutrophication phenomena. Eutrophication is a natural phenomenon that occurs when the water bodies receive an excessive input of nutrients, primarily nitrogen and phosphorus containing compounds resulting in an accelerated algal growth and increased primary productivity. This might initially appear as growth stimulation, but it could ultimately lead to oxygen depletion, alter species composition, and degrade overall aquatic ecosystem health. The NADESs compounds might have shown ready biodegradability trends but several of them L-proline, betaine, and choline acetate, contain nitrogen in their formulation, might act as a fertilizer which could cause a potential eutrophication effect.

The ecotoxicity results performed by our collaborators from University of Pisa (Publication 1), showed us that the algal growth assays on NADESs often induce biological effects that differ from those of their single components. The strongest algal growth stimulation was observed for NADES 2 (Bet:CA), NADES 3 (Bet:Gly), and NADES 5 (Bet:L-LacA), all containing betaine. While betaine alone showed no significant effect on algal growth, its combination with different hydrogen bond donors led to a marked stimulation, suggesting synergistic interactions between components. A similar behaviour was observed for NADESs containing L-proline, which slightly inhibited algal growth when tested alone at high concentrations but promoted growth when combined with other compounds in eutectic systems. For NADESs containing choline acetate (NADESs 11-15), algal growth trends closely followed those observed for choline acetate alone, indicating that this compound plays a dominant role in shaping the biological response. However, algal biomass values were consistently higher in the complete NADESs formulations than in solutions of choline acetate alone, suggesting synergistic effects between NADESs components, as previously reported for choline chloride-based DESs [123,124]. The only exception was NADES 11 (ChA:Im), where the growth-promoting effect of choline acetate appeared to be partially counterbalanced by the inhibitory behaviour of imidazole, leading to an additive rather than synergistic response.

During the evaluation of NADESs, an initial indication of potential eutrophication risk emerged from considering the mineralization of nitrogen-containing components and their biological effects[125]. Compounds such as L-proline, betaine, and choline acetate contain nitrogen within their structure, which upon biodegradation might be released as bioavailable nutrients into aquatic environments. At the same time, the possibility of synergistic interactions between these components in promoting microalgal growth led to the hypothesis that such systems could enhance nutrient-driven biological activity. Consequently, NADESs may behave similarly to fertilizers[126], enhancing algal growth and potentially contributing to eutrophication and subsequent oxygen depletion. This observation highlights an indirect environmental risk that is not captured by standard biodegradability and ecotoxicity assessments, emphasizing the need for a more comprehensive evaluation of the environmental sustainability of NADESs.

4.3 Biodegradation results and discussion of oxime functionalized nanodiamonds

4.3.1 Results

Physicochemical characterization of the oxime-functionalized nanodiamonds was performed to evaluate particle size distribution and surface functionalization in relation to biodegradability assessment. Dynamic light scattering (DLS) measurements (ZetaSizer Nano S, Malvern Instruments) were performed with Dr. Denys Bondar, TalTech to evaluate the hydrodynamic size distribution of ND dispersions before and after surface functionalization. The unmodified ND-COOH sample exhibited two populations in aqueous medium, consisting of a smaller fraction in the nanoscale range (~30 nm) and a larger aggregate population above 200 nm (Figure 8). In phosphate-buffered saline (PBS), ND-COOH showed a single population with an average hydrodynamic diameter of approximately 250 nm, indicating increased aggregation in the presence of electrolytes. After functionalization, the ND conjugates displayed a shift toward larger hydrodynamic diameters, reflecting the influence of the grafted organic moieties and changes in colloidal behaviour. ND-A1, which is structurally related to the functional fragment used in biodegradation studies (4-pyridinium oxime linked to PEG-diamine), showed a significantly increased aggregate size in PBS (~531 nm), while other functionalized samples exhibited broader or multimodal distributions. This increase in apparent particle size could be attributed to the formation of an organic corona and enhanced intermolecular interactions, as well as electrolyte-induced aggregation effects.

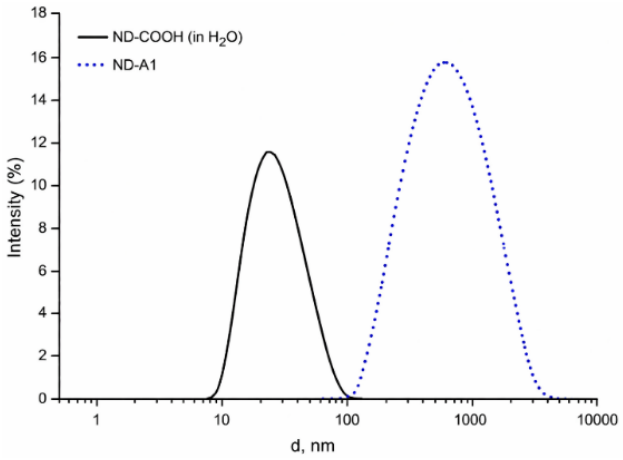

Figure 8. *Hydrodynamic size distribution of nanodiamond starting material (ND-COOH) in water and functionalized nanodiamond (ND-A1) measured by dynamic light scattering (DLS). Functionalization leads to an increase in aggregate size, indicating the formation of an organic corona and altered colloidal behaviour.*

The biodegradability of oxime-functionalized nanodiamonds was evaluated using the modified closed bottle test (OECD 301D) . The results indicated that the functional fragment containing a 4-pyridinium oxime linked to PEG-diamine(ND-4a) showed limited biodegradation under aerobic conditions, as shown in Figure 10. After 28 days, the biodegradation reached only 13%, which does not meet the criteria for readily biodegradable compounds. When the test duration was extended to 33 days, only a slight and slow increase was observed, with biodegradation reaching approximately 17%. This gradual increase suggests that the material undergoes partial biotransformation but remains largely persistent. Since PEG is generally considered biodegradable, the low overall biodegradation is likely due to the oxime-substituted pyridinium moiety, which may hinder microbial metabolism. Although full mineralization was not achieved during the test, within the test period, the partial degradation observed indicates that the organic corona of the nanodiamonds perhaps be classified as non-readily biodegradable and close to inherently biodegradable. Considering the reported low toxicity and high persistence of nanodiamonds, these materials may still be suitable for specialized applications where controlled environmental stability is required. This result suggests us that the surface functionalization, rather than the nanomaterial core itself, governs environmental biodegradability and that high-performance functional groups have the potential to significantly reduce microbial accessibility even when biodegradable components (PEG) are present.

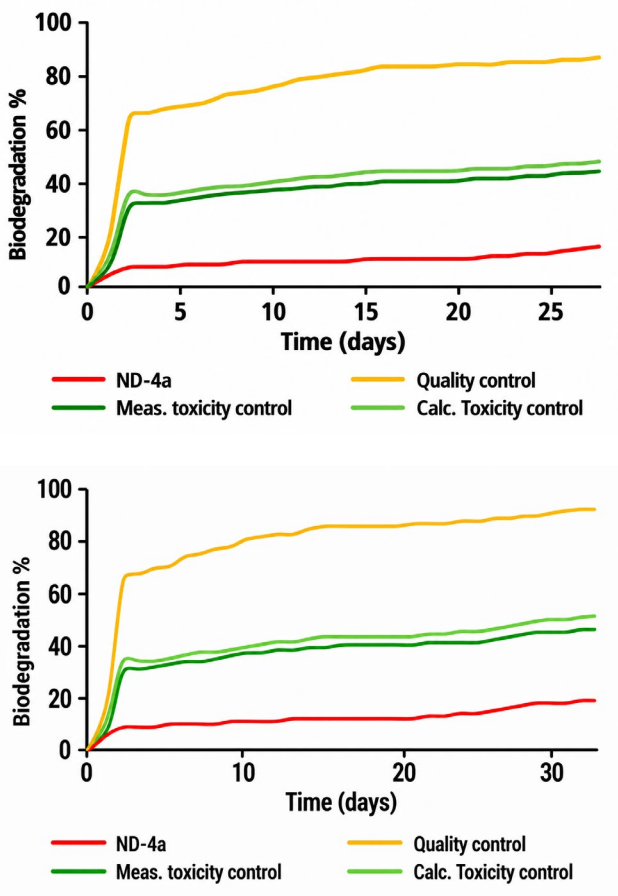

Figure 9. *Biodegradability profiles of 4-pyridinium oxime-linked PEG-diamine ND-4a for 28 and 33 days.*

4.3.2 Discussion

The modified OECD 301D Closed Bottle Test revealed that oxime-functionalized nanodiamonds exhibited low biodegradation under aerobic conditions, reaching only 13% mineralization after 28 days and approximately 17% after extension to 33 days. These values clearly fall below the threshold for ready biodegradability, indicating that the material is not readily biodegradable. The decision to extend the test duration beyond the standard 28 days was motivated by the slow but measurable increase in oxygen consumption, suggesting partial biotransformation rather than complete recalcitrance. Such behaviour is consistent with materials that undergo limited microbial modification without progressing toward full mineralization. Although PEG is generally regarded as biodegradable, the overall low biodegradation observed here is most plausibly credited to the oxime-substituted pyridinium moiety, which introduces aromaticity, permanent charge, and steric shielding that can hinder enzymatic access and microbial uptake. Similar findings have been reported for functionalized NDs and carbon-based nanomaterials bearing aromatic or cationic surface groups, where surface chemistry rather than the carbon core governs environmental persistence[127] . Overall, the observed biodegradability primarily reflects degradation of the surface-

functionalized organic moieties attached to the nanodiamonds, while the nanodiamond core itself is expected to remain environmentally persistent due to its highly stable carbon lattice structure. In pharmaceutical and biomedical contexts, this limited biodegradability does not necessarily represent a disadvantage; on the contrary, controlled environmental and biological stability is often desirable for drug delivery systems, imaging agents, or antidote platforms. The results therefore highlight an important trade-off between functional performance and environmental degradability, demonstrating that high-performance surface functionalization could substantially reduce microbial accessibility even in the presence of biodegradable components. Overall, these findings support the conclusion that the organic corona of functionalized NDs dictates their biodegradability and that oxime-based functional fragments contribute to persistence while enabling application-specific stability.

Fourier-transform infrared (FT-IR) spectroscopy (Bruker Tensor 27 spectrometer), performed by Dr. Denys Bondar, was used to confirm the successful covalent functionalization of ND surfaces. The candidate contributed to interpretation of the FT-IR spectra in relation to the biodegradability assessment. The spectrum of the pristine ND-COOH material indicates characteristic features of surface carboxyl groups, including a broad O–H stretching band centred around 3420 cm^{-1}, a distinct C=O stretching vibration at approximately 1775 cm^{-1}, and an O–H bending band near 1628 cm^{-1}. Additional bands in the fingerprint region (1000–1200 cm^{-1}) might be due to C–O stretching vibrations of carboxylic and related oxygen-containing functionalities. Following functionalization (ND-A1), notable spectral changes are observed (Figure 9). The broad O–H band decreases in intensity, indicating the consumption of surface carboxyl groups during the coupling reaction. A new band appears around 3125 cm^{-1}, corresponding to N–H stretching of newly formed amide groups, while the C=O stretching band shifts to lower wavenumbers (~1677 cm^{-1}), consistent with amide bond formation. Furthermore, additional bands observed at ~2936 cm^{-1} (C–H stretching), ~1461 cm^{-1} and ~1333 cm^{-1} (C–N and aromatic vibrations), and in the region of 1200–1000 cm^{-1} support the presence of the grafted organic moiety, including pyridinium and PEG-related functionalities. These spectral differences between ND-COOH and ND-A1 confirm the successful formation of covalent amide linkages and the introduction of the organic functional fragment onto the ND surface. It should be noted that, while FT-IR analysis verifies the surface functionalization of nanodiamonds, the biodegradation assessment in this study was conducted on the corresponding functional fragment (4-pyridinium oxime linked to PEG-diamine), representing the organic corona that governs the biodegradation profile.

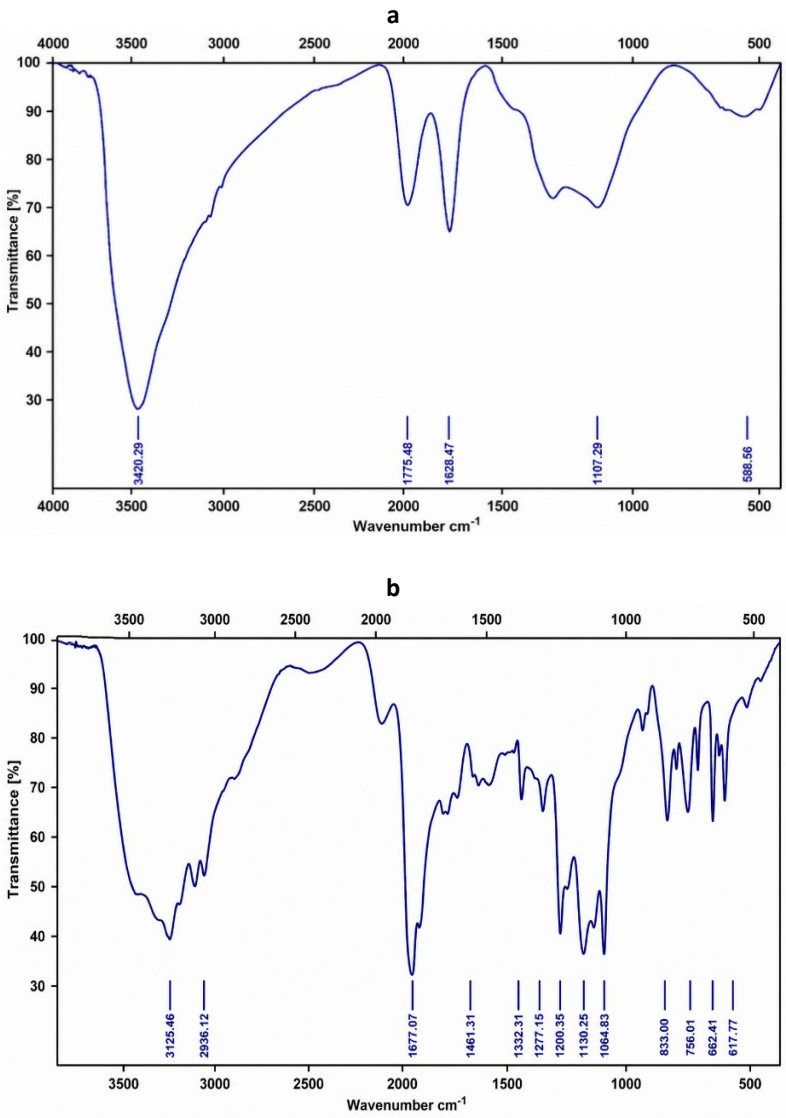

Figure 10. *FT-IR spectra of unmodified nanodiamond (ND-COOH) (a) and functionalized nanodiamond (ND-A1) (b).*

4.4 Biodegradation results and discussion of oxazole derivatives

4.4.1 Characterisation and biodegradability studies

High-performance liquid chromatography (HPLC) analysis was performed to confirm the purity and identity of the synthesized oxazole derivatives (7a, 7b, and 8aa) prior to biodegradation testing. The chromatograms of all compounds exhibited a single, well-

defined dominant peak with retention times of approximately 4.94 min (7a), 4.90 min (7b), and 5.03 min (8aa), respectively (Figure 11). The absence of significant secondary peaks indicates high purity and negligible presence of impurities or residual starting materials. This confirms that the substances subjected to biodegradation experiments were chemically well-defined. Consequently, any observed changes during biodegradation testing are possibly due to the transformation of the parent oxazole compounds rather than interference from impurities or background components, thereby ensuring the reliability of the biodegradation assessment.

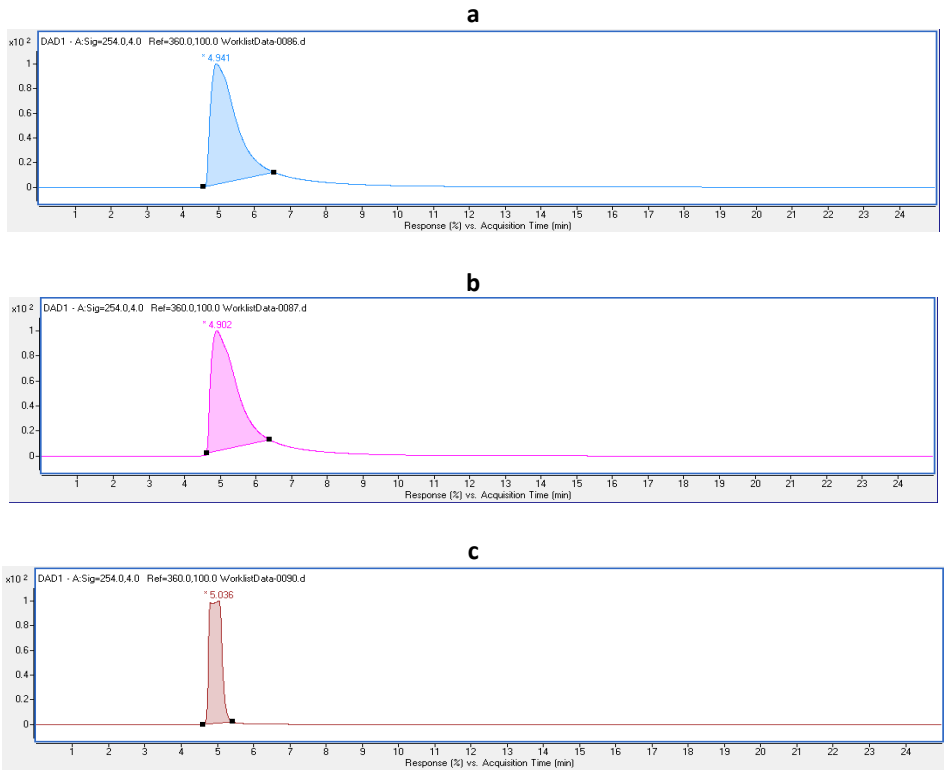

Figure 11. *HPLC chromatograms of oxazole derivatives 7a(a), 7b(b), and 8aa(c) showing single dominant peaks at retention times of ~4.94, 4.90, and 5.03 min, respectively, confirming high purity of the compounds.*

The biodegradability of selected piperazine-containing 1,3-oxazole-4-carbonitrile derivatives (7a, 7b, and 8aa) was evaluated using the OECD 301D Closed Bottle Test under aerobic aqueous conditions. The test was conducted over a 28-day incubation period, using a non-adapted microbial inoculum. All tested oxazole derivatives exhibited low levels of biodegradation, with mineralization values ranging from approximately 5-10% at day 28 (Figure 12). None of the compounds fulfilled the criteria for ready biodegradability according to OECD guidelines.Toxicity control experiments confirmed that the test compounds did not inhibit microbial activity, indicating that the observed low biodegradation was not due to toxic effects on the inoculum. Among the tested compounds, the derivative 8aa, which exhibited the lowest predicted aqueous solubility, showed similarly low biodegradation compared to 7a and 7b. Overall, the results indicate

limited mineralization of the investigated oxazole derivatives under OECD 301D screening conditions.

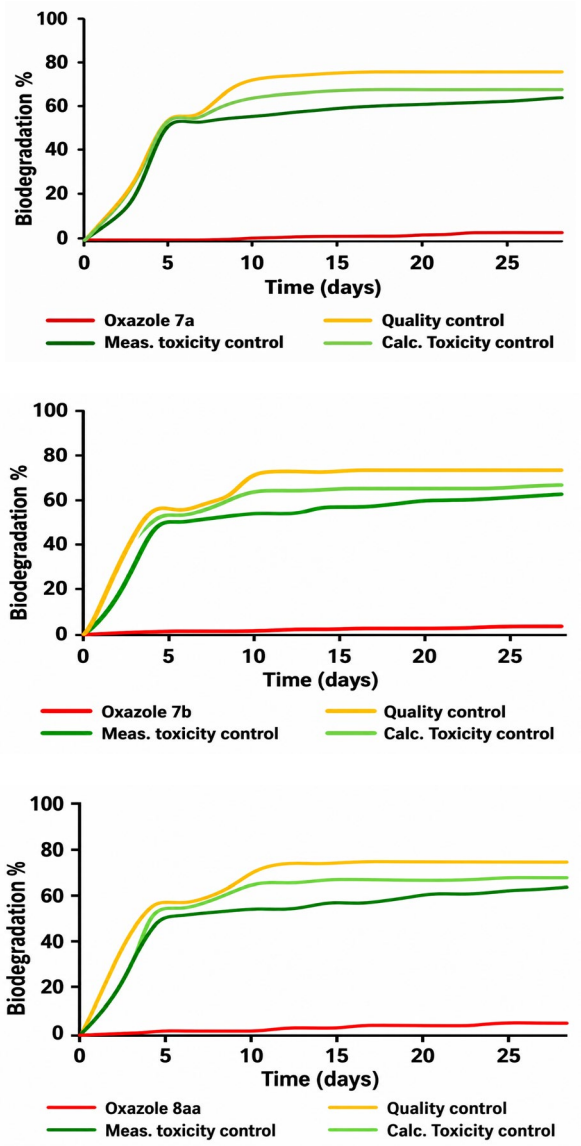

Figure 12. *Biodegradability profiles of oxazole derivatives 7a, 7b and 8aa.*

4.4.2 Discussion on oxazole biodegradability results

The low levels of mineralization observed for the piperazine-containing 1,3-oxazole-4-carbonitrile derivatives (7a, 7b, and 8aa) in the OECD 301D Closed Bottle Test, indicate that these compounds are not readily biodegradable under aerobic aqueous screening conditions. Biodegradation values of approximately 5-10% after 28 days suggest a high degree of persistence, which is consistent with the presence of heteroaromatic oxazole rings and the carbonitrile functionality, both of which are commonly associated with

reduced biodegradability in OECD screening tests. The limited biodegradation observed for the oxazole derivatives is consistent with literature reports that heterocyclic aromatic compounds, including nitrogen and oxygen-containing heterocycles, frequently exhibit resistance to microbial degradation and increased environmental persistence under aerobic aqueous conditions, likely due to the stability conferred by the aromatic heterocycle[128]. The piperazine moiety, while potentially increasing polarity, did not translate into enhanced biodegradability, likely due to steric protection and limited accessibility of enzymatically labile bonds. The absence of microbial inhibition in the toxicity control indicates that the low biodegradation is due to the inherent resistance of the compound rather than toxic effects on the microorganisms. Notably, compound 8aa, which showed the lowest predicted aqueous solubility, did not exhibit significantly lower biodegradation compared to 7a and 7b, indicating that solubility was not the primary limiting factor under the test conditions. A slight plateau observed in the quality control curve between day 5 and 10 is likely due to minor measurement variability or transient microbial adaptation and does not affect the overall interpretation of the results. Overall, the results suggest that the investigated oxazole derivatives are environmentally persistent under standard OECD 301D screening conditions and would not be classified as readily biodegradable, highlighting the need for further studies under extended or environmentally relevant conditions to better assess their long-term fate.

To mitigate this risk of persistence, the solution will be to consider pharmacological optimization and 'benign by design' principles through which the ready biodegradability of the compound will be assessed before their synthesis, and both the efficacy of the drug and its environmental fate is optimized [129]. Also, the structural modification of the compounds might have a significance in increasing its biodegradability. For heteroaromatic compounds the modification could be done by reducing the structural complexity and aromaticity of the compound, introducing metabolically and environmentally cleavable bonds and by tuning properties like solubility and bioavailability [130].

4.5 Cross-system comparison of biodegradability

A central objective of this study was to explore whether biodegradation behaviour can be compared across structurally different classes of emerging chemicals using a unified screening approach. The OECD 301D framework enabled direct comparison of mineralisation behaviour under identical experimental conditions.

The results support a general trend in which molecular complexity and material architecture influence biodegradation behaviour. The NADESs, composed of low-molecular-weight and biologically familiar building blocks, exhibited rapid and extensive biodegradation, reflecting efficient microbial utilisation under the test conditions. In contrast, the oxazole derivatives, characterised by heteroaromatic stability and electron-deficient ring systems, showed very limited biodegradation, indicating intrinsic resistance to microbial transformation. Intermediate behaviour was observed for the hybrid nanodiamond-based systems, where biodegradation appears to be influenced by the persistence of the nanomaterial core and the nature of the organic surface functionalization. The limited mineralisation of the oxime-functionalized nanodiamond conjugates illustrates how surface modification can restrict microbial accessibility even when the organic corona contains partially biodegradable elements.

Importantly, biodegradability should not be interpreted as a direct indicator of environmental safety. In the case of NADESs, rapid biodegradation may contribute to

increased dissolved organic carbon turnover and nutrient release, which, when considered together with ecotoxicity findings reported in collaborative studies, may be relevant to eutrophication-related effects. Conversely, more persistent systems such as oxazole derivatives and nanodiamond conjugates may remain in environmental compartments for longer periods, potentially leading to prolonged exposure under certain conditions.

Together, these observations indicate that environmental behaviour should be evaluated from an integrated perspective, in which biodegradability, molecular structure, material architecture, and secondary ecological effects are considered together. The comparative approach adopted in this work provides a useful framework for exploring potential structure–persistence relationships across chemically diverse systems, see Table 9.

Table 9. *Complexity vs Biodegradability vs Environmental Risk for the classes of compounds (materials) studied in this work*

System Class	Structural Complexity	Biodegradability (OECD 301D)	Environmental Considerations
NADESs	Low–moderate (bio-based)	High (readily biodegradable)	Potential eutrophication-related effects associated with nutrient release
Hybrid nanomaterials (ND conjugates)	High (hybrid)	Low	Limited biodegradation: environmental behaviour influenced by nanomaterial persistence and surface functionalization
Heterocyclic compounds, pharmaceutical candidates (oxazole derivatives)	Moderate–high (heteroaromatic pharmaceutical scaffold)	Very low	Limited biodegradation and potential persistence in aquatic environments

The future work may therefore integrate higher-tier simulation studies, degradation pathway analysis, and design-oriented approaches to support the development of materials with optimized functional performance and environmental compatibility.

5 Conclusion

This study presented a comparative assessment of the aerobic biodegradability of three classes of emerging substances (materials): natural deep eutectic solvents (NADESs), oxime functionalized nanodiamonds (NDs), and oxazole-based pharmaceutical candidates using the OECD 301D Closed Bottle Test as a unified screening platform.

- The results demonstrate that biodegradability under standardized aerobic conditions is strongly influenced by molecular structure and material complexity. Bio-based systems such as NADESs exhibited rapid biodegradation and fulfilled the criteria for ready biodegradability, whereas structurally complex heteroaromatic molecules and hybrid nanomaterials showed limited degradability, and can be considered environmentally persistent under screening conditions.
- Despite their favourable biodegradation profiles, when considered together with ecotoxicity data obtained in collaborative studies, NADESs may present indirect environmental risks associated with nutrient release and eutrophication-related effects. This finding highlights that biodegradability alone is not sufficient for comprehensive environmental safety assessment and must be considered alongside ecotoxicological and ecosystem-level responses.
- The oxime-functionalized nanodiamond conjugates demonstrated limited biodegradation under OECD 301D conditions, suggesting that both persistence of the nanomaterial core and stability of the surface functionalization contribute significantly to the environmental behaviour of such hybrid nanomaterials.
- The oxazole derivatives displayed low biodegradability, consistent with the known persistence of heterocyclic pharmaceutical compounds. These results underline the importance of incorporating biodegradation screening during early stages of chemical and drug development to identify persistence risks before environmental release.
- A key contribution of this work is showing that standardized biodegradation tests can be used not only as regulatory screening tools but also as comparative platforms for exploring potential structure–persistence relationships in chemically diverse systems. This interdisciplinary approach enables a more generalizable understanding of environmental fate.

Overall, the findings contribute to the advancement of proactive environmental risk assessment strategies and support the broader goal of evaluating the environmental compatibility of sustainable chemical systems at early stages of their lifecycle.

References

(1) *Guidance on Information Requirements and Chemical Safety Assessment: Part E: Risk Characterisation*; ECHA, 2016.

(2) Schäffer, A.; Fenner, K.; Wang, Z.; Scheringer, M. To Be or Not to Be Degraded: In Defense of Persistence Assessment of Chemicals. *Environ. Sci. Process. Impacts* **2022**, *24* (8), 1104–1109. https://doi.org/10.1039/D2EM00213B.

(3) Alexander, M. *Biodegradation and Bioremediation*; Academic Press, 1999.

(4) *Revised Introduction to the OECD Guidelines for Testing of Chemicals, Section 3*; OECD, 2006. https://doi.org/10.1787/9789264030213-en.

(5) Nyholm, N. The European System of Standardized Legal Tests for Assessing the Biodegradability of Chemicals. *Environ. Toxicol. Chem.* **1991**, *10* (10), 1237–1246. https://doi.org/10.1002/ETC.5620101002.

(6) Boethling, R.; Fenner, K.; Howard, P.; Klečka, G.; Madsen, T.; Snape, J. R.; Whelan, M. J. Environmental Persistence of Organic Pollutants: Guidance for Development and Review of POP Risk Profiles. *Integr. Environ. Assess. Manag.* **2009**, *5* (4), 539–556. https://doi.org/10.1897/IEAM_2008-090.1.

(7) Kümmerer, K. The Presence of Pharmaceuticals in the Environment Due to Human Use – Present Knowledge and Future Challenges. *J. Environ. Manage.* **2009**, *90* (8), 2354–2366. https://doi.org/10.1016/j.jenvman.2009.01.023.

(8) Abbott, A. P.; Boothby, D.; Capper, G.; Davies, D. L.; Rasheed, R. K. Deep Eutectic Solvents Formed between Choline Chloride and Carboxylic Acids: Versatile Alternatives to Ionic Liquids. *J. Am. Chem. Soc.* **2004**, *126* (29), 9142–9147. https://doi.org/10.1021/ja048266j.

(9) Smith, E. L.; Abbott, A. P.; Ryder, K. S. Deep Eutectic Solvents (DESs) and Their Applications. *Chem.Rev*. **2014**. *114* (21), 11060–11082. https://doi.org/10.1021/cr300162p.

(10) Wen, Q.; Chen, J. X.; Tang, Y. L.; Wang, J.; Yang, Z. Assessing the Toxicity and Biodegradability of Deep Eutectic Solvents. *Chemosphere* **2015**, *132*, 63–69. https://doi.org/10.1016/J.CHEMOSPHERE.2015.02.061.

(11) Çelik, G.; Stolte, S.; Müller, S.; Schattenberg, F.; Markiewicz, M. Environmental Persistence Assessment of Heterocyclic Polyaromatic Hydrocarbons – Ultimate and Primary Biodegradability Using Adapted and Non-Adapted Microbial Communities. *J. Hazard. Mater.* **2023**, *460*, 132370. https://doi.org/10.1016/j.jhazmat.2023.132370.

(12) Baaloudj, O.; Scrano, L.; Bufo, S. A.; Modley, L.-A. S.; Lelario, F.; Zizzamia, A. R.; Emanuele, L.; Brienza, M. Environmental Fate, Ecotoxicity, and Remediation of Heterocyclic Pharmaceuticals as Emerging Contaminants: A Review of Long-Term Risks and Impacts. *Organics* **2025**, *6* (1), 1. https://doi.org/10.3390/org6010001.

(13) Zhang, J.; Yu, S.-H. Carbon Dots: Large-Scale Synthesis, Sensing and Bioimaging. *Mater. Today* **2016**, *19* (7), 382–393. https://doi.org/10.1016/j.mattod.2015.11.008.

(14) Nunn, N.; Torelli, M.; McGuire, G.; Shenderova, O. Nanodiamond: A High Impact Nanomaterial. *Curr. Opin. Solid State Mater. Sci.* **2017**, *21* (1), 1–9. https://doi.org/10.1016/j.cossms.2016.06.008.

(15) Vaijayanthimala, V.; Lee, D. K.; Kim, S. V; Yen, A.; Tsai, N.; Ho, D.; Chang, H.-C.; Shenderova, O. Nanodiamond-Mediated Drug Delivery and Imaging: Challenges and Opportunities. *Expert Opin. Drug Deliv.* **2015**, *12* (5), 735–749. https://doi.org/10.1517/17425247.2015.992412.

(16) Fiket, Ž.; Dutour Sikirić, M.; Gal, D.; Petrović, M.; Strasser, V.; Kovač, V.; Frka, S.; Vdović, N.; Saikia, B. Stability of Nanodiamonds and Carbon Dots in Aqueous Environments: Insights into Aggregation Behavior and Additive Influence. *Environ. Sci. Nano* **2025**, *12* (8), 3904–3920. https://doi.org/10.1039/D5EN00264H.

(17) Makhado, B. P.; Oladipo, A. O.; Gumbi, N. N.; De Kock, L. A.; Andraos, C.; Gulumian, M.; Nxumalo, E. N. Unravelling the Toxicity of Carbon Nanomaterials – From Cellular Interactions to Mechanistic Understanding. *Toxicol. in Vitro* **2024**, *100*, 105898. https://doi.org/10.1016/j.tiv.2024.105898.

(18) Pikula, K.; Johari, S. A.; Golokhvast, K. Colloidal Behavior and Biodegradation of Engineered Carbon-Based Nanomaterials in Aquatic Environment. *Nanomaterials* **2022**, *12* (23), 4149. https://doi.org/10.3390/nano12234149.

(19) Mokhtari-Farsani, A.; Hasany, M.; Lynch, I.; Mehrali, M. Biodegradation of Carbon-Based Nanomaterials: The Importance of "Biomolecular Corona" Consideration. *Adv. Funct. Mater.* **2022**, *32* (6). https://doi.org/10.1002/adfm.202105649.

(20) Kümmerer, K. Sustainable Chemistry: A Future Guiding Principle. *Angew. Chem. Int. Ed.* **2017**, *56* (52), 16420–16421. https://doi.org/10.1002/anie.201709949.

(21) Schwarzenbach, R. P.; Escher, B. I.; Fenner, K.; Hofstetter, T. B.; Johnson, C. A.; von Gunten, U.; Wehrli, B. The Challenge of Micropollutants in Aquatic Systems. *Science (1979).* **2006**, *313* (5790), 1072–1077. https://doi.org/10.1126/science.1127291.

(22) *Detailed Review Paper on Biodegradability Testing*; OECD, 2002. https://doi.org/10.1787/9789264078529-en.

(23) Lead, J. R.; Batley, G. E.; Alvarez, P. J. J.; Croteau, M.-N.; Handy, R. D.; McLaughlin, M. J.; Judy, J. D.; Schirmer, K. Nanomaterials in the Environment: Behavior, Fate, Bioavailability, and Effects—An Updated Review. *Environ. Toxicol. Chem.* **2018**, *37* (8), 2029–2063. https://doi.org/10.1002/etc.4147.

(24) Alexander, Martin. *Biodegradation and Bioremediation*; Academic Press, 1999.

(25) Lyons, T. W.; Fike, D. A.; Zerkle, A. Emerging Biogeochemical Views of Earth's Ancient Microbial Worlds. *Elements* **2015**, *11* (6), 415–421. https://doi.org/10.2113/gselements.11.6.415.

(26) Wackett, L. P. New Chemicals Fuel the Evolution of Microbial Biodegradation. *Microbiol. Mol. Biol. Rev.* **2025**, *89* (4). https://doi.org/10.1128/mmbr.00207-24.

(27) Levy, G.; Lutz, I.; Krüger, A.; Kloas, W. Bisphenol A Induces Feminization in Xenopus Laevis Tadpoles. *Environ. Res.* **2004**, *94* (1), 102–111. https://doi.org/https://doi.org/10.1016/S0013-9351(03)00086-0.

(28) Hamilton, P. B.; Baynes, A.; Nicol, E.; Harris, G.; Uren Webster, T. M.; Beresford, N.; Straszkiewicz, M.; Jobling, S.; Tyler, C. R. Feminizing Effects of Ethinylestradiol in Roach (Rutilus Rutilus) Populations with Different Estrogenic Pollution Exposure Histories. *Aquat. Toxicol.* **2022**, *249*, 106229. https://doi.org/https://doi.org/10.1016/j.aquatox.2022.106229.

(29) Green, R. E.; Newton, I.; Shultz, S.; Cunningham, A. A.; Gilbert, M.; Pain, D. J.; Prakash, V. Diclofenac Poisoning as a Cause of Vulture Population Declines across the Indian Subcontinent. *J. Appl. Ecol.* **2004**, *41* (5), 793–800. https://doi.org/10.1111/j.0021-8901.2004.00954.x

(30) Godoy, A. A.; de Oliveira, Á. C.; Silva, J. G. M.; Azevedo, C. C. de J.; Domingues, I.; Nogueira, A. J. A.; Kummrow, F. Single and Mixture Toxicity of Four Pharmaceuticals of Environmental Concern to Aquatic Organisms, Including a Behavioral Assessment. *Chemosphere* **2019**, *235*, 373–382. https://doi.org/10.1016/J.CHEMOSPHERE.2019.06.200.

(31) Ortúzar, M.; Esterhuizen, M.; Olicón-Hernández, D. R.; González-López, J.; Aranda, E. Pharmaceutical Pollution in Aquatic Environments: A Concise Review of Environmental Impacts and Bioremediation Systems. *Front. Microbiol.* **2022**, *13*. https://doi.org/10.3389/fmicb.2022.869332.

(32) Fonseca, V. F.; Duarte, I. A.; Duarte, B.; Freitas, A.; Pouca, A. S. V.; Barbosa, J.; Gillanders, B. M.; Reis-Santos, P. Environmental Risk Assessment and Bioaccumulation of Pharmaceuticals in a Large Urbanized Estuary. *Science of The Total Environment* **2021**, *783*, 147021. https://doi.org/10.1016/J.SCITOTENV.2021.147021.

(33) Ferrari, Beno.; Mons, R.; Vollat, B.; Fraysse, Beno.; Paxé, N. U.; Giudice, R. LO; Pollio, A.; Garric, J. Environmental Risk Assessment of Six Human Pharmaceuticals: Are the Current Environmental Risk Assessment Procedures Sufficient for the Protection of the Aquatic Environment*? Environ. Toxicol. Chem*. **2004,** *23* (5), 1344-1354. http://www.argotech.com/.

(34) Huggett, D. B.; Brooks, B. W.; Peterson, B.; Foran, C. M.; Schlenk, D. Toxicity of Select Beta Adrenergic Receptor-Blocking Pharmaceuticals (B-Blockers) on Aquatic Organisms. *Arch. Environ. Contam. Toxicol.* **2002**, *43* (2), 229–235. https://doi.org/10.1897/03-246.

(35) Bittner, L.; Teixido, E.; Seiwert, B.; Escher, B. I.; Klüver, N. Influence of PH on the Uptake and Toxicity of β-Blockers in Embryos of Zebrafish, Danio Rerio. *Aquat. Toxicol.* **2018**, *201*, 129–137. https://doi.org/10.1016/J.AQUATOX.2018.05.020.

(36) Xia, L.; Zheng, L.; Zhou, J. L. Effects of Ibuprofen, Diclofenac and Paracetamol on Hatch and Motor Behavior in Developing Zebrafish (Danio Rerio). *Chemosphere* **2017**, *182*, 416–425. https://doi.org/10.1016/J.CHEMOSPHERE.2017.05.054.

(37) Lister, A. L.; Van Der Kraak, G. J. Regulation of Prostaglandin Synthesis in Ovaries of Sexually-mature Zebrafish (*Danio Rerio*). *Mol. Reprod. Dev.* **2009**, *76* (11), 1064–1075. https://doi.org/10.1002/mrd.21072.

(38) David, A.; Pancharatna, K. Developmental Anomalies Induced by a Non-Selective COX Inhibitor (Ibuprofen) in Zebrafish (Danio Rerio). *Environ. Toxicol. Pharmacol.* **2009**, *27* (3), 390–395. https://doi.org/10.1016/J.ETAP.2009.01.002.

(39) Cuthbert, R.; Parry-Jones, J.; Green, R. E.; Pain, D. J. NSAIDs and Scavenging Birds: Potential Impacts beyond Asia's Critically Endangered Vultures. *Biol. Lett.* **2007**, *3* (1), 91–94. https://doi.org/10.1098/rsbl.2006.0554.

(40) Triebskorn, R.; Casper, H.; Heyd, A.; Eikemper, R.; Köhler, H. R.; Schwaiger, J. Toxic Effects of the Non-Steroidal Anti-Inflammatory Drug Diclofenac: Part II. Cytological Effects in Liver, Kidney, Gills and Intestine of Rainbow Trout (Oncorhynchus Mykiss). *Aquat. Toxicol.* **2004**, *68* (2), 151–166. https://doi.org/10.1016/J.AQUATOX.2004.03.015.

(41) Gravel, A.; Wilson, J. M.; Pedro, D. F. N.; Vijayan, M. M. Non-Steroidal Anti-Inflammatory Drugs Disturb the Osmoregulatory, Metabolic and Cortisol Responses Associated with Seawater Exposure in Rainbow Trout. *Comp. Biochem. Physiol. C Toxicol. Pharmacol.* **2009**, *149* (4), 481–490. https://doi.org/10.1016/J.CBPC.2008.11.002.

(42) Schwaiger, J.; Ferling, H.; Mallow, U.; Wintermayr, H.; Negele, R. D. Toxic Effects of the Non-Steroidal Anti-Inflammatory Drug Diclofenac: Part I: Histopathological Alterations and Bioaccumulation in Rainbow Trout. *Aquat. Toxicol.* **2004**, *68* (2), 141–150. https://doi.org/10.1016/J.AQUATOX.2004.03.014.

(43) Xia, L.; Zheng, L.; Zhou, J. L. Effects of Ibuprofen, Diclofenac and Paracetamol on Hatch and Motor Behavior in Developing Zebrafish (Danio Rerio). *Chemosphere* **2017**, *182*, 416–425. https://doi.org/10.1016/J.CHEMOSPHERE.2017.05.054.

(44) Lister, A. L.; Van Der Kraak, G. J. An investigation into the role of prostaglandins in zebrafish oocyte maturation and ovulation. *Gen. Comp. Endocrinol.* **2008**, *159* (1), 46-57. https://doi.org/10.1016/j.ygcen.2008.07.017.

(45) David, A.; Pancharatna, K. Developmental Anomalies Induced by a Non-Selective COX Inhibitor (Ibuprofen) in Zebrafish (Danio Rerio). *Environ. Toxicol. Pharmacol.* **2009**, *27* (3), 390–395. https://doi.org/10.1016/J.ETAP.2009.01.002.

(46) Gonzalez-Rey, M.; Bebianno, M. J. Effects of Non-Steroidal Anti-Inflammatory Drug (NSAID) Diclofenac Exposure in Mussel Mytilus Galloprovincialis. *Aquat. Toxicol.* **2014**, *148*, 221–230. https://doi.org/10.1016/J.AQUATOX.2014.01.011.

(47) Thibaut, R.; Schnell, S.; Porte, C. The Interference of Pharmaceuticals with Endogenous and Xenobiotic Metabolizing Enzymes in Carp Liver: An In-Vitro Study. *Environ. Sci. Technol.* **2006**, *40* (16), 5154–5160. https://doi.org/10.1021/es0607483.

(48) Flippin, J. L.; Huggett, D.; Foran, C. M. Changes in the Timing of Reproduction Following Chronic Exposure to Ibuprofen in Japanese Medaka, Oryzias Latipes. *Aquat. Toxicol.* **2007**, *81* (1), 73–78. https://doi.org/10.1016/J.AQUATOX.2006.11.002.

(49) Wijaya, L.; Alyemeni, M.; Ahmad, P.; Alfarhan, A.; Barcelo, D.; El-Sheikh, M. A.; Pico, Y. Ecotoxicological Effects of Ibuprofen on Plant Growth of Vigna Unguiculata L. *Plants* **2020**, *9* (11), 1473. https://doi.org/10.3390/plants9111473.

(50) *Guidance Document on the Use of the Harmonised System for the Classification of Chemicals Which Are Hazardous for the Aquatic Environment*; OECD, 2002. https://doi.org/10.1787/9789264078444-en.

(51) *Assessment of chemicals | OECD*. https://www.oecd.org/en/topics/assessment-of-chemicals.html (accessed 2024-07-05).

(52) Nyholm, N. The European System of Standardized Legal Tests for Assessing the Biodegradability of Chemicals. *Environ. Toxicol. Chem.* **1991**, *10* (10), 1237–1246. https://doi.org/10.1002/ETC.5620101002.

(53) *OECD/OCDE 314*.

(54) Redman, A. D.; Bietz, J.; Davis, J. W.; Lyon, D.; Maloney, E.; Ott, A.; Otte, J. C.; Palais, F.; Parsons, J. R.; Wang, N. Moving Persistence Assessments into the 21st Century: A Role for Weight-of-Evidence and Overall Persistence. *Integr. Environ. Assess. Manag.* **2021**, *18* (4), 868–887. https://doi.org/10.1002/ieam.4548.

(55) Boethling, R.; Fenner, K.; Howard, P.; Klečka, G.; Madsen, T.; Snape, J. R.; Whelan, M. J. Environmental Persistence of Organic Pollutants: Guidance for Development and Review of POP Risk Profiles. *Integr. Environ. Assess. Manag.* **2009**, *5* (4), 539–556. https://doi.org/10.1897/IEAM_2008-090.1.

(56) *Test No. 301: Ready Biodegradability*; OECD, 1992. https://doi.org/10.1787/9789264070349-en.

(57) *OECD Guideline for Testing of Chemicals*.

(58) Madigan, M. T.; Bender, K. S.; Buckley, D. H.; Sattley, W. Matthew.; Stahl, D. Allan. *Brock Biology of Microorganisms*; Pearson, 2019.

(59) Hunter, W. R.; Battin, T. J. Microbial Metabolism Mediates Interactions between Dissolved Organic Matter and Clay Minerals in Streamwater. *Sci. Rep.* **2016**, *6* (1), 30971. https://doi.org/10.1038/srep30971.

(60) Hassan, S.; Bali, B. S.; Muneer, W.; Yaseen, A.; Bhat, S.; Zaman, M.; Ganiee, S. A.; Shah, A. J.; Ganai, B. A. A Review on Amino Acids as Proxies for Organic Matter Degradation in Aquatic Ecosystems: Implications for Nutrient Cycling, Climate Change, and Ecosystem Management. *Environ. Sci. Pollut.Res.* **2025**, *32* (7), 3593–3616. https://doi.org/10.1007/s11356-025-35949-9.

(61) *Biobased Chemicals and Bioplastics*; 2014. https://doi.org/10.1787/5jxwwfjx0djf-en.

(62) Jha, S.; Akula, B.; Enyioma, H.; Novak, M.; Amin, V.; Liang, H. Biodegradable Biobased Polymers: A Review of the State of the Art, Challenges, and Future Directions. *Polymers (Basel).* **2024**, *16* (16), 2262. https://doi.org/10.3390/polym16162262.

(63) Folino, A.; Pangallo, D.; Calabrò, P. S. Assessing Bioplastics Biodegradability by Standard and Research Methods: Current Trends and Open Issues. *J. Environ. Chem. Eng.* **2023**, *11* (2), 109424. https://doi.org/10.1016/J.JECE.2023.109424.

(64) Jordan, A.; Haiß, A.; Spulak, M.; Karpichev, Y.; Kümmerer, K.; Gathergood, N. Synthesis of a Series of Amino Acid Derived Ionic Liquids and Tertiary Amines: Green Chemistry Metrics Including Microbial Toxicity and Preliminary Biodegradation Data Analysis. *Green Chem.* **2016**, *18* (16), 4374–4392. https://doi.org/10.1039/C6GC00415F.

(65) Kusumahastuti, D. K. A.; Sihtmäe, M.; Kapitanov, I. V.; Karpichev, Y.; Gathergood, N.; Kahru, A. Toxicity Profiling of 24 L-Phenylalanine Derived Ionic Liquids Based on Pyridinium, Imidazolium and Cholinium Cations and Varying Alkyl Chains Using Rapid Screening Vibrio Fischeri Bioassay. *Ecotoxicol. Environ. Saf.* **2019**, *172*, 556–565. https://doi.org/10.1016/j.ecoenv.2018.12.076.

(66) Kapitanov, I. V.; Raba, G.; Špulák, M.; Vilu, R.; Karpichev, Y.; Gathergood, N. Design of Sustainable Ionic Liquids Based on L-Phenylalanine and l-Alanine Dipeptides: Synthesis, Toxicity and Biodegradation Studies. *J. Mol. Liq.* **2023**, *374*, 121285. https://doi.org/10.1016/j.molliq.2023.121285.

(67) Suk, M.; Haiß, A.; Westphal, J.; Jordan, A.; Kellett, A.; Kapitanov, I. V.; Karpichev, Y.; Gathergood, N.; Kümmerer, K. Design Rules for Environmental Biodegradability of Phenylalanine Alkyl Ester Linked Ionic Liquids. *Green Chem.* **2020**, *22* (14), 4498–4508. https://doi.org/10.1039/D0GC00918K.

(68) Reuschenbach, P.; Pagga, U.; Strotmann, U. A Critical Comparison of Respirometric Biodegradation Tests Based on OECD 301 and Related Test Methods. *Water Res.* **2003**, *37* (7), 1571–1582. https://doi.org/10.1016/S0043-1354(02)00528-6.

(69) Seo, J.-S.; Keum, Y.-S.; Li, Q. X. Bacterial Degradation of Aromatic Compounds. *Int. J. Environ. Res. Public Health* **2009**, *6* (1), 278–309. https://doi.org/10.3390/ijerph6010278.

(70) Fernandes, J. P.; Almeida, C. M. R.; Salgado, M. A.; Carvalho, M. F.; Mucha, A. P. Pharmaceutical Compounds in Aquatic Environments—Occurrence, Fate and Bioremediation Prospective. *Toxics* **2021**, *9* (10), 257. https://doi.org/10.3390/toxics9100257.

(71) Ortúzar, M.; Esterhuizen, M.; Olicón-Hernández, D. R.; González-López, J.; Aranda, E. Pharmaceutical Pollution in Aquatic Environments: A Concise Review of Environmental Impacts and Bioremediation Systems. *Front. Microbiol.* **2022**, *13*. https://doi.org/10.3389/fmicb.2022.869332.

(72) Baaloudj, O.; Scrano, L.; Bufo, S. A.; Modley, L.-A. S.; Lelario, F.; Zizzamia, A. R.; Emanuele, L.; Brienza, M. Environmental Fate, Ecotoxicity, and Remediation of Heterocyclic Pharmaceuticals as Emerging Contaminants: A Review of Long-Term Risks and Impacts. *Organics* **2025**, *6* (1), 1. https://doi.org/10.3390/org6010001.

(73) Çelik, G.; Stolte, S.; Müller, S.; Schattenberg, F.; Markiewicz, M. Environmental Persistence Assessment of Heterocyclic Polyaromatic Hydrocarbons – Ultimate and Primary Biodegradability Using Adapted and Non-Adapted Microbial Communities. *J. Hazard. Mater.* **2023**, *460*, 132370. https://doi.org/10.1016/j.jhazmat.2023.132370.

(74) Bhattacharya, K.; Mukherjee, S. P.; Gallud, A.; Burkert, S. C.; Bistarelli, S.; Bellucci, S.; Bottini, M.; Star, A.; Fadeel, B. Biological Interactions of Carbon-Based Nanomaterials: From Coronation to Degradation. *Nanomedicine* **2016**, *12* (2), 333–351. https://doi.org/10.1016/j.nano.2015.11.011.

(75) Pikula, K.; Johari, S. A.; Golokhvast, K. Colloidal Behavior and Biodegradation of Engineered Carbon-Based Nanomaterials in Aquatic Environment. *Nanomaterials* **2022**, *12* (23), 4149. https://doi.org/10.3390/nano12234149.

(76) Kümmerer, K.; Menz, J.; Schubert, T.; Thielemans, W. Biodegradability of Organic Nanoparticles in the Aqueous Environment. *Chemosphere* **2011**, *82* (10), 1387–1392. https://doi.org/10.1016/j.chemosphere.2010.11.069.

(77) Mokhtari-Farsani, A.; Hasany, M.; Lynch, I.; Mehrali, M. Biodegradation of Carbon-Based Nanomaterials: The Importance of "Biomolecular Corona" Consideration. *Adv. Funct. Mater.* **2022**, *32* (6). https://doi.org/10.1002/adfm.202105649.

(78) Partanen, S. B.; Mueller, N.; Fenner, K. High-Throughput Miniaturized Biotransformation Testing Using Activated Sludge Enables Rapid Chemical Persistence Assessment. *Environ. Sci. Technol. Lett.* **2025**, *12* (11), 1561–1566. https://doi.org/10.1021/acs.estlett.5c00859.

(79) Fenner, K.; Zahn, D.; Jöhncke, U.; Sigmund, G.; Mayer, P.; Hughes, C.; Arp, H. P. H.; Davenport, R. J.; Kapanen, A.; Reemtsma, T. Persistence Assessment of Chemicals: Trajectories toward New Approach Methodologies (P-NAMs). *Environ. Sci. Technol.* **2026**, *60* (15), 11243–11252. https://doi.org/10.1021/acs.est.6c00444.

(80) Zhang, Q.; De Oliveira Vigier, K.; Royer, S. S.; Franc¸ois, F.; Jerome, J. J. Deep Eutectic Solvents: Syntheses, Properties and Applications. *Chem. Soc. Rev* **2012**, *41*, 7108–7146. https://doi.org/10.1039/c2cs35178a.

(81) Choi, Y. H.; van Spronsen, J.; Dai, Y.; Verberne, M.; Hollmann, F.; Arends, I. W. C. E.; Witkamp, G. J.; Verpoorte, R. Are Natural Deep Eutectic Solvents the Missing Link in Understanding Cellular Metabolism and Physiology? *Plant Physiol.* **2011**, *156* (4), 1701–1705. https://doi.org/10.1104/PP.111.178426.

(82) Hikmawanti, N. P. E.; Ramadon, D.; Jantan, I.; Mun'im, A. Natural Deep Eutectic Solvents (NADESS): Phytochemical Extraction Performance Enhancer for Pharmaceutical and Nutraceutical Product Development. *Plants* **2021**, *10* (10), 2091. https://doi.org/10.3390/plants10102091.

(83) Mansour, F. R.; Bedair, A.; Hamed, M.; Magdy, G.; Ali, I.; Locatelli, M. Applications of (Natural) Deep Eutectic Solvents in Liquid Phase Microextraction: A Review. *Microchem. J.* **2024**, *198*, 110178. https://doi.org/10.1016/J.MICROC.2024.110178.

(84) Tian, Y.; Zhu, M.; Hu, T.; Liu, C. Natural Deep Eutectic Solvent—A Novel Green Solvent for Protein Stabilization. *Int. J. Biol. Macromol.* **2023**, *247*, 125477. https://doi.org/10.1016/J.IJBIOMAC.2023.125477.

(85) Chevé-Kools, E.; Choi, Y. H.; Roullier, C.; Ruprich-Robert, G.; Grougnet, R.; Chapeland-Leclerc, F.; Hollmann, F. Natural Deep Eutectic Solvents (NADESs): Green Solvents for Pharmaceutical Applications and Beyond. *Green Chem.* **2025**, *27* (28), 8360–8385. https://doi.org/10.1039/D4GC06386D.

(86) Li, H.; Yang, K.; Yang, Y.; Ding, L.; Li, X. Natural Deep Eutectic Solvents (NADESS) in Drug Delivery Systems: Characteristics, Applications, and Future Perspectives. *Int. J. Pharm.* **2025**, *675*, 125509. https://doi.org/10.1016/J.IJPHARM.2025.125509.

(87) García-Roldán, A.; Piriou, L.; Jauregi, P. Natural Deep Eutectic Solvents as a Green Extraction of Polyphenols from Spent Coffee Ground with Enhanced Bioactivities. *Front. Plant Sci.* **2023**, *13*. https://doi.org/10.3389/fpls.2022.1072592.

(88) Liu, Y.; Friesen, J. B.; McAlpine, J. B.; Lankin, D. C.; Chen, S.-N.; Pauli, G. F. Natural Deep Eutectic Solvents: Properties, Applications, and Perspectives. *J. Nat. Prod.* **2018**, *81* (3), 679–690. https://doi.org/10.1021/acs.jnatprod.7b00945.

(89) Mansour, F. R.; Bedair, A.; Hamed, M.; Magdy, G.; Ali, I.; Locatelli, M. Applications of (Natural) Deep Eutectic Solvents in Liquid Phase Microextraction: A Review. *Microchem. J.* **2024**, *198*, 110178. https://doi.org/10.1016/J.MICROC.2024.110178.

(90) Hayyan, M.; Hashim, M. A.; Al-Saadi, M. A.; Hayyan, A.; Al Nashef, I. M.; Mirghani, M. E. S. Assessment of Cytotoxicity and Toxicity for Phosphonium-Based Deep Eutectic Solvents. *Chemosphere* **2013**, *93* (2), 455–459. https://doi.org/10.1016/J.CHEMOSPHERE.2013.05.013.

(91) Nejrotti, S.; Antenucci, A.; Pontremoli, C.; Gontrani, L.; Barbero, N.; Carbone, M.; Bonomo, M. Critical Assessment of the Sustainability of Deep Eutectic Solvents: A Case Study on Six Choline Chloride-Based Mixtures. *ACS Omega* **2022**, *7* (51), 47449–47461. https://doi.org/10.1021/acsomega.2c06140.

(92) Peer, D.; Karp, J. M.; Hong, S.; Farokhzad, O. C.; Margalit, R.; Langer, R. Nanocarriers as an Emerging Platform for Cancer Therapy. *Nat. Nanotechnol.* **2007**, *2* (12), 751–760. https://doi.org/10.1038/nnano.2007.387.

(93) Farokhzad, O. C.; Langer, R. Impact of Nanotechnology on Drug Delivery. *ACS Nano* **2009**, *3* (1), 16–20. https://doi.org/10.1021/nn900002m.

(94) Saraiva, C.; Praça, C.; Ferreira, R.; Santos, T.; Ferreira, L.; Bernardino, L. Nanoparticle-Mediated Brain Drug Delivery: Overcoming Blood–Brain Barrier to Treat Neurodegenerative Diseases. *J. Control. Release* **2016**, *235*, 34–47. https://doi.org/10.1016/j.jconrel.2016.05.044.

(95) Bianco, A.; Kostarelos, K.; Prato, M. Applications of Carbon Nanotubes in Drug Delivery. *Curr. Opin. Chem. Biol.* **2005**, *9* (6), 674–679. https://doi.org/10.1016/j.cbpa.2005.10.005.

(96) Kostarelos, K.; Lacerda, L.; Pastorin, G.; Wu, W.; Wieckowski, S.; Luangsivilay, J.; Godefroy, S.; Pantarotto, D.; Briand, J.-P.; Muller, S.; Prato, M.; Bianco, A. Cellular Uptake of Functionalized Carbon Nanotubes Is Independent of Functional Group and Cell Type. *Nat. Nanotechnol.* **2007**, *2* (2), 108–113. https://doi.org/10.1038/nnano.2006.209.

(97) Mochalin, V. N.; Shenderova, O.; Ho, D.; Gogotsi, Y. The Properties and Applications of Nanodiamonds. *Nat. Nanotechnol.* **2012**, *7* (1), 11–23. https://doi.org/10.1038/nnano.2011.209.

(98) Schrand, A. M.; Hens, S. A. C.; Shenderova, O. A. Nanodiamond Particles: Properties and Perspectives for Bioapplications. *Crit. Rev. Solid State Mater Sci* **2009**, *34* (1–2), 18–74. https://doi.org/10.1080/10408430902831987.

(99) Zhu, Y.; Li, J.; Li, W.; Zhang, Y.; Yang, X.; Chen, N.; Sun, Y.; Zhao, Y.; Fan, C.; Huang, Q. The Biocompatibility of Nanodiamonds and Their Application in Drug Delivery Systems. *Theranostics* **2012**, *2* (3), 302–312. https://doi.org/10.7150/thno.3627.

(100) Krueger, A. The Structure and Reactivity of Nanoscale Diamond. *J. Mater. Chem.* **2008**, *18* (13), 1485. https://doi.org/10.1039/b716673g.

(101) Liu, Z.; Robinson, J. T.; Sun, X.; Dai, H. PEGylated Nanographene Oxide for Delivery of Water-Insoluble Cancer Drugs. *J. Am. Chem. Soc.* **2008**, *130* (33), 10876–10877. https://doi.org/10.1021/ja803688x.

(102) Kagan, V. E.; Konduru, N. V.; Feng, W.; Allen, B. L.; Conroy, J.; Volkov, Y.; Vlasova, I. I.; Belikova, N. A.; Yanamala, N.; Kapralov, A.; Tyurina, Y. Y.; Shi, J.; Kisin, E. R.; Murray, A. R.; Franks, J.; Stolz, D.; Gou, P.; Klein-Seetharaman, J.; Fadeel, B.; Star, A.; Shvedova, A. A. Carbon Nanotubes Degraded by Neutrophil Myeloperoxidase Induce Less Pulmonary Inflammation. *Nat. Nanotechnol.* **2010**, *5* (5), 354–359. https://doi.org/10.1038/nnano.2010.44.

(103) Eyer, P. The Role of Oximes in the Management of Organophosphorus Pesticide Poisoning. *Toxicol. Rev.* **2003**, *22* (3), 165–190. https://doi.org/10.2165/00139709-200322030-00004.

(104) Cetina, M.; Nagl, A.; Gašo-Sokač, D.; Kovač, S.; Bušić, V.; Saftić, D. Extensive Intramolecular and Intermolecular Interactions in Two Quaternary Salts of the Pyridoxal Oxime. *J. Chem. Crystallogr.* **2012**, *42* (7), 752–758. https://doi.org/10.1007/s10870-012-0312-y.

(105) Bharate, S. B.; Chao, C.-K.; Thompson, C. M. Comparison of the Reactivation Rates of Acetylcholinesterase Modified by Structurally Different Organophosphates Using Novel Pyridinium Oximes. *Environ. Toxicol. Pharmacol.* **2019**, *71*, 103218. https://doi.org/10.1016/j.etap.2019.103218.

(106) Sakurada, K.; Matsubara, K.; Shimizu, K.; Shiono, H.; Seto, Y.; Tsuge, K.; Yoshino, M.; Sakai, I.; Mukoyama, H.; Takatori, T. Pralidoxime Iodide (2-PAM) Penetrates Across the Blood-Brain Barrier. *Neurochem. Res.* **2003**, *28* (9), 1401–1407. https://doi.org/10.1023/A:1024960819430.

(107) Eyer, P. The Role of Oximes in the Management of Organophosphorus Pesticide Poisoning. *Toxicol. Rev.* **2003**, *22* (3), 165–190. https://doi.org/10.2165/00139709-200322030-00004.

(108) Petersen, E. J., *et al.* Potential Release Pathways, Environmental Fate, And Ecological Risks of Carbon Nanotubes. *Environ. Sci. Technol.* **2011**, *45* (23), 9837–9856. https://doi.org/10.1021/es201579y.

(109) aus der Beek, T.; Weber, F.-A.; Bergmann, A.; Hickmann, S.; Ebert, I.; Hein, A.; Küster, A. Pharmaceuticals in the Environment—Global Occurrences and Perspectives. *Environ. Toxicol. Chem.* **2015**, *35* (4), 823–835. https://doi.org/10.1002/etc.3339.

(110) Daughton, C. G. Environmental Stewardship and Drugs as Pollutants. *The Lancet* **2002**, *360* (9339), 1035–1036. https://doi.org/10.1016/S0140-6736(02)11176-7.

(111) Wilkinson, J. L. *et al.* Pharmaceutical Pollution of the World's Rivers. *Proc. Nat. Acad. Sci* **2022**, *119* (8). https://doi.org/10.1073/pnas.2113947119.

(112) Vitaku, E.; Smith, D. T.; Njardarson, J. T. Analysis of the Structural Diversity, Substitution Patterns, and Frequency of Nitrogen Heterocycles among U.S. FDA Approved Pharmaceuticals. *J. Med. Chem.* **2014**, *57* (24), 10257–10274. https://doi.org/10.1021/jm501100b.

(113) Schwarzenbach, R. P.; Escher, B. I.; Fenner, K.; Hofstetter, T. B.; Johnson, C. A.; von Gunten, U.; Wehrli, B. The Challenge of Micropollutants in Aquatic Systems. *Science (1979).* **2006**, *313* (5790), 1072–1077. https://doi.org/10.1126/science.1127291.

(114) D'souza, A.; Venuprasad, K. D.; Nayak, P.; Poonacha, L. K. A Review Article on Triazoles and Its Pharmacological Activities. *J. Pharm. Res. Int.* **2021**, 309–317. https://doi.org/10.9734/jpri/2021/v33i43A32491.

(115) Katritzky, A. R.; Rees, C. W..; Scriven, E. F. V. *Comprehensive Heterocyclic Chemistry II : A Review of the Literature 1982-1995 : The Structure, Reactions, Synthesis, and Uses of Heterocyclic Compounds*; Pergamon, 1996.

(116) Joule, J. A.; Mills, Keith.; Joule, J. A..; Mills, K. *Heterocyclic Chemistry*; Wiley, 2013.

(117) Vaidya, A.; Jain, S.; Jain, P.; Jain, P.; Tiwari, N.; Jain, R.; Jain, R.; K. Jain, A.; K. Agrawal, R. Synthesis and Biological Activities of Oxadiazole Derivatives: A Review. *Mini-Rev. Med. Chem.* **2016**, *16* (10), 825–845. https://doi.org/10.2174/1389557516666160211120835.

(118) *Bioisosteres in Medicinal Chemistry*; Brown, N., Ed.; Wiley, 2012. https://doi.org/10.1002/9783527654307.

(119) Daughton, C. G.; Ternes, T. A. Pharmaceuticals and Personal Care Products in the Environment: Agents of Subtle Change? *Environ. Health Perspect.* **1999**, *107* (suppl 6), 907–938. https://doi.org/10.1289/ehp.99107s6907.

(120) Friedrich, J.; Längin, A.; Kümmerer, K. Comparison of an Electrochemical and Luminescence-Based Oxygen Measuring System for Use in the Biodegradability Testing According to Closed Bottle Test (OECD 301D). *Clean* **2013**, *41* (3), 251–257. https://doi.org/10.1002/clen.201100558.

(121) Singhal, N.; Kumar, M.; Kanaujia, P. K.; Virdi, J. S. MALDI-TOF Mass Spectrometry: An Emerging Technology for Microbial Identification and Diagnosis. *Front. Microbiol.* **2015**, *6*. https://doi.org/10.3389/fmicb.2015.00791.

(122) Clark, A. E.; Kaleta, E. J.; Arora, A.; Wolk, D. M. Matrix-Assisted Laser Desorption Ionization–Time of Flight Mass Spectrometry: A Fundamental Shift in the Routine Practice of Clinical Microbiology. *Clin. Microbiol. Rev.* **2013**, *26* (3), 547–603. https://doi.org/10.1128/CMR.00072-12.

(123) Patel, R. MALDI-TOF MS for the Diagnosis of Infectious Diseases. *Clin. Chem.* **2015**, *61* (1), 100–111. https://doi.org/10.1373/clinchem.2014.221770.

(124) Zhang, Q.; De Oliveira Vigier, K.; Royer, S.; Jérôme, F. Deep Eutectic Solvents: Syntheses, Properties and Applications. *Chem. Soc. Rev.* **2012**, *41* (21), 7108. https://doi.org/10.1039/c2cs35178a.

(125) Juneidi, I.; Hayyan, M.; Hashim, M. A. Evaluation of Toxicity and Biodegradability for Cholinium-Based Deep Eutectic Solvents. *RSC Adv.* **2015**, *5* (102), 83636–83647. https://doi.org/10.1039/C5RA12425E.

(126) Baldwin, D. S.; Whittington, J.; Oliver, R. Temporal Variability of Dissolved P Speciation in a Eutrophic Reservoir—Implications for Predicating Algal Growth. *Water Res.* **2003**, *37* (19), 4595–4598. https://doi.org/10.1016/S0043-1354(03)00403-2.

(127) Glibert, P. M.; Seitzinger, S.; Heil, C. A.; Burkholder, J. M.; Parrow, M. W.; Codispoti, L. A.; Kelly, V. *The Role of Eutrophication in the Global Proliferation of Harmful Algal Blooms: New Perspectives and New Approaches*; 2005; Vol. 18. https://www.jstor.org/stable/43925687.

(128) Bhattacharya, K.; Mukherjee, S. P.; Gallud, A.; Burkert, S. C.; Bistarelli, S.; Bellucci, S.; Bottini, M.; Star, A.; Fadeel, B. Biological Interactions of Carbon-Based Nanomaterials: From Coronation to Degradation. *Nanomedicine* **2016**, *12* (2), 333–351. https://doi.org/10.1016/j.nano.2015.11.011.

(129) Baaloudj, O.; Scrano, L.; Bufo, S. A.; Modley, L.-A. S.; Lelario, F.; Zizzamia, A. R.; Emanuele, L.; Brienza, M. Environmental Fate, Ecotoxicity, and Remediation of Heterocyclic Pharmaceuticals as Emerging Contaminants: A Review of Long-Term Risks and Impacts. *Organics* **2025**, *6* (1), 1. https://doi.org/10.3390/org6010001.

(130) Puhlmann, N.; Mols, R.; Olsson, O.; Slootweg, J. C.; Kümmerer, K. Towards the Design of Active Pharmaceutical Ingredients Mineralizing Readily in the Environment. *Green Chem.* **2021**, *23* (14), 5006–5023. https://doi.org/10.1039/D1GC01048D.

(131) Jornada, D.; Dos Santos Fernandes, G.; Chiba, D.; De Melo, T.; Dos Santos, J.; Chung, M. The Prodrug Approach: A Successful Tool for Improving Drug Solubility. *Molecules* **2015**, *21* (1), 42. https://doi.org/10.3390/molecules21010042.

Acknowledgements

This thesis presents research conducted at the Department of Chemistry and Biotechnology, Tallinn University of Technology (TalTech), supported by funding that enabled its successful completion. and was supported in part by the BIOFORM (COVSG5) project funded by the Estonian Research Council, which enabled the successful completion of this work.

I am sincerely grateful to my supervisor Dr. Yevgen Karpichev, for his continuous support, patience, and guidance throughout the past five years. I truly appreciate his ability to manage diverse research topics while maintaining a clear scientific direction. His encouragement and support in all aspects of my work have been invaluable to the successful completion of this thesis.

I am also thankful to my colleagues in the Sustainable Chemistry and Engineering research team for creating a supportive and collaborative research environment. In particular, I would like to thank Denys Bondar for his support from day one, as well as Oleg, Zeba, Mahi, Nadia, Albina and all other colleagues, who contributed to my research in one way or another.

I would like to acknowledge the valuable contributions of my bachelor's students and Erasmus interns, whose dedication significantly supported my work. I am especially thankful to Pia-Justina Wellmann for her extensive involvement in CBT experiments, as well as for improving laboratory processes, data handling, and contributing to the development of standard operating procedures. I also thank Daria Maljuk for her assistance in multiple CBT experiments, Sofia Mosjakina for her support with CBT testing and inoculum characterization.

I would also like to acknowledge the BIOCEB Master's students whom I had the opportunity to teach in the biodegradation laboratory. Over four cohorts, teaching them the Closed Bottle Test not only contributed to the development of the CBT laboratory but also helped me improve my teaching and communication skills. I am grateful for their enthusiasm and support throughout this process.

I am particularly grateful to Morten Sük (Leuphana University), who introduced me to the Closed Bottle Test methodology and hosted me in his laboratory, marking the beginning of my journey in biodegradation research. His continued support during experimental challenges and data curation has been invaluable. I also thank Prof. Klaus Kümmerer for hosting me at Leuphana University and supporting my research development.

My sincere thanks go to Ms. Marlen Taggu (Tallinna Vesi) for providing the inoculum used in our biodegradation studies. I also acknowledge the Microbiome Research Group at TFTAK for performing the next-generation sequencing analysis of the inoculum. I am grateful to Prof. Jean-Manuel Raimundo (Aix-Marseille University) for hosting me during my research exchange. I would like to thank all collaborators from the University of Pisa (Italy) and Politecnico di Milano (POLIMI) for their contributions to my NADESs research, as well as all other collaborators who supported my projects.

I would like to thank the Department of Chemistry and Biotechnology and all faculty members for their support and collaboration throughout my research. Special thanks to Dr. Kristel Vene for her support during my early projects, Dr. Pirjo Spuul and Prof. Cecilia Sarmiento for facilitating research exchange visits and conference participation, and Mr. Ants Uus for his technical assistance and quick solutions to laboratory hurdles. I also thank Dr. Olga Bragina for her support in inoculum characterization and MALDI-TOF

analysis, and all researchers and PhD students in the department for contributing to my research in various ways.

My greatest strength throughout my PhD journey has been my family. I am especially grateful to my wife, Deepa, for her unwavering support, patience, and for accompanying me to Estonia, facing all challenges including the winters with strength and positivity. I would like to thank my parents, Mr. Nagappa and Indira, and my brothers Prashanth and his wife Pooja, Praveen and his wife Shwetha, for their constant encouragement and support. I also extend gratitude to my mother-in-law Akkamma Basavaraj and her family, and my extended family in my hometown Harihar. Special thanks to the kids in my family Aadhya, Bhuvi, Raju, Ruthu and Achhu for bringing me joy and laughter despite the physical distance, my Indian friends in Tallinn, and our Kannadiga community in Estonia, for their companionship and support.

AI-based language tools (Claude and ChatGPT) were used only for grammar correction and improvement of language clarity. All scientific content, interpretations, and conclusions were developed and verified by the author.

I apologize, if I have unintentionally missed mentioning anyone, and my sincere thanks go to everyone who has directly or indirectly contributed to my PhD journey.

Abstract

Biodegradability assessment of emerging green solvents, bioactive heterocycles, and hybrid nanomaterials

The increasing use of structurally diverse chemicals, including bio-based solvents, pharmaceutical scaffolds, and nano-enabled materials, raises some serious questions regarding their environmental fate and persistence in aquatic systems. Biodegradation plays a central role in determining whether such substances are rapidly removed from ecosystems or persist in it for prolonged exposure. This thesis evaluates the aerobic biodegradation profiles of three chemically distinct classes: natural deep eutectic solvents (NADESs), oxime-functionalized nanodiamonds, and piperazine-containing oxazole derivatives using the OECD 301D modified Closed Bottle Test, supported by high-resolution oxygen consumption measurements.

All investigated NADESs fulfilled the criteria for ready biodegradability, demonstrating rapid and extensive mineralization under aerobic conditions. Ecotoxicity assessment further indicated low acute toxicity toward aquatic organisms. However, their high organic carbon and nitrogen content suggests a potential risk of increased biological oxygen demand and nutrient enrichment, indicating that ready biodegradability alone does not fully ensure environmental safety.

In contrast, oxime-functionalized nanodiamonds exhibited negligible biodegradation, with the surface-bound organic functional fragment showing only limited degradation, indicating that the organic corona rather than the nanodiamond core governs the environmental fate profile of these hybrid materials. The surface-bound organic functionalization showed only limited and slow degradation, indicating at most inherent biodegradability. In general, the environmental fate of such hybrid materials is affected by the long-term stability of the nanomaterial core. Similarly, the investigated oxazole derivatives showed low biodegradation, with mineralization levels well below the OECD threshold for ready biodegradability. Toxicity control experiments confirmed that this limited degradation was not due to microbial inhibition but rather to the intrinsic stability and heteroaromatic character of the oxazole scaffold. Despite their promising biological activity, these compounds may persist in aquatic environments, highlighting the importance of incorporating biodegradation screening at early stages of pharmaceutical development.

Overall, the results support the expected relationship between molecular structure, biodegradability, and environmental persistence, with naturally derived systems showing high degradability, while structurally complex synthetic molecules and nanomaterials exhibit increased persistence. The results emphasize that comprehensive environmental risk assessment must integrate biodegradability, ecotoxicity, and secondary effects such as eutrophication, and support the development of safer, benign-by-design chemical systems.

Lühikokkuvõte

Tekkivate roheliste lahustite, bioaktiivsete heterotsüklite ja hübriidnanomaterjalide biolagunevuse hindamine

Struktuurselt mitmekesiste kemikaalide, sealhulgas biopõhiste lahustite, ravimilaadsete ühendite ja nanoosakestel põhinevate materjalide järjest ulatuslikum kasutamine tõstatab olulisi küsimusi nende keskkonnakäitumise ja püsivuse kohta veekeskkonnas. Biolagunemine mängib keskset rolli määramaks, kas sellised ained eemaldatakse ökosüsteemidest kiiresti või püsivad neis pikemaajaliselt. Käesolevas töös uuritakse kolme keemiliselt erineva ainerühma aeroobset biolagunemist: looduslikke sügaveutektilisi lahusteid (NADES-id), oksiimrühmadega funktsionaliseeritud nanoteemante ning piperasiini sisaldavaid oksasooli derivaate. Biolagunemist hinnati OECD 301D modifitseeritud suletud pudeli testi abil ning kõrge lahutusvõimega hapnikutarbimise mõõtmistega, tulemusi täiendati täpsete hapnikutarbimise mõõtmistega.

Kõik uuritud NADES-id vastasid kergesti biolagunevate ainete kriteeriumidele, lagunedes kiiresti ja ulatuslikult aeroobsetes tingimustes. Lisaks näitasid ökotoksilisuse katsed, et nende ainete akuutne toksilisus veeorganismidele on madal. Samas viitab nende kõrge orgaanilise süsiniku ja lämmastiku sisaldus võimalikule riskile suurendada bioloogilist hapnikutarvet ning põhjustada toitainete rikastumist veekeskkonnas. Seega ei taga ka hea biolagunevus üksinda täielikku keskkonnaohutust.

Seevastu oksiimrühmadega funktsionaliseeritud nanoteemandid biolagunesid väga vähesel määral. Pinnale seotud orgaaniline funktsionaalne fragment näitas vaid piiratud lagunemist, mis viitab sellele, et orgaaniline pind — mitte nanoteemandi tuum — määrab nende hübriidmaterjalide keskkonnas püsivuse profiili. Pinnale seotud orgaanilised rühmad lagunesid aeglaselt ja vaid piiratud ulatuses, mis viitab loomupärasele biolagunevusele. Üldiselt määrab selliste hübriidmaterjalide keskkonnakäitumise nanomaterjali tuuma pikaajaline stabiilsus.

Madalat biolagunemist näitasid ka uuritud oksasooli derivaadid. Nende mineralisatsioon jäi oluliselt alla OECD kergesti biolagunevuse piirväärtuse. Toksilisuse kontrollkatsed kinnitasid, et vähene lagunemine ei olnud põhjustatud mikroorganismide aktiivsuse pärssimisest, vaid tulenes eelkõige oksasoolistruktuuri suurest keemilisest stabiilsusest ja heteroaromaatsest iseloomust. Kuigi neil ühenditel on paljulubav bioloogiline aktiivsus, võivad need veekeskkonnas püsida. Seetõttu on oluline hinnata biolagunemist juba ravimiarenduse varajases etapis.

Kokkuvõttes toetab käesolev uuring oodatavat seost molekulaarse struktuuri, biolagunemisvõime ja keskkonnas püsimise vahel. Looduslikku päritolu süsteemid lagunevad hästi, samal ajal kui keerukama struktuuriga sünteetilised molekulid ja nanomaterjalid on püsivamad. Tulemused rõhutavad, et terviklik keskkonnariski hindamine peab hõlmama biolagunemist, ökotoksilisust ning võimalikke teiseseid mõjusid, näiteks eutrofeerumist. Samuti toetavad saadud tulemused ohutumate ja keskkonnasõbralikumate keemiliste süsteemide arendamist.

Appendix 1

Publication I

Nagappa, N. M.; Mero, A.; Husanu, E.; Usmani, Z.; Oliva, M.; Sanches, M. V.; Fumagalli, G.; Mele, A.; Mezzetta, A.; Gathergood, N.; Guazzelli, L.; Pretti, C.; Karpichev, Y. Biodegradability and Ecotoxicity Profiles of Choline Acetate, Betaine, and L-Proline NADESs: A Hidden Threat for Eutrophication? *Molecules* **2026**, 31 (2), 262. https://doi.org/10.3390/molecules31020262.

molecules

MDPI

Article

Biodegradability and Ecotoxicity Profiles of Choline Acetate, Betaine, and L-Proline NADESs: A Hidden Threat for Eutrophication?

Nandish M. Nagappa [1], Angelica Mero [2], Elena Husanu [3], Zeba Usmani [1], Matteo Oliva [4], Matilde Vieira Sanches [4,5], Giorgia Fumagalli [4], Andrea Mele [6], Andrea Mezzetta [2,*], Nicholas Gathergood [7], Lorenzo Guazzelli [2], Carlo Pretti [4,8,*] and Yevgen Karpichev [1,*]

1 Department of Chemistry and Biotechnology, Tallinn University of Technology (TalTech), 12618 Tallinn, Estonia; nandish.mudegowdru@taltech.ee (N.M.N.)
2 Department of Pharmacy, University of Pisa, 56126 Pisa, Italy
3 Center for Material Interfaces, Istituto Italiano di Tecnologia, 56025 Pontedera, Italy
4 Interuniversity Consortium of Marine Biology and Applied Ecology "G. Bacci", 47128 Livorno, Italy
5 Department of Biology & Centre for Environmental and Marine Studies (CESAM), University of Aveiro, 3810-193 Aveiro, Portugal
6 Dipartimento di Chimica, Materiali e Ingegneria Chimica "Giulio Natta", Politecnico di Milano, 20133 Milano, Italy
7 School of Chemistry, College of Science, University of Lincoln, Lincoln LN6 7TS, UK
8 Department of Veterinary Sciences, University of Pisa, 56122 Pisa, Italy
* Correspondence: andrea.mezzetta@unipi.it (A.M.); carlo.pretti@unipi.it (C.P.); yevgen.karpichev@taltech.ee (Y.K.)

Abstract

Deep Eutectic Solvents (DESs), particularly Naturally Available Deep Eutectic Solvents (NADESs), are increasingly regarded as green solvents due to their low vapor pressure, non-flammability, thermal stability, strong solvent power, and low toxicity. In line with Green Chemistry principles, the use of renewable and biocompatible components such as amino acids, lipids, and naturally derived acids enables the development of more sustainable solvent systems. This study addresses the need for environmentally safer NADESs by evaluating their physico-chemical suitability and environmental impact. Fifteen NADESs were prepared using naturally derived components and assessed for environmental safety. Biodegradability was evaluated using the OECD 301D Closed Bottle Test (CBT), while toxicity toward *Raphidocelis subcapitata* was examined to characterize ecotoxicological behavior. The results demonstrated that the synthesized NADESs exhibit high biodegradability levels and low toxicity toward microalgae. Toxicity control indicated no significant inhibition of microbial activity during biodegradation, suggesting favorable environmental compatibility. Overall, the findings indicate that the NADESs represent more sustainable solvent alternatives with low toxicological profiles. However, the potential role of these compounds in enhancing eutrophication processes cannot be excluded and warrants further investigation.

Keywords: naturally available deep eutectic solvents; biodegradation; ecotoxicity; *Raphidocelis subcapitata*; closed bottle test; hydrogen bond donor; hydrogen bond acceptor

Academic Editor: Gonzalo de Gonzalo

Received: 15 December 2025
Revised: 31 December 2025
Accepted: 7 January 2026
Published: 12 January 2026

1. Introduction

In the advent of the sustainability and green chemistry era, there is an ongoing quest to discover safer and more environmentally friendly solvents to replace traditional ones

derived from fossil-derived chemicals [1]. These conventional solvents pose significant environmental threats during production, use, and disposal [2]. The end-of-life cycle for these solvents is a problem because they are not biodegradable. This means that they must be burned, which creates CO_2 emissions, as they are often non-biodegradable. In addition, the impact of these solvents on human health has recently become a cause for concern in various industrial sectors. For example, *N*,*N*-dimethyl formamide (DMF) has recently been highlighted for its reproductive toxicity [3]. Consequently, its use, particularly in the pharmaceutical industry, has been prohibited within the European Union. In this context, the investigation of sustainable alternatives to fossil-based solvents has intensified in recent years. Among the neoteric solvents, the Deep Eutectic Solvents (DESs) represent a versatile alternative to volatile organic solvents, including those of natural origin [4]. The recent popularity of DESs is mainly due to their simple preparation and their relatively low cost [5,6]. DESs are typically obtained by mixing two or more compounds [7], which determines a decrease in the melting point of the mixture below that expected for the ideal eutectic [8]. At the basis of this deviation, there is the strong interaction between a hydrogen bond donor (HBD) and a hydrogen bond acceptor (HBA) that creates a strong microheterogeneity at the molecular level [9]. However, the real key to the success of DES is their tuneability, which allows for the customization of the system to suit specific needs. Simply modifying the chemical composition of the mixture allows its chemical and physical properties to be adapted for a specific application. An additional degree of modularity can be achieved by adjusting the molar ratio between the components [10]. A subset of DESs, inspired by nature and derived from plant-based products and other bio-resources, are called Natural Deep Eutectic Solvents (NADESs) [11]. In fact, they are composed entirely of bio-based compounds, which is the reason behind their biocompatibility [12–14].

Although the definition of DESs does not have a direct implication on most features, initially, the green characteristics of DESs were assumed based on the pharmaceutically acceptable profile that was reported in the material safety data sheets of the selected individual components [15]. Later, a few studies were devoted to investigating the DESs toxicity profile [16]. Indeed, bio-based chemicals may not be completely biodegradable, and hence, are not 100% environmentally friendly. However, despite the great interest of academia and industry in DESs and NADESs applications for gas capture [17], biomass valorization [18,19], wastewater entrapment [20] and wastewater treatment [21], material synthesis [22], the toxicity of these compounds is still an underrated issue. Limited recent research studies have investigated NADESs toxicity on different targets, such as human cells [23–25], bacteria [25–28], yeasts [25], invertebrates and microalgae [12,26,27], and fish [29], sometimes reporting conflicting results. Indeed, what emerged from different papers was a pool of different behaviors of HBA/HBD if assessed singularly or, instead, in a NADESs composition [12]. Moreover, several studies support the idea of DESs as "eco-friendly", assuming they are not toxic, given the fact they are formed by naturally occurring ingredients and are, for this reason, bio-renewable, biodegradable and bio-assimilable [30,31], while other publications report a clear toxicity linkable to some DESs components [23].

Among the NADESs components, choline is the most used compound to prepare DESs [32], due to its high biodegradability [33] and low toxicity [31] as well as low cost and widespread availability [34]. Although found in living organisms, the choline cation currently on the market is of fossil origin and is obtained from trimethylamine and ethylene oxide [33]. In particular, choline acetate (ChA) and bitartrate (TA) are much less commonly used than choline chloride (ChCl) in the preparation of DES, but they are a valuable halogen-free alternative. For example, DES based on ChTA have recently been used to increase the solubilization of drugs [35], plasticize starch [36] and extract flavonoids [37].

ChA-based DESs have also recently been studied from a physico-chemical and application perspective [38–41]. For example, ChA:glycolic acid (GA), ChA:levulinic acid (LA) and ChA:imidazole (Im) showed excellent performance in hemicellulose solubilization and were used in Kraft cellulose purification [42]. On the other hand, betaine (trimethylglycine, Bet), a zwitterionic compound bearing both formal positive and negative charges, has also been used to prepare DESs [5] and has been even suggested as the universal HBA [43]; like choline, betaine is also biocompatible [44], has a low toxicity profile [45,46], and is readily biodegradable. However, in contrast to ChCl, Bet can be derived from renewable sources and, in particular, by the transformation of the by-product of sugar production [42]. The use of Bet-based DESs has grown significantly in recent years and they are being used in numerous applications [47–50].

The proteinogenic amino acid L-proline (L-Pro) has recently received attention for designing ILs [51–53] and NADESs [54,55] for different applications. The ability of L-Pro to form enamines or imines when reacting with carbonyl groups, as well as its ability to induce chirality promoted by the cyclic structure of the molecule, have been exploited in a wide range of organic synthetic methodologies. L-Pro can promote a very broad diversity of transformations, which can be explained by the multiple catalytic roles allowed by its structural features.

Similarly, L-Pro can behave both as an acid or Brønsted base, or even show both behaviors during a mechanism, therefore, being a bifunctional catalyst. It is the only natural amino acid with a secondary amine functionality, a feature that raises the nitrogen pK_a and increases its nucleophilicity in comparison to other amino acids. L-Pro has several additional advantages, such as being inexpensive, commercially available, non-toxic and easily recoverable, which are important properties from the point of view of green chemistry [56]. L-Pro has recently become widely used as an ingredient in supplements, health foods and cosmetics. The use of L and D-Pro as an HBA in the preparation of DESs allows us to develop new reaction media with a dual solvent/catalyst role [57].

Previous research published by the co-authors of this study presented one of the most comprehensive ecotoxicological screens of NADESs evaluated using a broad battery of marine and freshwater bioassays [12]. The overall findings revealed a general absence of acute toxicity across the NADESs tested; however, some NADESs induced algal biostimulation responses in freshwater assays. This suggested that while NADESs are often labeled as "sustainable", their ecological effects, particularly for primary producers, may be more complex than predicted by single-species toxicity tests alone, especially under conditions where biostimulation could influence ecosystem functioning. Those results highlighted the need for further investigation of both ecotoxicological endpoints and biodegradation behavior to more reliably assess the environmental safety of NADESs.

In this study, a series of 15 different choline, betaine, and L-proline-based NADESs (Table A1) and their single components (Figure 1) was assessed for their biodegradability using the aerobic biodegradation method [58], in order to evaluate their persistence in aquatic systems and the potential release of nutrients, such as N and P by molecule dissolution.

Moreover, we evaluated the potential ecotoxic effect of these compounds and their respective single components in terms of freshwater microalgae *Raphidocelis subcapitata* growth stimulation and/or inhibition, hypothesizing an underrated effect of NADESs as potential eutrophication substances.

A. Hydrogen bond acceptors:

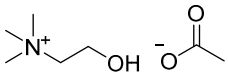

Choline acetate (**ChA**)

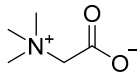

Betaine (**Bet**)

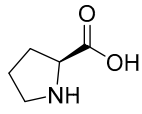

L-proline (**L-Pro**)

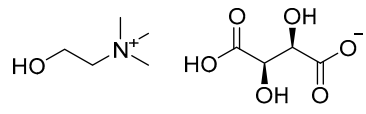

Choline bitartrate (**ChTA**)

B. Hydrogen bond donors:

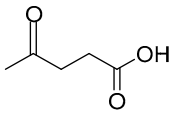

Levulinic acid (**LA**)

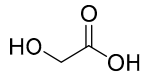

Glycolic acid (**GA**)

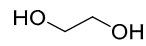

Ethylene glycol (**EG**)

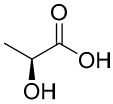

L-lactic acid (**L-LacA**)

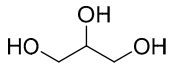

Glycerol (**Gly**)

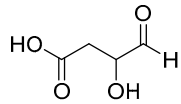

D,L-malic acid (**MA**)

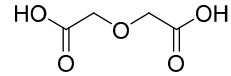

Diglycolic acid (**DGA**)

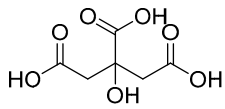

Citric acid (**CA**)

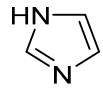

Imidazole (**Im**)

Figure 1. Chemical structures of hydrogen bond acceptors (**A**) and hydrogen bond donors (**B**) and their abbreviations used in this work.

2. Results

2.1. Biodegradation Results of NADESs

The biodegradability tests conducted for all of the test substances for 28 days were proven to be valid as the control, readily biodegradable sodium acetate, was eliminated by at least 60% by the end of 14 days.

All the tested NADESs, as well their single components, were observed to be classified as "readily biodegradable", showing biodegradation values > 60% after a 28-day Closed Bottle Test (Table A2). The only exception was Im, with a biodegradation value of 23% as an indisvidual HBD component, although when in combination with ChAc (NADES 11), it seemed to not affect whole NADESs' biodegradability score (67%). The biodegradability profiles observed for the studied NADESs are presented in Figure 2a–o.

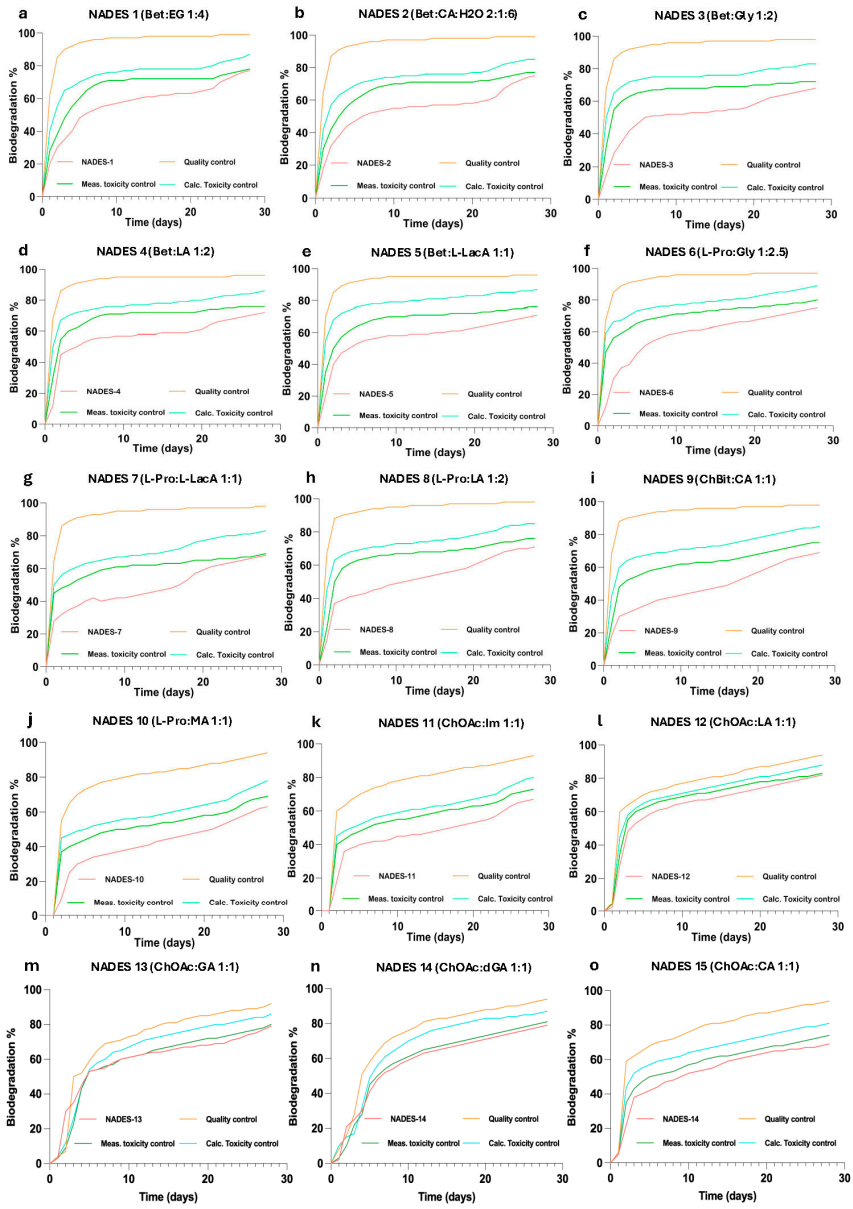

Figure 2. Biodegradability profiles of the Closed Bottle Test (CBT OECD 301D, 28 days) for the studied NADESs: (**a**) Bet:EG; (**b**) Bet:CA; (**c**) Bet:Gly; (**d**) Bet:LA; (**e**) Bet:L-LacA; (**f**) L-Pro:Gly; (**g**) L-Pro:L-LacA; (**h**) L-Pro:LA; (**i**) ChTA:CA; (**j**) L-Pro:MA; (**k**) CA:Im; (**l**) ChA:LA; (**m**) ChA:GA; (**n**) ChA:DGA; (**o**) ChA:CA. Quality control series: sodium acetate (6.41 mg/L) in inoculated mineral medium, used to verify microbial activity and test validity; rapid biodegradation of sodium acetate confirms inoculum viability. Measured toxicity control: contains both sodium acetate and the test compound in their respective concentrations, used to assess potential inhibitory or toxic effects of the test compound on microbial activity by comparison with the quality control series. Calculated toxicity control: theoretically calculated biodegradation curve from the sum of the expected oxygen consumption of the reference series and the test series, assuming no inhibitory effects of the test compound on microbial activity. Used to identify any potential inhibitory effects of test substance on microbial activity.

2.2. *Raphidocelis Subcapitata* Growth Bioassay

Figure 3 represents the growth behavior of *R. subcapitata* algae exposed to different concentrations of 15 NADESs. Each graphic shows the differences, in terms of concentration–response trend, between NADESs and their components. The concentration–response curve showed an algal growth stimulation with increasing concentrations in thirteen NADESs compared to that of the control. The only two tested NADESs where the algal growth was not different from that of the control were NADES 4 (Bet:LA) (Figure 3d) and NADES 11 (ChA:Im) (Figure 3k).

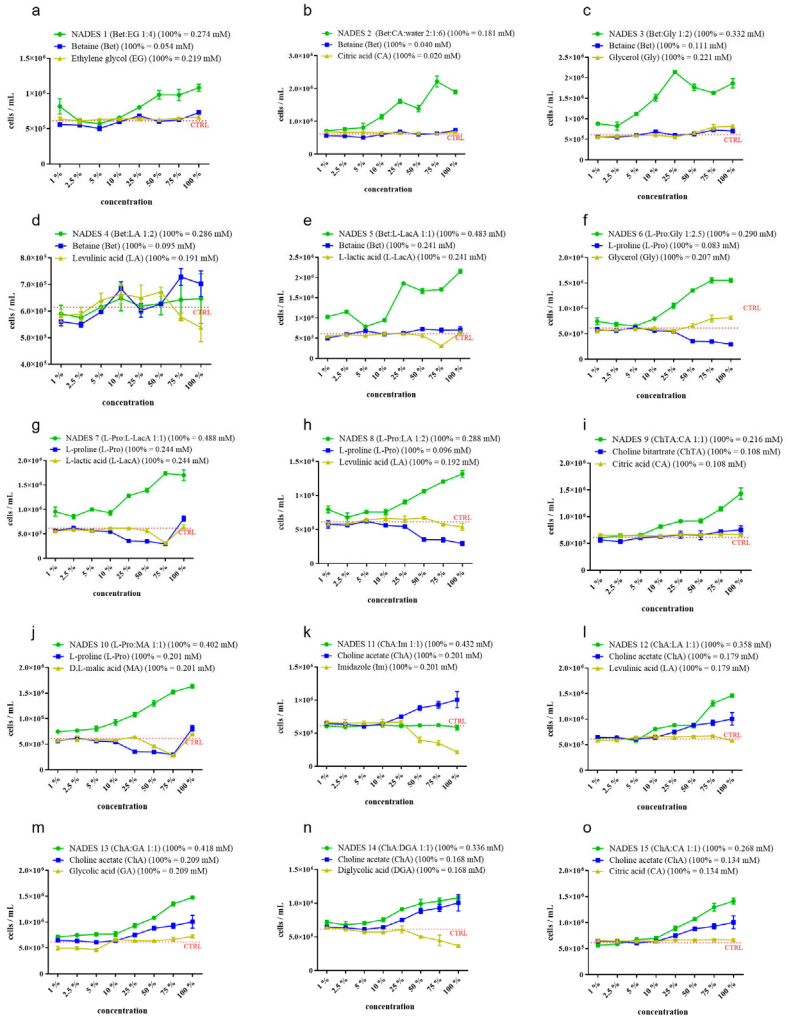

Figure 3. Concentration–response graphs of *R. subcapitata* exposed to NADESs and to their single components at the relative concentration as in the whole compound at the same concentration. The red dotted line is the mean algal concentration measured in the controls. (**a**) Bet:EG; (**b**) Bet:CA; (**c**) Bet:Gly; (**d**) Bet:LA; (**e**) Bet:L-LacA; (**f**) L-Pro:Gly; (**g**) L-Pro:L-LacA; (**h**) L-Pro:LA; (**i**) ChTA:CA; (**j**) L-Pro:MA; (**k**) CA:Im; (**l**) ChA:LA; (**m**) ChA:GA; (**n**) ChA:DGA; (**o**) ChA:CA. Results are expressed as mean algal concentration (cells mL^{-1}) ± standard deviation (n = 3) for each tested concentration of each tested substance.

The concentration–response curve showed an algal growth stimulation with increasing concentrations in thirteen NADESs compared to the control. The only two tested NADESs where the algal growth was not different from that of the control were NADES 4 (Bet: LA, Figure 3d) and NADES 11 (ChA:Im, Figure 3k).

Among the NADESs components, the one with the most stimulating effect in terms of algal growth was choline acetate, which represents the HBA of NADESs 11–12–13–14–15 (Figure 3k–o). Following the same trend, L-Pro in NADESs 7 and NADES 10 (Figures 3g and 3j, respectively) showed a slight growth stimulation at the maximum tested concentration, followed by a reduction in algal growth at 75%, 50% and 25%. The same compound, tested at concentrations as in NADESs 6 and 8 (Figures 3f and 3h, respectively), showed an inhibiting effect until 50%. This is linked to the fact that the concentration of L-Pro in NADESs 6 and 8 at 50% was similar to L-Pro in NADESs 7 and 10 at 25%. A similar trend, as for L-Pro in NADESs 7 and 10, was observed for MA and L-LacA (Figure 3e,g,j). However, in these cases, the inhibition effect was limited to the concentrations of 50% and 75% for MA and only at 75% for L-LacA.

Bet and ChTA displayed a similar effect on algal growth, having both shown biostimulation at the 100% concentration of NADESs 1,2,3,5 and 9 (Figure 3a–c,e,i). In addition, a biomass increase was also found at 50 and 75% of Bet in NADES 5, and at 75% of ChTA in NADES 9. Contrastingly, Bet exhibited a different algal growth pattern in NADES 4 (Figure 3d), where three peaks of biostimulation were found at 10, 75 and 100%, and an inhibition peak was displayed at 2.5%.

Concerning other tested components, they showed no effect as their growth patterns were very similar to those of the respective controls.

ANOVA results, with Tukey's post-test for multiple comparisons, for all concentration–response effects of each NADESs, are presented in Supporting Information (Table S1).

3. Discussion

Considering the continuously growing necessity of finding new green solutions aimed at decreasing the impact of human activities on the environment, the present study took in considering a pool of 15 NADESs, claimed as non-toxic systems, to evaluate their biodegradability potential and their effects on freshwater algal growth. The same analyses were accrued out on the single components to highlight possible differences when mixed in the NADESs.

The current study represents the natural development of our previous research work on NADESs [12], where the pool of 15 NADESs was evaluated in terms of ecotoxicological effects on two batteries of tests, a marine test and a freshwater test. Due to interesting results obtained in terms of microalgal growth biostimulation, particularly emphasized in the freshwater environment, a deeper investigation on biodegradability and the single component effect, in respect to the formed DES system, was considered necessary. Observing, as an example, biodegradability percentages of NADES single components after 28 days, we may notice that Im was the one with the lowest biodegradation value (23%). We may suggest that the inoculum used was likely deficient in key breakdown pathways for this particular chemical, since the biodegradability rose to 67% in the NADES with choline acetate, underlining complex interactions between components in whole NADES formulation.

Despite the very limited toxic effect of NADESs observed with tests involving invertebrates, their potential impact on the environment, if improperly disposed of, may lie in their characteristic as a nutrient source, thus increasing the already large pool of substances with the potential to disrupt biogeochemical cycles at a global scale [59]. This disruption might be intensified by extreme natural events linked to a Global Change Scenario, such as thermal heatwaves [60] and ocean acidification [61]. Regarding the latter, how NADESs

in aqueous solutions are able to reduce pH value and, as a consequence, enhanced algal growth was observed [12,62].

In addition to these statements, a ready biodegradability was observed for the majority of the assessed NADESs, with biodegradation values at 28 days between 60% and 81% for NADES compounds, and between 23% and 79% for their single components.

Our data coincides with the report on NADESs-based ChCl as HBA and a series of HBD (glycerol, ethylene glycol, urea, glucose, malonic acid, and lactic acid) studied by CBT [33], which demonstrated a biodegradability of beyond 60% in all cases. Irrespective of number of hydroxyl groups per mole or the presence of carboxylic derivatives, such as acids, esters, or amides, the biodegradability profiles were considered as "readily biodegradable". This feature may lead the general opinion to consider NADESs as completely "green" and "eco-friendly" substitutes to conventional organic solvents. However, the fact that they are readily biodegradable may enhance the load of dissolved ions/molecules with nutritional value, such as choline, also known as vitamin B4, and its degradation products, emphasizing the occurrence of eutrophication phenomena [63].

Due to lack of literature treating NADES effects on microalgae, to better understand current observations, it is important to deeply analyze all obtained results and compare NADES effects with their single component behavior. Among the NADESs, those showing the highest induction of algal growth were NADES 2 (Bet:CA), 3 (Bet:Gly) and 5 (Bet:L-LacA). All of these three systems have betaine in their formulation, which, notwithstanding a lack of effect while tested as single component, strongly enhanced algal proliferation when combined with Gly, CA, or L-LacA. Moreover, NADESs containing L-Pro as HBA, which tend to slightly reduce algal load while being assessed as single component at high concentrations (>0.29 mM), displayed a growth-stimulating effect when in combination with other HBDs (NADESs 6–7–8–10). Differently from those cases, effects of NADESs with ChA (NADESs 11–12–13–14–15), appeared to be more influenced by this latter component with respect to all other HBAs, given the similar shape of concentration–effect curves.

Moving the focus specifically to NADES components, it is possible to divide them into three main groups, depending on their effect. The first group, which comprises the majority of assessed compounds (betaine, ethylene glycol, citric acid, glycerol, glycolic acid, choline bitartrate, L-lactic acid, malic acid and levulinic acid), is composed by substances without significant effects, neither in enhancing nor inhibiting algal growth. The second group is composed of Im, L-Pro and DGA. These three compounds showed a limited inhibiting effect on algal growth when tested at concentrations > 0.08 mM for L-Pro, >0.107 mM for Im, and >0.1 mM for DGA (concentrations in the relative NADES solution, assessed at dilutions between 25% and 100%). The last group is composed of ChA only, which is present in NADESs 11–15 formulations (Figure 3k–o). As stated before, this particular compound showed a clear algal growth-enhancing effect, which followed the same concentration–response curve of the relative NADESs, appearing to be the main factor responsible for algal growth, if compared with concentration–response curves of each assessed whole NADESs. However, if compared with the relative whole system, the algal biomass measured at each ChA assessed concentration resulted in lower values. This, again, led us to hypothesize a synergistic effect between ChA and the other DES component, like in other assessed NADESs. The only exception was represented by NADES 11, where the two opposite effects of Im and ChA seemed to interact by simple addition (Figure 3k).

This hypothetical synergistic effect of the two components in the NADES composition, observed as an emphasized "overgrowth" effect of the entire systems if compared with both single compounds until 25% as a threshold concentration, has already been observed for ChCl-based DESs [64,65], but also for other toxic DESs, such as glyceline, ethaline and reline [27]. This last result was also observed in the present work with NADES 11 (ChA:Im

1:1), which, as reported before, has Im in its formulation. Im is also known to be linked to aquatic toxicity in other kinds of NADES-related compounds, such as ionic liquids [12]. However, while Im showed a certain degree of algal growth inhibition, no relevant effects were observed when it was assessed in combination with ChA as a whole DES.

Regarding biodegradability, with the exception of the previously discussed imidazole, no other relevant differences in terms of biodegradability percentages were observed between single components and NADESs, all with values still over 60%. However, the readiness of biodegradability of these compounds, considering that several of them, such as L-proline, betaine and choline acetate, contain nitrogen in their formulation, and the synergistic effect between some components in enhancing microalgal growth, may act as a perfect fertilizer with a potential eutrophication effect [66].

4. Materials and Methods

The NADESs used in this study and their composition, along with the ratio of the mixtures and their chemical structure, as well as the NADESs components, are listed in Table A1.

4.1. Chemicals

Choline acetate (ChA) 98% was purchased from IOLITEC (Heilbronn, Germany). Betaine (Bet) > 99% and L-Proline (L-Pro) > 99% were purchased from Tokyo Chemical Industry (TCI) (Tokyo, Japan). Ethylene glycol 99% (EG), levulinic acid (LA) 98%, imidazole (Im) 99%, and cholinium bitartarate (ChTA) > 98% were purchased from Thermo Fisher (Waltham, MA, USA). Glycerol (Gly) 99%, glycolic acid (GA) 99%, malic acid (MA) > 99%, diglycolic acid (DGA) 98%, and L-lactic acid (L-LacA) $\geq$ 98% were obtained from Sigma-Aldrich (Merck, Darmstadt, Germany). Ultrapure deionized water (Milli-Q Direct Water Purification System) was used for all solutions and media preparation. Potassium dichromate, $K_2Cr_2O_7$ (1 g/L) was purchased as a dehydrated salt (ACS reagent grade, purity $\geq$ 99.0%) from Sigma-Aldrich and used as a reference toxicant for algal growth inhibition assay. The composition and molar ratios of NADESs tested in this study are reported in Table A1. NADESs were prepared following the methodologies described in the literature [16,42].

4.2. Biodegradability Assessment

In the assessment of the biodegradability of organic compounds, the initial and simple test used is the Closed Bottle Test (modified OECD 301D), usually referred to as the aerobic biodegradation test [67,68].

Aerobic biodegradation testing was performed using the modified Closed Bottle Test (CBT), based on OECD 301D guidelines [68,69]. CBT setup with modifications, where biological oxygen consumption is measured with an optode oxygen sensor system using PTFE-lined PSt3 oxygen sensor spots (Fibox 3 PreSens, Regensburg, Germany), allows the measurement of BOD without dispensing it from the stock solution each time for each test and thereby reducing the number of parallels, as once we open a bottle to measure its BOD, we cannot use it anymore because it is exposed to the atmosphere; so, in that case, we would keep a stock solution and pour it into a new measuring flask each time. The modified setup has also been shown to improve the reproducibility compared to the original OECD 301D guidelines [69,70]. Compared to other standard aerobic biodegradation tests, CBT is better suited for testing compounds with different physico-chemical properties. It is also one of most stringent OECD tests for biodegradability, as the amount of inoculum added is very low and, thus, compounds passing CBT 301D should show good biodegradation not only under artificial wastewater treatment conditions but also in soil and groundwater systems.

Experimental Setup. Each CBT run consisted of four different series, each of which was run in duplicates. First was quality control (reference series), in which readily biodegradable sodium acetate in a known concentration (6.41 mg/L) was added to a flask of mineral medium inoculated with effluent from a wastewater treatment plant. As sodium acetate is known to be rapidly biodegradable, it acted as a reference and control for monitoring the activity of microbes in the inoculum. In the test series, a studied compound as the sole source of carbon was added to the inoculated mineral medium. The test compound was added in a concentration corresponding to theoretical oxygen demand (ThOD) of approximately 5 mg/L. ThOD was calculated assuming nitrification would take place as each of the 25 studied compounds included nitrogen atom(s) in their structure. The toxicity control series, containing both sodium acetate and the test compound in their respective concentrations, were used to evaluate test the compounds' toxicity against inoculum—if biodegradation values in these bottles were significantly lower compared to reference series, it was concluded that the test compound could be inhibiting or even being toxic to microbes in the WWTP effluent. To negate the effect of inoculum itself, blank bottles containing only inoculum and a mineral medium were added to each CBT run and the value of these bottles was subtracted from all the other bottles. To make sure seasonal variations in inoculum composition did not have an effect on biodegradation results, a total of 6 CBT runs from June to November were performed.

Inoculum. Effluent from a wastewater treatment plant was collected from a municipal wastewater treatment plant in Tallinn, Estonia (Paljassaare wastewater treatment plant, 59°27′55.5″ N 24°42′08.8″ E). WWTP effluent was filtered through a cellulose filter (membrane ø 240 mm) before being used as inoculum for aerobic biodegradation testing.

Results from each run were accepted if the following criteria were met: (i) difference in extremes of replicate values at the plateau is less than 20%, (ii) oxygen concentration in test series bottles must not fall below 0.5 mg/L at any time, (iii) sodium acetate in reference series must be degraded $\geq$ 60% by day 14. The blank bottles' oxygen consumption was also monitored to avoid the possibility of the system turning from aerobic to anaerobic. In the CBT runs, the oxygen consumption in all of the blank bottles did not exceed 34% of the initial oxygen concentration.

4.3. Ecotoxicity Assessment

Stock and working solutions

3N-BBM+V (Bold Basal Medium with 3-fold nitrogen and vitamins), as the algal culture medium, was prepared according to CCAP (Culture Collection of Algae and Protozoa) guidelines. Medium pH value was corrected to 8.00 $\pm$ 0.1.

4.4. Naturally Available Deep Eutectic Solvents (NADESs)

For all NADESs, a set of working concentrations was prepared, starting from 100 mg/L, which represents our 100%. Selected dilutions for each compound were 100–75–50–25–10–5–2.5–1%. Dilutions were carried out with algal culture medium 3N-BBM + V.

4.5. HBAs and HBDs

For each HBA and HBD, 1 g/L stock solution was prepared in ultrapure water. These stock solutions were further diluted to test the concentration of each individual component, matching the concentration they had in the corresponding NADES mixture. Dilutions were carried out with algal culture medium 3N-BBM + V. Results were plotted as percentages indicating the relative amount of compound at that tested NADES concentration.

4.6. Microalgal Bioassay

R. subcapitata was purchased from the reference center CCAP (Culture Collection of Algae and Protozoa—Scottish Association for Marine Science/SAMS Research Services Ltd., Oban, Scotland, UK). Axenic cultures were kept in 100 mL glass flask stored at 20 ± 2 °C, under natural white illumination (6000–8000 lx) with a 16:8 dark/light photoperiod. 3N-BBM + V was used for culturing *R. subcapitata*. Cultures were renewed every two weeks. The growth assessment of the freshwater alga *R. subcapitata* (batch: CCAP 1052/1A) was performed following ASTM procedures [71].

Before the test started, an algal working batch was prepared by inoculating 2 mL of maintenance cultures in 20 mL of fresh medium, maintaining it at 20 ± 2 °C under continuous illumination (6000–8000 lx) in order to obtain a logarithmic-phase algal culture. After 72 h, the algal concentration in the working batch was measured and diluted to reach a concentration of 10^6 cell/mL. For the growth inhibition bioassay, all samples at all concentrations were prepared in triplicate in sterile 24-well plastic plates. 20 µL of the diluted algal working batch was inoculated in each 2 mL replica of all samples and negative controls (medium). Plates were incubated at 20 ± 2 °C under continuous illumination (6000–8000 lx) for 72 h.

After 72 h, absorbance (λ = 670 nm) was measured in each well with a spectrophotometer (Jenway Genova Plus, Antylia Scientific, Chicago, IL, USA), using 1 cm optic-path plastic cuvettes. Algal concentration (Cells/mL) was calculated using the following equation, previously obtained by the CIBM (Livorno, Italy) research group:

$$Cells/mL = \frac{Abs_{670}}{8 \times 10^{-8}}$$

The reference toxicant was potassium dichromate. Stock solution was prepared by dissolving the dehydrated salt in ultrapure water at a concentration of 1 g/L. From the stock solution, five different concentrations of potassium dichromate were prepared, respectively, directly in algal growth medium (1.8–1–0.56–0.32–0.18) mg/L to check the reliability of the test. The results obtained for this assay fell into the laboratory control chart (EC_{50} 0.742 mg/L (0.648–0.808).

4.7. Statistical Analysis

For statistical analysis, two-way ANOVA was performed, followed by Tukey's multi-comparison test to evaluate the difference in algae growth between (1) DESs and control (2) HBA/HBD and control (3) DESs and HBA/HBD (4) HBAs and HBDs. Statistical analysis was performed with Graph-Pad Prism 7 software (GraphPad Software, La Jolla, CA, USA, www.graphpad.com, accessed on 30 April 2025). Statistically significant differences were reported with asterisks: $p < 0.05$ (*), $p < 0.01$ (**), $p < 0.001$ (***).

5. Conclusions

All the studied NADESs and the absolute majority of their components showed good biodegradation values (i.e., >60% = readily biodegradable). However, although they could be labeled as "green" and "safe" from a chemical point of view, they showed a clear stimulating effect of *R. subcapitata* growth. This effect was not always observed when single components were assessed at the same concentration as in the relative whole NADES, suggesting a putative synergistic effect for most of the substances while in the mixture. In particular, the NADESs with the most accentuate synergistic behavior were those containing betaine and proline, followed by those containing choline acetate and, less effectively, choline bitartrate. From observing different HBA/HBD combinations, results suggest that the hypothetical synergistic effect may be mainly linked to HBA

contribution. Considering that, it appears quite clear that to label NADESs as "green" or "eco-friendly", a deeper investigation on both molecular behavior in solutions and interactions at several organization levels, from molecules to ecosystem, is necessary in order to prevent unpredictable negative effects on the environment.

Supplementary Materials: The following supporting information can be downloaded at: https://www.mdpi.com/article/10.3390/molecules31020262/s1, Table S1: Tukey's multiple comparisons test data.

Author Contributions: N.M.N.: Conceptualization; methodology; investigation—biodegradability studies; data curation; validation; writing—original draft preparation. A.M. (Angelica Mero): Methodology; investigation—synthesis and analysis of NADESs. E.H.: Methodology; investigation—synthesis and purification of NADESs. Z.U.: Methodology; investigation—biodegradability study; writing—original draft preparation. M.O.: Investigation—synthesis and characterization of NADESs; data curation. M.V.S.: Methodology; investigation—ecotoxicity studies; data curation; validation; writing—original draft preparation. G.F.: Methodology; investigation—ecotoxicity studies; writing—original draft preparation. A.M. (Andrea Mele): Methodology; investigation—synthesis and properties of NADESs; data curation; writing—original draft preparation. A.M. (Andrea Mezzetta): Conceptualization; methodology; investigation—synthesis and properties of NADESs; resources, writing—original draft preparation; writing—reviewing and editing. N.G.: conceptualization; resources; funding acquisition; writing—reviewing and editing. L.G.: Conceptualization, funding acquisition; writing—reviewing and editing. C.P.: Conceptualization, methodology; resources; writing—reviewing and editing. Y.K.: Conceptualization, methodology; resources; funding acquisition; writing—reviewing and editing. All authors have read and agreed to the published version of the manuscript.

Funding: Funding from ERA-Net Cofund SUSFOOD2 Call 2017 (ImPrOVE) through Ministry of Rural Affairs of Estonia (Z.U., N.G., Y.K.) and through the Italian Ministry of University and Research (E.H., A.Mero, L.G.). L.G and A.M. acknowledge funding from European Union—Next Generation EU under the Italian Ministry of University and Research (MUR) project PRIN2022 SEED4GREEN—Code 20223W4RT9. N.M.N. and Y.K. acknowledge Marlen Taggu and AS Tallinna Vesi for providing wastewater treatment plant effluent for aerobic biodegradation tests.

Institutional Review Board Statement: Not applicable.

Informed Consent Statement: Not applicable.

Data Availability Statement: The original contributions presented in this study are included in the article. Further inquiries can be directed to the corresponding authors.

Conflicts of Interest: The authors declare that they have no known competing financial interests or personal relationships that could have appeared to influence the work reported in this paper.

Abbreviations

The following abbreviations are used in this manuscript:

ANOVA	Analysis of Variance
BBM	Bold Basal Medium
Bet	Betaine
CA	Citric Acid
CBT	Closed Bottle Test
ChA	Choline Acetate
ChCl	Choline Chloride
ChTA	Choline Tartarate (Bitartrate)
DES	Deep Eutectic Solvents
DGA	Diglycolic Acid
DMF	N,N-Dimethylformamide

EG	Ethylene Glycol
GA	Glycolic Acid
HBA	Hydrogen Bond Acceptor
HBD	Hydrogen Bond Donor
Im	Imidazole
ILs	Ionic Liquids
LA	Levulinic Acid
L-LacA	L-Lactic Acid
L-Pro	L-Proline
MA	Malic Acid
NADESs	Natural Deep Eutectic Solvents
OECD	Organisation for Economic Co-operation and Development
ThOD	Theoretical Oxygen Demand
WWTP	Wastewater Treatment Plant

Appendix A

Table A1. NADESs composition and molar ratio.

NADES	HBA	HBD	Molar Ratio
1.Bet:EG	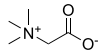 betaine	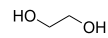 ethylene glycol	1:4
2.Bet:CA:water	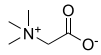 betaine	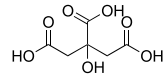 Citric acid	2:1:6
3.Bet:Gly	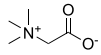 betaine	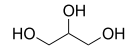 glycerol	1:2
4.Bet:LA	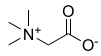 betaine	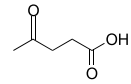 levulinic acid	1:2
5.Bet:L-LacA	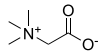 betaine	 L-lactic acid	1:1

Table A1. *Cont.*

NADES	HBA	HBD	Molar Ratio
6. L-Pro:Gly	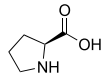 L-proline	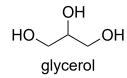 glycerol	1:2.5
7.L-Pro: L-LacA	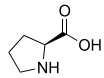 L-proline	 L-lactic acid	1:1
8.L-Pro:LA	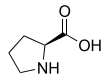 L-proline	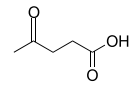 levulinic acid	1:2
9.ChTA:CA	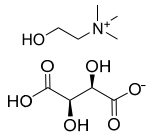 Choline bitartrate	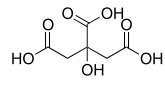 Citric acid	1:1
10.L-Pro:MA	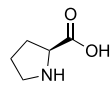 L-proline	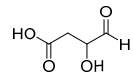 D,L-malic acid	1:1
11.ChA:Im	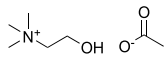 choline acetate	 Imidazole	1:1
12.ChA:LA	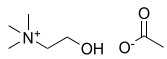 choline acetate	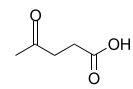 levulinic acid	1:1
13.ChA:GA	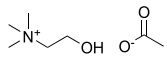 choline acetate	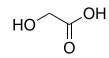 glycolic acid	1.1
14.ChA:DGA	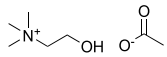 choline acetate	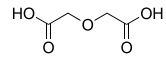 diglycolic acid	1:1
15.ChA:CA	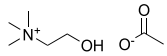 choline acetate	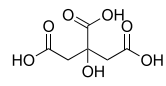 Citric acid	1:1

Table A2. NADESs and their single components, with the relative brutto-formula, molar mass, concentration for biodegradability test, and biodegradation achieved by CBT 301D (28 days).

NADES No.	HBA:HBD (Molar Ratio)	Structural Formula	Molar Mass (g/mol)	Test Substance (mg/L)	Biodegradation (28 days)
1	Bet:EG (1:4)	$C_{13}H_{35}NO_{10}$	365.42	3.57	76%
2	Bet:CA:water (2:1:6)	$C_{16}H_{42}N_2O_{17}$	371.86	5.06	70%
3	Bet:Gly (1:2)	$C_{11}H_{27}NO_8$	301.34	3.62	67%
4	Bet:LA (1:2)	$C_{15}H_{27}NO_8$	229.66	4.78	68%
5	Bet:L-LacA (1:1)	$C_8H_{17}NO_5$	263.759	3.60	70%
6	L-Pro:Gly (1:2.5)	$C_{13}H_{31}NO_{10}$	387.895	3.76	74%
7	L-Pro + L-LacA (1:1)	$C_8H_{15}NO_5$	205.210	3.77	65%
8	L-Pro:LA (1:2)	$C_{10}H_{21}NO_4$	347.364	3.29	69%
9	ChTA:CA (1:1)	$C_{12}H_{28}N_2O_6$	445.374	4.97	60%
10	L-Pro:MA (1:1)	$C_9H_{15}NO_7$	249.219	4.58	61%
11	ChA:Im (1:1)	$C_{10}H_{21}N_3O_3$	231.30	3.14	67%
12	ChA:LA (1:1)	$C_{12}H_{25}NO_6$	279.33	3.01	81%
13	ChA:GA (1:1)	$C_9H_{21}NO_6$	239.27	3.56	80%
14	ChA:DGA (1:1)	$C_{11}H_{23}NO_8$	297.30	3.87	77%
15	ChA:CA (1:1)	$C_{13}H_{25}NO_{10}$	373.36	4.32	66%
		Single NADES components			
	Betaine	$C_5H_{11}NO_2$	117.148	3.05	76%
	Ethylene glycol	$C_2H_6O_2$	62.068	3.88	65%
	Citric Acid	$C_6H_8O_7$	192.123	6.67	76%
	Glycerol	$C_3H_8O_3$	92.094	4.11	75%
	Levulinic Acid	$C_5H_8O_3$	116.116	3.30	72%
	L-Lactic Acid	$C_3H_6O_3$	90.078	4.69	65%
	L-Proline	$C_5H_9NO_2$	115.132	3.27	72%
	D,L-Malic Acid	$C_4H_6O_5$	134.087	6.98	73%
	Choline Acetate	$C_7H_{17}NO_3$	163.21	2.83	75%
	Imidazole	$C_3H_4N_2$	68.077	4.25	23%
	Glycolic Acid	$C_2H_4O_3$	76.05	7.92	79%
	Diglycolic Acid	$C_4H_6O_5$	134.09	6.98	76%
	Choline Bitartrate	$C_9H_{19}NO_7$	253.251	4.17	66%

References

1. Hessel, V.; Tran, N.N.; Asrami, M.R.; Tran, Q.D.; Van Duc Long, N.; Escribà-Gelonch, M.; Tejada, J.O.; Linke, S.; Sundmacher, K. Sustainability of Green Solvents—Review and Perspective. *Green Chem.* **2022**, *24*, 410–437. [CrossRef]
2. Winterton, N. The Green Solvent: A Critical Perspective. *Clean Technol. Environ. Policy* **2021**, *23*, 2499–2522. [CrossRef]
3. Sherwood, J.; Albericio, F.; de la Torre, B.G. *N*,*N*-Dimethyl Formamide European Restriction Demands Solvent Substitution in Research and Development. *ChemSusChem* **2024**, *17*, e202301639. [CrossRef]
4. Wang, Z.; Zhao, X.; Chen, Y.; Wei, C.; Jiang, J. A Review of Designable Deep Eutectic Solvents for Green Fabrication of Advanced Functional Materials. *RSC Sustain.* **2025**, *3*, 738–756. [CrossRef]
5. Zhang, Q.; De Oliveira Vigier, K.; Royer, S.; Jérôme, F. Deep Eutectic Solvents: Syntheses, Properties and Applications. *Chem. Soc. Rev.* **2012**, *41*, 7108–7146. [CrossRef]
6. Smith, E.L.; Abbott, A.P.; Ryder, K.S. Deep Eutectic Solvents (DESs) and Their Applications. *Chem. Rev.* **2014**, *114*, 11060–11082. [CrossRef]
7. Martins, M.A.R.; Pinho, S.P.; Coutinho, J.A.P. Insights into the Nature of Eutectic and Deep Eutectic Mixtures. *J. Solut. Chem.* **2019**, *48*, 962–982. [CrossRef]
8. Afonso, J.; Mezzetta, A.; Marrucho, I.M.; Guazzelli, L. History Repeats Itself Again: Will the Mistakes of the Past for ILs Be Repeated for DESs? From Being Considered Ionic Liquids to Becoming Their Alternative: The Unbalanced Turn of Deep Eutectic Solvents. *Green Chem.* **2023**, *25*, 59–105. [CrossRef]
9. Alizadeh, V.; Geller, D.; Malberg, F.; Sánchez, P.B.; Padua, A.; Kirchner, B. Strong Microheterogeneity in Novel Deep Eutectic Solvents. *ChemPhysChem* **2019**, *20*, 1786–1792. [CrossRef] [PubMed]

10. Mero, A.; Koutsoumpos, S.; Giannios, P.; Stavrakas, I.; Moutzouris, K.; Mezzetta, A.; Guazzelli, L. Comparison of Physicochemical and Thermal Properties of Choline Chloride and Betaine-Based Deep Eutectic Solvents: The Influence of Hydrogen Bond Acceptor and Hydrogen Bond Donor Nature and Their Molar Ratios. *J. Mol. Liq.* **2023**, *377*, 121563. [CrossRef]
11. Choi, Y.H.; van Spronsen, J.; Dai, Y.; Verberne, M.; Hollmann, F.; Arends, I.W.C.E.; Witkamp, G.J.; Verpoorte, R. Are Natural Deep Eutectic Solvents the Missing Link in Understanding Cellular Metabolism and Physiology? *Plant Physiol.* **2011**, *156*, 1701–1705. [CrossRef]
12. Vieira Sanches, M.; Freitas, R.; Oliva, M.; Mero, A.; De Marchi, L.; Cuccaro, A.; Fumagalli, G.; Mezzetta, A.; Colombo Dugoni, G.; Ferro, M.; et al. Are Natural Deep Eutectic Solvents Always a Sustainable Option? A Bioassay-Based Study. *Environ. Sci. Pollut. Res.* **2023**, *30*, 17268–17279. [CrossRef]
13. Usmani, Z.; Sharma, M.; Tripathi, M.; Lukk, T.; Karpichev, Y.; Gathergood, N.; Singh, B.N.; Thakur, V.K.; Tabatabaei, M.; Gupta, V.K. Biobased Natural Deep Eutectic System as Versatile Solvents: Structure, Interaction and Advanced Applications. *Sci. Total Environ.* **2023**, *881*, 163002. [CrossRef]
14. Azouz, H.H.; Hayyan, M. Preservation of Biological Systems and Materials Using Deep Eutectic Solvents: Pinnacles and Pitfalls. *Sep. Purif. Technol.* **2025**, *382*, 135584. [CrossRef]
15. Wen, Q.; Chen, J.X.; Tang, Y.L.; Wang, J.; Yang, Z. Assessing the Toxicity and Biodegradability of Deep Eutectic Solvents. *Chemosphere* **2015**, *132*, 63–69. [CrossRef]
16. Hayyan, M.; Hashim, M.A.; Al-Saadi, M.A.; Hayyan, A.; AlNashef, I.M.; Mirghani, M.E.S. Assessment of Cytotoxicity and Toxicity for Phosphonium-Based Deep Eutectic Solvents. *Chemosphere* **2013**, *93*, 455–459. [CrossRef] [PubMed]
17. Chen, Y.; Han, X.; Liu, Z.; Yu, D.; Guo, W.; Mu, T. Capture of Toxic Gases by Deep Eutectic Solvents. *ACS Sustain. Chem. Eng.* **2020**, *8*, 5410–5430. [CrossRef]
18. Chen, Y.; Mu, T. Application of Deep Eutectic Solvents in Biomass Pretreatment and Conversion. *Green Energy Environ.* **2019**, *4*, 95–115. [CrossRef]
19. Mero, A.; Mezzetta, A.; De Leo, M.; Braca, A.; Guazzelli, L. Sustainable Valorization of Cherry (*Prunus avium* L.) Pomace Waste via the Combined Use of (NA)DESs and Bio-ILs. *Green Chem.* **2024**, *26*, 6109–6123. [CrossRef]
20. Chen, Y.; Liu, Z.; Li, Y.; Tong, J.; Guo, Y.; Bi, Z.; Yang, X.; Wang, H.; Wang, J.; Zhao, D. Novel Reed + Deep Eutectic Solvent-Derived Adsorbents for Recyclable and Low-Cost Capture of Dyes and Radioactive Iodine from Wastewater. *Environ. Sci. Water Res. Technol.* **2022**, *8*, 2411. [CrossRef]
21. Chabib, C.M.; Ali, J.K.; Jaoude, M.A.; Alhseinat, E.; Adeyemi, I.A.; Al Nashef, I.M. Application of Deep Eutectic Solvents in Water Treatment Processes: A Review. *J. Water Process Eng.* **2022**, *47*, 102663. [CrossRef]
22. Yu, D.; Xue, Z.; Mu, T. Deep Eutectic Solvents as a Green Toolbox for Synthesis. *Cell Rep. Phys. Sci.* **2022**, *3*, 100809. [CrossRef]
23. Li, Y.; Luo, J.; Shan, S.; Cao, Y. High Toxicity of Amino Acid-Based Deep Eutectic Solvents. *J. Mol. Liq.* **2023**, *370*, 121044. [CrossRef]
24. Khorsandi, M.; Shekaari, H.; Mokhtarpour, M.; Hamishehkar, H. Cytotoxicity of Some Choline-Based Deep Eutectic Solvents and Their Effect on Solubility of Coumarin Drug. *Eur. J. Pharm. Sci.* **2021**, *167*, 106022. [CrossRef]
25. Rodríguez-Juan, E.; López, S.; Abia, R.; Muriana, F.J.G.; Fernández-Bolaños, J.; García-Borrego, A. Antimicrobial Activity on Phytopathogenic Bacteria and Yeast, Cytotoxicity and Solubilizing Capacity of Deep Eutectic Solvents. *J. Mol. Liq.* **2021**, *337*, 116343. [CrossRef]
26. Garralaga, M.P.; Lomba, L.; Leal-Duaso, A.; Gracia-Barberán, S.; Pires, E.; Giner, B. Ecotoxicological Study of Bio-Based Deep Eutectic Solvents Formed by Glycerol Derivatives in Two Aquatic Biomodels †. *Green Chem.* **2022**, *24*, 5228–5241. [CrossRef]
27. Lapeña, D.; Errazquin, D.; Lomba, L.; Lafuente, C.; Giner, B. Ecotoxicity and Biodegradability of Pure and Aqueous Mixtures of Deep Eutectic Solvents: Glyceline, Ethaline, and Reline. *Environ. Sci. Pollut. Res.* **2021**, *28*, 8812–8821. [CrossRef]
28. De Morais, P.; Gonçalves, F.; Coutinho, J.A.P.; Ventura, S.P.M. Ecotoxicity of Cholinium-Based Deep Eutectic Solvents. *ACS Sustain. Chem. Eng.* **2015**, *3*, 3398–3404. [CrossRef]
29. Ferreira, I.J.; Meneses, L.; Paiva, A.; Diniz, M.; Duarte, A.R.C. Assessment of Deep Eutectic Solvents Toxicity in Zebrafish (*Danio rerio*). *Chemosphere* **2022**, *299*, 134415. [CrossRef] [PubMed]
30. Brett, C.M.A. Perspectives for the Use of Deep Eutectic Solvents in the Preparation of Electrochemical Sensors and Biosensors. *Curr. Opin. Electrochem.* **2024**, *45*, 101465. [CrossRef]
31. Juneidi, I.; Hayyan, M.; Ali, M.; Ab, H. Evaluation of Toxicity and Biodegradability for Cholinium-Based Deep Eutectic Solvents. *RSC Adv.* **2015**, *5*, 83636–83647. [CrossRef]
32. Abbott, A.P.; Boothby, D.; Capper, G.; Davies, D.L.; Rasheed, R.K. Deep Eutectic Solvents Formed between Choline Chloride and Carboxylic Acids: Versatile Alternatives to Ionic Liquids. *J. Am. Chem. Soc.* **2004**, *126*, 9142–9147. [CrossRef]
33. Nejrotti, S.; Antenucci, A.; Pontremoli, C.; Gontrani, L.; Barbero, N.; Carbone, M.; Bonomo, M. Critical Assessment of the Sustainability of Deep Eutectic Solvents: A Case Study on Six Choline Chloride-Based Mixtures. *ACS Omega* **2022**, *7*, 47449–47461. [CrossRef]
34. Singh, B.S.; Lobo, H.R.; Shankarling, G.S. Choline Chloride Based Eutectic Solvents: Magical Catalytic System for Carbon–Carbon Bond Formation in the Rapid Synthesis of β-Hydroxy Functionalized Derivatives. *Catal. Commun.* **2012**, *24*, 70–74. [CrossRef]

35. Lu, C.; Cao, J.; Wang, N.; Su, E. Significantly Improving the Solubility of Non-Steroidal Anti-Inflammatory Drugs in Deep Eutectic Solvents for Potential Non-Aqueous Liquid Administration. *MedChemComm* **2016**, *7*, 955–959. [CrossRef]
36. Zdanowicz, M.; Jędrzejewski, R.; Pilawka, R. Deep Eutectic Solvents as Simultaneous Plasticizing and Crosslinking Agents for Starch. *Int. J. Biol. Macromol.* **2019**, *129*, 1040–1046. [CrossRef] [PubMed]
37. Liu, C.; Lei, J.; Liu, X.; Huang, Z.; Zhao, Y. Novel Ternary Deep Eutectic Solvent Coupled with In-Situ-Ultrasound Synergistic Extraction of Flavonoids from Epimedium Wushanense: Machine Learning, Mechanistic Investigation, and Antioxidant Activity. *Ultrason. Sonochem.* **2025**, *121*, 107547. [CrossRef] [PubMed]
38. Guglielmero, L.; Mero, A.; Koutsoumpos, S.; Kripotou, S.; Moutzouris, K.; Guazzelli, L.; Mezzetta, A. Choline Acetate-, L-Carnitine- and L-Proline-Based Deep Eutectic Solvents: A Comparison of Their Physicochemical and Thermal Properties in Relation to the Nature and Molar Ratios of HBAs and HBDs. *Int. J. Mol. Sci.* **2025**, *26*, 8625. [CrossRef]
39. Sernaglia, M.; Rivera, N.; Bartolomé, M.; Fernández-González, A.; González, R.; Viesca, J.L. Tribological Behavior of Two Novel Choline Acetate-Based Deep Eutectic Solvents. *J. Mol. Liq.* **2024**, *414*, 126102. [CrossRef]
40. Mangiacapre, E.; Barhoumi, Z.; Brehm, M.; Castiglione, F.; Di Lisio, V.; Triolo, A.; Russina, O. Choline Acetate/Water Mixtures: Physicochemical Properties and Structural Organization. *Molecules* **2025**, *30*, 3403. [CrossRef] [PubMed]
41. Di Pietro, M.E.; Tortora, M.; Bottari, C.; Colombo Dugoni, G.; Pivato, R.V.; Rossi, B.; Paolantoni, M.; Mele, A. In Competition for Water: Hydrated Choline Chloride:Urea vs Choline Acetate:Urea Deep Eutectic Solvents. *ACS Sustain. Chem. Eng.* **2021**, *9*, 12262–12273. [CrossRef]
42. Colombo Dugoni, G.; Mezzetta, A.; Guazzelli, L.; Chiappe, C.; Ferro, M.; Mele, A. Purification of Kraft Cellulose under Mild Conditions Using Choline Acetate Based Deep Eutectic Solvents. *Green Chem.* **2020**, *22*, 8680–8691. [CrossRef]
43. Abranches, D.O.; Silva, L.P.; Martins, M.A.R.; Pinho, S.P.; Coutinho, J.A.P. Understanding the Formation of Deep Eutectic Solvents: Betaine as a Universal Hydrogen Bond Acceptor. *ChemSusChem* **2020**, *13*, 4916–4921. [CrossRef] [PubMed]
44. Ferreira, I.J.; Paiva, A.; Diniz, M.; Duarte, A.R. Uncovering Biodegradability and Biocompatibility of Betaine-Based Deep Eutectic Systems. *Environ. Sci. Pollut. Res.* **2023**, *30*, 40218–40229. [CrossRef]
45. Rodrigues, L.A.; Cardeira, M.; Leonardo, I.C.; Gaspar, F.B.; Radojčić Redovniković, I.; Duarte, A.R.C.; Paiva, A.; Matias, A.A. Deep Eutectic Systems from Betaine and Polyols—Physicochemical and Toxicological Properties. *J. Mol. Liq.* **2021**, *335*, 116201. [CrossRef]
46. Benlebna, M.; Ruesgas-Ramón, M.; Bonafos, B.; Fouret, G.; Casas, F.; Coudray, C.; Durand, E.; Cruz Figueroa-Espinoza, M.; Feillet-Coudray, C. Toxicity of Natural Deep Eutectic Solvent Betaine:Glycerol in Rats. *J. Agric. Food Chem.* **2018**, *66*, 6205–6212. [CrossRef]
47. Nowacki, K.; Wysokowski, M.; Galiński, M. Synthesis and Characterization of Betaine-Based Natural Deep Eutectic Solvents for Electrochemical Application. *J. Mol. Liq.* **2025**, *424*, 127071. [CrossRef]
48. Jangir, A.K.; Bhawna; Verma, G.; Pandey, S.; Kuperkar, K. Design and Thermophysical Characterization of Betaine Hydrochloride-Based Deep Eutectic Solvents as a New Platform for CO_2 Capture. *New J. Chem.* **2022**, *46*, 5332–5345. [CrossRef]
49. Islam, S.; Rubio, C.; Rafikova, K.; Mutelet, F. Desulfurization and Denitrogenation Using Betaine-Based Deep Eutectic Solvents. *J. Chem. Eng. Data* **2024**, *69*, 2244–2254. [CrossRef]
50. Cysewski, P.; Jeliński, T.; Przybyłek, M. Exploration of the Solubility Hyperspace of Selected Active Pharmaceutical Ingredients in Choline- and Betaine-Based Deep Eutectic Solvents: Machine Learning Modeling and Experimental Validation. *Molecules* **2024**, *29*, 4894. [CrossRef]
51. Guo, H.-M.; Niu, H.-Y.; Xue, M.-X.; Guo, Q.-X.; Cun, L.-F.; Mi, A.-Q.; Jiang, Y.-Z.; Wang, J.-J. L-Proline in an Ionic Liquid as an Efficient and Reusable Catalyst for Direct Asymmetric α-Aminoxylation of Aldehydes and Ketones. *Green Chem.* **2006**, *8*, 682–684. [CrossRef]
52. Obregón-Zúñiga, A.; Milán, M.; Juaristi, E. Improving the Catalytic Performance of (S)-Proline as Organocatalyst in Asymmetric Aldol Reactions in the Presence of Solvate Ionic Liquids: Involvement of a Supramolecular Aggregate. *Org. Lett.* **2017**, *19*, 1108–1111. [CrossRef]
53. Nica Fernández-Stefanuto, V.; Corchero, R.; Rodríguez-Escontrela, I.; Soto, A.; Tojo, E. Ionic Liquids Derived from Proline: Application as Surfactants. *ChemPhysChem* **2018**, *19*, 2885–2893. [CrossRef] [PubMed]
54. Hao, L.; Wang, M.; Shan, W.; Deng, C.; Ren, W.; Shi, Z.; Lü, H. L-Proline-Based Deep Eutectic Solvents (DESs) for Deep Catalytic Oxidative Desulfurization (ODS) of Diesel. *J. Hazard. Mater.* **2017**, *339*, 216–222. [CrossRef]
55. Giri, C.; Karadendrou, M.-A.; Kostopoulou, I.; Kakokefalou, V.; Tzani, A.; Detsi, A. L-Proline-Based Natural Deep Eutectic Solvents as Efficient Solvents and Catalysts for the Ultrasound-Assisted Synthesis of Aurones via Knoevenagel Condensation. *Catalysts* **2022**, *12*, 249. [CrossRef]
56. Vachan, B.S.; Karuppasamy, M.; Vinoth, P.; Vivek Kumar, S.; Perumal, S.; Sridharan, V.; Menéndez, J.C. Proline and Its Derivatives as Organocatalysts for Multi- Component Reactions in Aqueous Media: Synergic Pathways to the Green Synthesis of Heterocycles. *Adv. Synth. Catal.* **2020**, *362*, 87–110. [CrossRef]

57. Zárate-Roldán, S.; Trujillo-Rodríguez, M.J.; Gimeno, M.C.; Herrera, R.P. L-Proline-Based Deep Eutectic Solvents as Green and Enantioselective Organocatalyst/Media for Aldol Reaction. *J. Mol. Liq.* **2024**, *396*, 123971. [CrossRef]
58. Assessment of Chemicals | OECD. Available online: https://www.oecd.org/en/topics/assessment-of-chemicals.html (accessed on 5 July 2024).
59. Levain, A.; Barthélémy, C.; Bourblanc, M.; Douguet, J.M.; Euzen, A.; Souchon, Y. Green Out of the Blue, or How (Not) to Deal with Overfed Oceans: An Analytical Review of Coastal Eutrophication and Social Conflict. *Environ. Soc.* **2020**, *11*, 115–142. [CrossRef]
60. Zhang, P.; Wang, T.; Zhang, H.; Wang, H.; Hilt, S.; Shi, P.; Cheng, H.; Feng, M.; Pan, M.; Guo, Y.; et al. Heat Waves Rather than Continuous Warming Exacerbate Impacts of Nutrient Loading and Herbicides on Aquatic Ecosystems. *Environ. Int.* **2022**, *168*, 107478. [CrossRef]
61. Silbiger, N.J.; Nelson, C.E.; Remple, K.; Sevilla, J.K.; Quinlan, Z.A.; Putnam, H.M.; Fox, M.D.; Donahue, M.J. Nutrient Pollution Disrupts Key Ecosystem Functions on Coral Reefs. *Proc. R. Soc. B* **2018**, *285*, 20172718. [CrossRef]
62. Leavitt, P.R.; Findlay, D.L.; Hall, R.I.; Smol, J.P. Algal Responses to Dissolved Organic Carbon Loss and PH Decline during Whole-Lake Acidification: Evidence from Paleolimnology. *Limnol. Oceanogr.* **1999**, *44*, 757–773. [CrossRef]
63. Baldwin, D.S.; Whittington, J.; Oliver, R. Temporal Variability of Dissolved P Speciation in a Eutrophic Reservoir—Implications for Predicating Algal Growth. *Water Res.* **2003**, *37*, 4595–4598. [CrossRef]
64. Zhao, B.Y.; Xu, P.; Yang, F.X.; Wu, H.; Zong, M.H.; Lou, W.Y. Biocompatible Deep Eutectic Solvents Based on Choline Chloride: Characterization and Application to the Extraction of Rutin from Sophora Japonica. *ACS Sustain. Chem. Eng.* **2015**, *3*, 2746–2755. [CrossRef]
65. Liu, Y.; Friesen, J.B.; Mcalpine, J.B.; Lankin, D.C.; Chen, S.-N.; Pauli, G.F. Natural Deep Eutectic Solvents: Properties, Applications, and Perspectives. *J. Nat. Prod.* **2018**, *81*, 679–690. [CrossRef] [PubMed]
66. Glibert, P.; Seitzinger, S.; Heil, C.; Burkholder, J.; Parrow, M.; Codispoti, L.; Kelly, V. The Role of Eutrophication in the Global Proliferation of Harmful Algal Blooms. *Oceanography* **2005**, *18*, 198–209. [CrossRef]
67. Nyholm, N. The European System of Standardized Legal Tests for Assessing the Biodegradability of Chemicals. *Environ. Toxicol. Chem.* **1991**, *10*, 1237–1246. [CrossRef]
68. OECD. *OECD Test Guidelines for Chemicals*; OECD: Paris, France, 1992.
69. Friedrich, J.; Längin, A.; Kümmerer, K. Comparison of an Electrochemical and Luminescence-Based Oxygen Measuring System for Use in the Biodegradability Testing According to Closed Bottle Test (OECD 301D). *CLEAN–Soil Air Water* **2013**, *41*, 251–257. [CrossRef]
70. Kitano, M. Updating of OECD Guidelines for the Testing of Chemicals. *Water Sci. Technol.* **1992**, *25*, 465–472. [CrossRef]
71. *ASTM E1218-21*; Standard Guide for Conducting Static Toxicity Tests with Microalgae. ASTM International: West Conshohocken, PA, USA, 2021.

Appendix 2

Publication II

Bondar, D.; Smirnova, O.; **Nagappa, N. M**.; Heinmaa, I.; Soukup, O.; Kobrlova, T.; Opravil, J.; Hrabinova, M.; Jun, D.; Starkov, P.; Spuul, P.; Kuča, K.; Mochalin, V. N.; Karpichev, Y. Nanodiamond Mediated Delivery of Pyridinium Oxime Antidotes to Central Nervous System for Potential Treatment of Exposure to Nerve Agents. *Chem. Biol. Interact.* **2025**, *420*, 111711. https://doi.org/10.1016/j.cbi.2025.111711

Chemico-Biological Interactions 420 (2025) 111711

Contents lists available at ScienceDirect

Chemico-Biological Interactions

journal homepage: www.elsevier.com/locate/chembioint

Nanodiamond mediated delivery of pyridinium oxime antidotes to central nervous system for potential treatment of exposure to nerve agents

Denys Bondar [a], Olga Smirnova [a], Nandish M. Nagappa [a], Ivo Heinmaa [b], Ondrej Soukup [c,d], Tereza Kobrlova [c], Jakub Opravil [d], Martina Hrabinova [d], Daniel Jun [d], Pavel Starkov [a], Pirjo Spuul [a], Kamil Kuča [e], Vadym N. Mochalin [f,g,*], Yevgen Karpichev [a,**]

[a] Department of Chemistry and Biotechnology, Tallinn University of Technology, 15 Akadeemia Rd., 12618, Tallinn, Estonia
[b] National Institute of Chemical Physics and Biophysics, 23 Akadeemia Rd., 12618, Tallinn, Estonia
[c] Biomedical Research Center, University Hospital Hradec Kralove, 581 Sokolska, 50005, Hradec Kralove, Czech Republic
[d] Department of Toxicology and Military Pharmacy, Military Faculty of Medicine, University of Defense, 1575 Trebesska, 50001, Hradec Kralove, Czech Republic
[e] Centre for Basic and Applied Research, Faculty of Informatics and Management, University of Hradec Kralove, 62 Rokitanskeho, 50 003, Hradec Kralove, Czech Republic
[f] Department of Chemistry, Missouri University of Science and Technology, Rolla, MO, 65409, USA
[g] Department of Materials Science & Engineering, Missouri University of Science and Technology, Rolla, MO, 65409, USA

ARTICLE INFO

Keywords:
Organophosphorus toxicants
Nanodiamonds
Oximes
Acetylcholinesterase reactivators
Blood-brain barrier
Central nervous system

ABSTRACT

Currently available antidotes against toxic organophosphorus compounds suffer from poor permeability across the blood-brain barrier (BBB) and due to this, are limited in their ability to restore the inhibited acetylcholinesterase (AChE) in the central nervous system (CNS). We designed functionalized detonation nanodiamond nanocarrier platforms to transport quaternary oxime antidotes into CNS. We showed that the nanodiamonds with covalently attached 4-oximinopyridinium moiety, cross the layer of Madin-Darby Canine Kidney (MDCK) cells, the surrogate BBB model, and demonstrate a dose-independent reactivation *in vitro* towards human AChE inhibited by nerve agents GB and VX, and pesticide paraoxon. Confocal microscopy visualization of tight junctions and actin cytoskeleton in MDCK and Human Umbilical Vein Endothelial Cells (HUVEC) revealed temporary disruption of tight junctions at higher nanoparticle concentrations without compromising cell viability or cytoskeletal integrity. Although reactivation was modest, the nanodiamond platform showed promise for delivering quaternary oxime to the central nervous system (CNS) *in vitro*. The results reveal the potential of detonation nanodiamonds as a promising delivery platform for charged therapeutic agents to CNS aimed to enhance treatment outcomes in organophosphorus poisoning.

1. Introduction

Acts of biological and chemical terrorism use toxic agents, for example, chemical warfare agents (CWA) to cause disease or death in man, animals, and plants [1]. Nanotechnology offers innovative and underutilized opportunities for defence against the threats of biological and chemical warfare [2]. Although the major world powers have agreed to abandon the use of CWAs [3], destroy their existing pilestocks [4], and control precursors, the key intermediates can be relatively easily synthesized [5]. The risk has also been enhanced by dual-use of artificial-intelligence-powered drug discovery, which could be misused for designing novel toxins [6]. Some of the most dangerous CWAs are the nerve agents [7] classified as G-agents, V-agents, and so-called A-agents known as Novichoks [8,9], which not long ago were used in attacks in the UK (Fig. 1A) [7]. Structurally similar to this group are organophosphorus (OP) pesticides [10,11]. The nerve agents inhibit serine esterases by covalently binding to a serine residue in the catalytic site of the enzyme [12]. Inhibition of human acetylcholine esterase (AChE) is the main mechanism for nerve agent toxicity resulting in the accumulation of neurotransmitter acetylcholine in synapses, leading to nervous

This article is part of a special issue entitled: ChEs and PON 2024 published in Chemico-Biological Interactions.

* Corresponding author. Department of Chemistry, Missouri University of Science and Technology, Rolla, MO, 65409, USA.
** Corresponding author. Department of Chemistry and Biotechnology, Tallinn University of Technology, 15 Akadeemia Rd., 12618, Tallinn, Estonia.
E-mail addresses: mochalinv@mst.edu (V.N. Mochalin), yevgen.karpichev@taltech.ee (Y. Karpichev).

https://doi.org/10.1016/j.cbi.2025.111711
Received 27 March 2025; Received in revised form 13 August 2025; Accepted 15 August 2025
Available online 16 August 2025

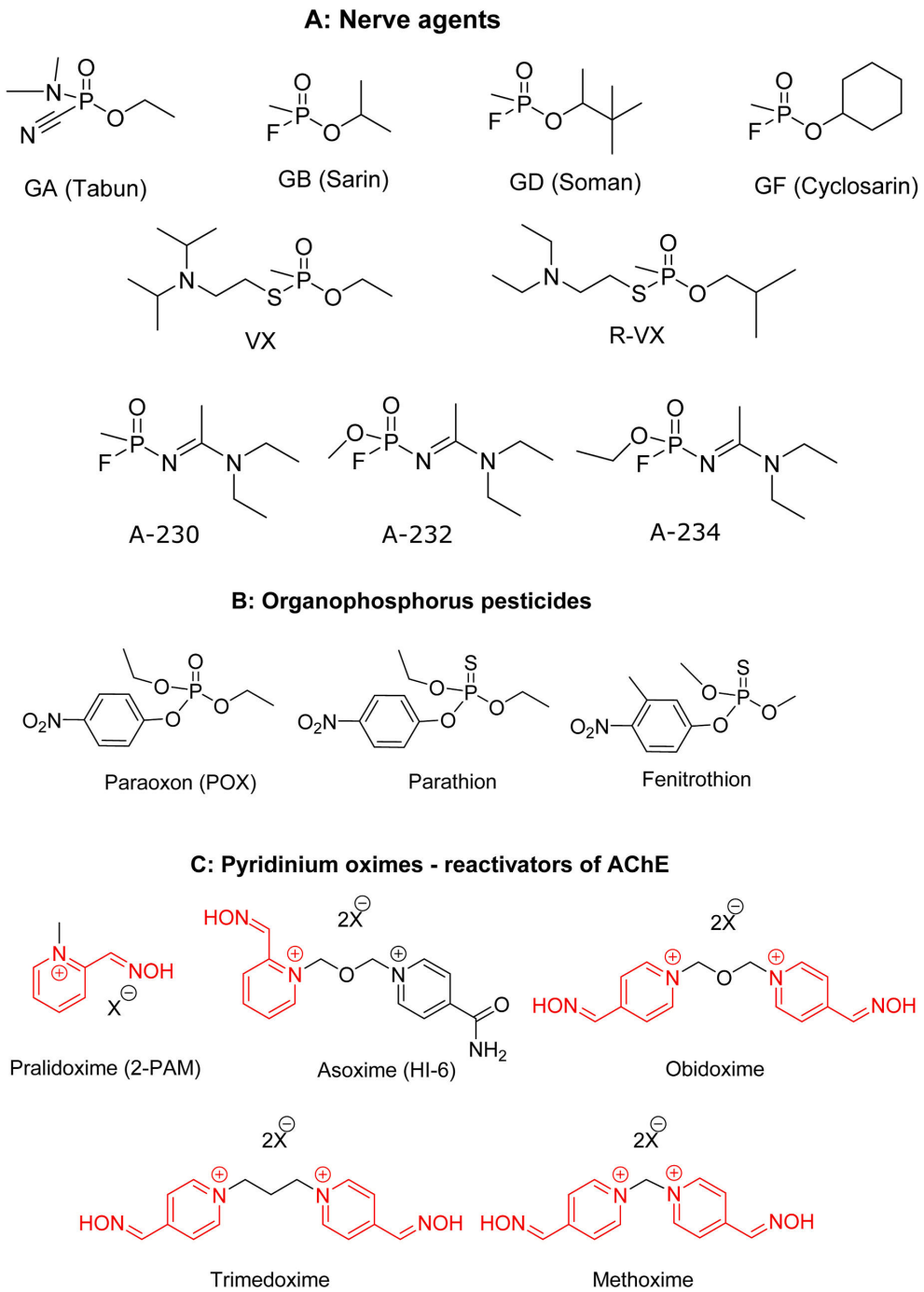

Fig. 1. Examples of toxic OP compounds and antidotes. (A) G-type, V-type, and A-type (Novichok) nerve agents. (B) Organophosphorus pesticides. (C) The most potent quaternary oximes - reactivators of the OP-inhibited AChE; the hydroximinomethyl pyridinium moiety is highlighted in color. (For interpretation of the references to color in this figure legend, the reader is referred to the Web version of this article.)

and respiratory failure and death within minutes of the exposure if it remains untreated [13].

Improving individual- and community-level resilience against potential attacks becomes part of sustained investment targeted at avoiding panic and reinforcing response if CWAs were used against civilians [14]. A core component of the "frontline" response to terrorism, first responders and spontaneous volunteers, will face health and safety risks requiring up-to-date protecting equipment and antidotes. Despite numerous efforts, there are still no available nerve agent antidotes that can easily cross the blood-brain barrier (BBB), effectively restore enzyme activity in the central nervous system (CNS) and prevent brain damage to improve survival rate and quality of life of the affected individuals [15]. Therefore, new delivery strategies enabling antidotes to cross the BBB efficiently are urgently needed.

Research on antidotes against OP poisoning continues for almost seven decades since pralidoxime (2-PAM) was employed [16], resulting in development of the potent AChE reactivators bearing hydroximinomethyl pyridinium fragment in their structure (Fig. 1C) [17,18]. Meanwhile, the efforts to improve oxime reactivation efficacy have yielded only a limited success [19–23] due to the presence of pyridinium moiety, which prevents access of the positively charged molecules to the CNS [24–27].

The current standard treatment of poisoning by toxic OP compounds usually consists of combined administration of anticholinergic drugs (atropine) and nucleophilic agents (quaternary oximes) [13,28]. Anticholinergic drugs block effects of the accumulated neurotransmitter acetylcholine, while the oximes reactivate AChE inhibited by the OP compounds [29–31]. However, the development of a versatile molecular scaffold with high efficiency towards inhibited AChE and ability to cross the BBB, remains a challenge [32]. Alternatively, poor accessibility of the quaternary oximes to the CNS can be improved by means of a delivery system, such as nanoparticle-based vehicle, capable of transporting the charged molecules across the BBB [33–36]. Our study focuses on this alternative approach, using nanodiamond particles as delivery vehicle.

The nanodiamonds (NDs) belong to the family of carbon nanoparticles (NPs) that have been attracting an increased interest of researchers over several decades due to their unique characteristics [37–39]. NDs possess diamond-like properties at the nanoscale, including chemically inert core, high Young's modulus, and fluorescence combined with tailorable surface chemistry [37,40,41] and fully accessible external surface in an ~5 nm diameter approximately spherical particle. Notably, NDs exhibited the lowest *in vitro* cytotoxicity among all carbon NPs [42]. There are several ways to fabricate NDs, which determine the properties of the resulting material [38,39,43,44]. The detonation NDs require post-synthesis purification through air oxidation [45] or ozone treatment [46], which in addition to removal of non-diamond carbon and mineral impurities, also homogenize surface chemistry *via* creation of carboxylic groups on the ND surface [39,41]. The uniform surface chemistry is crucial for further modification [47, 48]. Controlled surface modification enhances ND transport to target tissues and facilitates controlled drug release in cells and tissues [49–52]. Due to these outstanding properties, NDs were researched as a promising platform for drug delivery and biomedical applications [53–57]. In particular, NDs with covalently attached anticancer drug doxorubicin have been employed for targeted drug delivery to brain tumor cells [58]. Surface-modified NDs have been shown to induce reversible ND-mediated vascular barrier leakiness, akin to the enhanced permeability and retention (EPR) effect, which can be used to facilitate drug delivery through the *temporarily and reversibly* disrupted BBB [59–61]. In *ex vivo* mouse brain studies, the nanoparticles efficiently penetrated the blood-brain barrier without causing brain cell lesions or histomorphological changes, further confirming their biocompatibility and medical suitability [62].

In this study, we designed functionalized detonation NDs as non-toxic nanocarriers to transport covalently grafted oximinopyridinium AChE reactivators into the CNS. The nanoparticles with a pharmacophore covalently attached *via* biocompatible linker were prepared and characterized. We evaluated their ability to cross the BBB *in vitro* using MDCK and HUVEC cell lines as well-established models. The reactivation capacities of these ND based delivery vehicles towards human AChE inhibited by the CWAs sarin (GB) and VX, and by OP pesticide paraoxon (POX) were also studied. Although the observed enzyme reactivation efficiency in this first attempt remains low, it indicates the promise of this approach and highlights the necessity for further structural optimization and detailed mechanistic studies.

2. Results and discussion

Over the past decades, the transport of drugs by the nanocarriers (nanoparticles) across BBB has emerged as a method for drug delivery to the CNS [63,64]. Previous studies reported transport of noncovalently bound molecules by NDs in epithelial tissue cell lines but there were no reports on delivery of charged molecules across tight junction structures. In contrast to the epithelial cells, the BBB with abundant tight junctions represents an impermeable barrier to quaternary oxime antidotes. Our initial experiments confirmed this challenge: ND-COOH was unable to deliver noncovalently bound (adsorbed) quaternary oxime antidotes, pralidoxime (2-PAM) and asoxime (HI-6), through the MDCK cell monolayer (Supplementary S5 online). Hence, an alternative approach was explored in which NDs with covalently bound charged oxime AChE reactivator are transported across BBB.

A series of three oxime-grafted nanodiamonds was prepared starting from the highly pure ND-COOH material, as shown in Scheme 1 (detailed synthesis and characterization procedures are available in Supplementary S1 online). Functionalized fragments were synthesized using PEG3-diamine as a spacer and attaching 4-oximinomethylpyridine. Further modification of the functional fragments included reaction with haloacyl halides with different spacers ($n = 1, 2, 3$ for ND-A1, ND-A2, and ND-A3, correspondingly, see Scheme 1 and Supplementary S1 online). These constructs were coupled with ND-COOH using *N,N'*-carbonyldiimidazole as a coupling agent (Scheme 1 and Supplementary S1 online) [65,66].

Prior to cell imaging, intracellular uptake and reactivation capacity assays study, the obtained ND-based reactivators, ND-A1, ND-A2, and ND-A3 (Scheme 1), were characterized to confirm their structure and aggregation behavior.

2.1. Characterization of oxime-grafted nanodiamonds ND-A1, ND-A2, and ND-A3

Scanning Electron Microscopy. The morphologies of pristine (ND-COOH) and functionalized nanoparticles (ND-A1, ND-A2, and ND-A3) were characterized by SEM. All synthesized conjugates retain the overall texture and morphology of the starting material, albeit they visually appear slightly more agglomerated than ND-COOH (Fig. 2). Quantification and maximization of the number of oxime groups attached per ND particle is planned for future studies.

The most important characterization result, the evidence of covalent modification of the ND-COOH with functional groups, was obtained by FT-IR and NMR spectroscopy.

Infrared spectroscopy. Covalent binding employed in this work is based on chemistry of COOH groups on ND surface. FT-IR analysis clearly confirmed successful covalent functionalization of ND surfaces. The carboxyl functional groups on the surface of the starting ND-COOH material were detected using the characteristic O–H stretch (3420 cm^{-1}) and bend (1628 cm^{-1}) vibrations, as well as C═O stretch band at 1775 cm^{-1} (Fig. 3) [46,52]. Broad bands in the 'fingerprint region' (1000–1500 cm^{-1}) could be attributed to the combination of the overlapping peaks of C–O–C stretch and O–H deformational vibrations, epoxy C–O stretch and C–C stretch, see Supplementary S4 online.

In contrast to ND-COOH, the FT-IR spectra of ND-A1, ND-A2, and

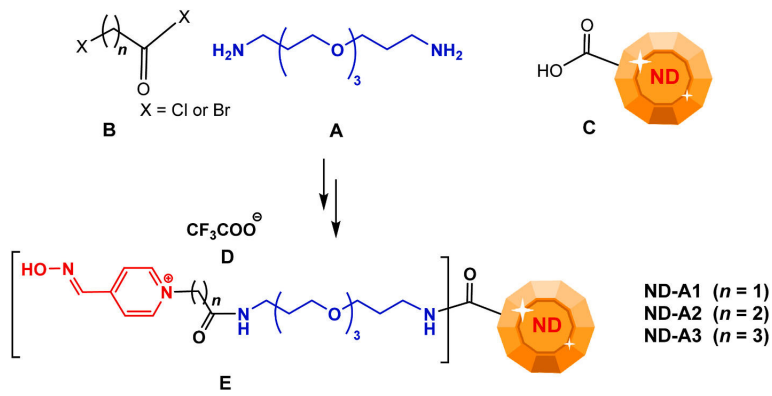

Scheme 1. Synthesis of oxime-functionalized nanodiamonds ND-A1, ND-A2, and ND-A3. Reactions and conditions: (A) PEG3-diamine, Boc_2O, DCM; (B) haloacyl halide, pyridine, DCM; (C) pyridine-4-carbaldoxime, acetonitrile; (D) CF_3COOH, DCM; (E) ND-COOH, N,N-carbonyldiimidazole, MeCN (more details in Scheme S1 and experimental procedure in Section S1); 4-hydroximininomethyl pyridinium fragment is highlighted in red, PEG3-diamine spacer is highlighted in blue.

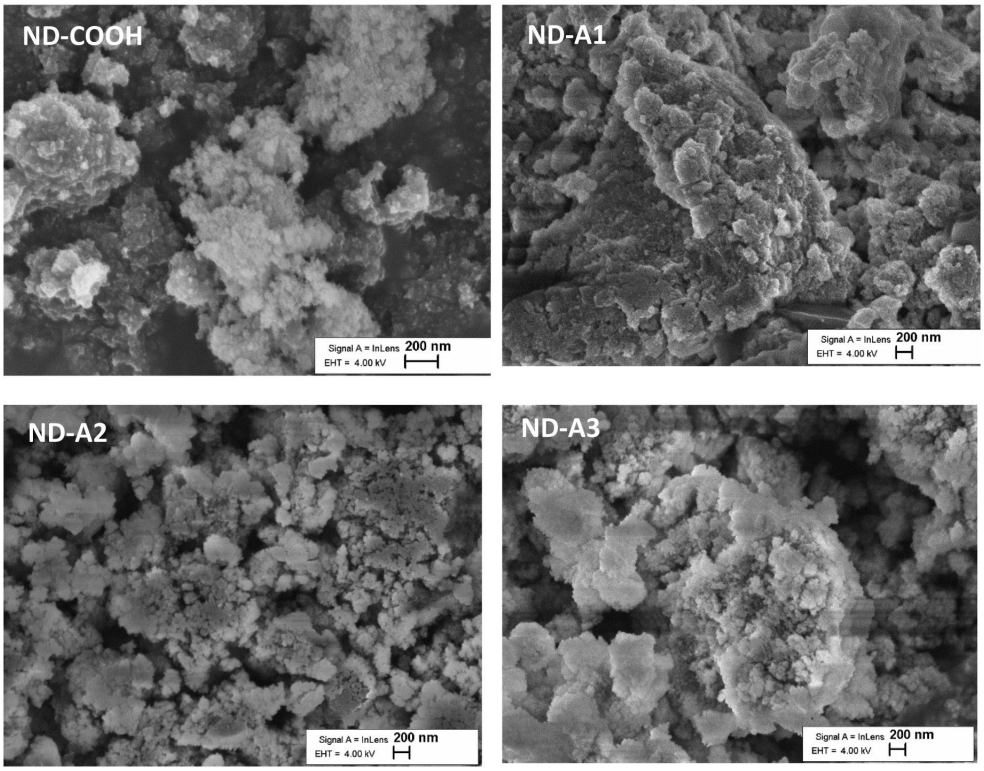

Fig. 2. SEM micrographs of nanodiamonds studied. (Top left) ND-COOH. The synthesized ND-oxime grafted nanodiamonds: (top right) ND-A1, (bottom left) ND-A2, and (bottom right) ND-A3.

ND-A3 showed new signals as the result of chemical modification. To confirm covalent attachment of molecules to nanoparticles in contrast to their adsorption, it is important to focus on specific FT-IR bands characteristic to either new bonds formed or the existing bonds that have been broken in the attachment reactions [40]. Coupling reaction of ND-COOH with 1,1′-carbonyldiimidazole (CDI) leads to formation of amide bonds, which were not present in the initial material nor in the coupling agent. Accordingly, the intensity of a broad O–H stretch band has decreased in the spectra of the conjugates compared to ND-COOH, and a new characteristic band of amide C(O)–N–H stretch near 3120 cm^{-1} appeared, accompanied by a red shift of the C═O stretch peak to 1670 cm^{-1}. Additionally, the peaks of C–H stretch at 2800-3000 cm^{-1}, C═N stretch near 1650 cm^{-1}, and aromatic C═C stretch between 1600 and 1500 cm^{-1} are seen in ND-A1, ND-A2, and ND-A3 (Fig. 3;

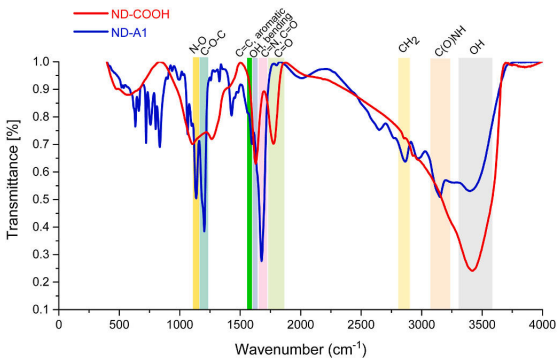

Fig. 3. FT-IR comparison spectra. (Red) ND-COOH. (Blue) ND-A1. (For interpretation of the references to color in this figure legend, the reader is referred to the Web version of this article.)

Supplementary S4 online), confirming the presence of methylene, amide, and pyridinium moieties, respectively.

^{13}C *MAS NMR*. The ^{13}C MAS NMR spectra of ND-COOH were obtained either *via* ^{1}H/^{13}C cross polarization (CP), which highlights carbons interacting with nearby protons (Fig. 4A), or *via* direct excitation followed by proton decoupling, revealing different types of carbons in the sample (Fig. 4B). Naturally, in the ND conjugates the number of carbon atoms adjacent to protons is significantly smaller than the total number of carbons. Peak deconvolution using Gaussians/Lorenzians (green lines in Fig. 4A and B) shows the contributions of different components (see also Table 1), while the red lines represent the convoluted spectra. Spinning sidebands (asterisks) appear at frequencies related to the sample spinning rate. Panels C and D in Fig. 4 display spectra of ND-A1, ND-A2, and ND-A3. They exhibit intensities in the direct excitation spectra approximately ten times greater than those obtained with the CP pulse sequence. The spectrum recorded without ^{1}H/^{13}C CP can be well described by eight different resonances with parameters given in Table 1. The most intense lines in the spectra with CP are ~40 times smaller than without CP (Fig. 4B). The ratio of combined intensity of carbon atoms in the two spectra corresponds to the anticipated fraction of carbon atoms on the surface of a ca. 5 nm diameter diamond particle [40,41,67]. Analysis of the CP spectrum shows that majority (60.8 %) of carbon atoms are composed by (i) typical graphite-like carbon 2C–CH_2 at 29.5 ppm and (ii) terminal 2C–CH_2 carbon at 37.5 ppm as, *e. g.,* in the core of adamantane, the smallest diamondoid. The resonance at 52 ppm (25.6 % of surface carbons and 12.6 % of all carbon atoms) could be assigned to the tertiary carbon, the peaks at 73 ppm (11.6 % of carbons and 5.7 % of all carbon atoms) and at 98 ppm (0.5 % of all carbon atoms) occur typically in alkyl moiety next to electron withdrawing groups. The spectrum obtained with direct excitation shows that at least half of the carbons are in the ND core sites, while the number of aromatic sp^2 carbons and COOH groups is relatively small. This agrees with the results reported in NMR studies of similar ND-COOH samples [68–70].

After surface modification, new peaks belonging to the ligand moiety appear in the spectra (Fig. 4C and D). The new peaks in the region of aromatic carbons at 120 ppm, 135 ppm, and 162 ppm can be assigned to pyridine ring, the new peak at 70 ppm to the carbons in [-C-C-*O*-] chains, and the peak at 29 ppm to sp^3 carbons of –CH_2- chains. The CP spectra of all three samples are similar, although the peaks in the aromatic region of ND-A1 and ND-A3 are weaker compared to ND-A2.

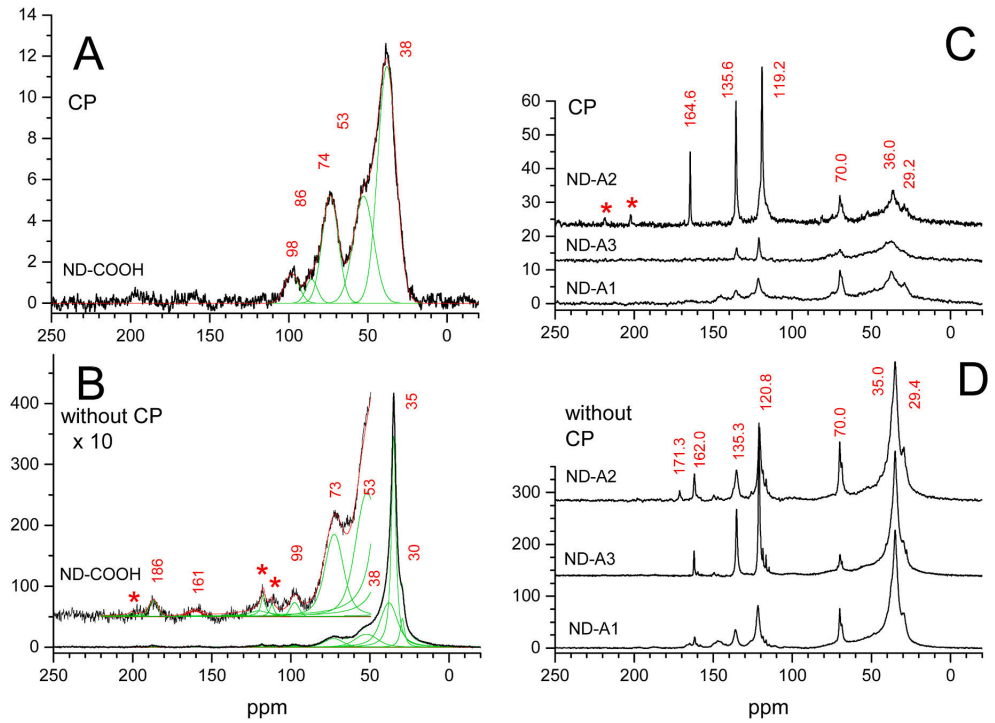

Fig. 4. ^{13}C MAS NMR spectra of ND-COOH and oxime-functionalized ND-A1, ND-A2, and ND-A3. (A, C) ^{1}H/^{13}C cross polarization (CP) sequence. (B, D) direct excitation (without CP).

Table 1
Chemical shift in the ^{13}C NMR spectrum. Measured (direct excitation) for ND-COOH with relative intensities contributed by different components.

	Core	Core, 4C–C	2C–CH_2	-CH_2-N-	2C–CH–*O*-	2C–C–2O	N–C═O C═N	COOH
Chemical shift (ppm)	29.5	34.9	37.5	51.8	72.8	98	161	187
Relative Intensity (%)	4.4	46.4	29.9	12.6	5.7	0.5	0.2	0.3

2.2. Size of the nanodiamond conjugates in colloidal solution

Particle size distributions of ND-COOH and oxime-functionalized ND-A1, ND-A2, and ND-A3 dispersed in demineralized water and phosphate buffer saline (PBS), modelling physiologically relevant environment, were measured by dynamic light scattering (DLS). The suspension of ND-COOH in MilliQ water is made up of two populations of the aggregates in the nanoscale range, a smaller population with hydrodynamic diameter ~30 nm and a larger fraction with a median above 200 nm (Fig. 5). ND-COOH in PBS showed a single fraction with the aggregates of ~250 nm diameter (Fig. 5). The higher degree of agglomeration in PBS may be attributed to the salting-out effect commonly occurring in electrolyte solutions. In PBS suspensions, ND-A1 showed high aggregation with hydrodynamic diameter 531 nm; ND-A2 produced two overlapping populations at 164 nm and 615 nm, respectively; and ND-A3 gave a broad distribution of fractions peaked at ~250 nm, see Fig. 5.

Overall, the data show that the introduction of organic moieties on the surface of ND-COOH leads to increased aggregation in PBS and water colloids. It should be also noted that the structure and nature of ND agglomerates are still debated and that these agglomerates are most likely weakly bonded and dynamic, meaning that at any moment of time there is an equilibrium between aggregated and disaggregated ND particles in solution, which shifts towards the single particles if their equilibrium concentration is reduced. Nonetheless, the observed aggregation is somewhat concerning, which maybe resolved by further optimization of dispersion methods.

2.3. Permeability and acetylcholinesterase reactivation

Permeability experiments with *in vitro* BBB model. The permeability of ND-A1 across the MDCK BBB model was studied in the double-well experiment and evaluated as the apparent permeability coefficient (P_{app}). In this model, compounds showing $P_{app} > 3 \times 10^{-6}$ cm/s have high potential to enter the CNS and compounds with $P_{app} < 1 \times 10^{-6}$ cm/s have very low chances to penetrate the BBB [71,72]. The MDCK assay evaluates the ability of compounds to permeate from the donor compartment through the MDCK cell membrane into the acceptor compartment. The concentration of ND-A1 or reference compounds in both compartments was measured by UV-VIS or fluorescence spectrophotometry (Table 2). Remarkably, the P_{app} value for ND-A1 extracted from these experiments is only about twice lower compared to either hormone testosterone or a reversible cholinesterase inhibitor donepezil, both known to be capable of crossing the BBB easily, and is similar to that of 7-methoxytacrine (7-MEOTA) [73]. In contrast, sulfasalazine (used here as negative standard), an antirheumatic drug with low lipophilicity and limited membrane crossing, showed P_{app} value ~26–30 times lower, see Table 2. Similarly, in the same experiments an established quaternary oxime antidote obidoxime (presented in Fig. 1) demonstrates an extremely low permeability, with P_{app} value comparable to that of sulfasalazine, see Table 2, as expected since low BBB permeability is a known long-standing issue for charged quaternary oxime antidotes.

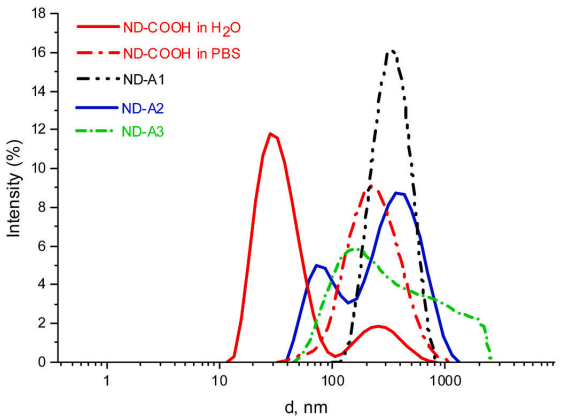

Fig. 5. Particle size distribution (represented as intensity of scattering) of nanodiamonds. (Red solid line) ND-COOH in MilliQ water. (Red dash-dotted line) ND-COOH in PBS. (Black dash-double dotted line) ND-A1 in PBS. (Blue dashed line) ND-A2 in PBS. (Green dash-dotted line) ND-A3 in PBS. (For interpretation of the references to color in this figure legend, the reader is referred to the Web version of this article.)

Interestingly, ND-A1 in a lower concentration (10 μg/mL in suspension) showed remarkably better permeability compared to higher concentration (100 μg/mL), see Table 2, which is probably due to an increased aggregation of functionalized NDs at higher concentrations [74–76] or to their accumulation inside the cells. Indeed, pilot measurement using cell lysis after the MDCK permeation experiment showed that approximately 13 % (for 10 μg/mL) and 30 % (for 100 μg/mL) of total amount of ND-A1 is accumulated inside the cells, confirming that NDs in higher concentrations tend to aggregate more and thus show a higher extent of intracellular entrapment.

Internalization of ND-A1 in the MDCK and HUVEC cells. We used the MDCK cells due to their unique capability to form an epithelial monolayer in a culture that contains functionally intact tight junctions to evaluate the uptake and internalization of ND-COOH and functionalized ND-A1. The ZO-1 antibody was used to stain tight junctions that appeared intact in non-treated cells (control in Fig. 6A). MDCK cells were treated with 10 μg/mL, 50 μg/mL, and 100 μg/mL of NDs for 1 h, 3 h, and 24 h. ND-COOH was visualized with brightfield imaging using differential interference contrast (DIC) (Fig. S1). ND-A1 exhibits intrinsic green fluorescence and therefore, its visualization is possible in a convenient way (Fig. 6 and Supplementary Fig. S2 online). We found that internalization of ND-A1 in MDCK cells is concentration-dependent, and the nanoparticles accumulated in the cells over time. We were not able to visualize ND-A1 added at 10 μg/mL inside the cells up to 24 h of

Table 2
Permeability of ND-A1 and reference compounds. Measured across the MDCK assay as *in vitro* BBB model.

Compound or material	Experimental estimation of BBB Penetration	CNS (±)
	P_{app} ± SD (× 10^{-6} cm s^{-1})	
ND-A1 10 μg/mL	14.55 ± 1.10	CNS +
ND-A1 100 μg/mL	4.68 ± 2.46	CNS ±
Testosterone	30.16 ± 3.99	CNS +
Donepezil	26.80 ± 2.70	CNS +
7-MEOTA	17.19 ± 3.56	CNS +
Sulfasalazine	0.96 ± 1.06	CNS -
Obidoxime	1.00 ± 0.33	CNS -

Note. CNS+ (green): stands for predicted BBB penetration; CNS (red): stands for no BBB penetration; CNS+/− (orange): stands for uncertain result.

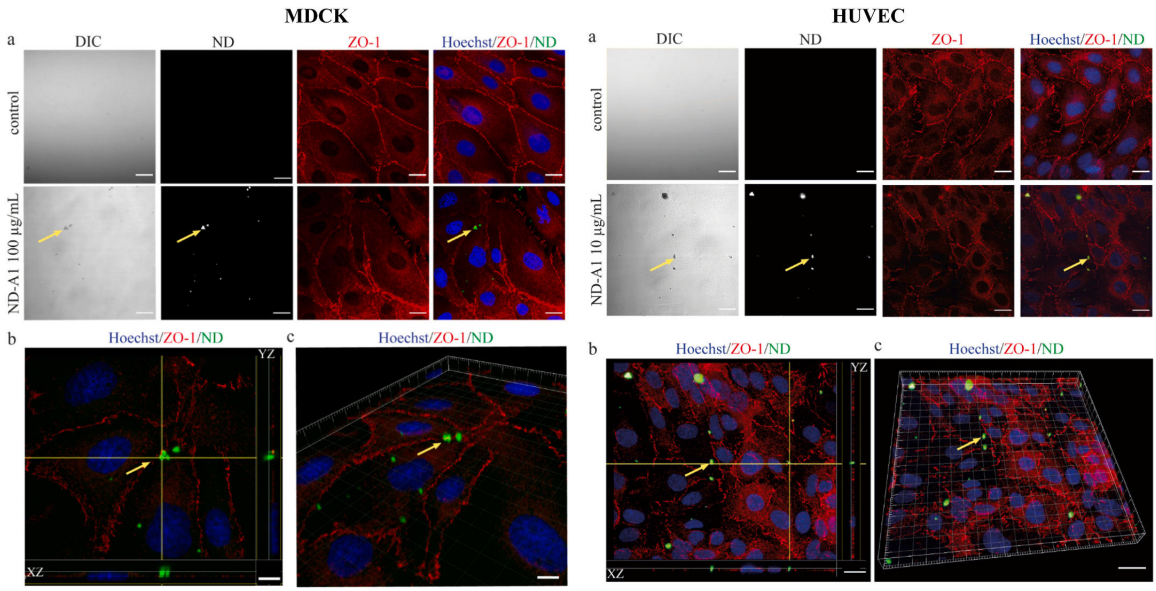

Fig. 6. Entry of ND-A1 into MDCK (left panel) and HUVEC (right panel) cells. (A) Confocal microscopy images show ND-A1 uptake in MDCK (left) and HUVEC (right) cells. The top panel presents untreated controls, while the bottom panel shows MDCK cells treated with 100 μg/mL ND-A1 for 3 h and HUVEC cells treated with 10 μg/mL ND-A1 for 1 h. Cells were fixed and stained with ZO-1 (red, cell junctions) and Hoechst 33342 (blue, nuclei). ND-A1 exhibits intrinsic fluorescence and appears green, visible through both DIC and 488 nm laser excitation. Merged images highlight internalized ND-A1 (yellow arrows). (B) Orthogonal views from the z-stack confirm intracellular localization of ND-A1 (yellow arrows).(C) 3D rendering further visualizes ND-A1 inside the cells, reinforcing its internalization. All images were processed using Imaris software. Scale bars: 20 μm. (For interpretation of the references to color in this figure legend, the reader is referred to the Web version of this article.)

exposure. The MDCK cells treated with 100 μg/mL ND-A1 for 3 h showed a clear intracellular ND-A1 fluorescence (Fig. 6A and Fig. S2), however, the tight junctions stained with ZO-1 seemed less intact and ruffled. The results are consistent with reported data on time- and concentration-dependent ND uptake *via* clathrin-mediated endocytosis [61]. The 3D reconstruction with Imaris software confirmed that the ND-A1 nanoparticles have successfully entered the MDCK cells as seen in the sectional and 3D view (Fig. 6A and C, left panel). Disruption of tight junctions was even more noticeable at 24 h (Fig. S2). Treatment of the cells with ND-COOH resulted in a similar concentration- and time-dependent intracellular accumulation of nanoparticles, and ZO-1 showed a similar change of its localization pattern over time as compared to the cells treated with ND-A1. Therefore, the internalization of our ND based conjugates is determined by the size and other properties of NDs and is not much sensitive to the attached molecules.

To confirm these results, another cell culture model of the human BBB, made of human umbilical endothelial cells (HUVEC), was employed. To enhance the cell-cell junctions, the cells were grown on gelatin-coated coverslips to a confluent layer and treated for 24 h with an astrocyte-conditioned medium mixed 50:50 with endothelial cell growth medium. As can be seen in the right panel of Fig. 6A the tight junctions stained by ZO-1 antibody are clearly visible but are less noticeable than in MDCK model, as expected. We observed that ND-A1 could successfully enter the HUVEC cells already at 1 h time point from the solution of the lowest concentration 10 μg/mL, see Fig. 6 right panel and Supplementary Fig. S3 online. The HUVEC cells were reconstructed using Imaris software and rotated to better illustrate the intracellular ND-A1 particles by using sectional and 3D view, see Fig. 6B and C, right bottom panel.

The tight junctions stained by ZO-1 were less pronounced in this cell line upon treatment with the nanoparticles, however, the difference between the ZO-1 patterns of untreated control and the cells incubated with our ND conjugates is obvious. Longer incubation periods with NDs disrupt the tight junctions between the cells considerably and in a concentration-dependent and time-dependent manner. The ND-A1 showed the formation of large aggregates upon entering the cell irrespective of their initial concentration, see Supplementary Fig. S5 online. However, the actin cytoskeleton of HUVEC cells seemed intact even after 24 h treatment with the highest concentration of NDs, see Supplementary Fig. S6 online. Therefore, the observations reveal that the ND-A1 nanoparticles were successfully internalized by the cells, supporting previous reports that NDs may induce temporary changes in cell permeability [61,77]. Although initial results suggest nanoparticle internalization *via* endocytosis without significant cytotoxicity, additional investigation is necessary to conclusively elucidate the internalization mechanism and its potential effect on tight junction integrity.

AChE reactivation using *in vitro* assays. Reactivation capacity of ND-A1, ND-A2, and ND-A3 towards human inhibited AChE was studied against their structural analogue 4-PAM (Scheme 1) as positive control and compared to four other selected pyridinium oximes (see structures in Fig. 1): pralidoxime (2-PAM), methoxime, obidoxime, and asoxime (HI-6). The reactivation capacities against human AChE inhibited by sarin, VX, and paraoxon for antidotes used in the doses of 10 μg/mL and 100 μg/mL for NDs and 10 μM and 100 μM for known quaternary oximes are presented in Table 3. The concentrations of the oximes converted into μg/mL are presented in the parentheses for comparison with the corresponding oxime-functionalized ND formulations.

These data show similar efficiency of ND conjugates to 4-PAM in their reactivation capacity towards POX- and VX-inhibited AChE. Importantly, although the values remain low compared to other pyridinium oximes, they are not lower than the corresponding values for 4-PAM. The lower dose of ND-A1 (10 μg/mL) revealing better permeability in the *in vitro* experiment, showed 3–4 times lower capacity than 2-PAM, methoxime, or asoxime (10 μM, which is equal to 1.75–3.59 μg/

Table 3
Reactivation potency of ND-A1, ND-A2, and ND-A3 and five selected quaternary oxime reactivators (4-PAM, pralidoxime, methoxime, obidoxime, and asoxime, see Fig. 1) against nerve agents- (GB, VX) and paraoxon- (POX) inhibited human AChE after 10 min of incubation.

Compound or material	GB		VX		POX	
	100 μg/mL (% ± SD)	10 μg/mL (% ± SD)	100 μg/mL (% ± SD)	10 μg/mL (% ± SD)	100 μg/mL (% ± SD)	10 μg/mL (% ± SD)
ND-A1	0.88 ± 0.35	0.58 ± 0.04	0.80 ± 0.00	0.70 ± 0.70	1.93 ± 0.92	1.93 ± 0.34
ND-A2	1.11 ± 0.41	1.17 ± 0.01	0.54 ± 0.47	0.71 ± 0.05	1.53 ± 0.38	2.48 ± 1.14
ND-A3	0.56 ± 1.74	1.13 ± 0.52	1.10 ± 0.45	0.82 ± 0.01	1.89 ± 0.44	0.95 ± 0.02
4-PAM	7.6[a] ± 0.6 (17.46[c])	0.1[b] ± 0.0 (1.75[c])	2.7[a] ± 0.2 (17.46[c])	0.4[b] ± 0.1 (1.75[c])	3.8[a] ± 0.6 (17.46[c])	1.9[b] ± 0.4 (1.75[c])
Pralidoxime (2-PAM)	35.8[a] ± 0.5 (17.46[c])	8.3[b] ± 0.3 (1.75[c])	9.2[a] ± 0.2 (17.46[c])	1.1[b] ± 0.0 (1.75[c])	28.9[a] ± 2.2 (17.46[c])	6.2[b] ± 0.4 (1.75[c])
Methoxime	30.2[a] ± 1.5 (32.92 [c])	6.1[b] ± 0.4 (3.29 [c])	12.0[a] ± 0.1 (32.92 [c])	1.5[b] ± 0.1 (3.29 [c])	40.5[a] ± 2.2 (32.92 [c])	8.0[b] ± 1.0 (3.29 [c])
Obidoxime	37.6[a] ± 1.3 (35.92 [c])	12.7[b] ± 0.1 (3.59 [c])	14.6[a] ±1.7 (35.92 [c])	1.5[b] ± 0.6 (3.59 [c])	66.5[a] ±1.2 (35.92 [c])	32.4[b] ± 2.2 (3.59 [c])
Asoxime (HI-6)	90.0[a] ± 2.6 (35.92 [c])	51.6 [b] ± 3.0 (3.59 [c])	48.8[a] ± 0.7 (35.92 [c])	4.2[b] ± 0.4 (3.59 [c])	27.1[a] ± 1.1 (35.92 [c])	5.6 [b] ± 2.2 (3.59 [c])

Note. 4-PAM, pralidoxime, methoxime, obidoxime, and asoxime were used in the experimental concentrations.
[a] 100 μM.
[b] 10 μM ((mean ± SD).
[c] the concentration of quaternary oxime reactivators in μg/mL is given in parentheses.

mL) in the case of POX, while obidoxime demonstrated remarkable 17-fold superiority. Reactivation capacity towards VX-inhibited AChE is 1.5–6 times higher for those oximes. Obidoxime and asoxime, the established antidotes-reactivators of AChE bearing 4-oximipyridinium moiety in their molecules (see Fig. 1) are most efficient towards sarin (GB), reaching 1-2 orders of magnitude, compared to ND-A1. The concentration-dependent effect was confirmed for all quaternary oximes (Table 3), whereas ND formulations demonstrated dose-independent behavior, which may be due to increased agglomeration of the functionalized NDs at higher concentrations. We note, however, that the use of ND conjugates in high concentrations is not practical anyway as their permeability across the BBB is lower at higher concentrations (see Table 2) and in general, nanoparticles are intended to be used in very low concentrations. Due to low reactivation efficiency (<2 %) registered in this first study, additional experiments with increased incubation time and alternative linker chemistries or improvement of the structure of the oximinopyridinium platform may be needed for further optimization of the ND formulations. Additionally, future comparative assays using non-conjugated oximes (3a, 3b, and 3c, Supplementary S3) will be essential to clearly assess the contribution of ND conjugation to reactivation efficiency.

Overall, these data illustrate the potential of the ND-based carriers to mediate the problem of AChE reactivation in CNS by facilitating the delivery of the antidotes bearing pyridinium oxime moieties across the BBB.

Cell viability and biodegradability. The viability of MDCK cells after treatment with ND-A1 was evaluated by MTT cytotoxicity assay showing the IC_{50} values higher than 500 μg/mL for all studied samples. It supports our prior assumption that the ND-A1 particles pass through the monolayer without hampering the cells in the BBB model assays. The NDs are non-toxic [78], so they are non-biodegradable and non-toxic nanomaterials [79–81]. The organic "corona" containing oxime moiety demonstrated insignificant biodegradability and did not pass the *readily* biodegradability Closed Bottle test OECD 301D, see Supplementary S9 and Supplementary Fig. S7 online. The *inherently* biodegradability may be reached in case of the extension of the experimental window [79], making oxime-grafted NDs suitable for special applications. Investigation into biodegradation under extended physiological conditions may also shed light on assessing environmental and clinical safety.

To summarize, the newly synthesized oxime-functionalized nanodiamonds are shown for the first time to be able to cross the cell monolayer model of the BBB without disrupting functionally intact tight junctions, particularly, at lower concentrations, and without damaging the cytoskeleton or exerting other cytotoxic effects on the MDCK and HUVEC cells. At higher concentrations, which we believe will not be practical, the functionalized NDs tend to aggregate in the cells within the time of the experiment. Nanodiamond-mediated delivery of positively charged moieties, antidotes against nerve agent poisoning, across the BBB opens doors to reactivation of AChE in CNS. Although the reactivation capacity measured in these initial experiments remains low, it compares favorably to the capacity of 4-PAM, structural analogue of our designed ND conjugates. At the same time, our results highlight the necessity for further structural optimization of the nanocarriers and oxime conjugation strategies to enhance their therapeutic efficacy.

3. Conclusion

This study presents an innovative approach for using functionalized nanodiamonds as a delivery platform for AChE antidotes across the BBB into the central nervous system. The 4-oximinopyridinium antidote was covalently linked to the ND-COOH particles *via* a biocompatible fragment. The designed ND conjugates were able to cross the well-established MDCK cell monolayer surrogate model of human brain-blood barrier. HUVEC-based assays were included as a human-derived endothelial model to support the findings. Initial microscopy results suggest concentration-dependent internalization of nanoparticles without significant disruption to tight junction integrity or cell viability; however, further clarification of internalization mechanisms is required. Although internalization was clearly observed, future studies should precisely determine the mechanisms involved and confirm reversibility of the minor disruption to tight junctions. However, we note that oxime-functionalized nanodiamonds do not seem to affect cell viability or integrity of the actin cytoskeleton. Most importantly, even in this first report, the oxime-modified nanodiamonds ND-A1 already showed low but measurable *in vitro* reactivation capacity towards human OP-inhibited AChE, which favorably compares to their structural analogue, 4-PAM. Given the observed low reactivation and issues of aggregation at higher concentrations, we believe that there is potential for further enhancement of the efficacy of the ND-based reactivators that can be achieved *via* optimization of the antidote structure and ND surface modification. Systematic evaluation of structure-activity relationships and optimization of nanoparticle dispersion methods may significantly improve therapeutic outcomes. In a broader context, this paper also shows that detonation NDs can be studied as delivery vehicles across the BBB for drugs used in treatment of other conditions and diseases specific to CNS, such as the Alzheimer disease, etc.

4. Materials and methods

Reagents and chemicals. All chemicals and solvents were purchased from Sigma–Aldrich, Alfa Aesar, Fisher Scientific or TCI Europe and used without further purification. Deionized water from a Milli-Q system was used in all sample preparations. Pralidoxime chloride was prepared in the Department of Toxicology and Military Pharmacy, Military Faculty of Medicine, University of Defense (Czech Republic).

Octadecylsilane-bonded silica gel SPE column (Phenomenex) was purchased from Chromservis s.r.o. (Czech Republic). GB (isopropyl methylphosphonofluoridate) and VX (*O*-ethyl *S*-diisopropylaminomethyl methylphosphonothiolate) with purity >95 % were obtained from the Military Technical Institute in Brno, Czech Republic. Paraoxon (*O,O*-diethyl *O*-(4-nitrophenyl) phosphate, POX) of analytical grade was purchased from Sigma–Aldrich.

Nanodiamond powder UD90 produced by detonation synthesis was supplied by NanoBlox, Inc., USA. The powder was characterized and purified from non-diamond carbon by a well-known standard procedure: oxidation in air followed by reflux in ~35 wt % aqueous HCl to remove traces of metals and metal oxides. After the HCl reflux, the ND was allowed to settle to the bottom of the flask. The excess HCl with dissolved salts was removed; ND powder was separated by centrifugation, rinsed multiple times with deionized water until neutral pH, and then dried in an oven at 110 C overnight. This purification procedure, as well as exhaustive characterization of the purified ND, were reported elsewhere [40,45,82–85]. The purified ND with acidic groups on the surface, labeled ND–COOH, was a starting material for all subsequent functionalization in this work. Oxime-functionalized NDs were prepared and purified as shown in detail in Supplementary S1 online, Fig. S8.

Characterization of products. ^{1}H and ^{13}C NMR spectra of the obtained compounds are presented in Supplementary S2 online. Ion exchange of TFA counterion in the final products was monitored by ^{19}F NMR following the procedure developed by Okaru et al. [86], see Supplementary Table S1 online. The High-Resolution Mass Spectroscopy (HRMS) identification of compounds was performed with an Agilent 6540 UHD Accurate-Mass Q-TOF LC/MS G6540A mass spectrometer. IR spectra were collected with a Tensor 27 FT-IR spectrometer. NMR spectra were recorded with Bruker Avance III 400 MHz NMR spectrometer operated at 400 MHz for ^{1}H NMR and 101 MHz for ^{13}C NMR. Spectra were recorded in deuterated chloroform ($CDCl_3$) or dimethyl sulfoxide (DMSO-d_6) where appropriate. All chemical shifts δ, ppm are relative to the internal standard TMS; coupling constants J are measured in Hertz (Hz). ^{13}C MAS NMR spectra were recorded with a Bruker AVANCE-II spectrometer at 14.1 T magnetic field using a home-built MAS probe for 25× 4 mm Si_3N_4 rotors, spinning at frequency 12.5 kHz. The spectra were recorded with a simple 90-degree pulse (4.5 μs) excitation followed by acquisition in high field ($H_1 = 100$ kHz) of proton decoupling. The relaxation delay between the excitations was 10 s. All intensities are normalized to the number of accumulations and to the weight of the sample to allow for quantitative estimates of the ratios of different carbon sites. Scanning electron microscopy (SEM) imaging was performed using Zeiss Ultra 55 with in-lens secondary electron detection at a 4 kV accelerating voltage.

Dynamic light scattering (DLS). The hydrodynamic diameter, particle size distribution, and zeta potential of the ND aggregates suspended in water and PBS were measured using ZetaSizer Nano S (Malvern Instruments) with He–Ne laser (633 nm, 10 mW) in back-scattering geometry ($\theta = 173°$). The data obtained was processed using Malvern DTS Software 7.11. Before the measurements, the samples were sonicated in TORBEO® 36810 Ultrasonic Cell Disruptor for 90 s (2 × 45 s) at 8 W effective radiated power for sonication. Suspension on NDs can be followed visually, see Supplementary S10 online.

MDCK assay double-well experiment. The Madin-Darby Canine Kidney (MDCK) assay was used to evaluate the diffusion through the MDCK cell membrane [87]. The cells were seeded on a polycarbonate membrane (1.12 cm^2 area with 3 μm pores) of the 12-well plates with 12 mm inserts. The apparent permeability coefficient (P_{app}) was calculated from Eq. (1):

$$P_{app} = \left(\frac{dC}{dt}\right) \cdot \frac{V_r}{(A \cdot C_0)} \quad (1)$$

A - area of the well/cell monolayer; dC/dt – rate of permeation; V_r - volume of the receiving compartment; C_0 - initial concentration of a tested compound. The tightness of MDCK monolayer was assessed by the permeability of fluorescein isothiocyanate (FITC) in concentration 0.4 mg/mL. Monolayer integrity was confirmed after each experiment, by ensuring that FITC level in the acceptor compartment did not surpass 1 % of its initial concentration in the donor compartment after 6 h.

HUVEC and MDCK assays for cell internalization studies. Pooled human umbilical vein endothelial cells (HUVEC) (200P–05 N) were cultured in Endothelial Cell Growth Medium (211–500), both from Cell Applications, Inc., passages between 3 and 6 were used. $7.5x10^4$ cells were plated for each experiment onto gelatin-coated coverslips (0.2 % gelatin, G1393-20 ML, Sigma). Astrocyte conditioned medium (1811, ScienCell Research Laboratories, Inc.) mixed 50:50 with Endothelial Cell Growth Medium was used to stimulate cell-cell junction formation. MDCK cells (84121903-1VL, Sigma-Aldrich) were cultured in Minimum Essential Medium (MEM) (15-010-CV, Corning®) supplemented with 10 % fetal bovine serum (FBS, Merck®). After forming confluent cell layers, NDs were added in 10, 50, or 100 μg/mL concentrations. Cells were incubated at 37 °C, 5 % CO_2 for 1, 3 or 24 h, followed by washing with PBS and fixation. CytoSMART cell counter (Corning™) was used for cell counting. Immunocytochemistry methods used for cell internalization studies are detailed in Supplementary S6 online.

Imaging and image analysis. The functionalized nanodiamonds ND-A1, ND-A2, and ND-A3 show bright green fluorescence, see Supplementary Fig. S9 online, when irradiated with ultraviolet light source with wavelength 254 nm and, in contrast to ND-COOH, can be successfully imaged by means of fluorescent and confocal microscopy. ND-treated stained cells were analyzed with confocal microscope Zeiss LSM 510 DUO using 63x/1.4 oil immersion objective and point scanning Ar lasers at wavelengths 488, 561 and 405 nm. Optical sectionals were acquired using sequential unidirectional scanning. Images were analyzed with Fiji ImageJ program [88] and Bitplane Imaris (Oxford Instruments) was used for 3D rendering and sectional view.

AChE reactivation assay. Reactivation potency of the oxime-grafted NDs and known reactivators pralidoxime, 4-PAM, methoxime, obidoxime, and asoxime was evaluated using human recombinant AChE. The enzyme was inhibited in phosphate buffer by GB (1 μM, 33 min), POX (1 μM, 45 min), and VX (0.1 μM, 45 min) dissolved in propan-2-ol. The concentrations and times were chosen to achieve complete enzyme inhibition. The excess of inhibitor was removed using octadecylsilane-bonded silica gel SPE cartridge. The inhibited AChE was incubated for 10 min with a reactivator solution (suspension) at 37 °C. Then the reaction was initiated by adding acetylthiocholine and AChE activity was measured spectrophotometrically at 412 nm, following the modified method of Ellman et al. [89], detailed previously [26,90,91]. Each concentration of reactivator was assayed in triplicate. The data from these assays were used to calculate reactivation potency R (Eq. (2)), corrected for oximolysis and inhibition of AChE by the reactivator.

$$R = \left(1 - \frac{\Delta A_0 - \Delta A_r}{\Delta A_0 - \Delta A_i}\right) \times 100\ [\%] \quad (2)$$

R - reactivation potency; ΔA_0 - absorbance change by intact AChE (propan-2-ol); ΔA_i - absorbance change by AChE after exposure to OP compounds.

***In vitro* cell viability assessment**. The standard MTT assay (Sigma–Aldrich) was used according to the manufacturer's protocol on the CHO–K1 (Chinese hamster ovary, ECACC, Salisbury, UK). The cells were cultured according to ECACC recommended conditions and seeded at a density of 8000 per well as described previously [92]. The tested compounds were dissolved (or dispersed in case of nanocarriers) in the F-12 growth medium. Cells were exposed to a tested compound for 24 h. Then the medium was replaced by a medium containing 10 μM of MTT and the cells were allowed to produce formazan for 3 h under surveillance. Thereafter, the medium with MTT was removed, crystals of formazan were dissolved in DMSO (100 μL), and cell viability was assessed spectrophotometrically by the amount of formazan produced, which was

determined spectroscopically. Absorbance was measured at 570 nm with 650 nm reference wavelength on Synergy HT (BioTek, USA). Half-maximal inhibitory concentration (IC_{50}) was calculated from the control-subtracted triplicates using four-parameter non-linear regression carried out in GraphPad Prism 5 software.

CRediT authorship contribution statement

Denys Bondar: Writing – original draft, Validation, Methodology, Investigation, Data curation. **Olga Smirnova:** Writing – original draft, Visualization, Methodology, Investigation, Formal analysis, Data curation. **Nandish M. Nagappa:** Writing – original draft, Investigation, Formal analysis, Data curation. **Ivo Heinmaa:** Writing – review & editing, Methodology, Investigation, Formal analysis. **Ondrej Soukup:** Writing – review & editing, Visualization, Methodology, Investigation, Data curation, Conceptualization. **Tereza Kobrlova:** Investigation, Data curation. **Jakub Opravil:** Investigation, Data curation. **Martina Hrabinova:** Investigation, Data curation. **Daniel Jun:** Writing – original draft, Resources, Investigation. **Pavel Starkov:** Writing – original draft, Methodology, Investigation. **Pirjo Spuul:** Writing – review & editing, Visualization, Supervision, Formal analysis, Conceptualization. **Kamil Kuča:** Writing – review & editing, Supervision, Conceptualization. **Vadym N. Mochalin:** Writing – review & editing, Supervision, Resources, Methodology, Conceptualization. **Yevgen Karpichev:** Writing – review & editing, Resources, Project administration, Methodology, Funding acquisition, Conceptualization.

Data availability statement

All data needed to evaluate the conclusions in the paper are present in the paper and/or the Supplementary Information.

Notes

The authors declare that they have no competing interests.

Declaration of competing interest

The authors declare the following financial interests/personal relationships which may be considered as potential competing interests: Yevgen Karpichev reports financial support was provided by North Atlantic Treaty Organization. Vadym Mochalin reports financial support was provided by US Army Research Office. Vadym Mochalin reports financial support was provided by National Eye Institute. Ondrej Soukup reports financial support was provided by Czech Science Foundation. Yevgen Karpichev, Vadym Mochalin have patent #US18/972,432 pending to Missouri S&T. If there are other authors, they declare that they have no known competing financial interests or personal relationships that could have appeared to influence the work reported in this paper.

Acknowledgments

In memory of Dr. Pavel Starkov, whose contribution to conceptualization and preparation of this paper was impactful. Although he is no longer with us, his dedication to science continues to inspire our research.

The authors express their appreciation to Maria Kuhtinskaja and Marina Kudrjašova, for their assistance in the products characterization, to Lucie Krbálek and Lucie Junova, for their technical assistance in the *in vitro* studies, and to Pia-Justina Wellmann, for her assistance in biodegradability studies of nanodiamonds.

DB and YK acknowledge funding from NATO SPS MYP grant No. G5565. OS and DJ acknowledge funding from the grant of Czech Science Foundation no 22-12859S. VNM acknowledges partial support from the Synthesis and Processing of Materials program in the Army Research Office (Project W911NF-18-1-0155) and the National Eye Institute of the National Institutes of Health under Award Number 1R15EY029813-01A1.

Appendix A. Supplementary data

Supplementary data to this article can be found online at https://doi.org/10.1016/j.cbi.2025.111711.

References

[1] F. Worek, T. Wille, M. Koller, H. Thiermann, Toxicology of Organophosphorus compounds in view of an increasing terrorist threat, Arch. Toxicol. 90 (2016) 2131–2145.
[2] M. Sharon, Nanotechnology to aid biological and chemical warfare defense, in: Nanotechnology in the Defense Industry, 2019, https://doi.org/10.1002/9781119460503.Ch6.
[3] P.J. Hotchkiss, The world's chemical-weapons stockpiles are gone — but A new challenge looms, Nature 623 (2023) 459.
[4] J.B. Tucker, The role of the chemical weapons convention in countering chemical terrorism, Terror. Political Violence 24 (2012) 105–119.
[5] P.F. Walker, A century of chemical warfare: building A world free of chemical weapons, One Hundred Years Chem. Warfare: Res. Deploy. Conseq. (2017) 379–400, https://doi.org/10.1007/978-3-319-51664-6_20.
[6] F. Urbina, F. Lentzos, C. Invernizzi, S. Ekins, Dual use of artificial-intelligence-powered drug discovery, Nat. Mach. Intell. 4 (2022) 189–191.
[7] D. Evison, D. Hinsley, P. Rice, Chemical weapons, BMJ 324 (2002) 332–335.
[8] D. Castelvecchi, Novichok nerve agents banned by chemical-weapons treaty, Nature (2019), https://doi.org/10.1038/D41586-019-03686-Y.
[9] M. Hrabinova, et al., A-Series agent A-234: initial in vitro and in vivo characterization, Arch. Toxicol. 98 (2024) 1135–1149.
[10] J. Bertolote, A. Fleischmann, M. Eddleston, D. Gunnell, Deaths from pesticide poisoning: a global response, Br. J. Psychiatry 189 (2006) 201–203.
[11] M.K. Mohan, et al., Oxime-functionalized anti-insecticide fabric reduces insecticide exposure through dermal and nasal routes, and prevents insecticide-induced neuromuscular-dysfunction and mortality, Nat. Commun. 15 (2024) 4844.
[12] R. Sharma, et al., Development and structural modifications of cholinesterase reactivators against chemical warfare agents in last decade: a review, Mini Rev. Med. Chem. 15 (2014) 58–72.
[13] H. Thiermann, N. Aurbek, F. Worek, Treatment of nerve agent poisoning, Issues Toxicol. 27 (2016) 1–42.
[14] B. Durodié, S. Wessely, Resilience or panic? The public and terrorist attack, Lancet 360 (2002) 1901–1902.
[15] L. Pulkrabkova, et al., Neurotoxicity evoked by organophosphates and available countermeasures, Arch. Toxicol. 97 (2023) 39–72.
[16] I. Wilson, B. Ginsburg, A powerful reactivator of Alkylphosphate-Inhibited acetylcholinesterase, Biochim. Biophys. Acta 18 (1955) 168–170.
[17] N. Singh, Y. Karpichev, A.K. Tiwari, K. Kuca, K.K. Ghosh, Oxime functionality in surfactant self-assembly: an overview on combating toxicity of organophosphates, J. Mol. Liq. 208 (2015) 237–252.
[18] J. Dhuguru, E. Zviagin, R. Skouta, FDA-approved oximes and their significance in medicinal chemistry, Pharmaceuticals 15 (2022) 66.
[19] A. Kovalevsky, D.K. Blumenthal, X. Cheng, P. Taylor, Z. Radić, Limitations in current acetylcholinesterase structure–based design of oxime antidotes for organophosphate poisoning, Ann. N. Y. Acad. Sci. 1378 (2016) 41–49.
[20] F. Worek, H. Thiermann, T. Wille, Oximes in organophosphate poisoning: 60 years of hope and despair, Chem. Biol. Interact. 259 (2016) 93–98.
[21] L. Gorecki, O. Soukup, J. Korabecny, Countermeasures in organophosphorus intoxication: pitfalls and prospects, Trends Pharmacol. Sci. 43 (2022) 593–606.
[22] G. Amitai, et al., Non-quaternary oximes detoxify nerve agents and reactivate nerve agent-inhibited human butyrylcholinesterase, Commun. Biol. 4 (2021) 573.
[23] L. Gorecki, J. Korabecny, K. Musilek, D. Malinak, E. Nepovimova, R. Dolezal, D. Jun, O. Soukup, K. Kuca, SAR study to find optimal cholinesterase reactivator against organophosphorous nerve agents and pesticides, Arch. Toxicol. 90 (2016) 2831–2859.
[24] Handbook of Toxicology of Chemical Warfare Agents, Elsevier, 2020, https://doi.org/10.1016/C2018-0-04837-9.
[25] L. Gorecki, et al., Rational design, synthesis, and evaluation of uncharged, "Smart" bis-oxime antidotes of organophosphate-inhibited human acetylcholinesterase, J. Biol. Chem. 295 (2020) 4079–4092.
[26] D. Jun, L. Musilova, K. Musilek, K. Kuca, *In Vitro* ability of currently available oximes to reactivate organophosphate pesticide-inhibited human acetylcholinesterase and butyrylcholinesterase, Int. J. Mol. Sci. 12 (2011) 2077–2087.
[27] B.J. Bennion, et al., Development of A CNS-Permeable reactivator for nerve agent exposure: an iterative, multi-disciplinary approach, Sci. Rep. 11 (2021) 15567.
[28] M. Eddleston, F.R. Chowdhury, Pharmacological treatment of organophosphorus Insecticide poisoning: the old and the (Possible) new, Br. J. Clin. Pharmacol. 81 (2016) 462–470.
[29] J. Renou, et al., Syntheses and *In Vitro* evaluations of uncharged reactivators for human acetylcholinesterase inhibited by organophosphorus nerve agents, Chem. Biol. Interact. 203 (2013) 81–84.

[30] G. Mercey, et al., Reactivators of acetylcholinesterase inhibited by organophosphorus nerve agents, Acc. Chem. Res. 45 (2012) 756–766.
[31] A.J. Franjesevic, et al., Resurrection and reactivation of acetylcholinesterase and butyrylcholinesterase, Chem. Eur J. 25 (2019) 5337–5371.
[32] K. Sakurada, H. Ohta, No promising antidote 25 years after the Tokyo subway sarin attack: a review, Leg. Med. 47 (2020) 101761.
[33] E. Barbu, É. Molnàr, J. Tsibouklis, D.C. Górecki, The potential for nanoparticle-based drug delivery to the brain: overcoming the blood-brain barrier, Expet Opin. Drug Deliv. 6 (2009) 553–565.
[34] A.M. Grabrucker, et al., Nanoparticle transport across the blood brain barrier, Tissue Barriers 4 (2016) E1153568.
[35] T. Kobrlova, J. Korabecny, O. Soukup, Current approaches to enhancing oxime reactivator delivery into the brain, Toxicology 423 (2019) 75–83.
[36] S. Ding, et al., Overcoming blood–brain barrier transport: advances in nanoparticle-based drug delivery strategies, Mater. Today 37 (2020) 112–125.
[37] K. Turcheniuk, V.N. Mochalin, Biomedical applications of nanodiamond, Nanotechnology 28 (2017) 252001 (Review).
[38] S.L.Y. Chang, P. Reineck, A. Krueger, V.N. Mochalin, Ultrasmall nanodiamonds: perspectives and questions, ACS Nano 16 (2022) 8513–8524.
[39] V.N. Mochalin, O. Shenderova, D. Ho, Y. Gogotsi, The properties and applications of nanodiamonds, Nat. Nanotechnol. 7 (2012) 11–23.
[40] V.N. Mochalin, et al., Covalent incorporation of aminated Nanodiamond into an epoxy polymer network, ACS Nano 5 (2011) 7494–7502.
[41] G.C.C. Costa, O. Shenderova, V. Mochalin, Y. Gogotsi, A. Navrotsky, Thermochemistry of Nanodiamond terminated by oxygen containing functional groups, Carbon 80 (2014) 544–550.
[42] X. Zhang, W. Hu, J. Li, L. Tao, Y. Wei, A comparative study of cellular uptake and cytotoxicity of multi-walled carbon nanotubes, graphene oxide, and nanodiamond, Toxicol. Res. 1 (2012) 62–68.
[43] B.I. Kharisov, O.V. Kharissova, L.S. Chávez-Guerrero, Synthesis techniques, properties, and applications of nanodiamonds, Synth. React. Inorg. Metal-Org. Nano-Metal Chem. 40 (2010) 84–101.
[44] V.V. Danilenko, On the history of the discovery of nanodiamond synthesis, Phys. Solid State 46 (2004) 581–584.
[45] S. Osswald, G. Yushin, V. Mochalin, S.O. Kucheyev, Y. Gogotsi, Control of Sp^2/Sp^3 carbon ratio and surface chemistry of nanodiamond powders by selective oxidation in air, J. Am. Chem. Soc. 128 (2006) 11635–11642.
[46] A. Kume, V.N. Mochalin, Sonication-assisted hydrolysis of ozone oxidized detonation nanodiamond, Diam. Relat. Mater. 103 (2020) 107705.
[47] W.-W. Zheng, et al., Organic functionalization of ultradispersed nanodiamond: synthesis and applications, J. Mater. Chem. 19 (2009) 8432–8441.
[48] A. Krueger, D. Lang, Functionality is key: recent progress in the surface modification of nanodiamond, Adv. Funct. Mater. 22 (2012) 890–906.
[49] V. Vaijayanthimala, et al., Nanodiamond-mediated drug delivery and imaging: challenges and opportunities, Expet Opin. Drug Deliv. 12 (2015) 735–749.
[50] J.M. Giammarco, V.N. Mochalin, J. Haeckel, Y. Gogotsi, The adsorption of tetracycline and vancomycin onto nanodiamond with controlled release, J. Colloid Interface Sci. 468 (2016) 253–261.
[51] Y.-A. Huang, et al., The effect of fluorescent nanodiamonds on neuronal survival and morphogenesis, Sci. Rep. 4 (2014) 6702.
[52] J. Beltz, et al., Effect of nanodiamond surface chemistry on adsorption and release of tiopronin, Diam. Relat. Mater. 100 (2019) 107590.
[53] V.N. Mochalin, et al., Adsorption of drugs on nanodiamond: toward development of a drug delivery platform, Mol. Pharm. 10 (2013) 3728–3735.
[54] F.F. An, X.H. Zhang, Strategies for preparing albumin-based nanoparticles for multifunctional bioimaging and drug delivery, Theranostics 7 (2017) 3667–3689.
[55] T. Lin, et al., Blood-brain-barrier-penetrating albumin nanoparticles for biomimetic drug delivery via albumin-binding protein pathways for antiglioma therapy, ACS Nano 10 (2016) 9999–10012.
[56] W.A. Banks, From blood-brain barrier to blood-brain interface: new opportunities for CNS drug delivery, Nat. Rev. Drug Discov. 15 (2016) 275–292.
[57] K.K. Liu, et al., Covalent linkage of nanodiamond-Paclitaxel for drug delivery and cancer therapy, Nanotechnology 21 (2010) 315103.
[58] X. Li, et al., TAT-conjugated nanodiamond for the enhanced delivery of doxorubicin, J. Mater. Chem. 21 (2011) 7966–7973.
[59] P. Moscariello, et al., Unraveling *In Vivo* brain transport of protein-coated fluorescent nanodiamonds, Small 15 (2019) 1902992.
[60] U. Roy, et al., Characterization of nanodiamond-based Anti-HIV drug delivery to the brain, Sci. Rep. 8 (2018) 16003.
[61] M.I. Setyawati, V.N. Mochalin, D.T. Leong, Tuning endothelial permeability with functionalized nanodiamonds, ACS Nano 10 (2016) 1170–1181.
[62] J. Kim, et al., A systematic study on the use of multifunctional nanodiamonds for neuritogenesis and super-resolution imaging, Biomater. Res. 27 (2023) 37.
[63] E. Nance, S.H. Pun, R. Saigal, D.L. Sellers, Drug delivery to the central nervous system, Nat. Rev. Mater. 7 (2022) 314–331.
[64] H. Helmbrecht, A. Joseph, M. Mckenna, M. Zhang, E. Nance, Governing transport principles for nanotherapeutic application in the brain, Curr. Opin. Chem. Eng. 30 (2020) 112–119.
[65] E.K. Woodman, J.G.K. Chaffey, P.A. Hopes, D.R.J. Hose, J.P.N. Gilday, *N*-Carbonyldiimidazole-Mediated amide coupling: significant rate enhancement achieved by acid catalysis with imidazole - HCl, Org. Process Res. Dev. 13 (2009) 106–113.
[66] N. Usachova, G. Leitis, A. Jirgensons, I. Kalvinsh, Synthesis of hydroxamic acids by activation of carboxylic acids with *N,N'*-Carbonyldiimidazole: exploring the efficiency of the method, Synth. Commun. 40 (2010) 927–935.
[67] J.-F. Cui, X.-W. Fang, K. Schmidt-Rohr, Quantification of C═C and C═O surface carbons in detonation nanodiamond by NMR, J. Phys. Chem. C 118 (2014) 9621–9627.
[68] A.M. Panich, Nuclear magnetic resonance studies of Nanodiamond surface modification, Diam. Relat. Mater. 79 (2017) 21–31.
[69] C. Presti, et al., NMR and EPR characterization of functionalized nanodiamonds, J. Phys. Chem. C 119 (2015) 12408–12422.
[70] O. Shenderova, et al., Hydroxylated detonation nanodiamond: FTIR, XPS, and NMR studies, J. Phys. Chem. C 115 (2011) 19005–19011.
[71] Q. Wang, et al., Evaluation of the MDR-MDCK cell line as A permeability screen for the blood–brain barrier, Int. J. Pharm. 288 (2005) 349–359.
[72] Z. Rankovic, CNS drug design: balancing physicochemical properties for optimal brain exposure, J. Med. Chem. 58 (2015) 2584–2608.
[73] O. Soukup, et al., A resurrection of 7-MEOTA: a comparison with tacrine, Curr. Alzheimer Res. 10 (2013) 893–906.
[74] C. Desai, K. Chen, S. Mitra, Aggregation behavior of nanodiamonds and their functionalized analogs in an aqueous environment, Environ. Sci., Process. Impacts 16 (2014) 518–523.
[75] A. Krüger, et al., Unusually tight aggregation in detonation nanodiamond: identification and disintegration, Carbon 43 (2005) 1722–1730.
[76] S.L.Y. Chang, D. Williams, M.R. Gutierrez, C. Dwyer, A.S. Barnard, Aggregation behavior of detonation nanodiamond in solution, Microsc. Microanal. 25 (2019) 1740–1741.
[77] K. Fox, et al., Nanodiamond-polycaprolactone composite: a new material for tissue engineering with sub-dermal imaging capabilities, Mater. Lett. 185 (2016) 185–188.
[78] A.M. Schrand, et al., Are diamond nanoparticles cytotoxic? J. Phys. Chem. B 111 (2007) 2–7.
[79] K. Kümmerer, J. Menz, T. Schubert, W. Thielemans, Biodegradability of organic nanoparticles in the aqueous environment, Chemosphere 82 (2011) 1387–1392.
[80] D. Daval, D. Xu, Biodegradation of materials: building bridges between scientific disciplines, npj Mater. Degrad. 7 (2023) 36.
[81] A. Mokhtari-Farsani, M. Hasany, I. Lynch, M. Mehrali, Biodegradation of carbon-based nanomaterials: the importance of "Biomolecular Corona" consideration, Adv. Funct. Mater. 32 (2022) 2105649.
[82] V.N. Mochalin, Y. Gogotsi, Wet chemistry route to hydrophobic blue fluorescent nanodiamond, J. Am. Chem. Soc. 131 (2009) 4594–4595.
[83] K. Turcheniuk, C. Trecazzi, C. Deeleepojananan, V.N. Mochalin, Salt-assisted ultrasonic deaggregation of nanodiamond, ACS Appl. Mater. Interfaces 8 (2016) 25461–25468.
[84] V.N. Mochalin, S. Osswald, Y. Gogotsi, Contribution of functional groups to the raman spectrum of nanodiamond powders, Chem. Mater. 21 (2009) 273–279.
[85] A. Pentecost, S. Gour, V.N. Mochalin, I. Knoke, Y. Gogotsi, Deaggregation of nanodiamond powders using Salt- and sugar-assisted milling, ACS Appl. Mater. Interfaces 2 (2010) 3289–3294.
[86] A.O. Okaru, et al., Application of ^{19}F NMR Spectroscosy for Content Decerminatdon of Fluorinatef Pharmaceutpcals, J. Anal. Methods Chem. 7 (2017) 9206297.
[87] L. Gorecki, et al., Structure-activity relationships of dually-acting acetylcholinesterase inhibitors derived from tacrine on *N*-Methyl-D-Aspartate receptors, Eur. J. Med. Chem. 219 (2021) 113434.
[88] J. Schindelin, et al., Fiji: an open-source platform for biological-image analysis, Nat. Methods 9 (2012) 676–682.
[89] G.L. Ellman, K.D. Courtney, V. Andres, R.M. Featherstone, A new and rapid colorimetric determination of acetylcholinesterase activity, Biochem. Pharmacol. 7 (1961) 88–95.
[90] D. Jun, et al., Reactivation of human acetylcholinesterase and butyrylcholinesterase inhibited by Leptophos-Oxon with different oxime reactivators *In Vitro*, Int. J. Mol. Sci. 11 (2010) 2856–2863.
[91] M. Hrabinova, J. Pejchal, V. Hepnarova, L. Muckova, L. Junova, J. Opravil, et al., A-series agent A-234: initial in vitro and in vivo characterization, Arch. Toxicol. 98 (2024) 1135–1149.
[92] K. Spilovska, et al., Novel tacrine-scutellarin hybrids as multipotent anti-alzheimer's agents: design, synthesis and biological evaluation, Molecules 22 (2017) 1006.

Abbreviations

AChE: acetylcholinesterase
BBB: blood-brain barrier
OP: organophosphorus
CWA: chemical warfare agents
CNS: central nervous system
DIC: differential interference contrast
DMSO: dimethyl sulfoxide;
EPR: enhanced permeability and retention (effect)
HUVEC: human umbilical vein endothelial
GB: isopropyl methylphosphonofluoridate (Sarin)
FITC: fluorescein isothiocyanate
ND: nanodiamonds
MAS NMR: the magic angle spinning nuclear magnetic resonance spectroscopy
MDCK: Madin-Darby canine kidney cell line;
MEM: minimum essential medium
2-PAM: 2-pyridinealdoxime methiodide;
4-PAM: 4-pyridinealdoxime methiodide;

PBS: phosphate buffer saline;
POX: O,O-diethyl *O*-(4-nitrophenyl) phosphate (paraoxon)
TFA: trifluoroacetic acid
TLC: thin layer chromatography
VX: O-ethyl *S*-diisopropylaminomethyl methylphosphonothiolate

Appendix 3

Publication III

Severin, O. O.; Bondar, D.; Bragina, O.; **Nagappa, N. M**.; Olev, J.; Brovarets, V. S.; Semenyuta, I. V.; Karpichev, Y. In Vitro Anticancer Activity and In Silico Target Profiling of 5-(Piperazin-1-Ylsulfonyl)-1,3-Oxazole-4-Carbonitriles. *Int J Mol Sci* **2026**, *27* (4), 1936. https://doi.org/10.3390/ijms27041936

International Journal of
Molecular Sciences

MDPI

Article

In Vitro Anticancer Activity and In Silico Target Profiling of 5-(Piperazin-1-ylsulfonyl)-1,3-oxazole-4-carbonitriles

Oleksandr O. Severin [1,2,†], Denys Bondar [1,3,†], Olga Bragina [1], Nandish M. Nagappa [1], Janari Olev [1], Volodymyr S. Brovarets [2], Ivan V. Semenyuta [2,*] and Yevgen Karpichev [1,*]

[1] Department of Chemistry and Biotechnology, Tallinn University of Technology (TalTech), 15 Akadeemia Rd., 12618 Tallinn, Estonia; nandish.mudegowdru@taltech.ee (N.M.N.)
[2] Department of Chemistry of Bioactive Nitrogen-Containing Heterocyclic Bases, V.P. Kukhar Institute of Bioorganic Chemistry and Petrochemistry of the NAS of Ukraine, Academician Kukhar Str., 1, 02094 Kyiv, Ukraine; brovarets@bpci.kiev.ua
[3] Department of Chemistry, Ghent University, Krijgslaan 281 (S3), 9000 Ghent, Belgium
* Correspondence: ivan@bpci.kiev.ua (I.V.S.); yevgen.karpichev@taltech.ee (Y.K.)
† These authors contributed equally to this work.

Abstract

Sulfonylated 5-piperazine-substituted 1,3-oxazole-4-carbonitriles were synthesized and evaluated for in vitro anticancer activity. Cytotoxicity was assessed in hepatocellular (HepG2, Huh7), breast (MCF-7, MDA-MB-231), cervical (HeLa), melanoma (M21), and neuroblastoma (Kelly, SH-SY5Y) cell lines, with HEK293 cells used as a non-malignant control. Compounds **7a**, **7b**, and **8aa** emerged as lead structures. Notably, compound **7b** showed the highest activity in Kelly neuroblastoma cells (IC_{50} = 1.3 μM) while exhibiting low cytotoxicity toward HEK293 cells (IC_{50} > 10 μM), indicating an improved selectivity profile relative to doxorubicin. In silico molecular docking suggested favorable interactions of the lead compounds with several cancer-associated proteins, with the highest predicted affinity observed for Aurora A kinase, along with additional predicted interactions with cyclin-dependent kinases. Predicted ADMET properties of compounds **7a**, **7b**, and **8aa** compared favorably with doxorubicin, although the lead compounds were not readily biodegradable under OECD 301D conditions. Overall, these findings identify oxazole-4-carbonitriles as promising anticancer candidates with a putative kinase-directed mechanism of action.

Keywords: oxazole; cancer; kinase; anticancer drugs; doxorubicin

Academic Editor: Georgia Zissimou

Received: 12 December 2025
Revised: 8 February 2026
Accepted: 13 February 2026
Published: 18 February 2026

1. Introduction

First reported in 1917, oxazoles became important after the discovery of penicillin antibiotics [1]. Structurally, oxazoles are planar, sp^2-hybridized five-membered rings with oxygen at position 1 and nitrogen at position 3, separated by carbon; see Figure 1 center. Their structure is isomeric to furan and pyridine. The electronic properties of oxazoles affect their reactivity, including participation in electrophilic and Diels–Alder reactions. Compared to pyridine, oxazoles are less resistant to oxidation, but more stable in acid and at elevated temperatures [2], facilitating their use in organic synthesis and drug development [3]. Their aromatic structure allows for substitutions at C-2, C-4, and C-5 to tune electronic, steric, and lipophilic properties. Oxazoles act as bioisosteres of amide or peptide bonds, enabling hydrogen bonding and molecular recognition, and serve as

drug-development building blocks via oxygen- and nitrogen-mediated interactions with enzymes and receptors [3].

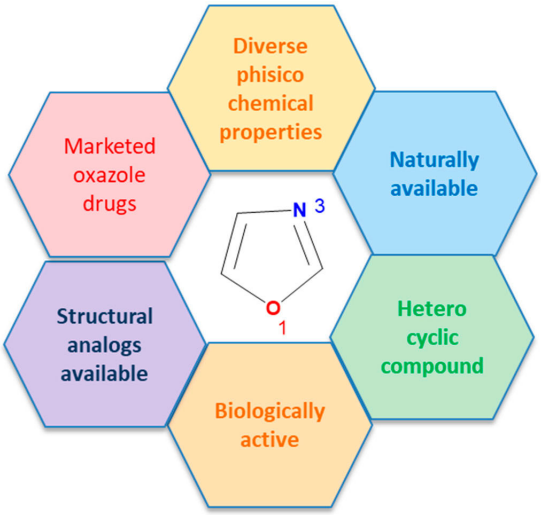

Figure 1. Key features and applications of oxazoles.

1,3-Oxazoles inhibit enzymes, block receptor activity, or interfere with microbial biosynthesis, supporting use as anticancer, antiviral, anti-inflammatory, and antibacterial agents; see Figure 2 [4]. Oxazole-containing drugs have been shown to demonstrate anticancer activity against multiple cancer types. Tivozanib, for example, binds the ATP-binding site and regulatory domain of VEGFR2, blocking autophosphorylation and signal transduction [5]. Also, the sulfonyl and cyano groups [5], and the piperazine moiety are present in various clinically used anticancer drugs: Prexasertib (Chk1 and Chk2 inhibitor) [6], Olaparib (PARP inhibitor) [6], Palbociclib (selective inhibitor of the cyclin-dependent kinases CDK4 and CDK6) [7], and Navitoclax (Bcl-2 inhibitor) [8] are the examples.

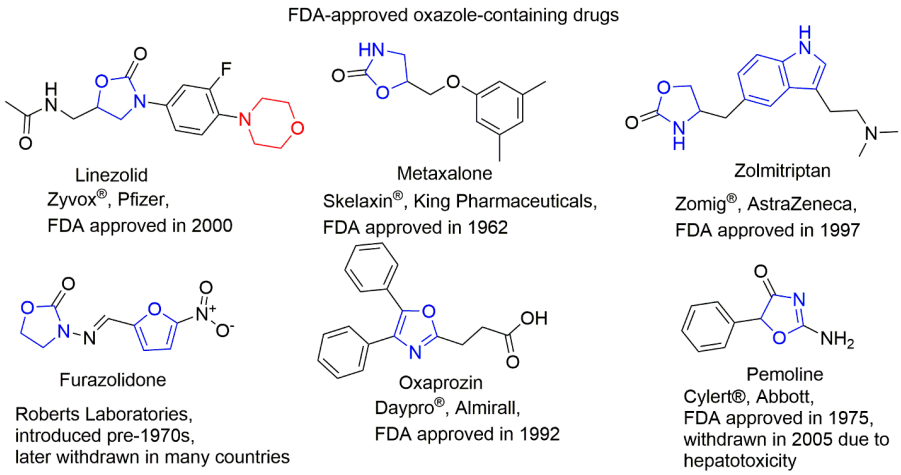

Figure 2. Clinical use of 1,3-oxazole-based drugs [2].

Cancer is the second leading cause of death worldwide. In 2018, it was responsible for nearly 9.6 million deaths and about 18.1 million new cases [9]. According to the 2025 report, cancer causes about 2.04 million new cases and 618 000 deaths each year in the United States, reflecting a rise among younger adults and women [10]. Kinase signaling is central in sustaining oncogenic development [11]. Thus, oxazoles are used in kinase inhibitor design, being potent inhibitors of class III receptor tyrosine kinases such as FLT3 (wild-type and mutant), FLT4, and c-KIT, with demonstrated activity in non-small-cell lung cancer [12]. Cyclin-dependent kinases (CDKs) regulate cell-cycle progression and transcription; however, high conservation of the ATP-binding site limits inhibitor selectivity [13]. The oxazole-based CDK7/9 inhibitor SNS-032 blocks RNA polymerase II phosphorylation, inducing transcriptional shutdown and cell death [14,15]. Oxazoles also target histone deacetylases 2 and 6) [15], poly(ADP-ribose) polymerase-2 (PARP-2) [16], and matrix metalloproteinases MMP-2 and MMP-9 [17], with antiproliferative effects in cervical, hepatocellular, breast, melanoma, and neuroblastoma cancers.

Cancer growth is associated with oncogene overexpression [18] and tumor suppressor inactivation [19], with MYCN amplification occurring in 20–25% of cases and correlating with aggressive disease [20]. N-MYC, one of three MYC subtypes proteins (C-MYC, L-MYC, and N-MYC), encodes a transcription factor [21] that regulates cell cycle, growth, apoptosis, DNA repair, metabolism, and immune response [22]. The stability of MYC protein is controlled by phosphorylation at the conserved MBI sequence, which directs proteolysis and ubiquitination [23]. Dephosphorylation of N-MYC at Ser62 by protein phosphatase 2A allows the SCF-FbxW7 E3 ubiquitin ligase to add a K48-linked ubiquitin chain [24]. Aurora-A kinase blocks this process, preventing metabolic degradation via an inhibitor-sensitive N-MYC/Aurora-A complex, leading to MYCN accumulation [25].

CD532 (IC_{50} = 45 nM; Figure 3, left) both inhibits Aurora A kinase activity and promotes MYCN degradation [26]. Alisertib (MLN8237; Figure 3, center) is an ATP-competitive Aurora A kinase inhibitor (IC_{50} = 1.2 nM) that disrupts cell cycle progression, induces apoptosis, and suppresses MYCN expression [27]. CCT137690 (Figure 3, right) is an isoxazole-containing compound that inhibits Aurora A (IC_{50} = 15 nM), Aurora B (IC_{50} = 25 nM), and Aurora C (IC_{50} = 19 nM), resulting in tumor growth inhibition in MYCN-overexpressing neuroblastoma models. These examples illustrate the therapeutic relevance of Aurora A kinase in neuroblastoma, while also highlighting the need for structurally diverse scaffolds capable of modulating Aurora A-associated pathways. In this study, a series of oxazole–piperazine–sulfonyl hybrids were synthesized and evaluated for their in vitro anticancer activity, with a primary focus on neuroblastoma models. Initial cytotoxicity screening identified compounds exhibiting selective activity against MYCN-amplified Kelly and SH-SY5Y neuroblastoma cell lines while sparing non-malignant HEK293 cells. The most active compounds (**7a, 7b**, and **8aa**) were further characterized by dose–response analyses and selectivity assessment, followed by evaluation of the lead compound **7b** across a broader panel of human cancer cell lines, including HeLa, HepG2, Huh7, MDA-MB-231, MCF7, and M21. To rationalize the observed biological profile, potential molecular targets were explored using in silico docking studies, and the pharmacokinetic properties of the lead compounds were assessed by ADME analysis.

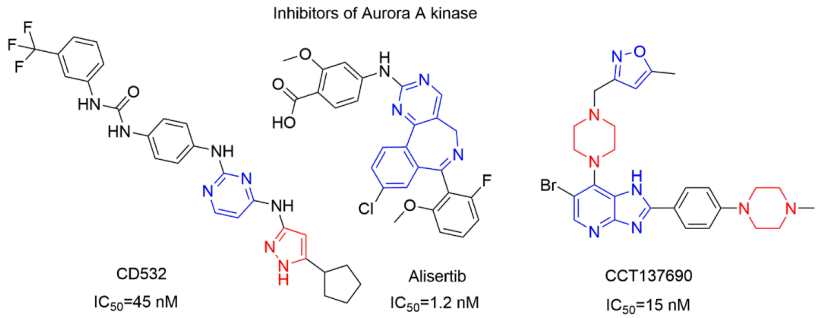

Figure 3. Inhibitors of Aurora A kinase.

2. Result and Discussion

2.1. Chemistry

Previously, we synthesized and studied sulfonyl derivatives of oxazole, which demonstrated significant antitumor activity. In our study several 5-arylsulfonyl-1,3-oxazole-4-carbonitriles exhibited high activity on the CNS cancer cell line [26]. In particular, the compound 2-(4-fluorophenyl)-5-(toluene-4-sulfonyl)-1,3-oxazole-4-carbonitrile demonstrated growth inhibition against glioblastoma cells SF-268 (GI_{50} = 4.61μM) and SF-539 (GI_{50} = 2.44 μM) and indicate low cytotoxicity with values LC_{50} >100 μM. Therefore, the anticancer activity of sulfonyl derivatives of 2-phenyl-4-cyano-1,3-oxazoles can be improved by inserting a piperazine moiety having multiple biotargets.

Synthesis of the target 5-(piperazin-1-yl)oxazole-4-carbonitriles **2a–2c** and **3aa–3ce** was carried out as follows (Scheme 1). First, the appropriate 2-acylamino-3,3-dichloroacrylonitriles **I** were dissolved in anhydrous THF, in the presence of triethylamine, and then Boc-protected piperazine was added, and the reaction mixture was stirred at 20–25 C for 48h. To remove the Boc-protecting group, the intermediate products **IA** were dissolved in dioxane, and hydrogen chloride gas was bubbled through the solution for 30 min. The reaction mixture was then left to stand for 24h. With the corresponding 5-(piperazin-1-yl)oxazole-4-carbonitrile hydrochlorides (**2a–2c**) in solution 1,4-dioxane, triethylamine was added, followed by the appropriate sulfonyl chloride. The reaction mixture was stirred and refluxed for 8h. The final products **3aa–3ce** were purified by recrystallization from EtOH.

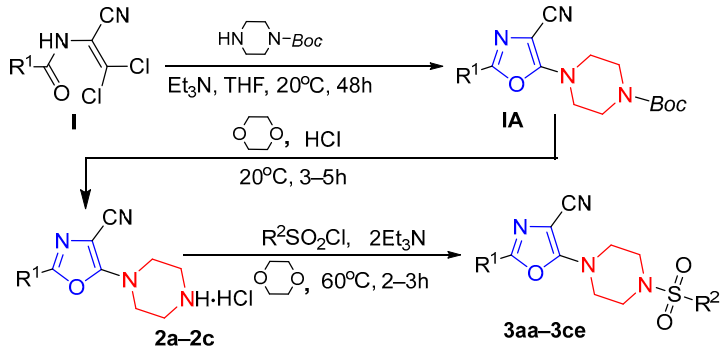

Scheme 1. General procedure for the synthesis of 5-(piperazin-1-yl)oxazole-4-carbonitrile hydrochlorides **2a–2c** and 5-(sulfonylpiperazin 1-yl)oxazole-4-carbonitriles **3aa–3ce**; the starting 2-acylamino-3,3-dichloroacrylonitriles are designated as (**I**), their Boc-protected piperazine derivatives are designated as (**IA**).

The structure-synthesized compound **2a**–**2c** and **3aa**–**3ce** is shown in Figure 4.

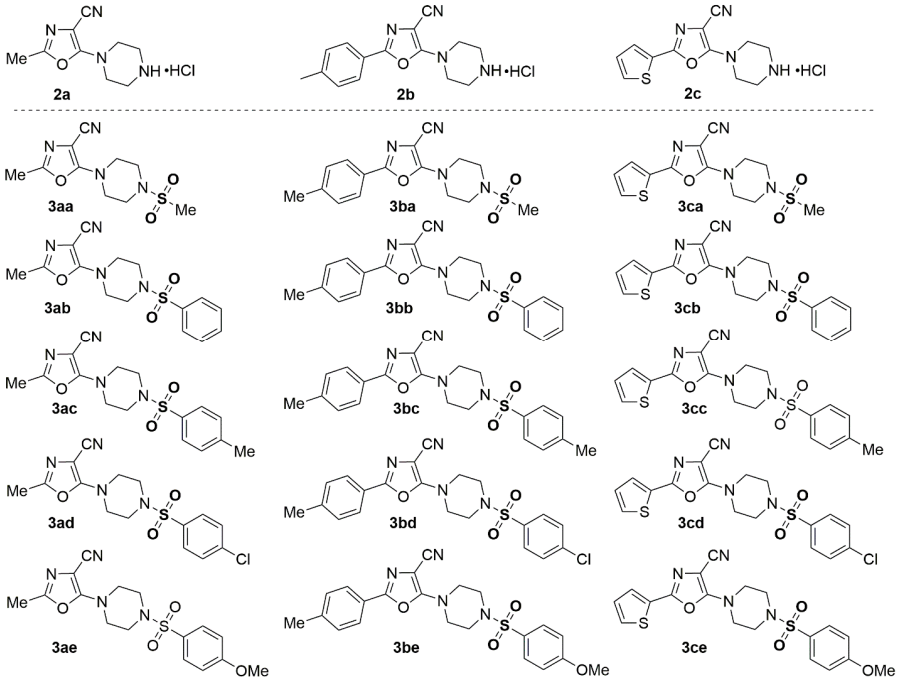

Figure 4. Structure of compounds **2a**–**2c** and **3aa**–**3ce**.

The target 5-(piperazin-1-ylsulfonyl)oxazole-4-carbonitriles were synthesized according to the procedure (Scheme 2). The corresponding 2-acylamino-3,3-dichloroacrylonitriles **I** were used as starting materials. Their reaction with an excess of NaSH in methanol solution led to cyclization, yielding substituted 5-mercaptooxazoles **II**. Alkylation of compounds 2 with benzyl chloride in ethanol in the presence of triethylamine afforded substituted 1,3-oxazoles **3** bearing a benzylthio group at position 5 of the oxazole ring. Oxidative chlorination of compounds **III** in aqueous acetic acid at 0–5 °C produced 2-aryl-4-cyano-1,3-oxazole-5-sulfonyl chlorides **IV**. Reaction of these intermediates with 1-phenylpiperazine in dioxane in the presence of excess triethylamine gave the corresponding 2-aryl-5-(4-phenylpiperazin-1-yl)sulfonyl-1,3-oxazole-4-carbonitriles **5a, 5b** (Scheme 2).

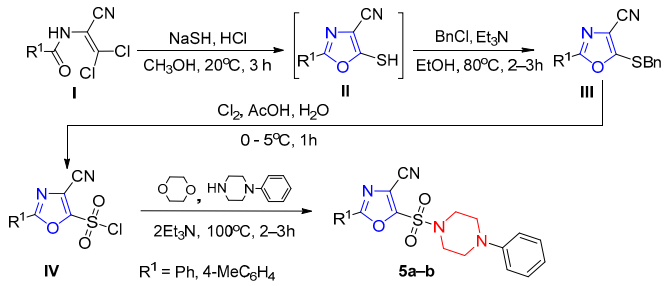

Scheme 2. Synthesis of 2-aryl-5-(4-phenylpiperazin-1-yl)sulfonyl-1,3-oxazole-4-carbonitriles **5a**, **5b**. The starting 2-acylamino-3,3-dichloroacrylonitriles are designated as (**I**); corresponding 5-mercaptooxazoles are designated as (**II**); corresponding 5-(benzylthio)-substituted 1,3-oxazoles are designated as (**III**); corresponding 2-aryl-4-cyano-1,3-oxazole-5-sulfonyl chlorides are designated as (**IV**).

Next, the substituted 4-cyano-1,3-oxazole-5-sulfonyl chlorides **4** with Boc-piperazine gave the corresponding Boc-protected sulfonamides **6**. Passing gaseous HCl through a dioxane solution of sulfonamides **6** resulted in the removal of the Boc protecting group and the formation of sulfonamide hydrochlorides **7a**, **7b**. Finally, the reaction of these compounds with the corresponding sulfonyl chlorides yielded sulfonamides **8aa**–**8bd**, containing two sulfonyl groups connected by a piperazine linker (Scheme 3) and structure-synthesized compound **7a**–**7b** and **8aa**–**8bd** shown in Figure 5.

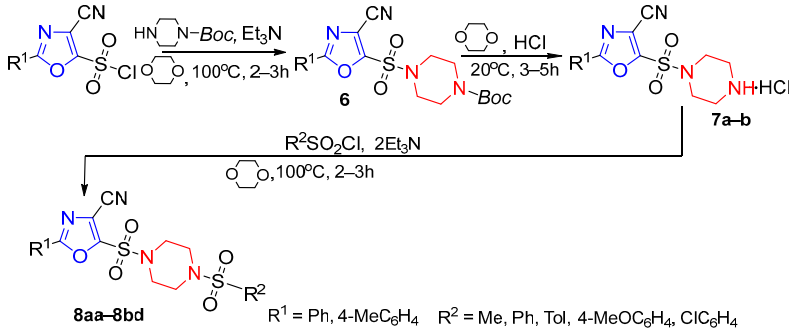

Scheme 3. Synthesis of 5-[4-(arylsulfonyl)piperazin-1-yl]sulfonyl-2-(4-aryl)-1,3-oxazole-4-carbonitriles **8aa**–**8bd**.

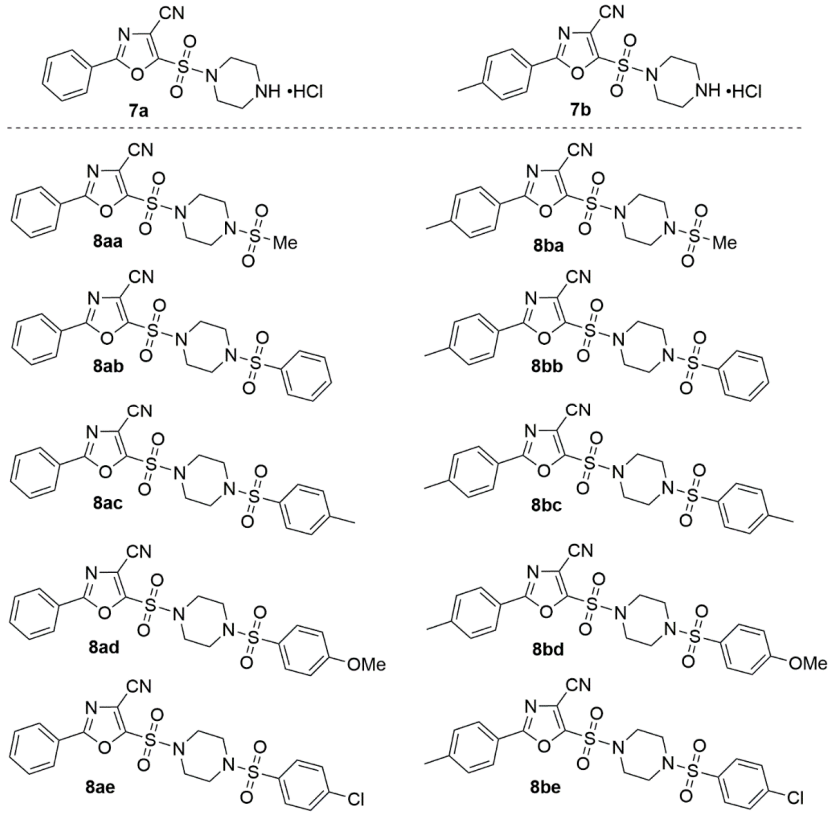

Figure 5. Structure of compound **7a**–**7b** and **8aa**–**8bd**.

The structure of the compounds **2a–2c**, **3aa–3ce**, **5a–5b**, **7a–7b** and **8aa–8bd** was confirmed using the ^{1}H, ^{13}C NMR and FTIR spectroscopy, and elemental analysis (see Supporting Information Figures S1–S96b).

2.2. Biology (In Vitro)

To evaluate the anticancer potential of the synthesized compounds, preliminary cytotoxicity was conducted at a fixed concentration of 2.5 μM using the WST-1 assay in a neuroblastoma Kelly cells and non-malignant human embryonic kidney cell line HEK293, shown in Figure 6. An initial cytotoxicity screening was designed to assess both anticancer activity and selectivity of the synthesized compounds. The screening was performed at a fixed concentration of 2.5 μM using the WST-1 assay in neuroblastoma Kelly cells, representing a malignant model, and non-malignant human embryonic kidney HEK293 cells as a control (Figure 6).

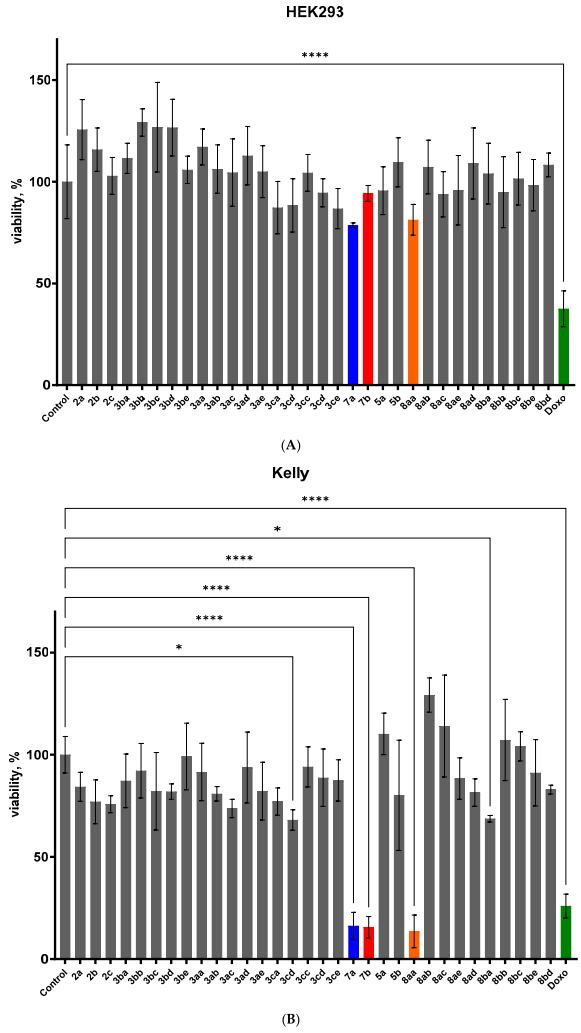

Figure 6. Cytotoxic effects of all compounds at 2.5 μM after 48 h incubation assessed by WST-1 assay. Cell viability data on HEK293 cells (**A**) and Kelly cells (**B**) with doxorubicin (green) as a negative control. The lead compounds are shown in color: **7a** (blue), **7b** (red), and **8aa** (orange). In both panels,

data of the cells treated with solvent are used as control (100% viability, $n \geq 3$); mean ± SD. Statistical significance between control and cells are represented as * where $p < 0.05$; as **** where $p < 0.0001$.

Neuroblastoma Kelly cells exhibited pronounced sensitivity to a subset of the synthesized compounds, with compounds **7a**, **7b**, and **8aa** inducing a marked reduction in cell viability. At a concentration of 2.5 µM, treatment with these compounds resulted in mean viability values below 25%. In contrast, non-malignant HEK293 cells maintained high viability upon exposure to most of the tested compounds, with more than 75% of compounds displaying viability values above 80% (Figure 6). This differential response indicates selective cytotoxicity toward neuroblastoma cells and provides a rationale for further dose-dependent evaluation of compounds **7a**, **7b**, and **8aa**. Such selectivity is particularly relevant in the context of neuroblastoma, where therapeutic resistance and treatment-related toxicity remain significant challenges. To characterize the cytotoxic potency of the most active candidates, compounds **7a**, **7b**, and **8aa** were evaluated in concentration-dependent studies following 48 h exposure in Kelly and SHSY5Y neuroblastoma cells, as well as in non-malignant HEK293 cells. Half-maximal inhibitory concentrations IC_{50} values were determined by nonlinear regression analysis of WST-1 absorbance data at 450 nm, as shown in Figure 7A–I.

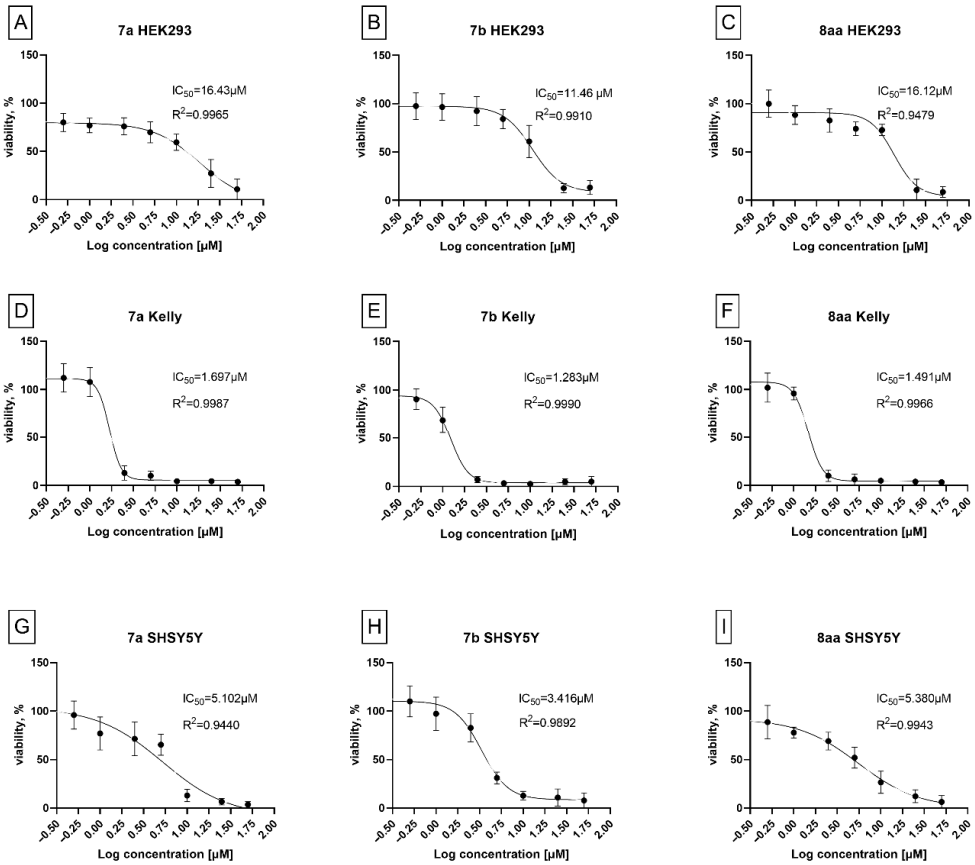

Figure 7. IC_{50} graphs for **7a**, **7b**, **8aa** in HEK cells (**A**–**C**) Kelly cells (**D**–**F**) and SHSY5Y cells (**G**–**I**) after 48 h incubation assessed by WST-1 assay; mean ($n \geq 3$) ± SD.

Neuroblastoma Kelly cells (see Figure 7D–F) exhibited pronounced sensitivity to the lead compounds, with IC_{50} values of 1.7 μM for **7a**, 1.3 μM for **7b**, and 1.5 μM for **8aa**. In contrast, SHSY5Y cells (Figure 7G–I) displayed reduced sensitivity, with IC_{50} values ranging from 3.4 to 5.4 μM, indicating variability in response among neuroblastoma models. Such differences may be associated with distinct genetic backgrounds, metabolic profiles, or cellular uptake mechanisms known to differ between neuroblastoma cell lines. Importantly, all three compounds showed low cytotoxicity in non-malignant HEK293 cells (Figure 7A–C), with IC_{50} values exceeding 10 μM. This differential activity profile demonstrates selective cytotoxicity toward neuroblastoma cells and suggests a favorable therapeutic window for compounds **7a**, **7b**, and **8aa**. To benchmark the cytotoxic potency of the lead compounds, their activity was compared with that of doxorubicin, a clinically established chemotherapeutic agent used in the treatment of solid tumors, including neuroblastoma. The IC_{50} values of doxorubicin were determined in both neuroblastoma Kelly cells and non-malignant HEK293 cells under identical experimental conditions (Figure 8A,B).

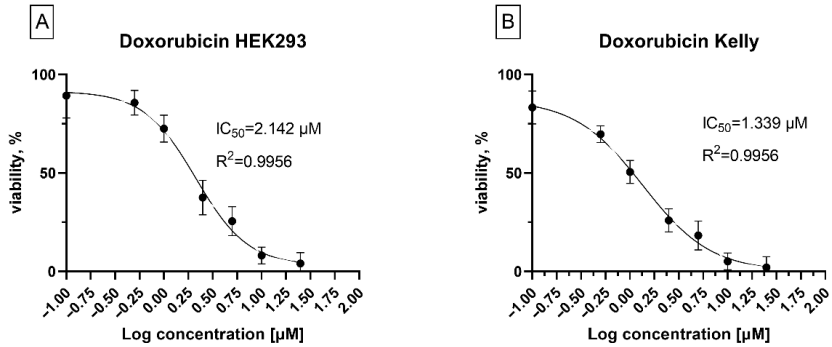

Figure 8. IC_{50} graphs for doxorubicin in HEK293 cells (**A**) and Kelly cells (**B**) after 48 h incubation assessed by WST-1 assay; mean ($n \geq 3$) ± SD.

In Kelly cells, doxorubicin exhibited an IC_{50} of approximately 1.3 μM, comparable to that observed for compound **7b**. In contrast, doxorubicin showed pronounced cytotoxicity in non-malignant HEK293 cells, with an IC_{50} of 2.1 μM, indicating limited selectivity toward malignant cells. By comparison, compound **7b** retained comparable potency in neuroblastoma cells while displaying substantially reduced cytotoxicity in HEK293 cells. This differential activity profile highlights the improved selectivity of compound **7b** and suggests a more favorable therapeutic window relative to doxorubicin.

To assess whether the observed cytotoxic activity of compound **7b** extends beyond neuroblastoma, its potency was further evaluated across a panel of human cancer cell lines, including hepatocellular carcinoma (HepG2, Huh7), breast cancer (MCF7, MDA-MB-231), cervical cancer (HeLa), melanoma (M21), and neuroblastoma (Kelly, SHSY5Y) (Figure 9).

As shown in Figure 9, compound **7b** demonstrated micromolar IC_{50} values (1.3–9.1 μM) across all cancer lines tested, with the most pronounced sensitivity observed in Kelly, SHSY5Y and M21 cells. This broad cytotoxic activity suggests that compound **7b** may interfere with fundamental cellular pathways such as cell cycle regulation or apoptotic signaling that are commonly dysregulated across multiple tumor types. These findings indicate that the anticancer activity of compound **7b** is not restricted to neuroblastoma and may involve shared regulatory pathways across multiple tumor types.

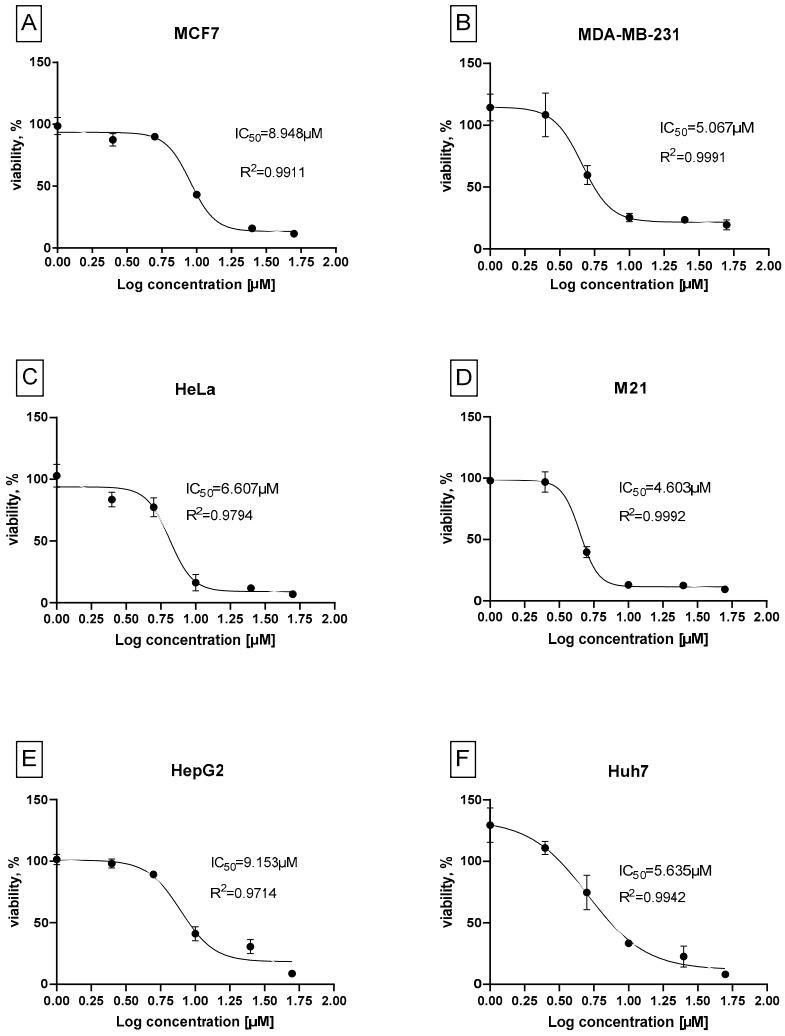

Figure 9. IC_{50} graphs for **7b** in various cancer cell lines after 48 h incubation assessed by WST-1 assay; (**A**) MCF7; (**B**) MDA-MB-231; (**C**) HeLA; (**D**) M21; (**E**) HepG2; (**F**) Huh7; mean ($n \geq 3$) ± SD.

2.3. Selectivity Index

To assess the therapeutic window and tumor-targeting selectivity of the synthesized oxazole derivatives, the selectivity index (SI) was calculated as the ratio of IC_{50} values in non-malignant HEK293 cells to those in malignant neuroblastoma cells (Kelly and SHSY5Y). Compounds **7a**, **7b**, and **8aa** demonstrated pronounced selectivity toward neuroblastoma cells. Specifically, compound **7b** exhibited an IC_{50} of approximately 1.3 μM in Kelly cells and >10 μM in HEK293 cells, yielding an SI > 7.7. Compound **7a** showed an IC_{50} of ~1.7 μM in Kelly cells and >10 μM in HEK293 cells, corresponding to an SI > 5.9, while compound 8aa displayed an IC_{50} of ~1.5 μM in Kelly cells and >10 μM in HEK293 cells, resulting in an SI > 6.7. In contrast, the reference chemotherapeutic agent doxorubicin exhibited limited selectivity, with IC_{50} values of ~1.3 μM in Kelly cells and ~2.1 μM in HEK293 cells, yielding an SI of approximately 1.6. Overall, these results highlight the markedly improved selectivity profile of compounds **7a**, **7b**, and **8aa** relative to doxorubicin and support their further investigation as neuroblastoma-selective anticancer agents.

2.4. Biodegradability

Active pharmaceutical ingredients (APIs) and their metabolites/transformation products are found as pollutants in the environment, impacting human and environmental health. Designing APIs with high biodegradability is desirable but there is no clear agreement on how to implement these criteria in practice [27].

In the CBT, the term "readily biodegradable" refers to those that pass the test with 60% or higher degradation, indicating they will biodegrade rapidly and completely in aquatic environments under aerobic conditions. The CBT experiments were run for 28 days; each day the oxygen concentration was measured and logged for each of the duplicates in the series. The three compounds **7a**, **7b**, and **8aa** did not show any significant biodegradation as the biodegradation % of all the three compounds after 28 days is only 5–10% and did not pass readily biodegradability test. The graphs are given on Figure S97.

Low biodegradability is caused by either toxicity of the studied compounds to the inoculum bacteria or their persistence under experimental conditions. The oxazoles **7a**, **7b**, and **8aa** demonstrated relatively low toxicity against the healthy cells and did not affect the toxicity control in the CBT (see Figure S97) confirming they remain chemically intact under CBT conditions. Indeed, environmental (bio)degradability helps in designing hit compounds that resist breakdown by enzymes in the human body yet finding a 'window of opportunity' where such hits are both metabolically stable enough and environmentally biodegradable remains a challenge [27,28].

2.5. Molecular Modeling

Consistent with our previous investigations [29–31] and supported by the experimental results obtained herein, compounds **7a**, **7b**, and **8aa** were selected as lead candidates for molecular docking studies, using three-dimensional structures obtained from the RCSB Protein Data Bank [29], where the following protein crystal structures were used: anaplastic lymphoma kinase in complex with Crizotinib—ALK (PDB ID: 2XP2); cyclin-dependent kinase series CDK2 (PDB ID: 3QXO), CDK4 (PDB ID: 7SJ3), CDK6 (PDB ID: 8I0M), CDK7 (PDB ID: 1UA2), CDK9 (PDB ID: 6Z45), as well as the checkpoint kinase 1—CHK1 (PDB ID: 1ZYS), apoptosis regulator BCL2 (PDB ID: 4LVT), Aurora-A kinase in complex with N-Myc (PDB ID: 5G1X) and poly[ADP-ribose] polymerase 1 PARP1 (PDB ID: 6I8T). First, molecular docking techniques were validated using redocking co-crystallized ligands into the proteins using docking scores from AutoDock Vina v1.2.5 program (reported as estimated binding free energies, ΔG, in kcal/mol). Next, molecular docking of **7a**, **7b**, and **8aa** was done, and the results are presented in Table 1 and Figure 10.

Table 1. The molecular docking results of ligands **7a**, **7a**, and **8aa** with cancer-related proteins, along with the redocking outcomes.

Compounds and Ligands	Binding Energy, ΔG, kcal/mol									
	ALK	**CDK2**	**CDK4**	**CDK6**	**CDK7**	**CDK9**	**CHK1**	**BCL2**	**Aurora A/ N-MYC**	**PARP1**
7a	−7.1	−7.9	−9.0	−8.0	−8.5	−8.0	−8.9	−7.4	**−10.8**	−8.1
7b	−7.2	−8.1	−9.0	−8.2	−9.1	−8.2	−8.7	−7.8	**−10.9**	−8.4
8aa	−7.5	−8.0	−9.1	−8.1	−9.0	−8.7	−9.1	−8.0	**−10.8**	−8.3
Crizotinib	−9.0	–	–	–	–	–	–	–	–	–
CID 57519664 [a]	–	−8.2	–	–	–	–	–	–	–	–
Abemaciclib	–	–	−9.1	–	–	–	–	–	–	–
CID 169552807 [b]	–	–	–	−9.2	–	–	–	–	–	–

Table 1. *Cont.*

Compounds and Ligands	Binding Energy, ΔG, kcal/mol									
	ALK	**CDK2**	**CDK4**	**CDK6**	**CDK7**	**CDK9**	**CHK1**	**BCL2**	**Aurora A/ N-MYC**	**PARP1**
ATP [c]	–	–	–	–	−9.3	–	–	–	–	–
CID 124155204 [d]	–	–	–	–	–	−9.0	–	–	–	–
CID 6914568 [e]	–	–	–	–	–	–	−9.4	–	–	–
Navitoclax	–	–	–	–	–	–	–	−11.5	–	–
ADP [f]	–	–	–	–	–	–	–	–	**−10.9**	–
CID 49873226 [g]	–	–	–	–	–	–	–	–	–	−8.8

Co-crystallized ligands [30]: [a] 5-nitro-2-[(4-sulfamoylphenyl)methylamino]benzamide; [b] 2-[(4-aminocyclohexyl)amino]-7-cyclopentyl-*N*,*N*-dimethylpyrrolo[2,3-d]pyrimidine-6-carboxamide; [c] Adenosine 5′-triphosphate; [d] (1S,3R)-3-acetamido-*N*-[5-chloro-4-(5,5-dimethyl-4,6-dihydropyrrolo[1,2-b]pyrazol-3-yl)pyridin-2-yl]cyclohexane-1-carboxamide; [e] *N*-[5-[4-(4-methylpiperazin-1-yl)phenyl]-1*H*-pyrrolo[2,3-b]pyridin-3-yl]pyridine-3-carboxamide; [f] adenosine 5′-diphosphate; [g] (1R)-2-(1-cyclohexylpiperidin-4-yl)-1-methyl-3-oxo-1*H*-isoindole-4-carboxamide.

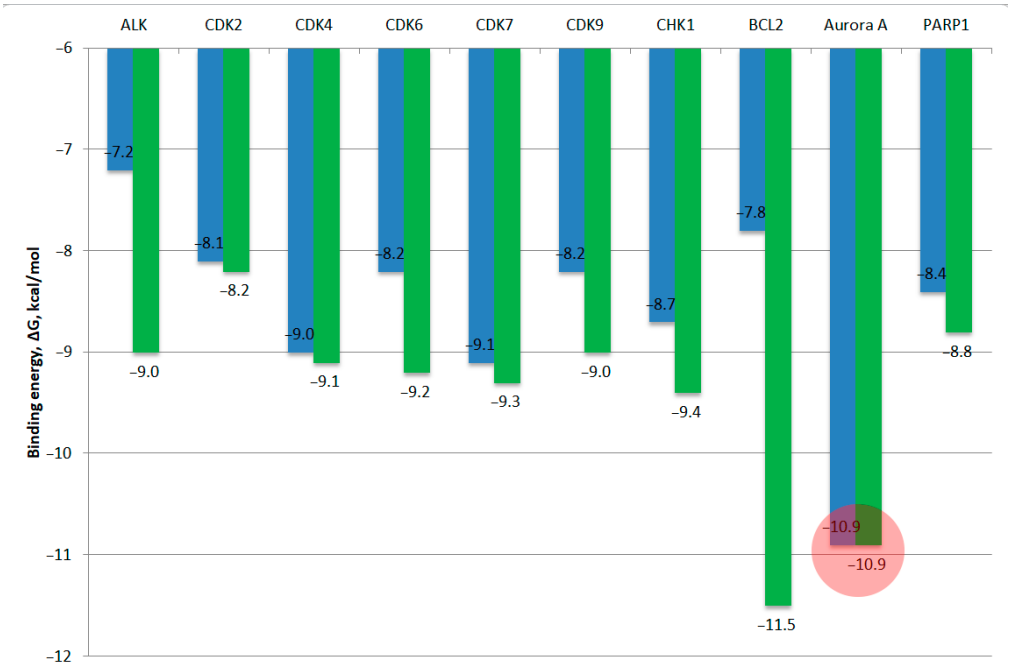

Figure 10. A demonstration of molecular docking results of ligand **7b** with neuroblastoma-associated proteins; blue—compound-**7b**; green—co-crystallized ligands.

Table 1 shows molecular docking validation by redocking co-crystallized ligands into the active sites of the target proteins: ALK kinase, as well as cyclin-dependent kinases CDK2, CDK4, CDK6, CDK7, CDK9, and CHK1 kinase, BCL2 and Aurora A kinase, and polymerase PARP1. The registered binding energies (ΔG) for these protein–ligand interactions varied from −8.2 to −11.5 kcal/mol, and RMSD values were 1.01–2.33 Å. According to the results of molecular docking, the most stable protein–ligand complexes of compounds **7a**, **7b**, and **8aa** were observed for the Aurora A kinase, with values of ΔG ranging from −10.8 to −10.9 kcal/mol. Molecular docking of these compounds into the other proteins did not show high complexation energies ΔG (from −7.2 to −9.1 kcal/mol). Notably, the studied compounds exhibit predicted binding affinities within the ATP-binding sites of several kinases, as reflected by their calculated binding

free energies (ΔG = −7.9–9.1 kcal/mol) in the ATP-binding centers of cyclin-dependent kinases (CDK2, CDK4, CDK6, CDK7, and CDK9), which is comparable to the redocking energy of ligands (ΔG = −8.2–9.3 kcal/mol). The low energy of the complexation was demonstrated by ALK kinase (ΔG = −7.1 to −7.5 kcal/mol) and the apoptosis regulator BCL2 (ΔG = −7.4 to −8.0 kcal/mol). Thus, the most energetically favorable complexation for the studied compounds was found to occur in the ATP-binding site of the Aurora A kinase, with a ΔG value of −10.8 to −10.9 kcal/mol, which is equal to the binding energy of adenosine 5′-diphosphate (ADP) with ΔG = −10.9 kcal/mol. This observation is consistent with the literature. First-generation Aurora A inhibitors are ATP-competitive molecules, many of which have progressed into different stages of clinical evaluation [31]. Successful piperazine-containing Aurora A kinase inhibitors include ENMD-2076 [32] and VX-680 [33], both evaluated in clinical studies. Next, we studied the molecular docking of compounds **7a**, **7b**, and **8aa** into the ATP-binding site of Aurora A kinase (Figure 11).

Figure 11 illustrates the result of the molecular docking of compounds **7a**, **7b**, and **8aa** into the ATP-binding site of Aurora A kinase. The complexation of compound **7a** (Figure 11a,b) with a binding energy of ΔG= −10.8 kcal/mol is stabilized by three hydrogen bonds; two hydrogen bonds formed between the carbonitrile group of compound and amino acids Asp274 (2.68 Å) and Lys162 (2.17 Å), and one bond present between the piperazine moiety and the amino acid residues Lys141 (2.22 Å). This ligand–protein complex is also stabilized by three electrostatic interactions between the compounds' sulfonyl group, the amino acid Lys162 (4.04Å), and the cofactors Mg^{2+} (4.28–4.39 Å). Notably a metal-acceptor interaction (2.57Å) is formed among the cofactor Mg^{2+} and the compounds' sulfonyl group. Also, this complex is stabilized by eight hydrophobic bonds (3.95–5.36 Å) with amino acids Ala160, Lys162, Leu139, Val147, and Leu263 with bond distances 3.92–5.08 Å.

The ligand–protein complex of compound **7b** (Figure 11c,d) with a binding energy of ΔG= −10.9 kcal/mol is stabilized by eight hydrogen bonds; two H-bonds between the compound carbonitrile group and amino acid residues Asp274 (2.66 Å) and Lys162 (2.31 Å), three H-bonds between the sulfonyl group and the amino acids Lys162 (2.22–3.47 Å), and Gly142 (3.48 Å), and three H-bonds between piperazine ring and amino acids—Lys141 (3.48 Å), Glu260 (2.65Å) and Asn (3.39 Å). Also, a metal–acceptor interaction (3.14 Å) exists between the cofactor Mg^{2+} and the **7b**′ sulfonyl group. Furthermore, this ligand–protein complex is stabilized by seven alkyl and Pi-alkyl hydrophobic bonds (3.75–5.43 Å) with amino acids Leu139, Val147, Lys162, and Leu263.

The **8aa** ligand-protein complex (Figure 11e,f) is characterized by a binding energy of ΔG= −10.8 kcal/mol and stabilized by eight hydrogen bonds. The first sulfonyl group forms two H-bonds with Lys258 (2.45–2.48 Å), and two H-bonds form between the piperazine ring and amino acids Asp256, Asp274 (3.38–3.42 Å). The second sulfonyl group forms one H-bond with Lys143 (2.74 Å), and the oxazole forms two H-bonds with the amino acid residues Lys143 (3.28 Å) and Lys162 (2.83 Å). The cofactor Mg1392 forms two metal–acceptor interactions with the oxazole ring (2.42 Å) and the second sulfonyl group (2.62 Å). Also, this ligand–protein complex is stabilized by three electrostatic interactions: between the compounds' first sulfonyl group and Trp277 (4.88 Å); among the oxazole ring and cofactor Mg1391 (4.03 Å), and the amino acid Asp274 (3.70 Å). In addition, the ligand-protein complex is stabilized by three hydrophobic bonds (3.63–4.79 Å) with amino acids Val147 and Leu263. Thus, the molecular docking results of compounds **7a**, **7b**, and **8aa** into the ATP-binding site of human Aurora A kinase are characterized by high binding energy, forming multiple H-bonds, electrostatic and hydrophobic interactions, and forming metal–acceptor interactions of compounds with Mg^{2+} cofactors, investigating the possible

anticancer mechanism of action of compounds **7a**, **7b**, and **8bb** by molecular docking demonstrates a binding model similar to the ADP molecule (Figure 12).

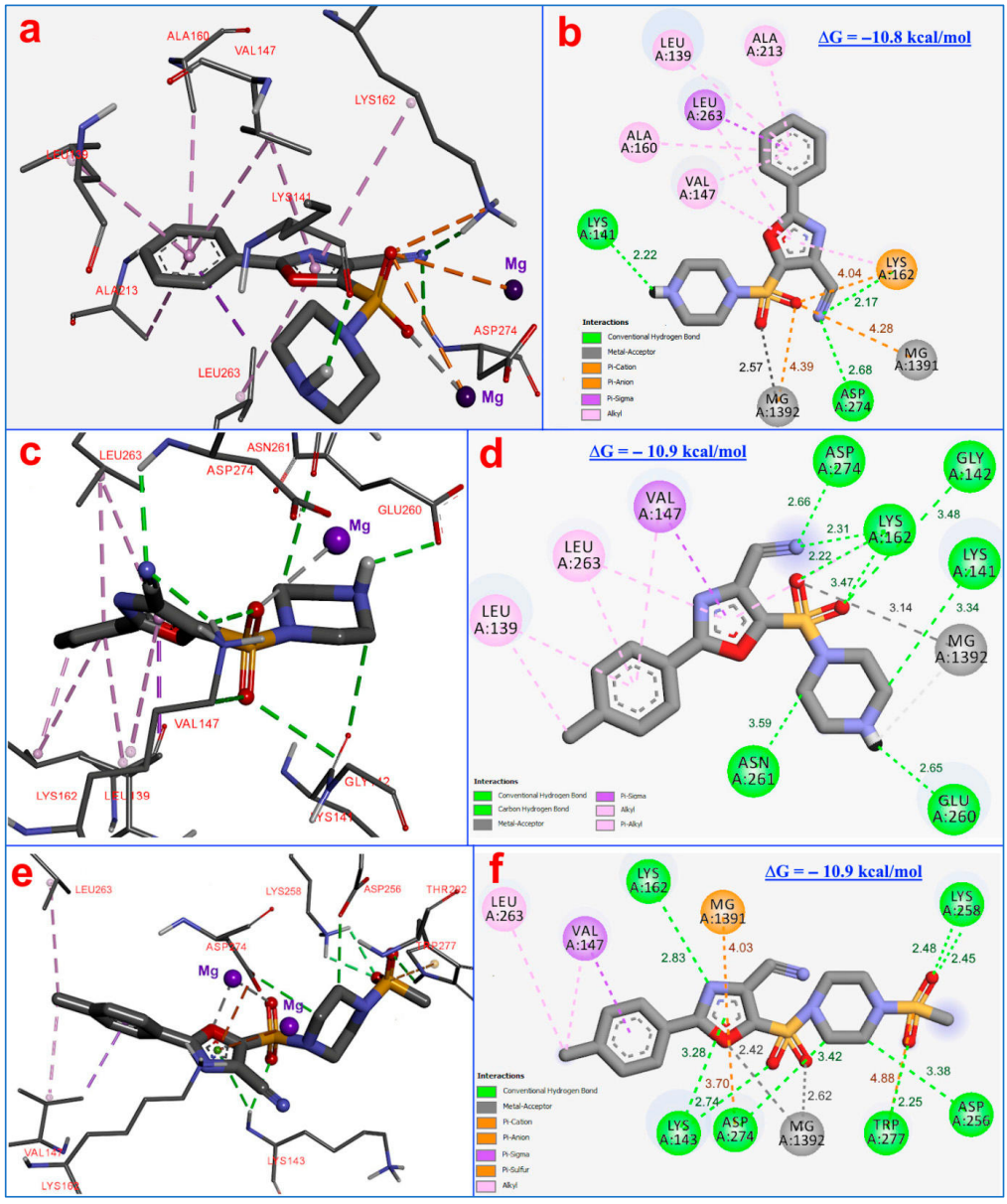

Figure 11. The molecular docking features of compounds **7a**, **7b**, and **8aa** with the ATP-binding site of Aurora A kinase; (**a**,**b**)—compound **7a**; (**c**,**d**)—compound **7b**; (**e**,**f**)—compound **8aa**; green—hydrogen bonds; orange—electrostatic interactions; violet—hydrophobic interactions.

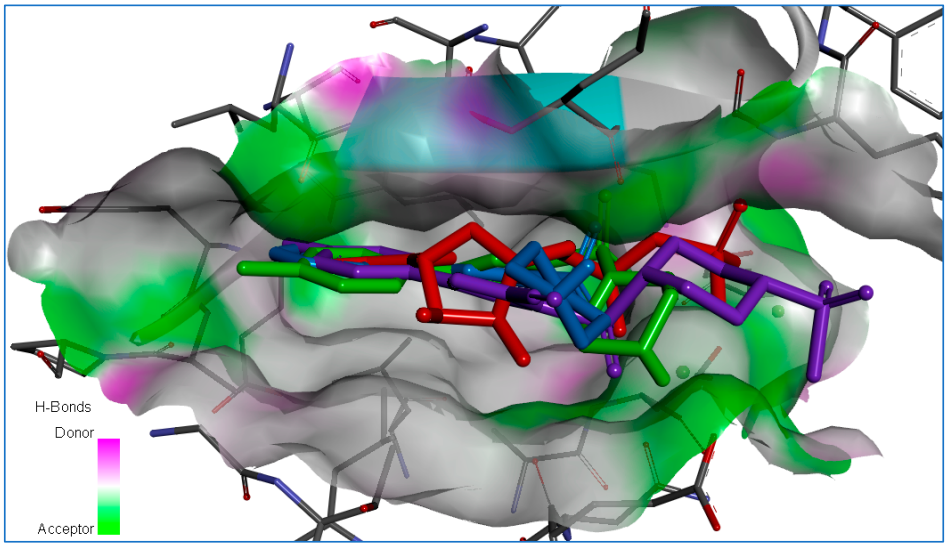

Figure 12. The docking position of the studied compounds in the ATP-binding site of Aurora-A kinase compared with ADP (PDB ID: 5G1X); red—ADP; blue—compound **7a**; green—compound **7b**; violet—compound **8aa**.

Our docking studies with the structure of Aurora-A kinase (PDB ID: 7ZTL) also confirm this interaction model [34]. Next, the pharmacokinetic aspects of compounds **7a**, **7b**, and **8aa** were investigated by ADMET 3.0 web tool [24].

2.6. Integrated Biology and Docking Discussion

The strong binding of the compounds **7a**, **7b**, and **8aa** with the ATP-binding site of the Aurora A kinase, with a ΔG value of −10.8 to −10.9 kcal/mol (ADP ΔG = −10.9 kcal/mol), is in good agreement with the literature data. First-generation Aurora A inhibitors are known to act as ATP-competitive agents that occupy the ATP-binding pocket, and many representatives of this class have progressed to various stages of clinical evaluation [35]. A successful example is the piperazine-containing Aurora A kinase inhibitor (IC_{50} = 1.86 nM) ENMD-2076, 6-(4-methylpiperazin-1-yl)-*N*-(5-methyl-1*H*-pyrazol-3-yl)-2-[(E)-2-phenylethenyl]pyrimidin-4-amine, which is currently in Phase I/II clinical trials [36]. In the literature, a selective Aurora A inhibitor (IC_{50} = 0.6 nM), Tozasertib (VX-680), *N*-[4-[4-(4-methylpiperazin-1-yl)-6-[(5-methyl-1*H*-pyrazol-3-yl)amino]pyrimidin-2-yl]sulfanylphenyl]cyclopropanecarboxamide, is described [37].

It is also known that Aurora A kinase inhibitors bind to the ATP site and cause significant conformational changes in the kinase structure, preventing binding to oncoprotein N-Myc, to block the formation of the Aurora A/N-Myc complex. The formation of this complex plays a crucial role in stabilizing the oncoprotein N-Myc, as key transcription factor that regulates cell cycle progression, cell proliferation, and the metastasis of neuroblastoma. Given the more favorable (i.e., more negative) binding energies compared to the reference in our study, Aurora A kinase represents a plausible molecular target for these compounds. In our opinion, the high activity of compounds **7a**, **7b**, and **8aa** against neuroblastoma cells Kelly expressing N-MYC is associated with their high energy of complex formation in the ATP-binding center of Aurora A kinase, disruption of its conformation, and, as a consequence, destabilization of the oncoprotein N-Myc with antimitotic and antiproliferative action. This hypothesis is supported by the literature data, indicating the development of specific methods for targeting Aurora A in cancer treatment, which initially concentrated

on designing various Aurora A kinase inhibitors and are currently in clinical trials [38]. Nevertheless, this proposed mechanism requires direct biochemical validation, such as kinase activity assays or assessment of N-Myc protein stability.

In contrast to Kelly cells, SHSY5Y neuroblastoma cells do not harbor MYCN amplification and are therefore less dependent on Aurora A-mediated stabilization of the MYCN protein. Despite this, SHSY5Y cells remained sensitive to treatment with compounds **7a**, **7b**, and **8aa**, albeit with moderately higher IC_{50} values (3.4–5.4 μM), suggesting the involvement of additional molecular pathways. Notably, SHSY5Y cells have previously been shown to respond to pharmacological inhibition of cyclin-dependent kinases (CDKs). For example, the selective CDK4/6 inhibitor Palbociclib induces G1 phase arrest and suppresses proliferation in neuroblastoma models, including SHSY5Y [39]. Moreover, CDK7 and CDK9—key regulators of transcriptional elongation via phosphorylation of RNA polymerase II—have emerged as therapeutic vulnerabilities, particularly in MYCN-low or MYCN-negative neuroblastoma subtypes [40]. In agreement with this, our docking results indicate favorable predicted binding affinities of compounds **7a**, **7b**, and **8aa** toward multiple CDKs, including CDK4 and CDK7 (ΔG = −9.0 to −9.1 kcal/mol), suggesting that inhibition of CDK-driven cell cycle and transcriptional programs may contribute to the observed cytotoxic effects, particularly in SHSY5Y cells.

Collectively, these findings support a broader multi-target activity profile for compounds **7a**–**8aa**, in which cytotoxicity may arise from the concurrent disruption of mitotic regulation via Aurora A and transcriptional or cell-cycle control via CDKs. Such multitargeted mechanisms are increasingly recognized as advantageous in anticancer drug development, as they may enhance therapeutic efficacy while reducing the likelihood of resistance, particularly in aggressive pediatric malignancies [41]. Consistent with this interpretation, the lead compound **7b** also exhibited cytotoxic activity across several non-neuroblastoma cancer cell lines, including M21 (melanoma), MCF7 (breast cancer), and Huh7 (hepatocellular carcinoma), with IC_{50} values in the low micromolar range. This pattern is characteristic of cytotoxic agents that interfere with fundamental processes such as cell cycle progression, mitotic spindle formation, or transcriptional regulation, which are commonly dysregulated in rapidly proliferating tumors [42].

Altogether, these results suggest that the therapeutic potential of the investigated oxazole derivatives may extend beyond neuroblastoma and warrants further evaluation in other high-proliferation tumor types. However, comprehensive mechanistic validation—including kinase activity assays, cell-cycle analysis by flow cytometry, and transcriptomic profiling—will be required to precisely delineate the relative contributions of Aurora A and CDK inhibition to the observed anticancer effects [43].

2.7. ADMET Evaluation

Table 2 presents the significant ADMET properties of compounds **7a**, **7b**, **8aa**, and doxorubicin (to compare) as calculated using the online ADMETlab 3.0 web server.

Table 2. ADMET characteristics of compounds **7a**, **7b**, and **8aa** in comparison with doxorubicin.

Parameter	Compounds			
	7a	**7b**	**8aa**	**Doxorubicin**
Physicochemical properties				
Molecular weight, g/mol	318.35	332.40	410.48	543.525
Rotatable bond count	3	3	4	5
Hydrogen bond acceptor count	7	7	9	12
Hydrogen bond donor count	1	1	0	7

Table 2. *Cont.*

Parameter	Compounds			
	7a	**7b**	**8aa**	**Doxorubicin**
Surface area, A^2 [a]	127.784	134.149	157.485	222.081
logP	1.424	2.013	2.048	1.208
Water solubility, log mol/L	−3.015	−2.879	−4.146	−2.915
Absorption				
Caco-2 permeability, log cm/s	−5.855	−5.47	−4.851	−6.77
Inhibitor of P-glycoprotein	No	No	Yes	No
Substrate of P-glycoprotein	No	No	No	Yes
Distribution				
BBB permeability [a]	−0.822	−0.87	−1.474	−1.379
CNS permeability [a]	−3.056	−2.621	−2.908	−2.846
Metabolism				
CYP2D6 substrate	No	No	No	No
CYP3A4 substrate	Yes	Yes	Yes	No
CYP1A2 inhibitor	No	No	No	No
CYP2C19 substrate	Yes	Yes	No	No
CYP2C19 inhibitor	Yes	No	Yes	No
CYP2C9 inhibitor	No	No	Yes	No
CYP2D6 inhibitor	No	No	No	No
CYP3A4 inhibitor	Yes	Yes	Yes	No
Excretion				
Plasma clearance, ml/min/kg	6.379	6.382	5.762	14.244
Half-life of the drug, hour	0.821	0.686	0.793	3.774
Toxicity				
Rat Oral Acute Toxicity (LD50), mol/kg [a]	2.456	2.471	2.491	2.408
Human Hepatotoxicity [a]	Yes	Yes	Yes	Yes
Max. tolerated dose (human), log mg/kg/day [a]	−0.158	−0.554	−0.429	0.081

[a] predicted using pkCSM web server.

The synthesized compounds exhibited acceptable physicochemical properties, including a rotatable bond count of (3–4) and a count of hydrogen bond donors (0–1) and acceptors (7–9). The topological polar surface area of compounds **7a**, **7b,** and **8aa** is 127–157 $Å^2$, which is slightly lower than the doxorubicin value (222 $Å^2$). The coefficient lipophilicity (logP) of compounds is in the acceptable range (0–3 log mol/L) and is 1.424 for compound 7a and 1.208 for doxorubicin. The compounds **7b** and **8aa** exhibit higher lipophilicity, with values of 2.013 and 2.048, respectively. The values of BBB permeability of compounds **7a** (−0.822) and 7b (−0.87) are below the permissible threshold (log BB < −1), and that of compound **8aa** (−1.474) is slightly below the threshold and equal to the corresponding value of doxorubicin (−1.379). The values of CNS permeability for all are <3 and are considered unable to penetrate the CNS. The absorption results show that compounds **7a** and **7b** are well permeable through intestinal cell membranes (logCaco-2 > 5.15), and compound **8aa** has moderate permeability (logCaco-2 = −4.815). Compounds **7a** and **7b** do not interact with P-glycoprotein as a biological barrier; however, compound **8aa** might be a P-glycoprotein inhibitor. The excretion of all compounds is estimated by plasma clearance, which ranges from 5.762 to 6.382 mL/min/kg, indicating moderate clearance (5–15 mL/min/kg). The doxorubicin plasma clearance is 2 times higher, amounting to 14.244 mL/min/kg. Additionally, the results of the compounds' half-lives are obtained, which ranges from 0.686 to 0.821 h, representing an ultra-short half-life value

(<1 h). Doxorubicin has a value of 3.774 h and is a short half-life drug. The toxicology properties of compounds **7a**, **7b**, and **8aa** are characterized by positive hepatotoxicity (similar to doxorubicin) and a low tolerated dose log (mg/kg/day) from −0.158 to −0.554; this dose for doxorubicin is higher (0.081). The values of the rat oral acute toxic doses (LD_{50}) of compounds **7a**, **7b,** and **8aa** are comparable to those of doxorubicin (2.4–2.5 mol/kg). Additionally, Figure 13 illustrates the ADMET characteristics of compounds **7a, 7b, 8aa** and doxorubicin as estimated by the ADMETlab 3.0 web server.

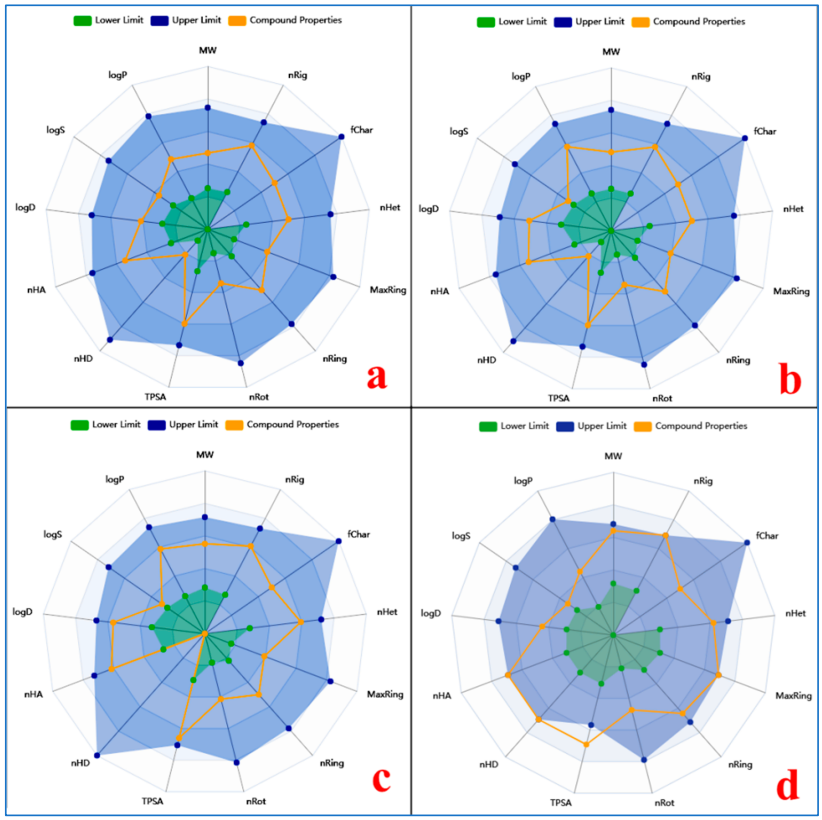

Figure 13. ADMET properties of compounds **7a**, **7b**, **8aa** (by ADMETlab 3.0); (**a**)—compound **7a**, (**b**)—compound **7b**, (**c**)—compound **8aa**, (**d**)—doxorubicin.

3. Experimental Section

3.1. Chemicals Materials and Methods

All chemicals were used without further purification in the synthetic procedures, including doxorubicin hydrochloride (batch WRS DR 02, was provided by Gemini PharmChem Mannheim GmbH/Synbias Pharma AG), commercially available reagents (Sigma-Aldrich, Taufkirchen, Germany), reagent-grade solvents (Lach-Ner, Neratovice, Czech Republic), and deutero solvents (Eurisotop, Saint-Aubin, France). The reaction progress was monitored using thin-layer chromatography (TLC) on silica gel 60 F254 plates (Merck KGaA, Darmstadt, Germany). Melting points (M.p.) were determined in open capillary tubes using a Stuart SMP40 apparatus with a 2 °C/min ramp, and values are reported in °C. NMR spectra (^{1}H and ^{13}C) and 2D HSQC plots were recorded on a Bruker Avance III 400 MHz spectrometer in DMSO-d_6, with residual $SO(CD_3)(CD_2H)$ (δH = 2.50 ppm) or $SO(CD_3)_2$ (δ_C = 39.52 ppm) as the internal standard. HPLS analysis

was conducted on an Agilent 6540 UHD Accurate-Mass Q-TOF LC/MS G6540A Mass Spectrometer. Elemental analysis (CHNS) was performed using a Vario Micro Cube device. Column chromatography was performed using Macherey-Nagel Silica 60, 0.04–0.063 mm silica gel. FT-IR spectra were recorded on a Shimadzu IRTracer-100 spectrometer (Kyoto, Japan) using KBr pellets (1% w/w), with a resolution of 2 cm^{-1} and detection at 254 nm. Dichloroacrylonitriles (**1a–1c**) were prepared as described in the literature [26,44,45]. The starting 4-cyano-2-aryloxazole-5-sulfonyl chlorides (see Scheme 2, structure IV) were synthesized according to a literature procedure [46]; structures **7a** and **7b** first reported in [47] were confirmed in this work. The synthetic procedures and spectral data of all compounds are collected in the Supplementary Information (Figures S1–S96).

3.2. Biology: In Vitro Anticancer Studies

Cell cultures. To evaluate the cytotoxicity and anticancer potential of the synthesized oxazole derivatives, a panel of human cancer cell lines—including HeLa (cervical carcinoma), HepG2 and Huh7 (hepatocellular carcinoma), MDA-MB-231 and MCF7 (breast adenocarcinoma), M21 (melanoma), and Kelly and SHSY5Y (neuroblastoma)—was employed. These cell lines were obtained from the American Type Culture Collection. Additionally, human embryonic kidney cells HEK293 cells were used as a non-cancerous control to assess selectivity toward malignant cells. Cells were cultured in DMEM supplemented with 10% bovine calf serum and 5% penicillin/streptomycin, and maintained under standard conditions (37 °C, 5% CO_2). Treatments were applied 24 h after seeding, followed by a 48 h incubation with either vehicle or compound-containing medium. Cell viability was assessed using the WST-1 assay, which quantifies mitochondrial activity through tetrazolium salt reduction by measuring IC_{50}, or the half maximal inhibitory concentration in this test against neuroblastoma cancer cell, we studied drug activity and possible cellular pathways of action. Additionally, to learn relative efficacy and SI of the hit compounds (**7a**, **7b** and **8aa**), as indicated by IC_{50}, doxorubicin was used in identical experiments, especially in targeting specific tumor types. The cells were propagated in Dulbecco's modified Eagle's medium (DMEM) (Gibco), supplemented with 10% bovine calf serum (Gibco) and 5% penicillin/streptomycin. All cell lines were incubated at 37 °C in a humidified 5% CO_2 and 95% air atmosphere.

Cell treatment procedures. The cells were plated at a density of 2.5 × 105 cells/well (The Countess Automated Cell Counter, Invitrogen, Bothell, WA, USA.) in 96-well plates and incubated overnight. After 24 h of incubation, 100 µL of either fresh media or fresh media containing diluted agents was added into each well and incubated for a further 48 h. The experiments with addition of MeOH were used as solvent control.

Cell viability measured by WST-1. The effects of agents on the viability of cells were determined using the cell viability assay WST-1 (Roche). WST-1 allows colorimetric measurement of cell viability due to reduction in tetrazolium salts to water-soluble formazan by viable cells. The amount of formed formazan dye correlates with the number of viable cells. The measurements were completed 48 h after the cell treatments. The experiments, with an addition of 5 µL of MeOH, were used as a solvent control. Five microliters per well of the WST-1 reagent was added to 100 µL of the cell culture medium, incubated at 37 °C for 2 h, after which the absorbance was measured at 450 nm by using a GENios Pro Microplate Reader (Tecan Group Ltd., Grödig, Austria). WST-1 reduction correlates with the number of metabolically active, viable cells, thus providing a quantitative readout of cytotoxicity.

Statistical analysis was performed using two-way Anova, together with Dunnett's multiple comparisons test. The graphs represent data from at least 3 independent experiments, all performed in triplicate, as the mean ± standard deviation. In the cell viability assay, data of treated with solvent cells showed as control cells. A statistical significance

between control and cells treated with compounds showed, where $p < 0.05$ is represented as *, $p < 0.01$ as **, $p < 0.001$ as *** and $p < 0.0001$ as ****. Statistical analysis was performed with GraphPad Prism 9.

3.3. Molecular Modeling Methods

Molecular docking was performed using AutoDock Vina v1.2.5 program [48]. The X-ray crystal structures of target proteins complexed with inhibitors were obtained from the RCSB Protein Data Bank (PDB). Prior to docking, protein structures were prepared using AutoDockTools (ADT) v.4.2 software [49], which provides a graphical user interface for model setup. Polar hydrogen atoms were added, all atoms were renumbered, and Gasteiger partial charges were assigned using ADT. The prepared protein structures were then saved in PDBQT format for use in docking simulations. The 2D and 3D structures of the ligands **7a**, **7b**, and **8aa** were generated and refined through pre-optimization using the ChemAxon MarvinSketch v.23.11.0 software [50]. The ligand structure optimization and its energy were minimized by the Avogadro v.1.2.0 program [51]. This procedure was performed using the Auto Optimize tool, which employed molecular mechanics calculations to refine the molecular geometry by minimizing the potential energy. We used the force field with MMFF94s, the "steepest descent" algorithm, and the default setting for "Steps per Update" of 4. Next, the three-dimensional structures of the ligands were prepared for docking studies using the AutoDockTools program and saved in PDBQT format for subsequent molecular docking. Docking studies were performed using AutoDock Vina with a grid spacing of 0.375 Å and a grid map ranging from 30 × 30 × 30 Å to 40 × 40 × 40 Å. The docking centers were the geometric centers of the co-crystallized ligands. Under these conditions, the optimized protein and ligand structures served as inputs for docking simulations targeting the defined active site. The AutoDock Vina scoring function was employed to evaluate and rank the docking poses based on their predicted binding affinities. The docking output files were rendered and examined for key interactions between the ligands and the amino acid residues constituting the active sites using BIOVIA Discovery Studio Visualizer 2019 [52]. To ensure the reliability of the docking results, five to six independent runs were performed, yielding up to nine distinct docking poses. Pose selection was based primarily on the AutoDock Vina-predicted binding affinities (kcal/mol) and RMSD values. Additionally, the presence and geometry of potential hydrogen bonds and electrostatic interactions were considered.

3.4. ADMET

The online tool, ADMETlab 3.0 web server [53], was used to calculate the ADMET properties of compounds **7a**, **7b**, and **8aa** in comparison to Doxorubicin [54]. ADMETlab 3.0 tool includes a multi-task DMPNN (directed message passing neural network) architecture based on molecular descriptors. This approach ensures high-speed calculation and performance for each endpoint, along with an elevated level of accuracy and robustness. Additionally, the pkCSM web server was used to predict some ADMET properties [55].

3.5. Biodegradability Study

Biodegradability of the selected oxazoles **7a**, **7b**, and **8aa** was determined using modified aerobic biodegradation test OECD 301D [56] known as Closed Bottle Test (CBT) [57], usually implied as an initial screening test for organic compounds [58].

CBT setup with modifications where biological oxygen consumption is measured with an optode oxygen sensor system using PTFE-lined PSt3 oxygen sensor spots (Fibox 3 PreSens, Regensburg, Germany), allows measuring BOD without dispensing it from the stock solution each time.

Each CBT run consisted of four different series, each done in duplicates. First was "reference series" in which readily biodegradable sodium acetate in a known concentration (6.41 mg/L) was added to a flask of mineral medium inoculated with effluent from a wastewater treatment plant. As sodium acetate is rapidly biodegradable it acted as a reference and control for monitoring activity of microbes in the inoculum [59]. In the test series a studied compound as a sole source of carbon was added to the inoculated mineral medium. The test compound was added in a concentration corresponding to theoretical oxygen demand (ThOD) of approximately 5 mg/L. The details of the calculated ThOD and the amount of test substance used to measure biodegradability in the CBT are listed in Table S1.

Effluent from wastewater treatment plant was collected at municipal wastewater treatment plant in Tallinn, Estonia (Paljassaare wastewater treatment plant, 59°27′55.5″ N 24°42′08.8″ E). Results from each run were accepted if the following criteria were met: (i) the difference in extremes of replicate values at the plateau is less than 20%, (ii) oxygen concentration in test series bottles must not fall below 0.5 mg/L at any time, and (iii) sodium acetate in reference series must be degraded ≥60% by day 14. Blank bottle oxygen consumption was also monitored to avoid the possibility of the system turning from aerobic to anaerobic.

4. Conclusions

Thirty-two 5-piperazine-containing 1,3-oxazole-4-carbonitriles were rationally designed and synthesized in yields ranging from 68% to 83%, and their structures were confirmed by ^{1}H and ^{13}C NMR spectroscopy, HPLC, and elemental analysis. In vitro cytotoxicity assays (WST-1) identified compounds **7a**, **7b**, and **8aa** as lead candidates, demonstrating reproducible micromolar activity against neuroblastoma cell lines (Kelly and SHSY5Y) while maintaining low toxicity toward non-malignant HEK293 cells (IC_{50} > 10 μM), resulting in favorable selectivity indices (SI > 5.9). Notably, compound 7b displayed potency comparable to doxorubicin in Kelly cells but with substantially reduced cytotoxicity in HEK293 cells. Across a broader cancer panel, **7b** retained low-micromolar IC_{50} values, indicating activity in rapidly proliferating tumor cell types.

In silico molecular docking suggested favorable binding of compounds **7a**, **7b**, and **8aa** to the ATP-binding site of Aurora A kinase in complex with N-MYCN, with calculated binding free energies comparable to that of ADP, supporting Aurora A as a plausible molecular target. Additional predicted interactions with cyclin-dependent kinases (CDK4 and CDK7) raise the possibility of a multi-target mechanism involving both mitotic and transcriptional or cell-cycle-associated pathways.

Predicted ADMET profiles indicated acceptable physicochemical properties and moderate clearance, although potential hepatotoxicity comparable to doxorubicin and limited biodegradability under OECD 301D conditions were observed, reflecting common trade-offs at the hit-to-lead stage. Overall, compounds **7a**, **7b**, and **8aa** represent promising lead structures for further preclinical investigation against neuroblastoma, with potential relevance for other rapidly proliferating solid tumors. The favorable in vitro selectivity and predicted multi-target binding profile provide a strong rationale for continued optimization and targeted mechanistic validation.

Supplementary Materials: The following supporting information can be downloaded at https://www.mdpi.com/article/10.3390/ijms27041936/s1.

Author Contributions: O.O.S.: Methodology; Investigation; Data Curation; Writing—Original Draft Preparation; D.B.: Methodology; Conceptualization; Investigation; Validation; Data Curation; Visualization; Writing—Original Draft Preparation, Writing—Reviewing and Editing; O.B.: Methodology;

Investigation; Validation; Data Curation; Visualization; Writing—Original Draft Preparation; N.M.N.: Methodology; Conceptualization; Investigation; Validation; Data Curation; Visualization; J.O.: Investigation; Validation; Data Curation; V.S.B.: Conceptualization; Resources; Funding Acquisition; Writing—Reviewing and Editing; I.V.S.: Methodology; Conceptualization; Investigation; Validation; Data Curation; Visualization; Writing—Original Draft Preparation; Writing—Reviewing and Editing; Y.K.: Conceptualization, Methodology; Resources; Funding Acquisition; Writing—Reviewing and Editing; Project Administration. All authors have read and agreed to the published version of the manuscript.

Funding: This research was financially supported by the Estonian Research Council, grant number COVSG5 (for D.B. and Y.K.), Estonian Ministry of Education and Research and Education and Youth Board scholarship (for O.O.S.), and National Research Foundation of Ukraine, grant number 2025.07/0168 (for I.V.S.). This project has received funding from the European Union's Horizon Europe research and innovation program under the Marie Skłodowska-Curie grant agreement number 101210683 (for D.B.).

Institutional Review Board Statement: Not applicable.

Informed Consent Statement: Not applicable.

Data Availability Statement: Data are available from the authors upon reasonable request.

Acknowledgments: In memory of Volodymyr S. Brovarets, whose contribution to conceptualization, accumulating resources, and preparation of this paper was impactful and alienable. Although he is no longer with us, his dedication to science continues to inspire our research. Authors acknowledge Ivar Järving and Kati Muldma for providing support in HPLC and elemental analysis respectively, Gemini PharmChem Mannheim GmbH/Synbias Pharma AG for providing doxorubicin hydrochloride used as the reference anticancer drug in this study, and Marlen Taggu (AS Tallinna Vesi) for providing wastewater treatment plant effluent for aerobic biodegradation tests.

Conflicts of Interest: The authors declare that they have no known competing financial interests or personal relationships that could have appeared to influence the work reported in this paper.

Abbreviations

HepG2, human hepatocellular carcinoma cell line; Huh7, human hepatocellular carcinoma cell line; MCF7, human breast cancer cell line; MDA-MB-231, triple-negative breast cancer cell line; HeLa, cervical carcinoma cell line; M21, Melanoma cells; Kelly, SH-SY5Y, neuroblastoma cell lines; HEK293, non-malignant human embryonic kidney cell line; ADP, adenosine diphosphate; ATP, adenosine triphosphate; N-MYC, proto-oncogene protein; MYCN, the gene encoding the proto-oncogene protein N-MYC; ADMET, absorption, distribution, metabolism, excretion, and toxicity; VEGFR2, vascular endothelial growth factor receptor; PARP1, poly(ADP-ribose) polymerase 1; EGFR, epidermal growth factor receptor; CBT, closed bottle test; CDK, cyclin-dependent kinase; CHK1, checkpoint kinase 1; DMEM, Dulbecco's modified Eagle medium; DMF, dimethylformamide; DOX, doxorubicin; FDA, Food and Drug Administration; HPLC, high-performance liquid chromatography; IC_{50}, half-maximal inhibitory concentration; PBS, phosphate-buffered saline; WST-1, water-soluble tetrazolium salt-1; ADT, AutoDockTools program.

References

1. Neha, K.; Ali, F.; Haider, K.; Khasimbi, S.; Wakode, S. Synthetic Approaches for Oxazole Derivatives: A Review. *Synth. Commun.* **2021**, *51*, 3501–3519. [CrossRef]
2. Joshi, S.; Mehra, M.; Singh, R.; Kakar, S. Review on Chemistry of Oxazole Derivatives: Current to Future Therapeutic Prospective. *Egypt. J. Basic Appl. Sci.* **2023**, *10*, 218–239. [CrossRef]
3. Chiacchio, M.A.; Lanza, G.; Chiacchio, U.; Giofrè, S.V.; Romeo, R.; Iannazzo, D.; Legnani, L. Oxazole-Based Compounds as Anticancer Agents. *Curr. Med. Chem.* **2020**, *26*, 7337–7371. [CrossRef] [PubMed]
4. Kakkar, S.; Narasimhan, B. A Comprehensive Review on Biological Activities of Oxazole Derivatives. *BMC Chem.* **2019**, *13*, 16. [CrossRef]

5. Nakamura, K.; Taguchi, E.; Miura, T.; Yamamoto, A.; Takahashi, K.; Bichat, F.; Guilbaud, N.; Hasegawa, K.; Kubo, K.; Fujiwara, Y.; et al. KRN951, a Highly Potent Inhibitor of Vascular Endothelial Growth Factor Receptor Tyrosine Kinases, Has Antitumor Activities and Affects Functional Vascular Properties. *Cancer Res.* **2006**, *66*, 9134–9142. [CrossRef]
6. Goulooze, S.C.; Cohen, A.F.; Rissmann, R. Olaparib. *Br. J. Clin. Pharmacol.* **2016**, *81*, 171–173. [CrossRef] [PubMed]
7. Deininger, M.; Buchdunger, E.; Druker, B.J. The Development of Imatinib as a Therapeutic Agent for Chronic Myeloid Leukemia. *Blood* **2005**, *105*, 2640–2653. [CrossRef] [PubMed]
8. Klempner, S.; Tran, P. Profile of Rociletinib and Its Potential in the Treatment of Non-Small-Cell Lung Cancer. *Lung Cancer Targets Ther.* **2016**, *7*, 91–97. [CrossRef]
9. Sung, H.; Ferlay, J.; Siegel, R.L.; Laversanne, M.; Soerjomataram, I.; Jemal, A.; Bray, F. Global Cancer Statistics 2020: GLOBOCAN Estimates of Incidence and Mortality Worldwide for 36 Cancers in 185 Countries. *CA Cancer J. Clin.* **2021**, *71*, 209–249. [CrossRef]
10. Siegel, R.L.; Kratzer, T.B.; Giaquinto, A.N.; Sung, H.; Jemal, A. Cancer Statistics, 2025. *CA Cancer J. Clin.* **2025**, *75*, 10–45. [CrossRef]
11. Blume-Jensen, P.; Hunter, T. Oncogenic Kinase Signalling. *Nature* **2001**, *411*, 355–365. [CrossRef]
12. Ryu, H.; Choi, H.-K.; Kim, H.; Kim, A.-Y.; Song, J.-Y.; Hwang, S.-G.; Kim, J.-S.; Kim, D.-U.; Kim, E.-H.; Kim, J.; et al. Antitumor Activity of a Novel Tyrosine Kinase Inhibitor AIU2001 Due to Abrogation of the DNA Damage Repair in Non-Small Cell Lung Cancer Cells. *Int. J. Mol. Sci.* **2019**, *20*, 4728. [CrossRef] [PubMed]
13. Łukasik, P.; Baranowska-Bosiacka, I.; Kulczycka, K.; Gutowska, I. Inhibitors of Cyclin-Dependent Kinases: Types and Their Mechanism of Action. *Int. J. Mol. Sci.* **2021**, *22*, 2806. [CrossRef] [PubMed]
14. Jiang, L.; Wen, C.; Zhou, H.; Liu, A.; Zhang, H.; Chen, X.; Ding, W.; Liu, J.; Shi, X. Cyclin-Dependent Kinase 7/9 Inhibitor SNS-032 Induces Apoptosis in Diffuse Large B-Cell Lymphoma Cells. *Cancer Biol. Ther.* **2022**, *23*, 319–327. [CrossRef]
15. Anh, D.T.; Hai, P.-T.; Huong, L.-T.-T.; Park, E.J.; Jun, H.W.; Kang, J.S.; Kwon, J.-H.; Dung, D.T.M.; Anh, V.T.; Hue, V.T.M.; et al. Exploration of Certain 1,3-Oxazole- and 1,3-Thiazole-Based Hydroxamic Acids as Histone Deacetylase Inhibitors and Antitumor Agents. *Bioorg. Chem.* **2020**, *101*, 103988. [CrossRef]
16. El-Ghobashy, N.M.; El-Sayed, S.M.; Shehata, I.A.; El-Ashmawy, M.B. Synthesis, Biological Evaluation, and Molecular Modeling Studies of New Benzoxazole Derivatives as PARP-2 Inhibitors Targeting Breast Cancer. *Sci. Rep.* **2022**, *12*, 16246. [CrossRef]
17. Kim, I.-S.; Yang, W.-S.; Kim, C.-H. Physiological Properties, Functions, and Trends in the Matrix Metalloproteinase Inhibitors in Inflammation-Mediated Human Diseases. *Curr. Med. Chem.* **2023**, *30*, 2075–2112. [CrossRef]
18. Bedoya-Reina, O.C.; Li, W.; Arceo, M.; Plescher, M.; Bullova, P.; Pui, H.; Kaucka, M.; Kharchenko, P.; Martinsson, T.; Holmberg, J.; et al. Single-Nuclei Transcriptomes from Human Adrenal Gland Reveal Distinct Cellular Identities of Low and High-Risk Neuroblastoma Tumors. *Nat. Commun.* **2021**, *12*, 5309. [CrossRef]
19. Martínez-Pacheco, M.L.; Hernández-Lemus, E.; Mejía, C. Analysis of High-Risk Neuroblastoma Transcriptome Reveals Gene Co-Expression Signatures and Functional Features. *Biology* **2023**, *12*, 1230. [CrossRef]
20. Tang, X.X.; Zhao, H.; Kung, B.; Kim, D.Y.; Hicks, S.L.; Cohn, S.L.; Cheung, N.-K.; Seeger, R.C.; Evans, A.E.; Ikegaki, N. The *MYCN* Enigma: Significance of *MYCN* Expression in Neuroblastoma. *Cancer Res.* **2006**, *66*, 2826–2833. [CrossRef] [PubMed]
21. Duffy, M.J.; O'Grady, S.; Tang, M.; Crown, J. MYC as a Target for Cancer Treatment. *Cancer Treat. Rev.* **2021**, *94*, 102154. [CrossRef]
22. Papadimitropoulou, A.; Makri, M.; Zoidis, G. MYC the Oncogene from Hell: Novel Opportunities for Cancer Therapy. *Eur. J. Med. Chem.* **2024**, *267*, 116194. [CrossRef]
23. Richards, M.W.; Burgess, S.G.; Poon, E.; Carstensen, A.; Eilers, M.; Chesler, L.; Bayliss, R. Structural Basis of N-Myc Binding by Aurora-A and Its Destabilization by Kinase Inhibitors. *Proc. Natl. Acad. Sci. USA* **2016**, *113*, 13726–13731. [CrossRef]
24. Sjostrom, S.K.; Finn, G.; Hahn, W.C.; Rowitch, D.H.; Kenney, A.M. The Cdk1 Complex Plays a Prime Role in Regulating N-Myc Phosphorylation and Turnover in Neural Precursors. *Dev. Cell* **2005**, *9*, 327–338. [CrossRef]
25. Hiyama, E.; Hiyama, K.; Yokoyama, T.; Ishii, T. Immunohistochemical Analysis of N-Myc Protein Expression in Neuroblastoma: Correlation with Prognosis of Patients. *J. Pediatr. Surg.* **1991**, *26*, 838–843. [CrossRef]
26. Kachaeva, M.V.; Pilyo, S.G.; Zhirnov, V.V.; Brovarets, V.S. Synthesis, Characterization, and in Vitro Anticancer Evaluation of 2-Substituted 5-Arylsulfonyl-1,3-Oxazole-4-Carbonitriles. *Med. Chem. Res.* **2019**, *28*, 71–80. [CrossRef]
27. Puhlmann, N.; Vidaurre, R.; Kümmerer, K. Designing Greener Active Pharmaceutical Ingredients: Insights from Pharmaceutical Industry into Drug Discovery and Development. *Eur. J. Pharm. Sci.* **2024**, *192*, 106614. [CrossRef] [PubMed]
28. Kapitanov, I.V.; Špulák, M.; Pour, M.; Soukup, O.; Marek, J.; Jun, D.; Novak, M.; Diz de Almeida, J.S.F.; França, T.C.C.; Gathergood, N.; et al. Sustainable Ionic Liquids-Based Molecular Platforms for Designing Acetylcholinesterase Reactivators. *Chem. Biol. Interact.* **2023**, *385*, 110735. [CrossRef] [PubMed]
29. Berman, H.M.; Westbrook, J.; Feng, Z.; Gilliland, G.; Bhat, T.N.; Weissig, H.; Shindyalov, I.N.; Bourne, P.E. The Protein Data Bank. *Nucleic Acids Res.* **2000**, *28*, 235–242. [CrossRef] [PubMed]
30. Kim, S.; Chen, J.; Cheng, T.; Gindulyte, A.; He, J.; He, S.; Li, Q.; Shoemaker, B.A.; Thiessen, P.A.; Yu, B.; et al. PubChem 2025 Update. *Nucleic Acids Res.* **2025**, *53*, D1516–D1525. [CrossRef]
31. Kollareddy, M.; Zheleva, D.; Dzubak, P.; Brahmkshatriya, P.S.; Lepsik, M.; Hajduch, M. Aurora Kinase Inhibitors: Progress towards the Clinic. *Investig. New Drugs* **2012**, *30*, 2411–2432. [CrossRef]

32. Veitch, Z.; Zer, A.; Loong, H.; Salah, S.; Masood, M.; Gupta, A.; Bradbury, P.A.; Hogg, D.; Wong, A.; Kandel, R.; et al. A Phase II Study of ENMD-2076 in Advanced Soft Tissue Sarcoma (STS). *Sci. Rep.* **2019**, *9*, 7390. [CrossRef]
33. Martens, S.; Goossens, V.; Devisscher, L.; Hofmans, S.; Claeys, P.; Vuylsteke, M.; Takahashi, N.; Augustyns, K.; Vandenabeele, P. RIPK1-Dependent Cell Death: A Novel Target of the Aurora Kinase Inhibitor Tozasertib (VX-680). *Cell Death Dis.* **2018**, *9*, 211. [CrossRef]
34. Diebold, M.; Schönemann, L.; Eilers, M.; Sotriffer, C.; Schindelin, H. Crystal Structure of a Covalently Linked Aurora-A–MYCN Complex. *Acta Crystallogr. D Struct. Biol.* **2023**, *79*, 1–9. [CrossRef] [PubMed]
35. Mou, P.K.; Yang, E.J.; Shi, C.; Ren, G.; Tao, S.; Shim, J.S. Aurora Kinase A, a Synthetic Lethal Target for Precision Cancer Medicine. *Exp. Mol. Med.* **2021**, *53*, 835–847. [CrossRef]
36. Yee, K.W.L.; Chen, H.-W.T.; Hedley, D.W.; Chow, S.; Brandwein, J.; Schuh, A.C.; Schimmer, A.D.; Gupta, V.; Sanfelice, D.; Johnson, T.; et al. A Phase I Trial of the Aurora Kinase Inhibitor, ENMD-2076, in Patients with Relapsed or Refractory Acute Myeloid Leukemia or Chronic Myelomonocytic Leukemia. *Investig. New Drugs* **2016**, *34*, 614–624. [CrossRef]
37. Harrington, E.A.; Bebbington, D.; Moore, J.; Rasmussen, R.K.; Ajose-Adeogun, A.O.; Nakayama, T.; Graham, J.A.; Demur, C.; Hercend, T.; Diu-Hercend, A.; et al. VX-680, a potent and selective small-molecule inhibitor of the Aurora kinases, suppresses tumor growth in vivo. *Nat. Med.* **2004**, *10*, 262–267. [CrossRef]
38. Vats, P.; Saini, C.; Baweja, B.; Srivastava, S.K.; Kumar, A.; Kushwah, A.S.; Nema, R. Aurora Kinases Signaling in Cancer: From Molecular Perception to Targeted Therapies. *Mol. Cancer* **2025**, *24*, 180. [CrossRef] [PubMed]
39. Rihani, A.; Vandesompele, J.; Speleman, F.; Van Maerken, T. Inhibition of CDK4/6 as a Novel Therapeutic Option for Neuroblastoma. *Cancer Cell Int.* **2015**, *15*, 76. [CrossRef] [PubMed]
40. Chipumuro, E.; Marco, E.; Christensen, C.L.; Kwiatkowski, N.; Zhang, T.; Hatheway, C.M.; Abraham, B.J.; Sharma, B.; Yeung, C.; Altabef, A.; et al. CDK7 Inhibition Suppresses Super-Enhancer-Linked Oncogenic Transcription in MYCN-Driven Cancer. *Cell* **2014**, *159*, 1126–1139. [CrossRef]
41. Raghavendra, N.M.; Pingili, D.; Kadasi, S.; Mettu, A.; Prasad, S.V.U.M. Dual or Multi-Targeting Inhibitors: The next Generation Anticancer Agents. *Eur. J. Med. Chem.* **2018**, *143*, 1277–1300. [CrossRef] [PubMed]
42. Hanahan, D.; Weinberg, R.A. Hallmarks of Cancer: The Next Generation. *Cell* **2011**, *144*, 646–674. [CrossRef] [PubMed]
43. Doostmohammadi, A.; Jooya, H.; Ghorbanian, K.; Gohari, S.; Dadashpour, M. Potentials and Future Perspectives of Multi-Target Drugs in Cancer Treatment: The next Generation Anti-Cancer Agents. *Cell Commun. Signal.* **2024**, *22*, 228. [CrossRef]
44. Matsumura, K.; Saraie, T.; Hashimoto, N. Studies of Nitriles. VII. Synthesis and Properties of 2-Amino-3,3-Dichloroacrylonitrile (ADAN). *Chem. Pharm. Bull.* **1976**, *24*, 912–923. [CrossRef]
45. Hirwe, N.; Deshpande, J. Studies in Chloral Amides. Part IX. Reactivity of α-Chlorine in α-Chloro-chloral-Toluic Amides. *Proc. Indian Acad. Sci. (Math. Sci.)* **1941**, *13*, 277–280. [CrossRef]
46. Kornienko, A.N.; Pil'o, S.G.; Prokopenko, V.M.; Brovarets, V.S. Synthesis of 2-Aryl-4-Cyano-1,3-Oxazole-5-Sulfonyl Chlorides and N-Substituted Sulfonamides. *Russ. J. Gen. Chem.* **2012**, *82*, 1855–1858. [CrossRef]
47. Severin, O.O.; Kachaeva, M.V.; Pilyo, S.G.; Kovalishyn, V.V.; Keith, K.A.; Harden, E.A.; Hartline, C.B.; James, S.H.; Zhirnov, V.V.; Brovarets, V.S. Synthesis, Characterization, and Study of Anti-HPV Activity and Cell Cytotoxicity of Novel 1,3-Oxazole-4-Carbonitrile and 4-Sulfonylamide-5-Phenyl-1,3-Thiazole Derivatives In Vitro. *Lett. Appl. NanoBioSci.* **2024**, *13*, 89. [CrossRef]
48. Eberhardt, J.; Santos-Martins, D.; Tillack, A.F.; Forli, S. AutoDock Vina 1.2.0: New Docking Methods, Expanded Force Field, and Python Bindings. *J. Chem. Inf. Model.* **2021**, *61*, 3891–3898. [CrossRef]
49. Morris, G.M.; Huey, R.; Lindstrom, W.; Sanner, M.F.; Belew, R.K.; Goodsell, D.S.; Olson, A.J. AutoDock4 and AutoDockTools4: Automated Docking with Selective Receptor Flexibility. *J. Comput. Chem.* **2009**, *30*, 2785–2791. [CrossRef]
50. ChemAxonChemAxon MarvinSketch 2013. ChemAxon. MarvinSketch, Version 23.11.0. ChemAxon: Budapest, Hungary, 2025. Available online: https://www.chemaxon.com (accessed on 5 September 2025).
51. Hanwell, M.D.; Curtis, D.E.; Lonie, D.C.; Vandermeersch, T.; Zurek, E.; Hutchison, G.R. Avogadro: An Advanced Semantic Chemical Editor, Visualization, and Analysis Platform. *J. Cheminform.* **2012**, *4*, 17. [CrossRef] [PubMed]
52. Dassault Systèmes Discovery Studio Visualizer 2025. BIOVIA, Dassault Systèmes, BIOVIA Discovery Studio Visualizer, 2021. Dassault Systèmes: San Diego, CA, USA, 2025. Available online: https://discover.3ds.com/ (accessed on 2 September 2025).
53. Fu, L.; Shi, S.; Yi, J.; Wang, N.; He, Y.; Wu, Z.; Peng, J.; Deng, Y.; Wang, W.; Wu, C.; et al. ADMETlab 3.0: An Updated Comprehensive Online ADMET Prediction Platform Enhanced with Broader Coverage, Improved Performance, API Functionality and Decision Support. *Nucleic Acids Res.* **2024**, *52*, W422–W431. [CrossRef]
54. Abo-Salem, H.M.; El Souda, S.S.M.; Shafey, H.I.; Zoheir, K.M.A.; Ahmed, K.M.; Mahmoud, K.; Mahrous, K.F.; Fawzy, N.M. Synthesis, bioactivity assessment, molecular docking and ADMET studies of new chromone congeners exhibiting potent anticancer activity. *Sci. Rep.* **2024**, *14*, 9636. [CrossRef]
55. Pires, D.E.V.; Blundell, T.L.; Ascher, D.B. PkCSM: Predicting Small-Molecule Pharmacokinetic and Toxicity Properties Using Graph-Based Signatures. *J. Med. Chem.* **2015**, *58*, 4066–4072. [CrossRef]

56. Assessment of Chemicals | OECD. Available online: https://www.oecd.org/en/topics/assessment-of-chemicals.html (accessed on 5 July 2024).
57. Friedrich, J.; Längin, A.; Kümmerer, K. Comparison of an Electrochemical and Luminescence-Based Oxygen Measuring System for Use in the Biodegradability Testing According to Closed Bottle Test (OECD 301D). *CLEAN Soil Air Water* **2013**, *41*, 251–257. [CrossRef]
58. Nyholm, N. The European System of Standardized Legal Tests for Assessing the Biodegradability of Chemicals. *Environ. Toxicol. Chem.* **1991**, *10*, 1237–1246. [CrossRef]
59. Gupta, A.K.; Alam, M.; Alam, S.; Ansari, A.; Mishra, S.; Husain, S.Q. Production of Ethanol from Jaggery. *Int. J. Res. Appl. Sci. Eng. Technol.* **2022**, *10*, 5042–5045. [CrossRef]

Curriculum vitae

Personal data	
Name:	Nandish Mudegowdru Nagappa
Date of birth:	18/01/1993
Place of birth:	Karnataka, India
Citizenship:	India
Contact data	
E-mail:	namude@taltech.ee
Education and degree awarded	
2021-2026	Tallinn University of Technology, Ph. D
2017-2020	University of Bologna, M.Sc.
2011-2015	Visvesvaraya Technological University, BE
Language competence	
Kannada	Native
English	Fluent
Hindi	Basic
Italian	Basic
Professional employment	
2021-2026	Early-Stage Researcher – TalTech
2015-2017	Process Engineer – Synthite Industries, India
Research Exchange visits:	
2022	Training on OECD 301D Biodegradation assessment method at Leuphana University, Luneburg, Germany.
2020	International research Exchange at Indian Institute of Science, Bengaluru, India.
Honors and awards	
2025	Best Poster presentation award at AI retreat, TalTech.
2017-2020	Emilia-Romagna (Er. Go) scholarship for Master Students from Govt of Italy.
Teaching and Supervision:	
2022-2025	Teaching Laboratory course on biodegradability study for BIOCEB Masters students (LKK0130).
2025	Bachelor Thesis advisor for Daria Maljuk, TalTech.
2024	Academic mentor for Erasmus+ exchange student Pia-Justina Wellmann, Leuphana University, Germany.

Elulookirjeldus

Isikuandmed	
Nimi	Nandish Mudegowdru Nagappa
Sünniaeg	18.01.1993
Sünnikoht	Karnataka, India
Kodakondsus	India
Kontaktandmed	
E-post	namude@taltech.ee
Haridus ja omandatud kraadid	
2021–2026	Tallinna Tehnikaülikool, doktorantuur (PhD)
2017–2020	Bologna Ülikool, magistrikraad (MSc)
2011–2015	Visvesvarayya Tehnikaülikool, bakalaureusekraad (BE)
Keeleoskus	
Kannada	Emakeel
Inglise	väga hea
Hindi	algtase
Itaalia	algtase
Töökogemus	
2021–2026	Nooremteadur (Early-Stage Researcher), TalTech
2015–2017	Protsessiinsener, Synthite Industries, India
Teadusvahetus ja koolitused	
2022	OECD 301D biolagunevuse hindamise meetodi koolitus, Leuphana Ülikool, Lüneburg, Saksamaa
2020	Rahvusvaheline teadusvahetus, India Teadusinstituut (IISc), Bengaluru, India
Autasud ja stipendiumid	
2025	Parima postriesitluse auhind, AI retreat, TalTech
2017–2020	Er.Go stipendium magistriõppeks, Itaalia valitsus
Õpetamine ja juhendamine	
2022–2025	BIOCEB magistrantidele biolagunevuse laborikursus (LKK0130)
2025	Bakalaureusetöö nõustaja, Daria Maljuk (TalTech)
2024	Erasmus+ üliõpilase Pia-Justina Wellmanni akadeemiline mentor (Leuphana Ülikool, Saksamaa)

ISSN 2585-6901 (PDF)
ISBN 978-9916-80-524-4 (PDF)